Genome instability : from genome content variations to gene expression plasticity

Alix Goupil

PSL
UNIVERSITÉ PARIS

THÈSE DE DOCTORAT
DE L'UNIVERSITÉ PSL

Préparée à Institut Curie

Instabilité génétique : des déviations du contenu génomique à la plasticité d'expression des gènes

Genome instability: from genome content variations to gene expression plasticity

Soutenue par
Alix GOUPIL
Le 04 juin 2021

École doctorale n° 515
Complexité du vivant

Spécialité
Biologie cellulaire

Composition du jury :

Jean-René, HUYNH, PhD Directeur de Recherche, Collège de France	*Président*
Raquel, OLIVEIRA, PhD Principal Investigator, IGC	*Rapportrice*
Jens, JANUSCHKE, PhD Principal Investigator, University of Dundee	*Rapporteur*
Pauline, SPÉDER, PhD Directrice de Recherche, Institut Pasteur	*Examinatrice*
Cédric, MAURANGE, PhD Directeur de Recherche, IBDM	*Examinateur*
Renata, BASTO, PhD Directrice de Recherche, Institut Curie	*Directrice de thèse*

institutCurie | PSL

Résumé du manuscrit en français

Contexte

Dans les organismes multicellulaires, une coordination parfaite entre prolifération, mort et différentiation cellulaire est essentielle pour le développement, le fonctionnement et l'homéostasie des tissus et organes. Un niveau de contrôle important est le maintien d'un contenu génomique stable (euploïdie), qui dans la plupart des cellules animales dépend de la présence de deux copies de chaque chromosome (diploïdie). Pour assurer la stabilité du génome et l'homéostasie tissulaire, la prolifération cellulaire est contrôlée au cours du cycle cellulaire où une cellule mère duplique entièrement son matériel génétique avant sa redistribution égale entre les deux cellules filles pendant la mitose. Lors de la mitose, l'ADN se condense et s'individualise en chromosomes mitotiques en prophase. Les centrosomes sont les principaux centres organisateurs des microtubules (MTs) des cellules animales et nucléent des MTs et forment les deux pôles du fuseau mitotique bipolaire. Une fois, les chromosomes alignés sur la plaque métaphasique, la ségrégation correcte des chromosomes en anaphase assure la répartition égale de l'information génétique entre les deux cellules filles dont la séparation physique se fait par cytokinèse, essentielle au maintien de la stabilité génétique.

Cependant, des déviations du contenu chromosomique peuvent survenir et parmi elles, on distingue la polyploïdie, caractérisée par le gain de l'ensemble des chromosomes et l'aneuploïdie, définie par le gain ou la perte de chromosome entier. En contexte pathologique, la polyploïdie et l'aneuploïdie résultent principalement d'erreurs en mitose. Un défaut de cytokinèse, par exemple, conduit au doublement du contenu en ADN et en organelles cytoplasmiques, tels que les centrosomes, tandis qu'une ségrégation incorrecte des chromosomes génère des cellules aneuploïdes (Meraldi et al., 2002; Levine and Holland, 2018). Ces variations sont généralement associées à des pathologies. L'aneuploïdie est associée à des troubles du développement neurologique (Antonarakis et al., 2004) et comme source d'instabilité génétique, alimente l'évolution complexe du génome des cancers. La duplication du génome entier est également fréquente dans les tumeurs et est considérée comme une source importante d'instabilité chromosomique (Dewhurst et al., 2014), notamment par la génération de cellules aneuploïdies lors de divisions multipolaires. Néanmoins les contributeurs de cette multipolarité en présence d'ADN et de centrosomes en excès restent inconnus.

Des changements de ploïdie sont également observés en contexte physiologique dans certaines cellules spécialisées. Dans ce contexte, ils surviennent en réponse à un stress ou font partie du programme de différentiation, et confèrent un certain avantage aux cellules. La polyploïdie, par exemple, présente dans de nombreux tissues de la larve de drosophile, les hépatocytes ou encore mégacaryocytes humains, permet une augmentation de la taille des cellules et de leur capacité métabolique. L'aneuploïdie est aussi décrite dans les tissus sains, comme dans le contexte de l'inversion de la ploïdie dans les hépatocytes ou le rectum de drosophile (Duncan et al., 2010; Schoenfelder et al., 2014). Cependant, la fréquence des cellules aneuploïdes et la manière dont ces déviations du contenu chromosomique sont générées dans les organismes multicellulaires de type sauvage restent sujet à débat. Un aperçu comparatif et dynamique des niveaux d'aneuploïdie, mécanismes de génération et du devenir des cellules aneuploïdes dans les différents tissus d'un organisme sain est manquant.

Mes travaux de thèse ont été initié à partir de deux projets indépendants : (A) investiguer la formation du fuseau mitotique dans des cellules polyploïdes ; (B) Investiguer la fréquence, la genèse et le devenir de cellules aneuploïdes dans les tissus sains de la drosophile en utilisant une nouvelle sonde génétique détectant la perte de chromosome *in vivo*.

Résultats Section A - Goupil, Nano et al. 2020, Journal of Cell Biology

"Chromosomes function as a barrier to mitotic spindle bipolarity in polyploid cells"

Dans le but de caractériser les conséquences de la polyploïdie sur la division cellulaire *in vivo*, j'ai utilisé un model permissif au défaut de cytokinèse (induit par la déplétion de Pavarrotti/MKLP1) : les cellules souches neuronales (ou neuroblastes NBs) du cerveau larvaire de *Drosophila melanogaster* (Adams et al., 1998; Gatti and Baker, 1989; Nano et al., 2019), accumulant ainsi de l'ADN et des centrosomes à chaque cycle. L'analyse en temps réel de NBs polyploïdes exprimant la tubuline-GFP et l'histone-RFP ont montré des divisions multipolaires. J'ai identifié une première étape de regroupement de centrosomes en excès suivie par un défaut de coalescence des multiples pôles générant des fuseaux multipolaires. La multipolarité et la duplication du génome sont connus pour être des sources d'instabilité chromosomiques dans les cancers humains. J'ai donc confirmé ces observations dans une lignée de cellules cancéreuses humaines (OVCAR-8) traitée avec un inhibiteur de la polymérisation d'actine connu pour induire un défaut de cytokinèse.

Trois voies de nucléation des MTs sont impliquées dans la formation du fuseau mitotique : à partir des centrosomes, de la chromatine et des MTs préexistants. Pour analyser leur contribution respective, j'ai diminué l'expression d'acteurs clés de chacune de ces voies, individuellement. J'ai découvert que seule la déplétion des centrosomes restaurait la bipolarité du fuseau mitotique dans des NBs polyploïdes de petite taille. En effet, les cellules ayant atteint un niveau plus élevé de polyploïdie se divisaient de façon multipolaire même en absence de centrosomes. Ces résultats suggèrent que les centrosomes mais surtout la présence d'ADN en excès contribue à cette multipolarité.

En contexte d'amplification centrosomale seule (non-polyploïde), les cellules cancéreuses et les NBs sont capables de regrouper les centrosomes surnuméraires grâce à l'activité de la kinésine Ncd/HSET. L'abolition du niveau de Ncd par l'utilisation de mutation a confirmé que Ncd était nécessaire au regroupement initial des centrosomes observé dans les NBs polyploïdes. Inversement, la surexpression de Ncd n'a pas restauré la bipolarité, suggérant que même un excès de Ncd n'était pas suffisant pour permettre la coalescence des pôles du fuseau et donc que Ncd ne constitue par un facteur limitant dans les NBs polyploïdes.

En collaboration avec Gaëlle Letort, experte en simulation informatique au Collège de France nous avons modélisé ces cellules *in sillico* et identifié des contributeurs de la multipolarité. Après avoir testé différents paramètres, nous avons découvert qu'au-delà du nombre de centrosomes, la quantité mais surtout la conformation spatiale de l'ADN empêchaient la coalescence des pôles du fuseau avec le positionnement d'ADN en excès agissant comme une barrière physique. L'ablation par laser des chromosomes positionnés entre deux pôles du fuseau et leur coalescence en conséquence ont confirmé cette propriété « barrière » de l'ADN dans des cellules cancéreuses humaines polyploïdes. De façon intéressante, la bipolarité a pu aussi être rétablie en augmentant la stabilité et donc la longueur des MTs pour contourner cette barrière dans les cellules polyploïdes.

En conclusion, mes résultats montrent que la polyploïdie induit des divisions multipolaires dans les NBs de drosophile et les cellules cancéreuses humaines. Cette multipolarité est due à la présence de chromosomes en excès agissant comme une barrière physique bloquant la coalescence des pôles du fuseau. Cette barrière d'ADN maintient les pôles du fuseau écartés, inhibant le contact et le glissement des MTs nucléés à partir des centrosomes. Cette découverte remet en question l'opinion actuelle qui suggérait que les extra-centrosomes étaient les seuls contributeurs à la multipolarité du fuseau mitotique.

Pour évaluer quantitativement la perte de chromosome chez la drosophile, nous avons développé un outil génétique basé sur le système bien connu GAL4 (activation)/ GAL80 (inhibition) (Suster et al., 2004) et l'expression d'un marqueur de fluorescence GFP (Siudeja et al., 2015). En principe, en présence du GAL80, GAL4 est inhibé et par conséquent la GFP est réprimée. Cependant, lors de la perte aléatoire d'un chromosome, s'il s'agit de celui contenant la séquence du GAL80, GAL4 est libéré et active l'expression de la GFP. Cet outil permet donc de suivre en temps réel l'apparition et le devenir des cellules aneuploïdes GFP positives *in vivo*.

J'ai testé 20 lignées différentes de drosophile, chacune contenant une copie du répresseur GAL80 inséré à différentes localisations sur trois des quatre chromosomes. De façon inattendue, pour la plupart des lignées, j'ai observé un taux très élevé de cellules vertes dans le cerveau de la larve, contrairement aux disques imaginaux qui étaient pour la majorité GFP négatifs. J'ai découvert que ces cellules GFP représentaient essentiellement des groupes de NBs avec leur cellules filles associées en utilisant des marqueurs spécifiques des différent types cellulaires qui composent le cerveau larvaire. De façon intéressante, les NBs GFP étaient diploïdes, comme j'ai pu le montrer en utilisant des sondes FISH à ADN. De plus, la fréquence de GFP restait inchangée en présence de chromosomes balanceurs non-homologues inhibant la recombinaison des chromosomes en mitose. Ces data suggèrent que l'apparition du signal GFP dans ces NBs n'est pas due à la perte du GAL80 par aneuploïdie, ni par recombinaison mitotique.

Le système GAL4/GAL80 est basé sur une stœchiométrie entre ces deux acteurs, nous avons donc émis l'hypothèse que la quantité de GAL80 était insuffisante pour inhiber tout le GAL4. J'ai donc généré de nouvelles lignés contenant deux copies de GAL80. Même si la fréquence des cellules GFP+ était considérablement diminuée pour les doubles insertions sur les chromosomes 2 et 3, deux ou quatre copies de GAL80 sur le chromosome X n'étaient toujours pas suffisantes pour abolir le signal GFP. Par l'utilisation de sondes spécifiques contre l'ARN du GAL80 et marquées avec un fluorophore, j'ai confirmé par FISH le manque d'expression de GAL80 dans les NBs GFP+.

Pour obtenir une vision dynamique du système, j'ai filmé les cerveaux pendant plus de 48H et observé différents comportements : (1) le maintien de la GFP dans la plupart des NBs GFP+ et sa transmission aux cellules filles au cours de divisions cellulaires ; (2) l'apparition ou (3) la disparition du signal GFP dans des NBs, suggérant que le système est dynamique et partiellement réversible. Cette dynamique et la spécificité de l'expression de GAL80 dans les NBs suggèrent une possible régulation épigénétique, spécifique au cerveau pendant le développement de la drosophile. La régulation épigénétique est souvent utilisée au cours du développement pour fournir une certaine adaptabilité face à différentes conditions environnementales (Friedrich et al., 2019). J'ai donc testé si différentes conditions induisant du stress pouvaient influencer le système en utilisant la double insertion du GAL80 sur le chromosome X comme rapporteur des modifications du pattern d'expression des gènes. Effectivement, des variations dans la température d'incubation des mouches et dans la composition de leur nourriture influençaient significativement la fréquence de cellules GFP +. Ces résultats montrent que les NBs du cerveau de la larve en développement présentent un nouveau mode de régulation de l'expression des gènes qui semble être dynamique, réversible et susceptible d'être influencé par différentes conditions environnementales.

En conclusion, même si ce système décrit ci-dessus ne permet pas de détecter la perte de chromosomes dans tous les tissus de drosophile au cours du développement, il a permis de mettre en lumière une nouvelle régulation et plasticité d'expression des gènes dans le cerveau en développement qui diffère des autres organes. Cette découverte aura des implications importantes pour la communauté des drosophilistes qui utilisent fréquemment ce système GAL4/GAL80 pour contrôler l'expression de transgènes. Néanmoins plusieurs questions restent en suspens. En effet, les mécanismes de régulation épigénétique responsables de ce mosaïsme d'expression des gènes dans les NBs restent à être découverts. De plus, la question de la spécificité du cerveau par rapport aux autres organes est très intrigante. Ce mosaïsme pourrait représenter un manque de control du paysage épigénétique en raison du développement extrêmement rapide du tissu ou à l'inverse une plasticité contrôlée nécessaire à une telle diversité neuronale. Cette plasticité épigénétique du cerveau pourrait aussi permettre une évolution rapide, essentielle à la survie de l'organisme.

Remerciements

J'ai vécu une expérience unique aux côtés de personnes uniques…

Merci à la Fondation pour la Recherche Médiale, La Ligue Nationale Contre le Cancer, l'European Research Council, l'Institut Curie, l'UMR144, l'ED Complexité du vivant et PSL pour avoir encadré et financé ma thèse et mes travaux 🤑. Merci également à toutes les personnes de l'administration, du laboratoire de préparation de l'UMR144 et des plateformes de microcopie et de milieu de mouches, pour m'avoir aidée et permise de réaliser ce doctorat dans les meilleures conditions possibles 🔬.

Merci à tous mes collaborateurs et à toutes les personnes qui ont participé à ce travail et aux discussions : les laboratoires de **Allison Bardin**, **Daniele Fachinetti** et **Cayetano Gonzalez,** et mon comité de thèse, **Allison Bardin, Phong Tran** et **Jorge Merlet**. Merci également aux membres de mon jury de de thèse **Raquel Oliveira**, **Jens Januschke**, **Pauline Spéder**, **Cédric Maurange** et **Jean-René Huynh** pour avoir pris le temps d'examiner mon travail et pour cette inspirante discussion lors de ma soutenance 💡.

Merci à tout le labo, membres présents mais aussi passés, **Renata Basto**, **Simon Gemble**, **Diana Vargas-Hurtado**, **Jean-Philippe Morretton**, **Véronique Marthiens**, **Maddalena Nano**, **Anthony Simon**, **Manon Budzyk**, **Céline Jacquet**, **Oumou Goundiam**, **Sandrine Passemard**, **Frances Edwards**, **Riham Salame**, **Clara Basto**, **Agata Banach-Latapy**, **Marine Saint-Blancat**, **Giulia Fantozzi**, **Carole Pennetier**, **Gisela D'angelo, Carmo C. Soares** pour nos échanges quotidiens, pour la bonne humeur, la chaleureuse atmosphère et la joyeuse ambiance qui résident dans le labo ✨ .

Renata, merci pour ton encadrement et ton soutien, j'ai énormément appris à tes côtés et j'4ai vécu une expérience extraordinaire. Ce fut un travail intense et exigeant, j'ai pu me surpasser et grandir grâce à toi, merci ! 🙏

Simon, **JP** et **Diana**, vous qui êtes devenus mes amis, merci pour votre aide, votre soutien, vos potins, vos rires, tous ces moments à la Montagne… merci pour tout en fait.

Simon, mon binôme et voisin de bureau, je t'ai tellement embêté pour des bêtises mais tu m'as toujours rassurée et aidée, pendant toutes ces années tu as été un soutien au quotidien 😻. Oh et merci aussi pour tes GIFs et « Gentle reminder » 🤪.

JP, tu es vraiment extra pour remonter le moral et détendre les gens avec des rires, des massages et des commérages… surtout des commérages 🙈🙉🐵, notamment avec ton acolyte, **Céline**, merci aussi pour ton aide au quotidien et ta bonne humeur au café des matins 9h ☕ .

My dear Dianita, tu es Tic et je suis Tac (ou l'inverse je ne sais jamais) 🐿️, nous nous comprenons et bien des fois, je n'aurais pas pu avancer sans toi à mes côtés, sans ton sourire et ta positivité, tu es une personne merveilleuse 😍.

Maddalena, merci pour ton aide, tu étais un modèle pour moi quand j'ai rejoint le labo, grâce à toi j'ai appris la rigueur, les « bonnes pratiques du labo » et j'ai repris un projet fantastique qui m'a beaucoup passionné 🤩.

Véro, merci pour ta bienveillance, ton aide mais aussi ta passion et ton formidable savoir scientifique, discuter une heure (ou plutôt des heures 🐵) avec toi c'est comme faire des jours de bibliographie 🤯.

Anthony, merci pour ton aide au quotidien, tu es d'un grand soutien pour le labo, anticipant nos besoins et sachant quoi faire, comment le faire et où sont les choses 🧐 … Je me serais perdue plusieurs fois sans toi aux alentours.

Manon, merci, c'était tellement cool d'avoir enfin quelqu'un qui comprend à quel point la drosophile c'est génial 🪰 et qui a ton optimiste et ta dynamique. (PS : Bon courage pour la BM ! 💪)

Riham, merci pour ton aide sur le projet et surtout ta gentillesse, ta volonté de bien faire, et… ta cuisine ! Tu es une vraie cheffe et c'est un régal pour nos papilles 😋.

Céline, merci à toi aussi pour ton aide au quotidien et nos pauses du matin 9h

Merci aussi à tous mes amis, avec un clin d'œil particulier aux membres du BDE, à **Julie Girard** et **Margaux Fricaud**, les meilleures qui essayaient tant bien que mal de comprendre ce que je faisais 💛 et à **Anne-Lou Terret** qui pour le coup comprenait bien les joies et les … « moins joies » de la thèse 😉. Un merci particulier aussi à **Flavien Brouillet**, mon binôme de soirée 🐓🕺, pour toutes ces nuits à danser pour relâcher la pression et toutes ces heures à discuter de tout et de rien à l'heure du déj ou du café alors qu'on disait « J'ai une expérience, je ne peux pas rester longtemps » Impossible pour nous, beaucoup trop bavards !

Merci à ma famille, **Maman**, **Papa**, **mes frères** et autres **Goupillons**, à **Los Valinos** et la **Big Mif** pour votre soutien et vos encouragements durant toutes ces longues années d'études 💗.

Et enfin, merci à toi mon amour, **Félix Valin**, les mots me manquent pour te dire sincèrement combien tu as été un soutien toutes ces années. Tu as accepté et même parfois accompagné pendant mes longues heures de travail les soirs et les week-ends, tu as supporté ma mauvaise humeur quand j'étais stressée, tu m'as écouté parler de mes recherches parce que je bloquais sur un truc alors que tu ne comprenais pas un mot. Tu as été patient et attentionné, et je te serai toujours reconnaissante pour cela. La consécration de cette thèse, c'est aussi à toi que je la dois, merci ❤️.

Thesis outlines

This manuscript resumes experimental findings carried out during my almost four years of thesis in the laboratory of Renata Basto at the Institut Curie in Paris, France. My work is organised around two independent initial projects: (1) investigation of spindle formation in polyploid cells (*Chapter 2 - Results – Section A*); (2) the establishment of a probe for chromosome loss *in vivo* (*Chapter 2 - Results – Section B*). All results are presented in the form of articles containing independent abstracts, introductions, materials and methods, and discussions.

Chapter 1 - Introduction and *Chapter 3 – Discussion and Perspectives* of the manuscript are built around these sections and try to gather these different concepts with further detail and relate them to the current literature.

The data provided in *Chapter 2 - Results – Section A* originate from a project that aimed to investigate the consequences of polyploidisation on cell division. Polyploidy, defined as the doubling of the whole chromosome set, was shown to correlate with multipolar figures in following mitosis. However, contributors of this multipolarity in a context of excessive DNA and cytoplasmic organelles remained to be investigated. Based on preliminary data from a former PhD student Maddalena Nano, I investigated spindle formation in polyploid cells. I used *in vivo* approaches in *Drosophila* neural stem cells and *in vitro* culture of cancer cells to carry out mitotic processes in cells where polyploidisation was induced through cytokinesis failure. Combining DNA and spindle perturbations with computer modelling in collaboration with Gaëlle Letort, I found that in polyploid cells the presence of excessive DNA acts as a physical barrier blocking spindle pole coalescence and bipolarity. This discovery challenges the current view that suggested extra-centrosomes as only contributor to spindle multipolarity. These findings gave rise to a co-first author publication in the Journal of Cell Biology in spring 2020, entitled *"Chromosomes function as a barrier to mitotic spindle bipolarity in polyploid cells"* (Goupil et al., 2020a).

The data in *Chapter 2 - Results – Section B* originate from the aim of generating a novel tool to quantitively probe chromosome loss *in vivo* in *Drosophila* tissues. Aneuploidy, defined as the gain or loss of whole chromosomes, has been observed in various physiological tissues, however the frequency of this error remained highly debatable. In addition, tools developed so far to assess aneuploidy lack a temporal dimension. To circumvent this, I used the expression of a GFP report gene driven by the GAL4/UAS system and its inhibition by GAL80. In principle, the random loss of the chromosome carrying the *GAL80* sequence leads to GFP appearance in aneuploid cells that can therefore be followed in live tissues. I found that chromosome loss was extremely infrequent in most tissues of the wild type fly.

While developing this tool, I discovered that in the larval brain, green cells where not a by-product of chromosome loss but rather an unexpected mis-regulation in the expression of the *GAL80* gene. I discovered mosaicism and plasticity of the *Drosophila* brain for gene expression which differs from other organs and that is influenced by environmental stimuli. These unexpected results have strong implications for the *Drosophila* community as it can result in false positive in clonal experiments. The paper is available in a preprint version on BioRxiv and is entitled *"Drosophila neural stem cells show a unique dynamic pattern of gene expression that is influenced by environmental factors"* (Goupil et al., 2020b). Of note, similar findings were discovered by the lab of Cayetano Gonzalez at the Institute for research in biomedicine (IRB) in Barcelona, Spain. Currently, we are preparing a new version of the paper which will contain the findings of the two teams and this will be submitted soon.

In addition, new experimental data using this probe to quantitatively assess aneuploidy versus epigenetic regulation in spindle-related mutant flies are produced by Riham Salame under the supervision of Renata Basto and myself. These results will be present in a publication entitled *"Identification of suppressors of a novel form of epigenetic instability in the Drosophila brain*" (Salame R., Goupil A. and Basto R., in preparation).

Table of contents

List of Abbreviations

APC/C	Anaphase promoting complex/cyclosome
CA	Centrosome amplification
CB	Central brain
CIN	Chromosome instability
CDK	Cyclin dependent kinase
CKI	CDK inhibitor
CMP	Chromatin-mediated pathway
CNS	Central nervous system
CPC	Chromosome passenger complex
E(var)	Enhancer of variegation
EM	Electron-microscopy
ESC	Embryonic stem cells
GIN	Genetic instability
GMC	Ganglion mother cell
HP1	Heterochromatin protein 1
ISC	Intestinal stem cell
KT	Kinetochore
MAP	Microtubule-associated protein
MCC	Mitotic checkpoint complex
MK	Megakaryocytes
MT	Microtubule
MTOC	Microtubule organizing center
MVA	Mosaic variegated aneuploidy
NB	Neuroblast
NEBD	Nuclear envelope breakdown
NSC	Neural stem cell
OE	Overexpression
OL	Optic lobe
PcG	Polycomb group

PCM	Pericentriolar material
PEV	Position effect variegation
Pre-RC	Pre-replication complex
RNAi	RNA interference
SAC	Spindle assembly checkpoint
SAF	Spindle assembly factor
SPG	Sub-perineurial glia
Su(var)	Suppressor of variegation
TF	Transcription factor
TGC	Trophoblast giant cells
TrxG	Thritorax group
VNC	Ventral nerve cord
WGD	Whole genome duplication
WGS	Whole genome sequencing
WT	Wild type
γ-tuRC	γ-tubulin ring complex

Chapter 1 - Introduction

1. The cell cycle

1.1. Cell cycle phases and control

All multicellular organisms originate from one unique cell, the zygote. Over the course of development, successive divisions generate a high number of cells that will populate the organs and acquire different morphologies and functions. In most cases, eukaryote somatic cells contain the same diploid genetic content, meaning that they contain two copies of each chromosome. To ensure genome stability and tissue homeostasis, cell proliferation is controlled over the cell cycle where a mother cell fully duplicates its genetic material before its equal re-distribution between the two daughter cells during mitosis.

Cell cycle phases. The concept of cell cycle was born from the work performed by Howard and Pelc in 1953, where using radioactive DNA incorporation in plant they described the existence of a timeframe in cellular life (Howard and Pelc, 1953). The canonical cell cycle is composed of two main phases, the long interphase and the short mitosis. Interphase is temporally organized in a step-wise series of different phases of growth (gap phases G1 and G2) and DNA synthesis (S-phase) (reviewed in (Norbury and Nurse, 1992))(**Figure 1**). In more detail, the G1 phase has a metabolic role with the synthesis of nutrients, RNA and proteins and prepares DNA for replication (Tobey et al., 1973). G1 is also the phase when cells chose to proliferate or to exit the cell cycle and to enter the G0 phase to remain quiescent until their reactivation, or to terminally differentiate into specialized cells and ensure specific functions. Indeed, G0 is a resting phase for non-growing and non-proliferating cells. If cells decide to continue to cycle, they enter S-phase and initiate DNA replication. During this phase, the DNA-double helix opens and unwinds and the replication machinery starts to synthetize DNA in order to obtain an identical copy forming two sister-chromatids for all chromosomes. The G2 phase is also a growth phase with increased cell mass and organelle number to prepare cells for chromosome segregation in mitosis (M-phase).

Regulation of the cell cycle progression. The transitions from one phase to the following one are regulated by protein complexes including cyclins and cyclin-dependent kinases (CDKs). CDKs are serine/threonine protein kinases which phosphorylate key substrates that control essential functions of each phase such as DNA synthesis or mitotic entry (reviewed in (Morgan,

1995; Pines, 1995; Vermeulen et al., 2003)). The level of CDKs in their inactivated form are constant over the cell cycle but the oscillation of the levels of cyclins and their location (Peng et al., 1997) activates specific CDK at specific time and place. Thus, several cyclins and CDKs sequentially form complexes to drive cell cycle progression (Evans et al., 1983; Pines and Hunter, 1991; Morgan, 1995; Hochegger et al., 2008). Briefly, the G1 phase starts by the formation of complexes of cyclin D with CDK4 and CDK6 (Sherr, 1994). Cyclin E/CDK2 and cyclin A/CDK2 complexes permit S-phase entry and progression, respectively (Walker and Maller, 1991; Girard et al., 1991; Ohtsubo et al., 1995). Mitotic entry in turn is allowed by the cyclin B /CDK1 complex (King et al., 1994) (**Figure 1**).

Quality control of cell cycle phases. All phases of the cell cycle have crucial roles and their quality control involves specific checkpoints (reviewed in (Hartwell and Weinert, 1989; Barnum and O'Connell, 2014)) (**Figure 1**). In G1, specific checkpoints and the restriction point R which is a point of no return, control sufficient cell growth and the absence of DNA damage before commitment to S-phase (Vaziri et al., 2003; Foster et al., 2010). After this, the cell is engaged to enter the cell cycle and starts DNA synthesis in S-phase. Prior mitosis in G2, another checkpoint controls for sufficient growth and the correct replication of DNA (reviewed in (Cuddihy and O'Connell, 2003). The control of growth in G1 and G2 ensures nutrient distribution in daughter cells. Interestingly, the first observations that allow this type of conclusions or hypothesis came from a study showing that the size of newly born daughter cells affect the speed of the next cell cycle. In that sense, larger cells progress faster through G1 and G2 phases than smaller cells (Killander and Zetterberg, 1965; Cross, 1988). In addition, in presence of DNA damage, the activation of the sensor checkpoint protein 1 (Chk1) (Latif et al., 2004) and the tumor suppressor p53 (Giono and Manfredi, 2006) induces cell cycle arrest to allow DNA repair prior DNA replication (G1/S transition) or prior mitosis (G2/M transition). In extreme cases, p53 can trigger terminal responses as senescence or cell death through apoptosis (Purvis et al., 2012; Carvajal and Manfredi, 2013). Finally, in mitosis the spindle assembly checkpoint (SAC) ensures the correct attachment of chromosomes to the mitotic spindle, ensuring their faithful segregation in anaphase (further details in section 1.2.5. Spindle assembly checkpoint and mitotic defects and reviewed in (Musacchio and Salmon, 2007)).

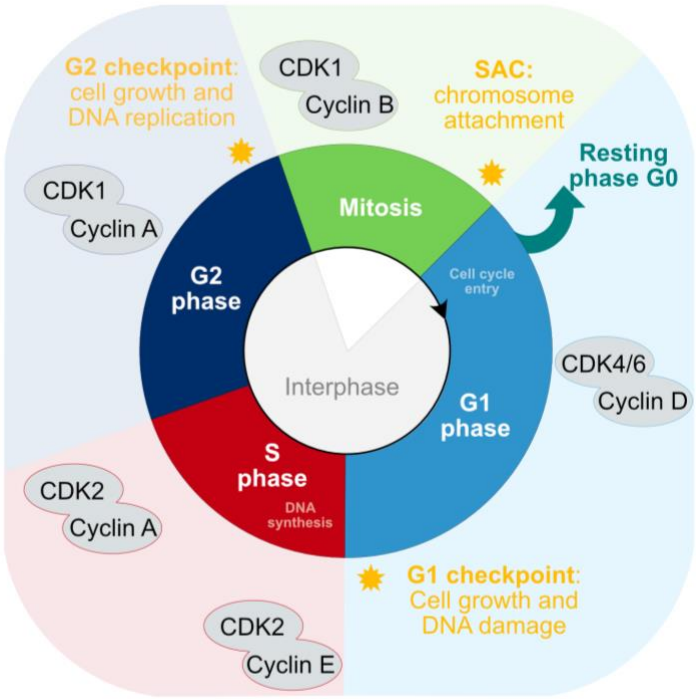

Figure 1. Cell cycle phases and regulators. Schematic representation of the successive phases of the cell cycle and regulators of cell cycle phase transition and quality control. Interphase is composed of growth gap phases (G1- and G2-phase), separated by a phase of DNA synthesis (S-phase). During mitosis, replicated DNA is segregated into two daughter cells (M-phase). Transitions from one phase to another are regulated by specific Cyclin/CDK complexes schematized in grey ovals and checkpoints, shown in orange, control the quality of key events in each phase.

1.2. Mitosis in more detail

The process of cell division, namely mitosis has been extensively study for more than a century. Originally, the word “mitosis” which comes from the Greek word of “thread”, was chosen by Flemming in 1882 (Flemming, 1882). Indeed, in his study, he precisely described the splitting of the nuclei and the migration of “threads” to opposite poles, namely condensed chromosomes segregating between the two daughter cells. The establishment of the mitotic spindle serves as a scaffold that generate forces required for chromosome separation. The critical steps of mitosis and the different components of the spindle apparatus are described in more detail in the following sections.

1.2.1. Mitotic phases

Mitosis is subdivided into sequential phases which all imply important and specific function and organisation (**Figure 2**). During prophase, DNA condenses and individualises into visible mitotic chromosomes (Flemming, 1882; Sedat and Manuelidis, 1978). Meanwhile in the cytoplasm, two organelles, the centrosomes start to nucleate microtubules (MTs) and form larger asters (Zhai et al., 1996). In some cell types, it is at this step that the two centrosomes separate to locate at both sides of the nucleus (Magidson et al., 2011). In other cells, centrosome separate after nuclear envelope breakdown (NEDB) (Toso et al., 2009). NEDB marks the entry in prometaphase and the centrosomes enhance MT-nucleation and form the two poles of a bipolar mitotic spindle (Peter et al., 1990; Zhai et al., 1996). In parallel, mitotic chromosomes are captured by MTs and move to align to the spindle equator in a process known as chromosome congression (Darlington, 1937). The correct alignment of all chromosomes on the so-called metaphase plate corresponds to the metaphase. Shortly after, anaphase begins, the cohesion between sister chromatids is broken, chromosomes move poleward and spindle poles separate (Saunders, 1993). In telophase, the cell physically divides its cytoplasm by cytokinesis (more detail in following paragraph) while nuclear envelope reforms around decondensing chromosomes, generating two newly born cells (**Figure 2**). In principle, upon normal cell division, the two daughter cells are genetically identical as they inherited the same genome content. However, they can vary in fate depending of the mode of division. If the division is symmetric, the two cells are similar. In contrast, upon asymmetric division, daughter cells are asymmetric in fate through the inheritance of differential fate determinants and in some cases, as in *Drosophila* neuroblasts (NBs), they are also asymmetric in size (Horvitz and Herskowitz, 1992; Rhyu et al., 1994; Yu et al., 2006).

Cytokinesis. This last step of cell division is crucial for the physical separation of the daughter cells. It is characterized by the assembly of a central spindle - anti-parallel MTs establishing at anaphase – and furrow ingression at the site of abscission. This site is specified in late metaphase by the localization of the chromosome passenger complex (CPC). There, one component of the CPC, Aurora B phosphorylates proteins of the motor complex centralspindlin : the MT-plus end kinesin Pavarotti (Pav) and Tumbleweed (MKLP1 and RACGAP in humans, respectively)(Adams et al., 1998; Giet and Glover, 2001; Eggert et al.,

2004; Goldstein et al., 2005; Guse et al., 2005; Neef et al., 2006). Then, at the spindle midzone, the centralspindlin mediates the activation of the small GTPase Rho1 (RHOA in humans) (Hime and Saint, 1992; Somma et al., 2002). Rho1 with its effector proteins formins and profilins favor the formation of actin filaments to establish the actin contractile ring. Its contractility is mediated by (1) the motor activity of the nonmuscle Myosin II, (2) the presence of scaffold proteins such as Anillin (Field et al., 2005; Piekny and Glotzer, 2008; Frenette et al., 2012; Kim et al., 2017) and (3) the tethering of mechanical-force generators at the membrane (reviewed in (Cabernard, 2012)).

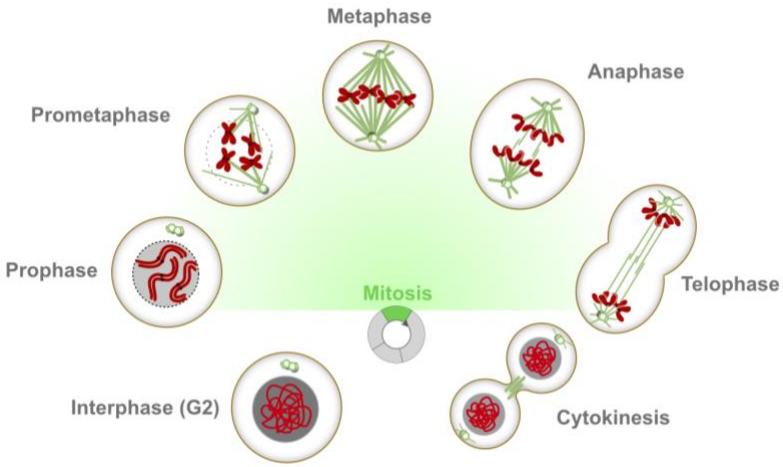

Figure 2. Mitotic phases. Schematic representation of the mitotic cell cycle. Mitosis starts in prophase with the condensation and individualization of chromosomes (in red). At NEBD in prometaphase, the two centrosomes nucleate MTs (in green) and form the two poles of a bipolar mitotic spindle. When all chromosomes are aligned at the cell equator in metaphase, sister-chromatids are segregated in anaphase. After telophase, cell division ends with the physical separation in two cells by cytokinesis.

1.2.2. Spindle apparatus

The spindle apparatus is the coupling of dynamic components that collectively organize in a harmonious manner to ensure efficient mitosis. The canonical spindle in most vertebrate cells involves individualized chromosomes, a MT-based skeleton and centrosome organelles (**Figure 3**), all orchestrated by MT-associated proteins (MAPs) and molecular motors.

CHROMOSOMES

Mitotic chromosome structure. The original description of mitotic "threads" presenting a site of constriction was made by Flemming using light-microscopy (Flemming, 1880, 1882), but the term "chromosoma" was given several years later by Waldeyer (Waldeyer, 1888). It turns out that after complete replication in the previous S-phase, mitotic chromosomes consist of a pair of sister-chromatids hold together by the centromere, which gives rise to this fascinating X-shape topology (reviewed in (Walczak et al., 2010; Batty and Gerlich, 2019). Centromeres are made of repetitive DNA (Brown et al., 1994; Farr et al., 1995) where centromeric proteins localize (Earnshaw and Rothfield, 1985) and recruit the large multiprotein complex kinetochore (KT), point of connection with the mitotic spindle (reviewed in (Cleveland et al., 2003; Hori and Fukagawa, 2012)). In most animal cells, monocentric chromosomes contain one unique centromere sequence and thus, have a single KT. In contrast, holocentric species, such as all nematodes or diverse plants and insects, present several MT-binding sites called "diffusive" KTs distributed along their chromosome surface (Pimpinelli and Goday, 1989; Maddox et al., 2004).

Mitotic chromosome formation. The genomic DNA contained in a nucleus is a very long structure that goes up to approximately 2 meters in diploid human cells (Ross, 1999). To limit its length, it organizes into nucleosomes (Olins and Olins, 1974) which are structural units composed of DNA wound on histone proteins (Kornberg, 1974). Over the cell cycle, the chromatin subdivided into several chromosomes face vast changes in their 3D organization. In interphase, the chromatin is compacted but decondensed into a mesh of chromosomes intertwined with each other and enclosed inside the nucleus, where it ensures gene expression for cell function. At mitotic entry, in early prophase, chromatin starts condensing and organizes into consecutive loops. Each chromosome individualizes into compacted cylindrical chromosomal bodies. This individualization is essential for the cleavage plane to be free of chromosomes to ensure proper cytokinesis (Steigemann et al., 2009). Electron-microscopy (EM) observations of mitotic chromosomes depleted for histones, supported a model in which non-histone scaffold proteins were responsible for the loop structure of chromatin (Paulson and Laemmli, 1977; Marsden and Laemmli, 1979; Earnshaw and Laemmli, 1983). Non-histone proteins such as topoisomerase II are recruited by the scaffold protein condensin which is a ring-shaped complex (Earnshaw and Laemmli, 1983; Earnshaw et al.,

1985; Hirano and Mitchison, 1991, 1994; Hirano et al., 1997). Depletion of condensin subunits in C. *elegans* (Hagstrom et al., 2002) and chicken DT40 cells (Hudson et al., 2003) leads to aberrant localization of non-histone proteins which compromises the overall chromosome scaffold and structural integrity but does not abolish chromosome condensation *per se*. More recent *in vitro* studies proposed alternative routes for mitotic chromosome formation: (1) a chromatin-inherent driving force of condensation induced by histone modifications in yeast (Wilkins et al., 2014) and vertebrate cells (Zhiteneva et al., 2017) and (2) the increase Mg^{2+} ion concentration promoting chromatin condensation by charge neutralization (Maeshima et al., 2018).

TUBULIN AND MICROTUBULES

Observations of living cells by Inoué in 1953 confirmed the existence of "spindle fibrils" that drive chromosome segregation (Inoué, 1953). Their architecture was characterised few years later with the emergence of EM and improved fixation protocols to preserve their structure. Several groups described the same tubular structure because of their "less dense core" (Roth et al., 1960; Harris, 1961; Roth and Daniels, 1962). Finally, in 1963, Slautterback, Ledbetter and Porter based on studies performed in Hydra and plant cells, respectively, named them "microtubules" and brought to light their ubiquity nature. Further they also propose that MTs play important and essential functions for diverse cellular processes such as protein transport, cell signalling or to maintain cell shape (Slautterback, 1963; Ledbetter and Porter, 1963).

Using the affinity of MTs for colchicine, a drug that blocks mitotic cells in metaphase by inhibiting MT-nucleation (Weisenberg et al., 1968), Borisy and colleagues identified the subunit components of MTs, named "tubulin" later by Mohri (Borisy and Taylor, 1967; Mohri, 1968). MTs are assemblies of α- and β-tubulin heterodimers (Feit et al., 1971; Bryan and Wilson, 1971; Luduena and Woodward, 1973) that polymerize (Nogales et al., 1999) to arrange into several proto-filaments, typically thirteen in most animal and plant cells (Tilney et al., 1973; Desai and Mitchison, 1997). They have the property to rapidly switch between phases of growth and shrinkage. This process that alternates events of MT rescue and catastrophe is called dynamic instability (Mitchison and Kirschner, 1984) (**Figure 3A**). Importantly, MTs are polarized with the plus-end being the dominant site for tubulin incorporation or disassembly and depending on the polarity of MT fibers, their interaction

within the mitotic spindle can be parallel or anti-parallel (Nogales et al., 1999). MTs can emanate from pre-existing MTs and form clusters of branched-MTs as it was shown using depolymerization/repolymerization *in vitro* assays (O. Wasteneys and E. Williamson, 1989) and confirmed in higher plants (Murata et al., 2005) and in mammalian cells (Reilein et al., 2005).

Additionally to the intrinsic dynamicity of MTs, MAPs and motors impact and enhance MT properties (reviewed in (Desai and Mitchison, 1997; Wittmann et al., 2001; Bodakuntla et al., 2019)). To give a few examples, the kinesin-related protein MCAK (Mitotic Centromere Associated Kinesin) and Katanin are involved in MT depolymerization and severing, respectively (Wordeman and Mitchison, 1995; McNally et al., 1996; Hunter et al., 2003; Díaz-Valencia et al., 2011). Mei38 (TPX2) or Mars (HURP) and CAMSAP (a minus-end stabilizer cap) favor MT nucleation and stability (Oakley, 1992; Brunet et al., 2004; Santarella et al., 2007; Yang and Fan, 2008; Jiang et al., 2014; Akhmanova and Hoogenraad, 2015). Minus-end directed motors such as Ncd (HSET) or dynein and kinesin-5 motors generate forces that allow the focusing of poles and the sliding of overlapping anti-parallel MTs (Endow et al., 1994; Cole et al., 1994; Heald et al., 1996; Burbank et al., 2007). All these proteins in concert with the different components of the mitotic spindle tailor spindle architecture (reviewed in (Helmke et al., 2013)).

Three subclasses of MT organization design the mitotic spindle (reviewed in (Meunier and Vernos, 2012)) (**Figure 3B**). (1) MTs emanating from the centrosomes- the astral MTs- extend towards the cell cortex. In contrast to the two other MT subclasses, astral MTs are not essential for chromosome segregation (Khodjakov et al., 2000). In combination with specific molecular motors, they are involved in centrosome separation in prophase and ensure correct spindle positioning and orientation (Gönczy et al., 1999; Giansanti et al., 2001; Morin and Bellaïche, 2011). (2) The most abundant and dynamic class of MTs are interpolar MTs, which form the inner mass of the mitotic spindle between the two poles. Close to the poles, they arranged into a parallel manner toward the center, while near the chromosome region their interaction is anti-parallel and overlapping (Mastronarde et al., 1993). At anaphase, their organization into anti-parallel bundles between separating chromosomes constitutes the major component of the central spindle, which is essential for cytokinesis (Glotzer, 2009). (3) At last, the most robust because cold-stable (Rieder, 1981) are KT-fibers. In most vertebrate cells, they form bundles of 20-40 parallel MTs that attach chromosome KTs to spindle poles

and ensure sister chromatid segregation (Rieder, 1981; McEwen et al., 1997; Rieder, 2005; Walczak et al., 2010). EM revealed that KT-fibers can extend from KTs to spindle poles in a continuous manner (**Figure 3C**), in a variety of cell types and organisms (Rieder, 1981; Witt et al., 1981; Church and Lin, 1982; Nicklas et al., 1982; McDonald et al., 1992). However, this direct connection is not necessary for chromosome segregation (Sikirzhytski et al., 2014) and it was shown using correlative light-EM that for most human chromosomes, those were discontinuous with short KT-fibers interacting with interpolar MTs or with KT-fibers of adjacent chromosomes (Sikirzhytski et al., 2018) (**Figure 3C**). In contrast, the worm *C. elegans* has holocentric KTs. Thus, KT-MTs are not bundles but rather a few MTs that anchor chromosomes over their entire length to the whole spindle network (Redemann et al., 2017). In *Drosophila*, in addition to KT-MTs connecting monocentric KTs to poles, a fourth set of MTs connect spindle poles to chromosome arms (reviewed in (Brust-Mascher and Scholey, 2007)).

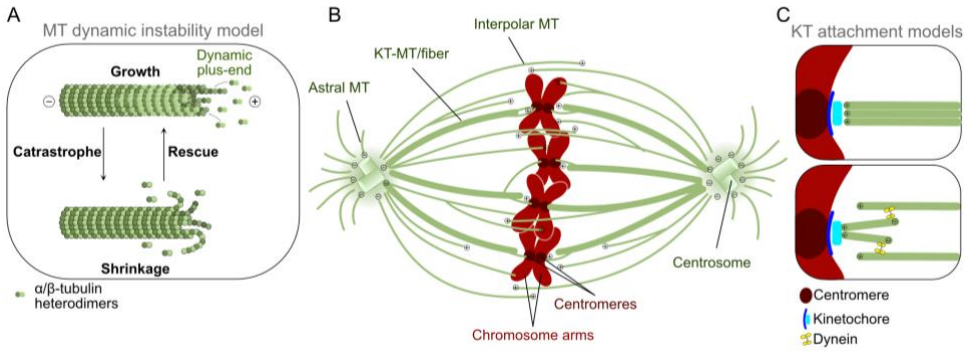

Figure 3. MT population in the mitotic spindle and properties. Schematic representations of (A) the dynamic instability model of MTs, (B) the canonical mitotic spindle in animal cells and (C) the different models for KT attachment. (A) MTs are assemblies of α- and β-tubulin heterodimers (in dark and light green, respectively). At the dynamic plus-end, MTs growth or shrink due to event of catastrophe or rescue, respectively. (B) The mitotic spindle is composed of centrosomes at poles, MTs (in green) and chromosomes (in red). Different MT classes populate the spindle: (1) astral MTs emanate from centrosomes and extend towards the cell cortex; (2) interpolar MTs overlap and constitute the inner mass of the spindle and (3) KT-MTs or fibers connect chromosome KTs to spindle poles. (C) KTs are connected to the poles in a continuous manner (upper panel) or indirectly by cross-linking with other MTs in a dynein-dependent manner (lower panel).

CENTROSOMES

Centrosome structure. Revealed by EM, centrosomes are composed of a pair of centrioles orthogonally oriented and surrounded by an electron dense pericentriolar material (PCM) (Anderson 1992). The PCM is a complex but highly organized matrix of more than 100 proteins responsible for MT-nucleation (Zheng et al., 1995; Moritz et al., 1995; Andersen et al., 2003; Mennella et al., 2012; Sonnen et al., 2012; Bauer et al., 2016). Centrioles are ninefold symmetrical MT-based organelles and their structure varies between organisms and cell types. For example, in somatic *Drosophila* cells, centrioles are composed of one central hub plus nine-radially arranged spokes forming the cartwheel and nine-fold symmetric MT-doublets (Callaini et al., 1997; Debec et al., 1999), while spermatocytes present MTs-triplets (**Figure 4A**). In vertebrates, centrioles are also composed of MTs-triplets and additional MT walls called distal or subdistal appendages serve for cortex anchoring of the mother centriole (Tanos et al., 2013). Indeed, the two centrioles always differ in age, structure and potential and are referred as "mother" and "daughter" centrioles (Vorobjev and Chentsov, 1982; Graser et al., 2007; Anderson and Stearns, 2009).

Centrosome functions. Discovered by Boveri, van Benenden and others in the 19th century, this cytoplasmic non-membrane bound organelle is considered as the major MT organizing center (MTOC) in animal cells (Boveri, 1887; Bornens, 2002; Scheer, 2014; Fu et al., 2015). Centrosomes, as central organizer of cellular events, have many functions that depend on cell cycle phase and cell types. To give a few examples, in interphase, the single centrosome can serve as a seed for cilia or flagella genesis, it confers cell shape, polarity or contribute to cell movement and intercellular organization (reviewed in (Doxsey et al., 2005)). Upon cell division, the two centrosomes constitute the two poles of the mitotic spindle. Thus, the exact number of centrosomes per cell is crucial and highly controlled to ensure all these functions.

Centrosome duplication cycle. The centrosome duplication cycle is in concert with the cell cycle (Delattre et al., 2006; Fu et al., 2015) (**Figure 4B**). In outline, the duplication cycle starts in G1 with the disengagement of the two centrioles which in turn leads to the loss of their orthogonality and spacing (Tsou et al., 2009). At that stage, both centrioles become mother centrioles and seed for the future new daughter centrioles. In S-phase, procentrioles assemble perpendicular to mother centrioles, on cartwheels. The elongation of the centriolar MTs

continues until G2. It results in the formation of two centrosomes, attached to each other by the tether and composed of two centrioles. At mitotic entry, the two centrosomes start maturating, separate and the PCM drastically expands which has the consequence of extensive MT-nucleation capacity and dynamics (**Figure 4C**). Mature centrosomes form the two poles of the bipolar mitotic spindle. All these events are tightly regulated and coordinated at the molecular level to ensure the formation of two centrosomes with two centrioles (**Figure 4B**) (Consequences of variations in centrosome copy number are described in the section 1.3. Centrosome number alterations and consequences). For simplicity, I will give the molecular detail for centrosome duplication and maturation in *Drosophila* neuroblasts (NBs) which is the main experimental model of my thesis project.

In *Drosophila* NBs, and in contrast to human cells, the two centrioles disengage in late telophase which initiates procentriole formation and migrate far apart to duplicate centrioles independently (Rusan and Peifer, 2007; Rebollo et al., 2007). One critical step for centriole duplication is the incorporation of Sas-4 (spindle assembly abnormal 4; CPAP in humans) in the newly formed centrioles, and its phosphorylation by the cell cycle regulator Cdk1. This enables the recruitment of key proteins, Polo kinase (Polo like kinase 1 or PLK1 in humans) and Asl (Asterless; CEP152) which stands the kinase activity of Sak (PLK4) (Dzhindzhev et al., 2010; Novak et al., 2014). Sak is considered as the master regulator of centriole duplication and deregulation of its level (loss or overexpression) leads to centrosome copy number variation (loss or amplification)(Bettencourt-Dias et al., 2005; Habedanck et al., 2005). Indeed, Sak is required for the recruitment and phosphorylation of the core centriole component Ana2 that in turn recruits the essential cartwheel component Sas-6. This step is essential for centriole biogenesis as the cartwheel serves as a seed for procentriole formation (Dzhindzhev et al., 2010, 2014). In G2, centrioles elongate by the incorporation of MTs on the cartwheel through Sas-4 recruitment. Newly formed daughter centrioles acquire MT-nucleation capacity after the so called “centriole to centrosome conversion” which was shown to involve the key proteins CEP135-Ana1-Asl (Fu et al., 2016).

In mitosis, the two new centrosomes enter in a maturation process, which consists of PCM recruitment and consequent MT-nucleation. Polo and Asl initiates this maturation by the recruitment of Spd2 (spindle defective 2; CEP192) and Cnn (centrosomin; CDK5RAP2/CEP215) (Sunkel and Glover, 1988; Dix and Raff, 2007; Varmark et al., 2007; Dobbelaere et al., 2008;

Giansanti et al., 2008; Conduit et al., 2014b; a). Both PCM proteins bear the sequential and self-assembling PCM matrix organized into layers of key proteins. The most inward protein is Bld10. The second layer is made of Sas-4, Polo and Spd2. Then, Plp (pericentrin like protein), Asl, Sak, Cnn and γ-tubulin constitute another layer. And at last, Spd2, Polo, Cnn and γ-tubulin compose the most outward layer from where MTs grow (Terada et al., 2003; Fu and Glover, 2012; Lawo et al., 2012; Mennella et al., 2012; Sonnen et al., 2012). With maturation, centrosomes form large mitotic asters of MTs which will compose the two poles of the mitotic spindle (Khodjakov and Rieder, 1999; Terada et al., 2003; Conduit et al., 2014b). At mitotic exit, each daughter cell retains one of the two centrosomes (**Figure 4B**). Interestingly, photo-convertible tracing of centrosomes during asymmetric division of *Drosophila* NBs, highlighted an asymmetry in centrosome inheritance in daughter cells with the daughter centrosome remaining in the NBs and the mother centrosome inherited by the more committed ganglion mother cell (GMC)(Januschke et al., 2011).

All these components, centrosomes, MTs and chromosomes tune together and form a tightly regulated equilibrium. Indeed, modification in one of these components can affect the others. For example, disruption of CENP-A, a centromeric protein essential for KT establishment perturbs MT-KT interaction and the overall MT dynamics. This, in turn, compromises spindle pole integrity observed by PCM dispersion due to mis-localization of MT minus-end at poles (Gemble et al., 2019).

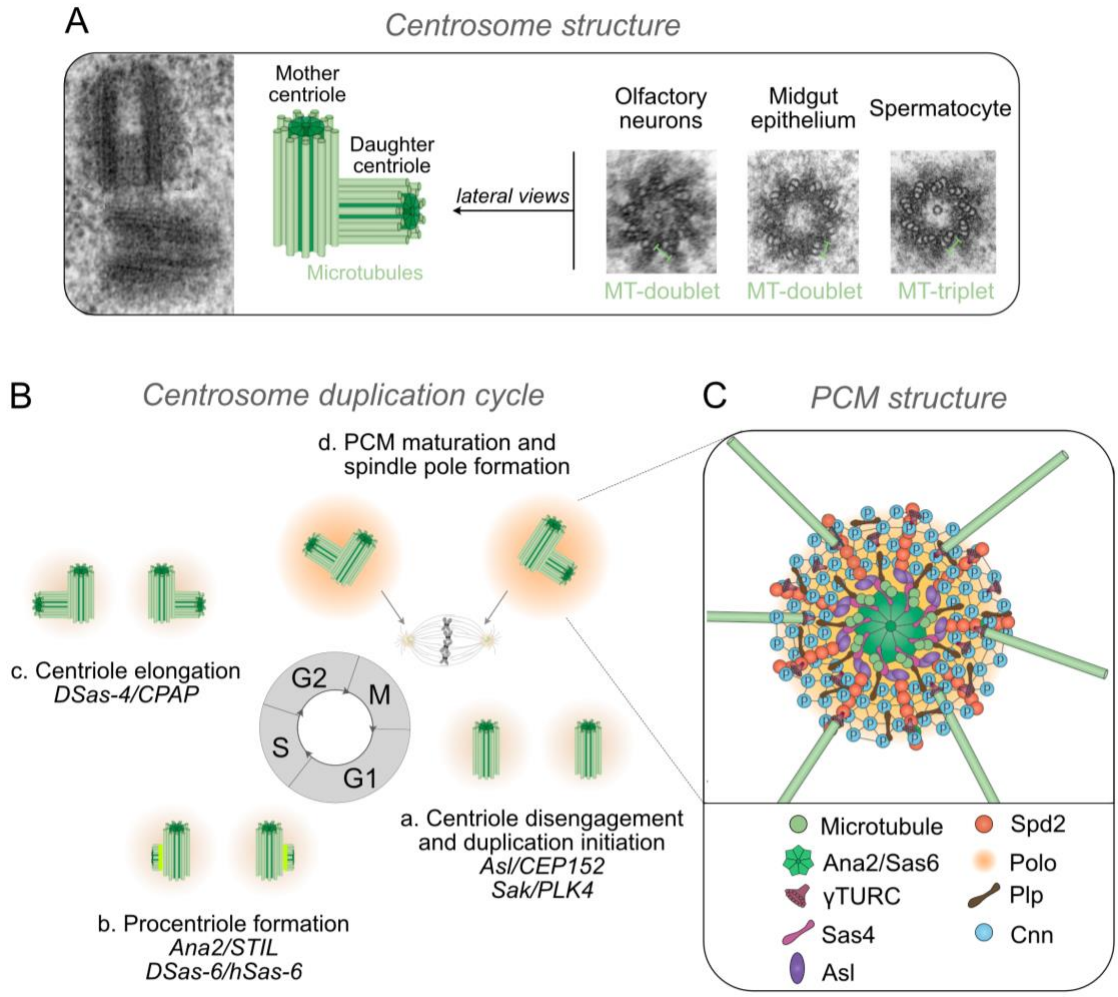

Figure 4. Centrosome structure and duplication cycle. (A) EM images (adapted from (Gottardo et al., 2015)) and schematic representation of *Drosophila* centrosomes. Mother and daughter centrioles are composed of nine MT-doublets in most somatic cells and nine MT-triplets in germ cells. (B) Schematic representation of key events and players (*Drosophila*/ human homologues in italic) in the centrosome duplication cycle. Centriole duplication occurs in concert with the cell cycle and starts with centriole disengagement at the end of M- or beginning G1-phase depending on cell type (a.). In S-phase, procentrioles assemble perpendicular to the two mother centrioles (b.) and elongate until G2 (c.). While in human cells, centrosomes separate at mitotic entry, in *Drosophila* NBs the two centrosomes migrate apart from each other right after disengagement. At mitosis, PCM expends and the two mature centrosomes form the two poles of a bipolar spindle (d.). (C) Schematic representation of the PCM layers of the mature centrosome in mitotic *Drosophila* NBs. (Schemes adapted from (Conduit et al., 2015)).

1.2.3. Several pathways for MT-nucleation and chromosome capture

The establishment of a robust bipolar spindle is driven by the coordination of three different MT-nucleation pathways. MTs can nucleate from all components describe above: centrosomes, chromosomes and pre-existing MTs (Hayward et al., 2014).

FROM CENTROSOMES – THE CENTROSOME PATHWAY

While centrosomes are not essential for cell division, they highly contribute to spindle formation, shape and robustness. After its discovery in *Aspergillus nidulans* (Oakley and Oakley, 1989; Oakley et al., 1990), the major nucleator protein γ-tubulin (γ-tub) was shown to be ubiquitous in eukaryotes (Oakley, 1992). Indeed, immunofluorescence analysis in *Drosophila*, *Xenopus* and mammalian cells revealed that γ-tub is located at centrosomes (Zheng et al., 1991; Joshi et al., 1992), more precisely associates with PCM (Stearns et al., 1991). Immuno-EM tomography of purified *Drosophila* centrosomes which lack MTs, revealed a dense array of γ-tub positive structures arranged into a ring-shaped template for MT-nucleation, therefore named the γ-tub ring complex (γ-tuRC) (Moritz et al., 1995) (**Figure 5A**). In biochemical studies, γ-tuRC purified from *Xenopus* is sufficient for MT-nucleation at the similar speed of purified *Drosophila* centrosomes (Zheng et al., 1995).

The depletion of γ-tub *in vivo* strongly compromised MTOC kinetics and structure, but does not abolish MT-nucleation from the PCM in different systems (Sunkel et al., 1995; Sampaio et al., 2001; Strome et al., 2001; Hannak et al., 2002). Thus, an additional model for MT-nucleation boost in mitosis emerged. Recent studies using biochemical reconstitution (Hernández-Vega et al., 2017; Woodruff et al., 2017) and *in vivo* analysis (Baumgart et al., 2019) propose that the PCM as behaving as phase-separated macromolecules concentrates soluble tubulin at centrosome site driving MT-nucleation (reviewed in (Woodruff, 2018)).

FROM CHROMOSOMES – THE CHROMATIN-MEDIATED PATHWAY (CMP)

An alternative pathway to centrosomes is the nucleation of MTs from the chromatin, either from KTs to form KT-fibers, or directly from the DNA itself. Injection of purified centrosomes and DNA into frog's eggs arrested in metaphase provide the first evidence of the differential contribution of centrosome and DNA for spindle assembly (Karsenti et al., 1984). It appeared later that cells can have an intrinsic property of bipolar spindle assembly around the

chromatin. This MT-nucleation at the vicinity of chromosomes was first demonstrated in *Xenopus* egg extract experiments where mitotic spindles could assemble around DNA-coated beads in absence of centrosomes and KTs (Heald et al., 1996). This model gained support at the end of the 90's/early 2000 through the observation of successful mitotic spindle assembly and bipolarization in acentrosomal cells such as oocytes (Matthies et al., 1996; Bennabi et al., 2016), and in cells where centrosomes were genetically (Basto et al., 2006) or chemically (Wong et al., 2015) removed or laser-ablated (Khodjakov et al., 2000). Further studies showed that the chromatin can directly impact spindle morphology and morphometrics (Dinarina et al., 2009) with the help of motor proteins (Gaetz and Kapoor, 2004). However, this pathway is not exclusive of cells lacking centrosomes. For example, in *Drosophila* embryos, MTs can be detected repolymerizing from both centrosomes and mitotic chromosomes after a cold-treatment (Hayward et al., 2014).

The first evidence for MT-nucleation from KTs came from studies that analyzed MT-nucleation capacity of isolated chromosomes (Telzer et al., 1975; Bergen et al., 1980; Mitchison and Kirschner, 1985a). This was in light of what was shown *in vitro* and *in vivo* in cells recovering from MT-poison treatments (Telzer et al., 1975; Witt et al., 1980; De Brabander et al., 1981; Mitchison and Kirschner, 1985a; Torosantucci et al., 2008) and strengthen by a more recent study in budding yeast (Kitamura et al., 2010). However, it remains debatable whether KTs have direct MT-nucleation capacity and if true, this was proposed to be a rare event or cell-type dependent (Khodjakov et al., 2003; Maiato et al., 2004b). Already in 1985, Mitchison and Kirschner challenged this view by proposing an alternative model where pre-formed MTs could be captured by KTs rather than directly nucleating from (Mitchison and Kirschner, 1985b). Recent studies in human cells confirm these data and show that small MTs accumulate near most KTs (75%) (Sikirzhytski et al., 2014, 2018). This pre-formed fibers are then captured by KTs and connected to centrosomes by branched and load-bearing MT (Khodjakov et al., 2003; Maiato et al., 2004; Sikirzhytski et al., 2014, 2018). Dynein is known to generate forces at pre-formed KTs for their poleward movement or their dynamic interaction with adjacent KTs and other MTs within the spindle (Rusan et al., 2002; Sikirzhytski et al., 2014) (**Figure 3C**).

The contribution of chromosome arms- and KT-dependent MT-nucleation to the assembly of the mitotic spindle is distinguishable (O'Connell et al., 2009). However, both share similarities in the molecular mechanism behind MT-nucleation. A first body of literature

suggests that this involves the Ras-related nuclear (Ran) pathway (Ran pathway in *Drosophila* reviewed in (Chen et al., 2015)). Briefly, Ran, a nuclear transport protein can switch from an inactive Ran-GDP to an active Ran-GTP. This conversion is mediated by the regulator of chromosome condensation 1 (RCC1) which is a GTP exchange factor (Ohtsubo et al., 1989; Kalab et al., 1999). RCC1 is coated on chromatin mass and at NEBD, a gradient of active Ran-GTP establishes, which has been observed using fluorescence resonance energy transfer (FRET) technics in *Xenopus* egg extracts (Kalab et al., 2002) and human cells (Kaláb et al., 2006). This gradient, also observed *in vivo* in *Drosophila* embryos, allows the release of importin-sequestered spindle assembly factors (SAFs) at the vicinity of chromosomes (Gruss et al., 2001; Nachury et al., 2001; Wiese et al., 2001; Trieselmann and Wilde, 2002) (**Figure 5B**– upper panel). The first to be identified was the MAP TPX2 (Mei-38 in *Drosophila*) which favors MT assembly around the chromatin (Wittmann et al., 2000; Gruss et al., 2001, 2002; Tulu et al., 2006; Li and Goshima, 2011; Hayward and Wakefield, 2014). Others SAFs where subsequently discovered and all have functions in MT stability and organization (reviewed in (Meunier and Vernos, 2012)). A particular important is Mars (HURP in mammals, (Koffa et al., 2006)) which is required for KT-MTs assembly in *Drosophila* S2 cells (Yang and Fan, 2008) and *Drosophila* embryos (Hayward and Wakefield, 2014). The requirement of Ran gradient for chromatin-dependent MT-nucleation in living centrosome-containing cells was further confirmed in many siRNA and microinjections experiments in *C. elegans* (Bamba et al., 2002; Askjaer et al., 2002), *Drosophila* (Silverman-Gavrila and Wilde, 2006) and mammalian systems (Nachury et al., 2001; Tulu et al., 2006; Kaláb et al., 2006). In contrast, in acentrosomal mouse and *Drosophila* oocytes, Ran in not required as meiotic spindles properly assemble when it is depleted (Dumont et al., 2007; Cesario and McKim, 2011) suggesting that a redundant pathway compensates for Ran loss. Further, in the absence of Ran-GTP gradient in sperm cells, the chromatin is still capable to nucleate and stabilize MTs via CPC activity (Maresca et al., 2009). The molecular pathway of the CPC, described by the Funabiki lab and others, involves the kinase subunit of the CPC, Aurora B which inactivates by phosphorylation MT-destabilizing proteins such as MCAK, at mitotic centromeres (Andrews et al., 2004; Lan et al., 2004; Sampath et al., 2004) (**Figure 5B** – lower panel). Interestingly, a study in *Xenopus* egg extracts observed CPC at MTs and chromosomes and suggested the presence of a feedback mechanism between Aurora and MTs for spindle assembly around chromosomes (Rivera et al., 2012). Here again, CPC requirement depends on the model system. Accordingly, CPC is not required

for spindle assembly in human RPE1 cells but it favors MT-nucleation at chromosomes in HeLa and LLC-PTK1 cells recovering from MT-poisons (Tulu et al., 2006; Katayama et al., 2008; Tan and Kapoor, 2011; Haase et al., 2017). Most likely, the Ran-GTP- and CPC-dependent pathways collaborate to first nucleate MTs around the chromatin and second to stabilize these nascent MTs preferentially near KTs (Tulu et al., 2006; Maresca et al., 2009).

Recent studies described the accumulation of free tubulin not only at centrosomes but also around chromatin favoring local MT-nucleation, in *Drosophila* (Yao et al., 2012; Schweizer et al., 2015) and *C. elegans* (Hayashi et al., 2012), and therefore contributing to spindle formation. Very recently, the Giet lab observed that the absence of the tubulin-specific chaperon dTBCE abolished MT-growth from the chromatin after cold-treatment in *Drosophila* NBs. Further, using fluorescent live imaging, they show that dTBCE is responsible for the recruitment of tubulin around chromatin during prophase which is required for proper spindle assembly in these centrosome-containing cells (Métivier et al., 2020).

From pre-existing MTs – the Augmin pathway

A MT can also emanate from a pre-existing MT which participates to the formation of a mesh of branched-MTs (**Figure 5C**). This third pathway was found by depol/repol assays showing clusters of branched-MTs (O. Wasteneys and E. Williamson, 1989) and confirmed later in higher plants (Murata et al., 2005) and mammalian epithelial cells (Reilein et al., 2005). It involves the recruitment of γ-tub on MTs for their nucleation, just as it occurs at plant cell cortex (Murata et al., 2005). However, the name and the molecular components of this new MT-nucleation pathway was found and characterized by Goshima and colleagues who performed a genome-wide RNAi screen in *Drosophila* S2 cells to identify genes essential for mitotic spindle assembly (Goshima et al., 2007, 2008). They discovered that the depletion of several unknown genes Dgt1-6 (for dim γ-tubulin 1 to 6) decreased the γ-tub staining at spindle poles (Dgt1-2) or selectively within the spindle core (Dgt3-6). Fluorescently tagged Dgt4-6 uniformly localized to the inner mass of spindle-MTs, which was lost upon depolymerization. Live imaging of Dgt-depleted cells presented lower spindle-MT density and defects in chromosome alignment and spindle bipolarization, which most likely explained the mitotic delay phenotype (Goshima et al., 2007). They called it the Augmin complex from the Latin verb “augmentare”, which means to increase (Goshima et al., 2008), as it is required for

the increase of MT-nucleation within the spindle, independently of centrosomes. Actually, Augmin is a multiprotein-complex composed of 8 subunits sequentially identified in *Drosophila*: the five Dgt subunits (Dgt2-6) which are essential for γ-tub recruitment (Goshima et al., 2007, 2008), the two MAPs mitotic spindle density 1 (msd1/Dgt9) and 5 (msd5/Dgt7) (Wainman et al., 2009; Uehara et al., 2009) and another regulator of γ-tub recruitment wee Augmin component (Wac/Dgt8) (Meireles et al., 2009; Uehara et al., 2009). In Humans HAUS, for homologous to Augmin subunits is also a complex of 8-subnits (HAUS1-8) and shares conserved components with the *Drosophila* Augmin complex (Uehara et al., 2009; Lawo et al., 2009; Kamasaki et al., 2013; David et al., 2019).

In principle, the Augmin complex serves as site for MT-nucleation, it recruits γ-tub on pre-existing MTs which results in the establishment of a branched MT network. The precise function and requirement of Augmin on spindle assembly is organism- and cell type-dependent. Overall Augmin is not essential for spindle formation in most centrosome-containing cells but is involved in many processes such as (i) spindle density, robustness and morphology, (ii) K-fiber amplification, stability and tension, (iii) chromosome alignment and (iv) mitotic timing in many systems (Goshima et al., 2008; Uehara et al., 2009; Lawo et al., 2009; Meireles et al., 2009; Hayward et al., 2014; David et al., 2019). In contrast, in absence of functional centrosomes, Augmin is essential for spindle formation and bipolarity. Indeed, upon centrosome disruption in *Drosophila* embryos, ectopic MT-asters, known as acentriolar MTOC (aMTOC), form and ultimately cluster to form an acentriolar barrel-shaped spindle. This was proposed to be Augmin-dependent, as co-depletion of MT-nucleation from centrosomes and Augmin abolished aMTOC nucleation and spindle formation (Hayward et al., 2014). Further, it was shown that in acentrosomal cells, kinesin motors act on branched-MT produced by the Augmin pathway to favor aMTOC clustering and pole focusing in *Xenopus* egg extracts (Petry et al., 2011), *Drosophila* oocytes (Colombié et al., 2013) and upon early mouse development (Watanabe et al., 2016).

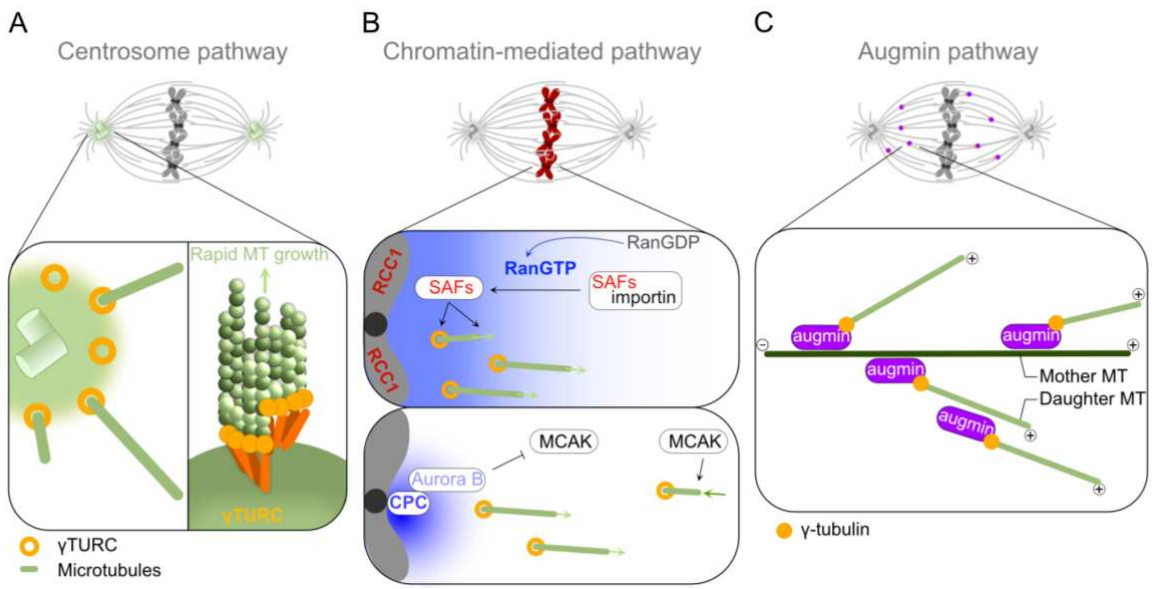

Figure 5. Several pathways for MT-nucleation. Schematic representation of MT-nucleation from centrosomes (A), chromosomes (B) and pre-existing MTs (C). (A) The recruitment of γ-tuRC on the PCM of centrosomes implements massive MT-nucleation. (B) Ran-GTP- and CPC-dependent pathways collaborate to nucleate and stabilize MTs at chromosome site. Ran-GTP gradient enables the release of SAFs from sequestration by importin which favors MT-nucleation at the vicinity of chromosomes. Aurora B from the CPC stabilizes MTs near KTs by inhibiting MT-depolymerizers such as MCAK. (C) The Augmin complex recruits γ-tubulin and serves as seed for the nucleation of branched-MTs.

1.2.4. Models for chromosome capture and bi-orientation

The first model for chromosome capture during mitotic spindle formation is the "search and capture" (S&C) model proposed by Kirschner and Mitchison in their review written in 1986. In this model, it is believed that MTs nucleate from centrosomes in all directions until they face obstacles. Consequently, chromosomes are randomly captured by MT plus-end growing from these asters. Once bi-oriented meaning that sister-chromatids are attached to opposite poles, KT-MT attachment is stably maintained and chromosomes align at the metaphase plate (Kirschner and Mitchison, 1986). This model gained credibility since the capture of chromosomes by MTs was directly visualized by time-lapse video microscopy of living vertebrate cells (Hayden et al., 1990; Rieder and Alexander, 1990) and in yeast (Tanaka et al., 2005). Importantly, this model of MT-searching behavior was justified by the principle of MT dynamic instability (Mitchison and Kirschner, 1984; Holy and Leibler, 1994). However, this

view, while intuitive, has been challenged by mathematical and theoretical modelling. Indeed, using this model, computer simulations predict longer hours to efficiently assemble the mitotic spindle, capture and align the 96 chromosomes of a human cell, which does not match with several minutes calculated from experimental data (Wollman et al., 2005). Thus, while the S&C model remained accepted for the last part of the twentieth century, it does not fit with kinetics of KT attachment in animal cells and does not explain chromosome capture and bi-orientation in the absence of centrosomes. Thus, alternative models have been proposed (reviewed in (Rieder, 2005; Heald and Khodjakov, 2015) and notably the pre-formation of MT fibers that are then captured by KTs and connected to centrosomes. This is favored by the existence of guidance gradients – Ran pathway and CPC - that stimulates MT growth at chromosome sites and thus, speeds up the formation of the mitotic spindle. Another stimulating factor is the variety of molecular factors present in the cytoplasm that drive spindle organization and bipolarity.

After their capture in prometaphase, chromosomes congress toward the cell equator to be aligned on the metaphase plate. This congression first involves forces generated by the KT-fibers leading to chromosome bi-orientation (reviewed in (Maiato et al., 2017)). In parallel, interpolar MTs dynamically interact with chromosomes through the action of plus-end-directed motor proteins, chromokinesins (Vanneste et al., 2011). Chromokinesins exert random polar ejection forces that push the chromosome arms away from the poles toward the spindle equator and thus, avoid that chromosome arms hide KTs (Darlington, 1937; Rieder et al., 1986; Rieder and Salmon, 1994; Brouhard and Hunt, 2005; Barisic et al., 2014). Interestingly, polar ejection forces are surprisingly low to avoid chromosome arm deformation or damage but are sufficient to guide their movement (Brouhard and Hunt, 2005). Combination of growth property of spindle-MT with forces generated by chromokinesin-mediated ejection on the arms and MT motors on KT-fibers strongly facilitate the correct alignment of chromosomes. If chromosomes are not well-bi-oriented and mis-attached, this can lead to defects in chromosome segregations. Thus, a mitotic checkpoint is present to control chromosome attachments prior anaphase onset.

1.2.5. Spindle assembly checkpoint and mitotic defects

To ensure genome stability, it is essential that chromosomes are well bi-oriented and sister-chromatids correctly attached to opposite poles prior separation and repartition into daughter cells. The safeguard of unattached and mis-attached KTs is the SAC (reviewed in (Musacchio and Salmon, 2007; Walczak and Heald, 2008; Lara-Gonzalez et al., 2012)). The SAC was discovered initially in budding yeast following genetic screens to identify mutant genes that do not arrest in response to MT-poisons (Hoyt et al., 1991; Li and Murray, 1991). In these two independent studies, the authors identified the MAD (mitotic-arrest deficient) genes *MAD1*, *MAD2* and *MAD3* (BUBR1 in humans) and the BUB (budding uninhibited by benzimidazole) genes *BUB1* and *BUB3* (Hoyt et al., 1991; Li and Murray, 1991). Then, the MSP1 (multipolar spindle 1) kinase was found as another component of this checkpoint, as mutant budding yeast failed to arrest after MT depolymerization (Weiss and Winey, 1996). Initially, the SAC was only considered as a mitotic checkpoint that inhibits cell division when the mitotic spindle is perturbed. It is micromanipulation and laser ablation experiments in eukaryotes that highlighted the SAC as sensor of unattached KTs (Rieder et al., 1995; Li and Nicklas, 1995), more precisely that the lack of tension on unattached KTs is the inhibitory signal that maintained the SAC "on" (Li and Nicklas, 1995). As an overall definition, the SAC is a "anaphase-wait" signal that senses attachment or tension at KTs and by inhibiting metaphase-anaphase transition purveys time for cell to correct erroneous attachments.

Mechanistically, at the sister-chromatid resolution level, the securin/separase/cohesin pathway (reviewed in (Nasmyth and Haering, 2009)) functions to prevent premature sister-chromatids separation before all chromosomes are well attached and oriented. Crystal structure analysis and gel electrophoresis experiments have shown that cohesin is a ring-shaped protein complex that encircles sisters for cohesion (Haering et al., 2002, 2008; Ivanov and Nasmyth, 2007). Securin forms dimers with separase to sequester it and impede it cleaves cohesin (Uhlmann et al., 2000). In parallel, the binding of Bub1, an essential SAC kinase, on unattached KT catalyzes the formation of the mitotic checkpoint complex (MCC) sequentially composed of Mad2, Mad3/BubR1 and then Cdc20 (Sudakin et al., 2001). The MCC inhibits the APC/C (anaphase promoting complex complex/cyclosome) activity by its binding with the APC/C cofactor Cdc20 (Sudakin et al., 2001). The APC/C is an E3 ubiquitin ligase that targets a variety of proteins for degradation by the proteasome (reviewed in (Peters, 2002)), including

cyclins (Glotzer et al., 1991) and securins (Cohen-Fix et al., 1996), which are involved in cell cycle progression and sister-chromatid cohesion, respectively.

Temporally, in prometaphase, Aurora B senses the absence of tension on incomplete or incorrect KT attachments and signals to the SAC to halt anaphase onset. Both kinases Bub1 and Aurora B cooperate to enhance MCC formation and thus, inhibition of the APC/C (Morrow et al., 2005). Inhibition of Aurora B (Ipl1 in *S. cerevisiae*) leads to chromosome mis-attachment in budding yeast and in human cells (Chan and Botstein, 1993; Kim et al., 1999; Biggins et al., 1999; Biggins and Murray, 2001; Tanaka et al., 2002; Murata-Hori and Wang, 2002). Different types of erroneous attachments exist and are called (1) synthelic when KTs of both sister-chromatids attach to the same pole, (2) merotelic when a KT connects both poles and (3) monotelic when the KT of only one sister chromatid is attached to one of the poles. In such cases, the SAC provides extra-time for error-corrections (reviewed in (Ricke and Van Deursen, 2011) which involves the regulation of MT dynamics at KTs (Bakhoum et al., 2009). Aurora B in the CPC, plays an important role in error-correction mechanisms as KT stretching sensor (Salimian et al., 2011) and recruiter-regulator of centromeric proteins such as the MT depolymerizing protein MCAK (Lan et al., 2004; Andrews et al., 2004; Helenius et al., 2006; Knowlton et al., 2006; Bakhoum et al., 2009).

Finally, when a chromosome is well attached, it generates tension within the KT (KT-MT attachment related) and tension from chromosome bi-orientation (attachment to opposite poles). Consequently, the KT-MT interaction is stabilized, Mad1 and Mad2 are ejected from KTs, the MCC is dismantled, Cdc20 is released, binds to APC/C which then becomes activated. APC/C activation induces the ubiquitin-dependent degradation of securin, which releases separase that in turn cleaves cohesin. The cohesin ring opens and sister-chromatids are free to separate. Meanwhile, the proteolysis of Cyclin B by APC/C inactivates the master mitotic kinase, CDK1, which promotes cell cycle progression and exit from mitosis (Luca et al., 1991; Holloway et al., 1993).

1.3. Centrosome number alterations and consequences

The duplication of centrosome is tightly regulated during the cell cycle (Gönczy, 2012) as centrosome copy number alterations or structural dysfunctions can have deleterious consequences on spindle assembly or cell survival. Indeed, mutations of genes encoding proteins of the centrosome machinery are frequently found in human pathologies such as

cancer (De Almeida et al., 2019; Denu and Burkard, 2020) or microcephaly (reviewed in (Nano and Basto, 2016). In this section, I will focus on two numerical defects: centrosome loss and the opposite condition, centrosome amplification and discuss their contribution to pathologies, such as brain growth disorders and tumorigenesis.

1.3.1. Centrosome loss

Centrosomes are considered as major actors of spindle formation, thus, one would except that removal of centrosome would decrease spindle robustness and cause chromosome segregation errors. While this seemed to be true to a low extend in the *Drosophila* epithelial wing disc (Poulton et al., 2014), mutant flies for the *sas4* gene can normally develop to adulthood and NBs that lack centrioles did not show mitotic errors. Instead, mitotic timing was slightly prolonged and *sas4* NBs also showed defects in spindle position (Basto et al., 2006). Further, they generated tumors when transplanted into the abdomen of host flies (Castellanos et al., 2008). Interestingly this tumorigenic potential is not due to the generation of genetic instability (GIN), but due to the perturbation of asymmetric division and thus, daughter cell fate leading to the over-proliferation of NBs (Castellanos et al., 2008).

In contrast centrosome loss can also decrease the fitness and survival of cells. For example, *sas4* mutation in the developing mouse brain induced microcephaly which is defined as a drastic reduction in brain size (Insolera et al., 2014; Bazzi and Anderson, 2014). As in *Drosophila* NBs, no mitotic errors were identified, but the accumulation of metaphase cells suggested also a mitotic delay, concomitantly to the p53-dependent cell death of the neural progenitor pool (Insolera et al., 2014; Bazzi and Anderson, 2014). *In vitro* studies using centrinone drug (Wong et al., 2015) and auxin-inducible degradation of PLK4 (Lambrus et al., 2015) to deplete centrosomes, revealed the existence of a novel p53-dependent pathway which is independent of DNA damage, stress or segregation errors. This pathway, named the mitotic surveillance pathway involves the USP28–53BP1–p53–p21 signaling and was firstly characterized in human cells (Lambrus et al., 2016; Meitinger et al., 2016). Depletion of 53BP1 (53 binding protein 1) or USP28 (ubiquitin specific peptidase 28) rescued the growth-arrest phenotype observed in cells without centrioles. This pathway was recently shown to be conserved *in vivo* in mouse brain (Xiao et al., 2020) and to contribute to microcephaly (Phan et al., 2021).

Interestingly, centrinone treated cancer cells continue to proliferate in absence of centrosomes, albeit with a reduced mitotic fidelity (Wong et al., 2015). Centrosome loss also leads to chromosome defects in chicken DT40 cells (Sir et al., 2013) and is associated with prostate cancer progression (Wang et al., 2020). However, this link between centrosome loss and GIN might be influenced by the fact that cells were already aneuploid prior centrosome loss in these three contexts. Thus, the role of centrosome loss in cancer remains unclear and debatable.

1.3.2. Centrosome amplification

Centrosome amplification (CA), a condition in which a cell contains more than two centrosomes, arises from different mechanisms including centrosome overduplication, *de novo* synthesis or polyploidization through cell fusion, mitotic slippage or cytokinesis failure (reviewed in (Nigg, 2002; Ganem et al., 2007); the different ways of polyploid cell generation are discussed in the section 2.1.2 Polyploidy - Routes to polyploidy)

CA is a common feature of cancer cells as it was found in most solid and hematological cancer cell lines, and at several steps of the tumorigenic process (Lingle et al., 1998; Pihan et al., 1998; Sato et al., 1999; Skyldberg et al., 2001; Giehl et al., 2005; Krämer et al., 2005; Hsu et al., 2005; Guo et al., 2007; Chan, 2011). Concerning tumor progression and metastatic transformation, a study combining 3D epithelial organoids and mammary epithelial cells in culture demonstrated that the presence of extra-centrosomes disrupts cell-cell adhesion causing invasion behaviors (Godinho et al., 2014). Consequently, for certain tumors, the presence of supernummary centrosomes correlates with high tumor aggressiveness and poor prognosis. CA was also proposed to occur in early stage of cancer development. Indeed, extra-centrosomes can initiate tumorigenesis through different mechanisms such as the loss of cell polarity (Lingle et al., 1998), stem cell asymmetric division (Basto et al., 2008) and most likely as being source of GIN due to error-prone mitosis.

Consequences of CA *in vivo* depend on the model organism and the tissue analyzed. In *Drosophila* larvae for example, as compared to centrosome loss, CA has different outcomes in wing discs and brains. Interestingly, while both conditions have tumorigenic potential when transplanted into host flies, this relies on different mechanisms. In brains the perturbation of asymmetric cell division induces an over-proliferation of neuronal progenitors (Basto et al.,

2008). On the other hand, CA in wing disc cells leads to chromosome mis-segregation and aneuploid cells are eliminated by apoptosis (Sabino et al., 2015) and delamination (Dekanty et al., 2012). During mouse brain development, CA causes aneuploidy, cell death and consequent microcephaly (Marthiens et al., 2013). In adult mouse skin, CA also fails to promote tumorigenesis (Kulukiana et al., 2015; Vitrea et al., 2015), unless p53 is depleted (Serçin et al., 2016; Coelho et al., 2015). In various other mouse tissues, global and transient CA promotes spontaneous tumorigenesis *in vivo* (Levine et al., 2017).

The link between CA and error-prone mitosis was first investigated by Boveri more than 100 years ago. He described the behavior of extra-centrosomes during mitosis, showing that CA correlates with multipolar figures. This multipolarity has the effect of generating more than two cells, which would be aneuploid as these cells will contain abnormal chromosome number. He proposed this mechanism as being the origin of malignant tumors (Harris and Boveri, 2008). This hypothesis was in light with previous works from the pathologist Hansemann who was the first to suggest a link between GIN and tumorigenesis as he observed unequal repartition of mitotic chromosomes in human epithelial tumors, albeit here it was after bipolar divisions (Hansemann, 1897). Later, live analysis revealed that cancer cells with supernumerary centrosomes only rarely undergo multipolar divisions and when they do so, aneuploid daughter cells are mostly unviable (Ganem et al., 2009). Consequently, many studies have investigated the different mechanisms used by cells to prevent multipolar spindle formation in the presence of supernumerary centrosomes (reviewed in (Godinho et al., 2009).

Centrosome inactivation. *Drosophila* NBs where centrosome number was amplified by the over-expression (OE) of Sak/PLK4, use centrosome inactivation as one strategy to limit the number of spindle poles. In this context, inactive centrosomes are devoid of (or highly limited) in MT-nucleation capacity and do not participate in spindle assembly (Basto et al., 2008). The same mechanism is used by the epithelial cells in *Drosophila* wing disc (Sabino et al., 2015). However, it remains unknown whether this strategy is used in mammalian or cancer cells and what designate the centrosomes to be inactivated from the others that remain active.

Centrosome clustering. The clustering of supernumerary centrosomes into two main groups for pseudo-bipolar spindle formation is the best characterized strategy to prevent multipolarity, and dominantly happens in cancer cells with CA (Ring et al., 1982; Brinkley,

2001; Quintyne et al., 2005; Kwon et al., 2008). This bipolarity is established in a two-step manner. First centrosome clustering into several poles which then coalescence to form a (pseudo-) bipolar spindle. However, this mode of division is error-prone. Both the Pellman and Cimini labs showed that transition by a multipolar figure before bipolarization leads to merotelic attachments and generation of aneuploid cells (**Figure 6**), yet to a less extend than what would happen upon multipolar divisions (Ganem et al., 2009; Silkworth et al., 2009). Thus, using this strategy, tumor cells with CA ensure their viability concomitantly with increase GIN (Silkworth et al., 2009; Ganem et al., 2009).

In genome-wide screens, several actors were identified to favor spindle bipolarity in CA cells, such as the SAC providing sufficient time for clustering or actin-dependent cortical and spindle intrinsic forces acting on astral MTs and many others (Kwon et al., 2008; Leber et al., 2010). The best known and conserved clustering factors are dynein and Ncd (HSET in mammals) (Mountain et al., 1999; Karabay and Walker, 1999; Goshima et al., 2005; Basto et al., 2008; Kwon et al., 2008; Kleylein-Sohn et al., 2012; Chavali et al., 2016). When present at a minimal distance, clustering factors bundle and slide MTs to focus spindle poles and cluster centrosomes (Rhys et al., 2018) (**Figure 6**). Interestingly, knowing that cancer cells frequently present CA, this clustering mechanism is a good candidate to target by therapeutic drugs to force multipolarity that ultimately would lead to cell death (Ganem et al., 2009). Some assays are currently ongoing using drugs targeting clustering motors (reviewed in (Myers and Collins, 2016; Sabat-Pośpiech et al., 2019)).

So far, I described cell division. I insisted on the importance of the establishment of a proper bipolar mitotic spindle to ensure the maintenance of the correct number of chromosomes per cell, which is essential for genome stability and tissue homeostasis. However, some variations to diploidy content can occur in different contexts, pathological or physiological and to different extend, aneuploidy or polyploidy. This will be discussed in the following section.

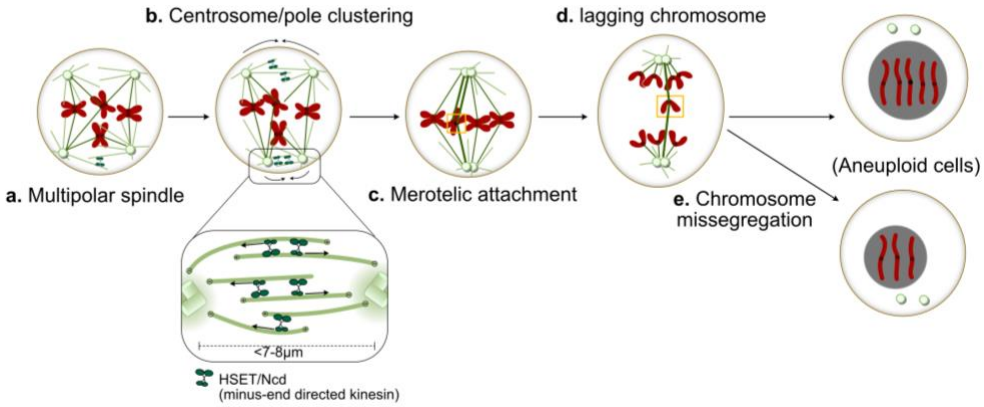

Figure 6. Centrosome clustering and merotelic attachment in cells with CA. Schematic representation of the process of centrosome clustering and consequent mis-attachment of chromosomes. Extra-centrosomes can cluster to establish a bipolar spindle. This clustering is mediated by the minus-end directed kinesin HSET/Ncd, which generates forces to slide overlapping MTs emanating from centrosomes in close proximity (≤7-8µm). This multipolar-bipolar transition can generate merotelic attachments of KTs and lead to the mis-segregation of the lagging chromosome. It has the consequence of generating aneuploid cells that have lost or gained one chromosome.

2. Variations in genome content

The DNA content in cells is represented by the C-value which is a multiple of the unreplicated haploid genome (Bennett and Smith, 1976). Consequently, as for most eukaryotes, a diploid nucleus contains 2C DNA content, prior duplication. In principle, all cells of one organism carry the same genome content and this is a criterion for genetic stability. However, unprogrammed alterations in ploidy can occur and most of the time, are linked to developmental growth disorders and cancer development. Among these changes in chromosome copy number, polyploidy and aneuploidy are distinguishable. Polyploidy is characterised by the gain of the whole chromosome set. In turn, aneuploidy is the gain or loss of individual chromosomes. Curiously, it appears somehow paradoxical that in physiology, changes in ploidy take place in certain specialised cells to adapt or ensure specific functions essential for tissue homeostasis. In this context, polyploidy and aneuploidy would have beneficial consequences. This duality of ploidy variation will be defined and discussed in this section.

2.1. Physiological variations to the genome content: How, where and why?

2.1.2. Polyploidy

After its discovery more than 100 years ago, polyploidy has been frequently observed across the plant (Lutz, 1907; Gates, 1908; Winkler, 1916; Stebbins, 1947; Otto, 2007) and animal kingdoms (reviewed in (Van De Peer et al., 2017)), although rarer in the latter (Muller, 1925; Orr, 1990; Mable, 2004). Remarkably, it appears that the major contributor to biological mass in nature is polyploidy rather than cell proliferation (reviewed in (Sugimoto-Shirasu and Roberts, 2003)). In agriculture crops of coffee or banana for example, polyploidization is used for plant breeding as it correlates with mass increase (reviewed in (Sattler et al., 2016)). In such context, polyploidy mostly concerns the whole organism and it is transmitted to the germline and inherited by next generations. This is in contrast with somatic polyploidy which is a condition where only few cells within tissues carry multiple copies of the diploid chromosome set. To facilitate comprehension, somatic polyploidy will be simply referred as polyploidy.

Polyploidy in animals is more frequent than usually expected. In *Drosophila*, most larval tissues and part of adult tissues are polyploid (Smith and Orr-Weaver, 1991; Edgar and

Orr-Weaver, 2001; Lee et al., 2009). In mammals, polyploidy concerns various specialized cells such as megakaryocytes (MKs) (Ravid et al., 2002; Trakala et al., 2015), trophoblast giant cells (TGCs) (Barlow and Sherman, 1974; Sher et al., 2013), muscle cells (McCrann et al., 2008; Cao et al., 2017), osteoclasts (Xing, 2012), and hepatocytes (Faktor and Uryvaeva, 1975; Yim, 1982; Kudryavtsev et al., 1993; Duncan, 2013; Gentric and Desdouets, 2014). In humans for example, polyploidy frequency can reach up to ~50% or ~70% in some tissues (Mollova et al., 2013; Gandarillas and Freije, 2014). In physiological context, polyploidization which is part of the developmental program or a stress-response, enables cells to have specific functions (reviewed in (Øvrebø et al., 2018)). Several modes of polyploidization exist. Two cells can fuse to form a polyploid cell through a process of cell-cell fusion but it is a rare event. In most cases, polyploidization arises from variants of the cell cycle and the transition from the canonical mitotic cycle to an endoreplication cycle. Upon endoreplication, cells escape either the whole M-phase or the last steps of mitosis, which result in endocycle or endomitosis, respectively. Depending on the mean of polyploidization, mono- or multi-nucleated cells will be produced (**Figure 7**).

Routes to polyploidy

Cell-cell fusion. This cell cycle independent mechanism which is the basis of egg fertilization, also occurs in somatic cells for differentiation and polyploidization of bone and skeletal muscle cells (Yagi et al., 2005; Quinn et al., 2017). Indeed, myoblasts fused to generate myofibrils (reviewed in (Abmayr and Pavlath, 2012) and macrophages fused to produce osteoblasts (reviewed in (Helming and Gordon, 2009). The mechanism and molecular pathway for cell-cell fusion is highly complex but for major steps, it involves cell migration, cell recognition and membrane fusion (reviewed in (Brukman et al., 2019)). It is experimentally inducible using specific molecules (Yang and Shen, 2006), optical manipulations (Steubing et al., 1991) or viral infection (Johnson and Rao, 1970; Rao and Johnson, 1970). Cell-cell fusion was a strategy to investigate the contribution of cell cytoplasm to the choice-making of cell cycle stage.

Endocycle. Cells endocycle by escaping the whole mitotic phase and thus, alternate between phases of growth (G-phases) and DNA synthesis (S-phase) (**Figure 7A**). Molecular mechanisms for endocycle onset and maintenance are organism- and cell type-dependent but in any case,

it concerns the lack of mitosis by suppression of the mitotic machinery, notably the disruption of cyclin/CDK complex activity, responsible for mitotic entry. In the absence of nuclear division, endocycle generates a cell with a single polyploid nucleus.

During *Drosophila* larval developmental, most tissues, with the exception of brain and imaginal discs, stop dividing to reach high levels of polyploidy (Smith and Orr-Weaver, 1991), as in the salivary glands where up to 10 rounds of DNA replication generate cells with up to 2048C (Rudkin, 1972; Urata et al., 1995). DNA labelling experiments showed that in these tissues, polyploidization occurs by endocycling as the DNA incorporation was cyclic and not continuous. In addition, chromosomes are defined as polytene (Pearson, 1974; Hammond and Laird, 1985) as all copies of sister-chromatids remained attached together and aligned to form large chromosomes with banded patterns. The onset of endocycle depends on the inhibition of the mitotic phase and the initiation of DNA replication. The APC/C, activated by the variant Fizzy-related Fzr (CDH1 in humans) targets mitotic cyclins for degradation and thus, prevents entry in mitosis. Indeed, *Fzr* mutant embryos present additional mitosis due to the accumulation of mitotic cyclins in post-mitotic salivary gland cells preventing from endocycle onset (Sigrist and Lehner, 1997). In addition to mitosis inhibition, one essential step for endocycle is the formation of pre-replication complexes (pre-RCs) in G1. This is possible by the APC/C-dependent degradation of the pre-RC inhibitor Geminin and the oscillation of Cyclin E transcription. Fluctuations of Cyclin E levels are regulated by the feed-back loop of the transcription factor E2F and its inhibitor $CRL4^{CDT2}$ (Zielke et al., 2011) and are necessary for multiple rounds of endocycle (Follette et al., 1998). In principle when Cyclin E levels are down, pre-RCs can form. When Cyclin E levels go up, Cyclin E/CDK2 complex forms and licenses replication initiation. Importantly, not all DNA is re-replicated at each cycle. In the salivary gland, under-replicated regions represent 20% to 30% of the whole genome (Rudkin, 1969; Hammond and Laird, 1985; Smith and Orr-Weaver, 1991; Lilly and Spradling, 1996). This differential replication mostly concerns the late-replicated heterochromatin regions (Dickson et al., 1971; Gall et al., 1971) and was proposed to be a mechanism for cells to do not invest much in regions poor in gene expression. In more recent studies using deep-sequencing and immunoprecipitation approaches in *Drosophila* polyploid cells, Nordman and colleagues precisely reported common and tissue-specific under-replicated regions - also present in euchromatin -, that are dependent on the Supressor of UnderReplication SuUR (Nordman et al., 2011). This suppressor localizes to these regions and

blocks replication fork progression (Nordman et al., 2014). Over-replication of specific regions also occurs and serves as a template for robust gene expression, like for chorion genes in *Drosophila* follicle cells (Orr-Weaver and Spradling, 1986; Delidakis and Kafatos, 1987). This differential DNA replication is a common feature of *Drosophila* polytene cells but was shown to be absent in polyploid MKs and TGCs that are essential for blood platelet production and mammalian placenta compartmentalisation, respectively. As an explanation, the expression of DNA replication factors is increased in MKs and TGCs (Sher et al., 2013).

At adult stage, various *Drosophila* cell types such as gut enterocytes, certain brain cells, ovarian nurse and follicle cells become polypoid but to different extend. The molecular mechanisms of polyploidisation slightly differs from larval tissues. For example, in *Drosophila* epithelial follicle cells, the onset of mitotic-to-endocycle switch depends on Notch pathway activation (Deng et al., 2001). Indeed, *Notch* mutant follicles remain undifferentiated and continue to divide (Deng et al., 2001; López-Schier and St. Johnston, 2001), while ectopic expression of *Delta* ligand induces precocious follicle endocycles. (Jordan et al., 2006). In more detail, the binding of Notch to Delta at the cell surface, signals the inhibition of the phosphatase String (Cdc25 in mammals) and promotes the transcription of *Fzr* (Schaeffer et al., 2004). APC/C^{Fzr} remains activated and degrades mitotic cyclins. Consequently, mitosis is inhibited and Cyclin E/CDK promotes S-phase entry (Duronio et al., 1996; Shcherbata et al., 2004) and mediates over-replication of chorion genes (Calvi et al., 1998). The Delta-Notch signalling is also responsible for the mitotic-to-endocycle transition of *Drosophila* enterocytes in the adult gut (Xiang et al., 2017) and of glial cells in the larval brain (Von Stetina et al., 2018).

In mammals, endocycle mainly depends on the use of CDK inhibitors (CKIs), like the CIP/KIP family, to prevent mitotic entry (Ullah et al., 2009). For example, *in vitro*, the removal of fibroblast growth factor 4 (FGF4) from the cell culture medium induces the accumulation of the CKIs $p21^{CIP1}$ and $p57^{KIP2}$, which inhibit CDK1 activity and supress the mitotic machinery. Consequently, fibroblasts start endocycling and differentiate into TGCs (Ullah et al., 2008).

Endomitosis. In contrast to endocycle, endomitotic cells enter M-phase but do not divide (**Figure 7A**). The moment cell exits mitosis determines the number of nuclei in the subsequent polyploid cell. Because in endomitotic cells, sister chromatids are not aligned, DNA has an interphase appearance, in contrast to *Drosophila* polytene chromosomes. Of note, in

endomitotic cells, not only the amount of DNA is increased but also the cytoplasmic content such as centrosome organelles.

Polyploidization of the mammalian MKs generate mono-nucleated polyploid cells with separated chromatids. MKs undergo mitosis until anaphase but only partially separate sister-chromatids. After assembling multipolar spindles, MKs skip late anaphase and cytokinesis, generating cells that contain a single multilobate polyploid nucleus. Endomitosis is initiated by the secreted signal thrombopoietin (Nagata et al., 1997a; b) and after up to 6 rounds of polyploidization, the DNA content of MK nuclei reaches up to 128C (Winkelmann et al., 1987; Ravid et al., 2002).

If polyploidization arises from cytokinesis failure, polyploid cells are multi-nucleated as chromosomes did segregate (**Figure 7B**). This is the case of mammalian hepatocytes where cytokinesis failed due to the inhibition of key regulators such as Rho-GTPase proteins or ROCK kinases. In the liver, polyploidization initiation is dependent on insulin signals (reviewed in (Gentric and Desdouets, 2014)).

Abortive cell cycle. In the review (Storchova and Pellman, 2004), Storchova and Pellman suggested the novel notion of "abortive cell cycle" as any process that affects cell division. It includes all the defects that halt mitotic progression, such as defects in DNA replication, sister-chromatids cohesion, cytokinesis or DNA damage. Here, cells are able to exit or slip after mitotic arrest without dividing and becoming thus polyploid. Abortive cell cycle as cytokinesis failure or mitotic slippage (**Figure 7B**) are sources of unprogrammed polyploidization and can be experimentally induced.

Direct perturbations in any of the actors involved in the cytokinetic process inhibit the furrow ingression and cells fail to accomplish division and become polyploid with multiple nuclei (**Figure 7B**). Many labs used chemical treatment (Andreassen et al., 1996) and/or genetic perturbations (Eggert et al., 2004; Somma et al., 2002; Ganem et al., 2014) to dissect cytokinesis mechanisms and to investigate the consequences of cytokinesis failure. In addition, unreplicated DNA or persistent DNA damage due to replication stress (Ichijima et al., 2010) or dysfunctional telomeres (Davoli et al., 2010; Pampalona et al., 2012; Stewénius et al., 2005) lead to the formation of chromosomes bridges which act as obstacles in the cleavage furrow and are major cause of cytokinesis failure (Jensen and Watson, 1999; Russo et al., 2015).

Mitotic slippage in turn, is a condition where cells halt in prometaphase but bypass the spindle checkpoint and exit mitosis without nuclear division resulting in one cell with one polyploid nucleus (**Figure 7B**). Concomitant perturbations of SAC and spindle dynamics or bipolarization (reviewed in (Ohashi, 2016)) induce mitotic slippage. For example, the formation of a monopolar spindle, through Eg5 inhibition plus disruption of the SAC induces slippage and the generation of mononucleated polyploid cell (Ohashi et al., 2015). In addition, the slow degradation of Cyclin B upon prolonged mitotic arrest causes mitotic slippage in human cells (Brito and Rieder, 2006).

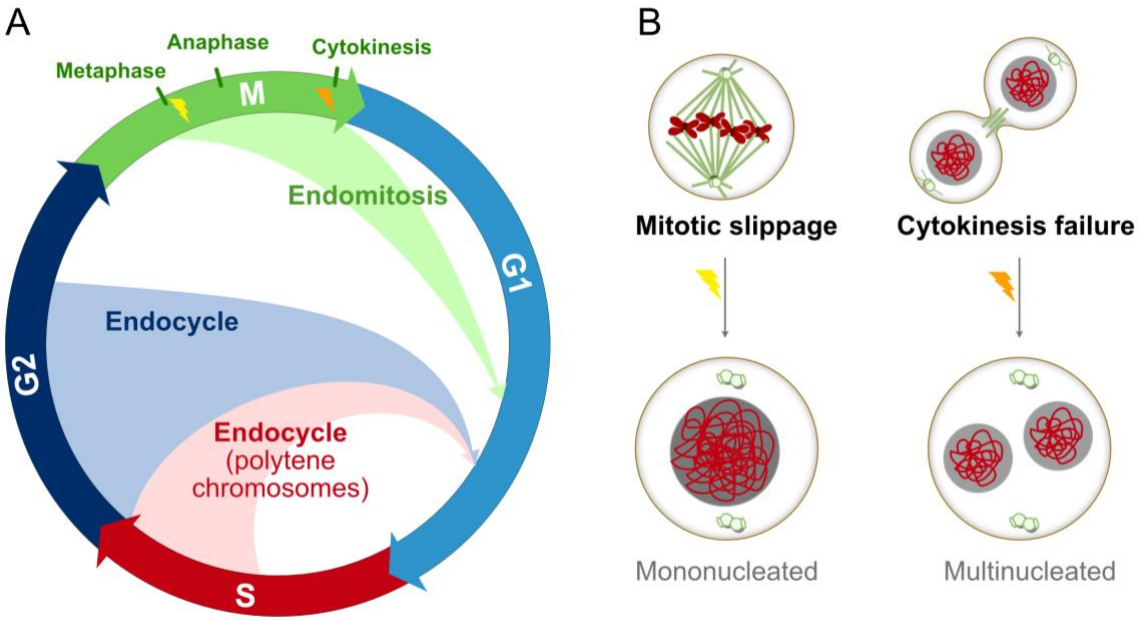

Figure 7. Different routes for polyploidization. (A) Schematic representation of the different cell cycle variants for endoreplication: endocycle (in red and blue) and endomitosis (in green). (B) Upon mitotic slippage, cell exists mitosis prior anaphase, generating a mononucleated polypoid cell. If a cell fails cytokinesis, the resulting polyploid cell presents multiple nuclei. In both contexts, cytokinesis failure and mitotic slippage, the doubling of the genome is accompanied by the concomitant increase in the cytoplasmic content and notably organelles such as centrosomes (in green).

POLYPLOIDIZATION FOR FUNCTION

During development and at adulthood, polyploidization is part of the differentiation program for cells to support specialized functions and confers several advantages (reviewed in (Orr-weaver, 2015; Frawley and Orr-Weaver, 2015; Øvrebø et al., 2018; Fox et al., 2020). Indeed, polyploidy facilitates growth, notably upon organogenesis and participates in tissue repair and stress-response.

Increase in cell size. Polyploidization produces large cells with wider nuclei (reviewed in (Schoenfelder and Fox, 2015)). In a short time-window as upon organogenesis, endoreplication is a faster strategy for cell growth and is less energy-demanding because cells simply increase in cell volume without dividing. In agreement, it was shown that rapid *Drosophila* larval growth was due to the increase in cell size of most larval tissues rather than an increase in cell number (reviewed in (Edgar and Orr-Weaver, 2001; Edgar, 2006)). The development of the worm *C. elegans* is also driven by endoreplication (Lozano et al., 2006).

In addition to their contribution to organ size, large polyploid cells sustain also barrier functions as they present several advantages. First, due to their large size, polyploid cells can envelop the organ while limiting the number of cell-cell junctions which can represent more vulnerable cell-cell fragile junctional sites in terms of tissue integrity. Second, it avoids barrier disruption upon cell divisions as it maintains intercellular junctions. This is the case for example of the TGC barrier which separates the maternal and foetal compartments of the placenta in mammals (Barlow and Sherman, 1974; Watson and Cross, 2005; Zybina and Zybina, 2005; Sher et al., 2013). Another example is the glial tissue layer of the *Drosophila* nervous system which serves as a blood-brain barrier (Stork et al., 2008; Desalvo et al., 2011; Hatan et al., 2011; Unhavaithaya and Orr-Weaver, 2012). Polyploidization is essential for the sub-perineurial glia (SPG) to sustain their function as inhibition of DNA replication decreases their ploidy and thus, their size leading to the rupture of septate junctions. Interestingly, this phenotype was rescued by inhibiting proliferation of the underlaying tissue. Further, the authors also found that SPG ploidy concomitantly increases with the increase number of neuronal number after brain tumour induction (Unhavaithaya and Orr-Weaver, 2012). These data show that polyploid SPG growth is able to accommodate during development. In addition, the primary role of polyploidization in this context is the resulting increase in cell volume rather than the polyploidy status itself. However, the balance between mono- and

multi-nucleated polyploid cells, produced by endocycle or endomitosis respectively, is important as any change in this ratio impairs barrier integrity (Von Stetina et al., 2018).

Another evidence of the importance of size increase in polyploid cells is the production of platelets by cytoplasmic budding from MKs. Indeed, larger MKs will produce more platelets. In these cells, polyploidization and not endomitosis *per se* is essential for its function, as a switch in their mode of polyploidization - from endomitosis to endocycle - does not have major consequences on platelet production (Trakala et al., 2015).

Finally, polyploidization can also be induced at adulthood, not as a part of the developmental or differentiation programs but as an adaptive response, such as upon wound healing after tissue injury. Certain tissues are able to regenerate after genetic or physical alterations, through polyploidization of cells located at the damage site. The process of "wound-induced polyploidisation" was shown to occur in *Drosophila* epithelia such as the epidermis, hindgut or imaginal discs (Losick et al., 2013; Tamori and Deng, 2013; Losick, 2016). Upon mammalian liver regeneration, cells become polyploid after hepatectomy (Faktor and Uryvaeva, 1975; Gerlyng et al., 1993; Duncan, 2013; Gentric and Desdouets, 2014).

Increase in metabolic capacity. The increase in gene copy number correlates with increase biosynthesis and metabolic capacity in certain polyploid cells (Frawley and Orr-Weaver, 2015). Upon oogenesis and early development, mammalian trophoblasts (Baines and Renaud, 2017) and *Drosophila* nurse and follicle cells (Bastock and St Johnston, 2008) sustain metabolic functions and provide nutrients to support egg and embryo development. This was also proposed to occur in mammalian MKs (Hancock et al., 1993), in hepatocytes to increase the metabolic capacity of the liver (Donne et al., 2020) and in *Drosophila* glial cells that are nutrient providers for the brain (Spéder and Brand, 2014).

One of the most striking examples is the factory function of nurse cells in the *Drosophila* ovary. One oocyte is surrounded by about 15 nurse cells with polytene chromosomes that can reach 512C-1024C (Dej and Spradling, 1999). Their major role consists in synthetizing all maternal nutrients as mRNAs, proteins or mitochondria, which are transported to the oocyte by cytoplasmic bridges (reviewed in (Pepling, 2016)). However, the direct link between this metabolic function and their polyploidy status remains uncertain. When polyploidization is disrupted in nurse cells, it induces the degeneration of both nurse cells and oocytes (Reed and Orr-Weaver, 1997). Another example is the support role of follicle

cells which are polyploid but to a much lower extend (16C) than nurse cells. Follicle cells produce the eggshell surface and the increase in gene copy number which is essential to sustain its function, comes from polyploidization and over-replication of specific genomic regions as the chorion gene (Calvi et al., 1998).

Robustness and protection against stress. In addition to their role in metabolism, increase gene copy number in polyploid cells can also has a protective role against mutations or DNA damage because multiple copies would favour correction and confer damage resistance. In addition, apoptosis is inhibited in certain polyploid cells that favours survival and life lengthening (Mehrotra et al., 2008; Lee et al., 2009; Hassel et al., 2014; De Renty et al., 2014). While a direct link has never been demonstrated, several studies showed that polyploidization of cardiomyocytes facilitate cardiac muscle contraction under stress (reviewed in (Pandit et al., 2013). In the mammalian skin, differentiation and polyploidization - by endomitosis or endocycle - of keratinocytes are strictly linked (Gandarillas et al., 2000) and it was proposed that due to their large size, polyploid cells increase their mechanical resistance and could protect them upon UV light exposure (Zanet et al., 2010). Moreover, the absence of cell division would protect them from tumour formation (De Castro et al., 2013; Sanz-Gómez et al., 2018, 2020). Interestingly, in response to compromised genome integrity, as upon telomere dysfunction, hepatocytes maintain the capacity to regenerate the liver after hepatectomy and favour polyploidization over cell proliferation (Denchi et al., 2006).

2.1.1. Aneuploidy

ROUTES TO ANEUPLOIDY

Numerical aneuploidy, mentioned here simply as aneuploidy, is a state of abnormal chromosome number which originates from mitotic errors and several routes lead to this erroneous segregation of chromosomes. It includes any defect in essential mitotic events that affect chromosome structure and segregation such as chromosome condensation, sister-chromatid cohesion, KT assembly, spindle formation and bipolarisation (reviewed in (Holland and Cleveland, 2012; Schukken and Foijer, 2018; Levine and Holland, 2018)).

Aneuploidy can originate from polyploid cells that return to a mitotic cell cycle. First evidence of reduction mitosis was described in the 1970s with the generation of diploid cells

from a tetraploid fibroblast cell line (Martin and Sprague, 1969; Pera and Rainer, 1973) and confirmed later *in vivo* from transplanted hematopoietic stem cells, which were polyploid by cell-cell fusion (Wang et al., 2003). However, this phenomenon known as "ploidy reversal" or "ploidy conveyor" occurs in certain physiological contexts and is a source of aneuploidy. One example is the error-prone polyploid mitosis in the *Drosophila* adult rectal papillae (Fox et al., 2010). Live-imaging of the *Drosophila* rectum revealed that mitotic polyploid papillar cells establish multipolar spindles and divide to form three cells, consequently aneuploid (Schoenfelder et al., 2014). In the mammalian liver, it was for long time believed that upon tissue regeneration after injury, polyploid hepatocytes re-entered mitosis generating cells with random chromosome aneuploidies (Duncan et al., 2010). In this study, authors FACS sorted polyploid hepatocytes from mouse liver and induce cell division. Live imaging of polyploid cells with extra-centrosomes -due to cytokinesis failure- showed different types of mitotic errors. In some cases, multipolar divisions of tetraploid cells lead to the generation of three daughter cells, one near-tetraploid and two near-diploid. In most cases, divisions were bipolar but with transient multipolar figures leading to chromosome mis-segregation (Duncan et al., 2010). This view was recently challenged by two studies. Using lineage tracing, authors demonstrated that ploidy reduction in mice hepatocytes only rarely involves erroneous chromosome repartition (Matsumoto et al., 2020; Lin et al., 2020). But mechanisms by which chromosomes are properly distributed in daughter cells - one tetraploid and two diploid - remain unknown.

Division of diploid cells can also generate aneuploid daughter cells. Indeed, errors in spindle assembly and bipolarization lead to aberrant KT-MT attachments. Multipolar divisions obviously lead to the generation of highly aneuploidy cells. In bipolar divisions, chromosomes can be mis-positioned, usually caused by mis-attachment and ultimately will mis-segregate. Merotelic KT attachments cause lagging chromosomes which at anaphase lag between the two chromatin masses generating aneuploidy (Cimini et al., 2001, 2003) and frequently micro-nuclei when the mis-segregated chromosome fails to incorporate in the main nucleus (Thompson and Compton, 2011). Merotelic attachments and lagging chromosomes are enriched by multipolar to bipolar spindle transitions in polyploid or diploid cells with extra-centrosomes (Silkworth et al., 2009; Ganem et al., 2009). Another type, polar chromosomes, do not align on the metaphase plate and instead localize near one spindle pole due to mono- or syntelic KT-attachments. Incorrect chromosome attachment or alignment can arise from

mutations or sporadic defects in the dynamics of spindle assembly and motor proteins, KT structure, KT-MT attachment stability and erroneous correction (reviewed in (Gregan et al., 2011; Levine and Holland, 2018).

In principle, the SAC safeguards from mitotic errors to occur. But the SAC can be bypassed or weakened by mutations affecting its efficiency. Consequently, the lack of time caused by SAC defects, does not permit the attachment of all chromosomes or the correction of erroneous attachments leading to chromosome mis-segregation. For example, mutations in BUBR1 and TRIP13 causes SAC inactivation and mosaic variegated aneuploidy in mammalian cells (Yost et al., 2017; Sieben et al., 2020).

Finally, other indirect factors have impacts of cell division accuracy. Certain genes, initially not linked to aneuploidy but involved in the cellular stress response, were identified in two genetic screens as affecting chromosome segregation fidelity (Conery and Harlow, 2010; Meena et al., 2015). Second, mutations in oncogenes or tumour suppressor such as Rb-E2F and Ras were shown to enhance SAC gene expression or cause sister chromatid cohesion defects (Hernando et al., 2004; Manning et al., 2010; Cui et al., 2010; Orr and Compton, 2013). Finally, a recent study on epithelial cells suggested that surrounding tissue architecture may also favour faithful mitotic division (Knouse et al., 2018).

DEBATABLE PHYSIOLOGICAL LEVELS: TECHNICAL ISSUES FOR ANEUPLOIDY DETECTION

Many studies have investigated the karyotype of cells, organs and tissues and it was initially proposed that a certain level of aneuploidy could be tolerated in healthy tissues. Conflicting results emerged and the frequency of abnormal karyotypes in normal organisms remain under debate. It appeared that the variety of different technics used to map aneuploidy might be the issue.

Major organs of debate are brain and liver. Initial studies using karyotype analysis on metaphase spreads reported from 25 to 70% of aneuploid hepatocytes in the developing mouse liver (Faggioli et al., 2011a) and 30% in mouse neural stem cells (NSC) (Rehen et al., 2001; Yang et al., 2003; Kaushal et al., 2003). Fluorescent *in situ* hybridization analyses on interphase nuclei confirmed high levels of aneuploidy in hepatocytes (Faggioli et al., 2011a) and similar rates in post-mitotic neurons (Rehen et al., 2001; Kaushal et al., 2003) which were shown to participate to the adult neural circuit (Kingsbury et al., 2005). Same trends were

observed in humans for both tissues using the same technics of chromosome labelling (Rehen et al., 2005; Pack et al., 2005; Yurov et al., 2007). However, the emergence of new technologies such as single-cell sequencing challenged these data and demonstrated that abnormal karyotypes are rare in normal mammalian tissues (Knouse et al., 2014; Douville et al., 2020). For example, the revisited rate of aneuploid neurons was reduced to < 5% in human brains (Knouse et al., 2014; Cai et al., 2014; van den Bos et al., 2016). Interestingly, low aneuploidy levels were also recently described in wild type (WT) *Drosophila* tissues (Gogendeau et al., 2015; Sabino et al., 2015; Resende et al., 2018).

The discrepancy between the variety of studies most likely originate from technical issues due to the limitations of the different methods used to assess aneuploidy (review in (Bakker et al., 2015)). Karyotype analysis of metaphase chromosomes is limited in the analysis of mitotically active cells. Spectral karyotyping and FISH are known to present false positive and negative due to probe clusters and conversely low binding efficiency. Single cell sequencing appeared as a more reliable and unbiased technology with a higher resolution. However, it is limited in cell number analysis as it requires the dissociation of cells from the tissue, remains an expansive technology and lacks a dynamic view of aneuploidy in organisms at it corresponds to a snapshot. Monitoring aneuploid cells *in vivo* would be very informative on the mechanisms of origin and to follow their outcome. The second part of my PhD project aimed to develop such a tool in *Drosophila* (*Chapter 2 - Results – Section B*).

2.2. Unprogrammed variation in genome content: a double-edged sword

Aneuploidy is infrequent in physiological context because chromosome imbalance affects cellular physiology and consequent organism homeostasis. When out of control, unprogrammed variations to the genome content are associated with pathological conditions such as cancer (Beroukhim et al., 2010), microcephaly (Marthiens et al., 2013) or miscarriage (Jia et al., 2015) and consequences differ whether ploidy variations occur during development or aging.

2.2.1. Ploidy alterations: growth defects and aging

CONSEQUENCES OF CONSTITUTIONAL AND MOSAIC ANEUPLOIDY ON TISSUE DEVELOPMENT

More than 100 hundred years ago, in its dispermic experiment in sea urchin, Boveri linked abnormal karyotype with lethality. He observed that aneuploid embryos, originating from multipolar divisions of the polyploid zygote, presented strong developmental disorders and ultimately died (Boveri, 1902). Several decades later, Bridges made same conclusions in *Drosophila*. A *Drosophila* strain carrying an extra-copy of the small chromosome IV were viable but presented developmental defects, decrease body size and sterility (Bridges, 1921a; b). Constitutional aneuploidy, defined as a condition where all cells of the body are aneuploid, originates in gametes from errors in meiosis. In humans, the majority of trisomies and monosomies are embryonic lethal. One autosomal trisomy viable to adulthood is the trisomy of the chromosome 21, however patients present a Down syndrome, characterised by important developmental growth disorders and mental retardation (Lejeune et al., 1959). Most trisomies are also lethal in mouse (Dyban and Baranov, 1987).

Interestingly, somatic aneuploidy, by opposition, concerns a fraction of cells within the whole organism and differentially impacts tissue development and homeostasis. A rare condition, mosaic variegated aneuploidy (MVA) where nearly 25% of cells are aneuploidy, is associated with developmental delay and notably a microcephaly phenotype (Warburton et al., 1991). Consistently with the fact that the brain is susceptible to aneuploidy, induction of chromosome mis-segregation in mice causes drastic reduction in brain size due to loss of neural progenitor pool (Marthiens et al., 2013).

PLOIDY VARIATIONS IN AGING

Whether aneuploidy increases with age and whether this is associated with age-related pathologies are long-term debates. Several studies reported the accumulation of abnormal karyotypes in aging cells of mammalian tissues (Baker et al., 2013), such as in the brain (Iourov et al., 2009; Yurov et al., 2014, 2018; Faggioli et al., 2011b, 2012), liver (Duncan et al., 2010; Faggioli et al., 2011a; Duncan et al., 2012), blood lymphocytes (Jacobs et al., 1961) and oocytes (Jones, 2008). In the brain, for example, the increase of chromosome-specific aneuploidy was proposed to be at the origin of age-related neurodegeneration (Iourov et al., 2009; Shepherd

et al., 2018) as in Alzheimer's disease (AD) (Yurov et al., 2014) but this assumption remains controversial (van den Bos et al., 2016). Polyploidy is also believed to increase rate with age, as recently reported in the *Drosophila* (Nandakumar et al., 2020) and mammalian brain (López-Sánchez et al., 2017). Another striking example is the exponential increase of aneuploid oocytes with maternal aging in mouse and humans (reviewed in (Ma et al., 2020)).

In addition to the potential increase of aneuploidy frequency with age, one can mention the opposite, namely aneuploidy as a source of aging. One of the best examples is MVA which is also associated with premature aging known as progeroid syndromes. This link was further confirmed in mice carrying a BUBR1 mutation- the most affected gene in MVA patients - which presented high levels of aneuploidy and consequent increase in senescence and aging (Sieben et al., 2020). Importantly, gene expression comparison between young and old mice revealed age-associated down-regulation of SAC and centromere proteins (Zahn et al., 2007; Andriani et al., 2017), such as BUBR1. Conversely, BUBR1 OE expands mice healthy lifespan (Baker et al., 2013).

2.2.1. The aneuploid and polyploid paradoxes

THE ANEUPLOID PARADOX

Initial studies on budding yeast were crucial for understanding of detrimental effects of aneuploidy on cell physiology. Torres and colleagues generated a collection of yeast strains carrying extra-copies of single chromosomes and showed that extra-chromosomes were actively transcribed and that overall chromosome gain negatively impacts cell growth and proliferation, mainly by extended G1 phase (Torres et al., 2007). Authors proposed that transcriptome changes perturb the protein imbalance causing proteotoxic stress that in turn, deregulates cellular processes and decreases cellular fitness (Torres et al., 2007, 2008). Several proteomic analyses in aneuploid yeast confirmed the dysregulation of the proteasome (Pavelka et al., 2010; Dephoure et al., 2014), such as formation of protein aggregates (Oromendia et al., 2012) as a source of toxicity, in addition to perturbations in redox homeostasis (Dephoure et al., 2014). Interestingly, aneuploidy in mammalian cells similarly affects cell metabolism at the transcriptome (Upender et al., 2004) and proteome level (Stingele et al., 2012; Tang et al., 2011), and reduces proliferation capacity (Williams et al., 2008). A comparative study in yeast, plant, mouse and human cells confirmed that

aneuploidies of different chromosomes and in different organisms involve similar cellular pathways causing an anti-proliferative response (Sheltzer et al., 2012). Aneuploidy also interferes with cell survival. The increase production of reactive oxygen species mediated by metabolic and energetic stresses (Dephoure et al., 2014), activates the ATM kinase (Guo et al., 2010) which in turn triggers P53-dependent cycle arrest or apoptosis of aneuploid cells (Li et al., 2010). In agreement, oxidative stress causes P53-dependent senescence of aneuploid human mesenchymal stem cells (Estrada et al., 2013). Chromosome mis-segregation and resulting DNA damage also signals the ATM-P53 pathway activation and induces aneuploid cell death (Jeganathan et al., 2007; Thompson and Compton, 2010; Janssen et al., 2011). In *Drosophila* unlike mammalian cells, the elimination of aneuploid cells does not involve a p53-dependant mechanism and differs between tissue. In wing discs, aneuploidy is eliminated by epithelial cell delamination and p53-independent death, while aneuploid NBs prematurely differentiate into neurons (Dekanty et al., 2012; Gogendeau et al., 2015). However, current knowledge on the precise signaling pathways involved in aneuploidy elimination is limited.

In regards of this literature, aneuploidy has proliferative disadvantage in multiple species and contexts. Thus, it appears somehow paradoxical that abnormal karyotypes are a hallmark of highly proliferative cancer cells (Taylor et al., 2018). Interestingly, this duality of aneuploid condition can also be applied to non-cancer cells, as aneuploidy commonly emerge in mammalian cell cultures. For example, 25% of non-transformed mouse cells are aneuploid (Didion et al., 2014) and chromosome 12 gain is common in human pluripotent stem cells as it confers growth benefit (Mayshar et al., 2010; Taapken et al., 2011; Ben-David et al., 2014). This conflicting idea named the “paradox of aneuploidy” intrigued many labs and aneuploidy was proposed to act both as oncogene and tumour suppressors *in vivo* (Weaver and Cleveland, 2007; Weaver et al., 2007). Of note, many studies investigating aneuploidy consequences were performed in a peculiar condition of single chromosome aneuploidy. An overview of chromosomes gains and losses and more complex karyotypes, which are typical of cancer cells will be necessary to understand implications of aneuploidy on cell homeostasis. It is tempting to assume that certain combinations or specific chromosome imbalance would favour proliferation, while other would highly decrease cell fitness.

To understand how aneuploidy could be tolerated, whole genome sequencing (WGS) analysis of aneuploid yeast that presented a rescue in proliferation capacity after two weeks in culture, revealed the existence of aneuploidy-tolerating mutations that normalize protein

stoichiometries (Torres et al., 2010). In addition, certain aneuploid strains were shown to growth faster than euploid controls under pressure (Pavelka et al., 2010) and the acquisition of new karyotypes after stress-induced aneuploidy and consequent chromosome instability (CIN) facilitate drug-resistance (Chen et al., 2012). Several studies reported similar observations, that aneuploidy favours rapid adaptive mechanisms and resistance to genetic, chemical and environmental perturbations (Selmecki et al., 2006, 2009; Yona et al., 2012; Kaya et al., 2015; Millet and Makovets, 2016; Linder et al., 2017). Aneuploidy could indeed confer advantages in adverse situations, with the dysregulation of transcriptome and proteasome being a source of variability for stress-resistance and permit cell survival. Importantly, aneuploidy can also be tolerated *in vivo*. Mice deficient for the SAC, to induce CIN, undergone normal development to adulthood (Michel et al., 2001; Babu et al., 2003; Jeganathan et al., 2007; Weaver et al., 2007). In physiological conditions, upon liver regeneration, ploidy reversal generates low levels of tolerated aneuploid cells that through phenotypic variability drives adaption to stress (Duncan et al., 2010) and can be source of tumour formation (Matsumoto et al., 2021).

THE POLYPLOID PARADOX

Even if less studied than aneuploidy, polyploidy also presents a paradox. First, polyploidy is frequently found in healthy tissues. In such contexts, polyploidization is tolerated and is even essential for certain cell type to sustain specialised functions. In opposite, when unscheduled polyploidy is usually associated with cell cycle arrest or even cell death. Importantly, however, in a third context, polyploidy is also found in a large variety of tumours and is reported as early event of tumorigenesis that fuels rapid GIN.

Programmed polyploid cells arise from different mechanisms and can sustain many different functions (described in the section 2.1.2. Polyploidy - Polyploidization for function). However, despite all these differences, they have several common points: 1) in physiological context, polyploidization is part of a program and thus, is maintain under control; 2) in the majority of cases, polyploid cells are terminally differentiated and thus, 3) polyploidy mostly rhythms with the lack of cell division. This low proliferation capacity of polyploid cells is essential to limit GIN as in several examples, as ploidy reversal in the mammalian liver and *Drosophila* rectum, the return to a mitotic cycle is synonymous of multipolar cell divisions,

that can lead to unbalanced chromosome copy number in daughter cells. Thus, when unscheduled, strong mechanisms limit polyploid cell proliferation, with few exceptions. *In vitro* culture, the control relies on the P53 and Hippo pathway that induces cell cycle arrest or apoptosis most likely in response to CA characterising cells that failed cytokinesis (Ganem et al., 2014; Zhang et al., 2017). In contrast, in *Drosophila*, physiological endocycling cells seem to downregulate *p53* expression, even though its OE is not sufficient to induce an apoptotic response (Mehrotra et al., 2008; Zhang et al., 2014a). Interestingly, in *Drosophila*, the tolerance for unscheduled polyploidy is tissue-dependent: in wing discs polyploid cells are eliminated (unpublished data), while in the larval brain, polyploidy is tolerated and NBs that failed cytokinesis continue cycling (Gatti and Baker, 1989; Karess et al., 1991; Nano et al., 2019). Mechanisms behind these differential behaviours and the precise signalling cascade that sense polyploidy and control its tolerance or elimination remain open questions.

Paradoxically, a large variety of cancer cells undergone whole genome duplication (WGD). In this context, polyploidy is associated with high proliferation capacity of cancer cells. In addition, we have shown in the lab that unscheduled polyploid cells suffer from strong error-prone mitosis and high levels of DNA damage ((Nano et al., 2019; Goupil et al., 2020a); *Chapter 2 - Results – Section A*). It is thus intriguing and unknown how polyploid cells can bypass this block to continue proliferate in P53-competent conditions (Dewhurst et al., 2014; Zhang et al., 2014b). Regulation by Cyclin D activity was proposed as a mechanism for WDG tolerance in P53-proficient cells in mammalian models (Potapova et al., 2016; Crockford et al., 2017). How and through which mechanisms polyploidy fuels GIN and decreases tissue homeostasis are current issues in the polyploidy field. In addition, one has to consider the concomitant increase of genome content with the increase in cell size and cytoplasmic components. Thus, polyploidy rises many questions about cell scaling and whether, cells and its machinery can sustain major functions when all its components are doubled. As part of this considerable question, I dedicated the first part of my thesis to decipher the impact of concomitant increase in DNA content and centrosome number on polyploid cell division and thus, genome stability (*Chapter 2 - Results – Section A*).

2.2.3. Whole genome duplication and aneuploidy: sources of CIN and GIN

Transient chromosome mis-segregation and stable propagation of abnormal chromosome copy number is very rare. In most cases, aneuploidy and polyploidy are sources of CIN characterised by an increase rate of whole chromosome gains and losses over time (reviewed in (Geigl et al., 2008)). Indeed, proliferative aneuploid and polyploid cells experience various mitotic errors such as chromosome bridges, mis-segregation, multipolar divisions, cytokinesis failure or micronuclei formation, in various species including yeast (Mayer and Aguilera, 1990; Molnar and Sipiczki, 1993; Storchová et al., 2006), *Drosophila* (Fox et al., 2010; Unhavaithaya and Orr-Weaver, 2012; Nano et al., 2019; Goupil et al., 2020a) or mammals (Duncan, 2013; Nicholson et al., 2015; Wangsa et al., 2018). Further, it is important to mention that all these defects can lead to structural rearrangements which defined GIN. For example, micronuclei or defective DNA replication causes DNA damage and breaks, chromosome pulverisation and consequent genome shuffling (Crasta et al., 2012; Russo et al., 2015; Passerini et al., 2016; Notta et al., 2016; Ly and Cleveland, 2017; Wangsa et al., 2018). In addition, we reported in the lab, unprogrammed polyploid cells with multiple nuclei - generated through multipolar divisions ((Goupil et al., 2020a); *Chapter 2 - Results – Section A*) - performing DNA damage due forced entry in mitosis of delayed nuclei, termed chronocrisis (reviewed in (Gemble and Basto, 2020)). We propose this as an additional source of GIN (Nano et al., 2019). Cancer genome analysis confirmed the association between the experience of WGD and higher rate of other genetic alterations (Zack et al., 2013; De Bruin et al., 2014; Dewhurst et al., 2014). Thus, aneuploidy and polyploidy are status, while CIN and GIN are dynamic processes that evolve and lead to complex and abnormal karyotypes. The emergence of a large body of studies will help to define mechanisms linking variations to chromosome copy number and cancer genome evolution.

As mention above, in most mammalian tissues and *in vitro* culture, the control of polyploidization relies on the P53 pathway which induces cell cycle arrest or eventually apoptosis of aneuploid and polyploid cells (Livingstone et al., 1992; Andreassen et al., 2001; Ganem and Pellman, 2007; Ganem et al., 2014; Kuffer et al., 2013; Marthiens et al., 2013; Hinchcliffe et al., 2016). Interestingly, in P53-deficient models, polyploidy arises in response to damage and promotes tumorigenesis (Fujiwara et al., 2005; Krzywicka-Racka and Sluder, 2011; Davoli and de Lange, 2012). Programmed polyploidy also drives tumour formation in

physiological contexts (Duncan et al., 2010; Schoenfelder et al., 2014; Matsumoto et al., 2021). Thus, WGD was proposed to be involved in tumorigenesis, from initiation to evolution and metastasis, for several reasons. First nearly 40% of cancers experience WGD and this rate can reach 70% in specific tumour subtypes (Kaneko and Knudson, 2000; Carter et al., 2012; Zack et al., 2013; Dewhurst et al., 2014; Notta et al., 2016). Then, most aneuploid tumours contain extra-centrosomes which might originate from an abortive cell cycle (Meraldi et al., 2002). In addition, computational analysis of human cancer genomes reported that WGD is an early event (Zack et al., 2013; Blakely et al., 2017) and that increase number of chromosome sets could catalyses further aneuploidy and GIN, which drive intra-tumour heterogeneity and phenotypic variability, beneficial for tumour evolution and response to anti-cancer drugs for example (Gerlinger et al., 2012; Zhang et al., 2014b; Kuznetsova et al., 2015). Another advantage of the presence of extra-copies is the compensation for adverse defects of chromosome loss or deleterious mutations and tolerance for mitotic errors (Dewhurst et al., 2014).

3. Gene expression plasticity: differentiation and cell identity – lessons from *Drosophila*

As detailled above, equal repartition of the genome content into the two daugther cells is crucial for genetic stability and tissue homeostasis. However, while being genetically identical, daugther cells can differ in fate and thus, in function. The inheritance of specific markers and consequent modification in the expression of specific genes establishes novel cell identities without changing the genetic information. In this section I will introduce the notion of epigenetic regulation and the establishment of specific pattern of gene expression. After a brief description of the main actors and regulators of gene expression, I will discuss its role in the differentiation process and its stability over time and inheritance. For simplicity, I will mainly focus on *Drosopila* characteristics and examples, as my work, related to epigenetic regulation, was developped in *Drosophila (Chapter 2 - Results – Section B).*

3.1. Regulation of gene expression and epigenetic marks

Brief introduction to *Drosophila* genome

The diploid *Drosophila* genome is composed of 4 chromosome pairs: one sexual pair (XX or XY) and three autosome pairs. Among autosomes, the chromosome 4 is very small mainly composed of heterochromatin. The large chromosomes 2 and 3 are metacentric composed of left and right arms, named 2L/3L and 2R/3R, respectively (Metz, 1914; Deng et al., 2007). Based on the banded pattern of polytene chromosomes, Bridges codified these regions and created the first map of *Drosophila* chromosomes. In this map, still used to date, each chromosome arm is divided in 20 units (X = 1–20; 2L = 21– 40; 2R = 41–60; 3L= 61–80; 3R = 81–100; and the small fourth 4R = 101–102), in turn subdivided into 6 lettered segments (A to F) composed of numbered bands (Bridges, 1935). This mapping gained into resolution and precision with the improvement of microscopy (Lefevre, 1976; Saura et al., 1999). The annotated molecular mapping emerged with WGS (Adams et al., 2000). The estimated size of the *Drosophila* genome is ~180Mb (Bosco et al., 2007) and its annotation identified ~17,700 genes (reviewed in (Kaufman, 2017)). The expression of those genes is regulated at different scales: directly by gene regulatory sequences, by chromatin compaction and chromatin folding into 3D structures (**Figure 8**)(reviewed in (Cavalli and Misteli, 2013)).

DIRECT REGULATION: PROMOTORS AND TRANSCRIPTION FACTORS

In a simplistic view, the promoter is a regulatory sequence that locates usually upstream of the gene and serves as a site for transcription initiation through the binding of the enzyme RNA polymerase. The binding of specific proteins, named transcription factors (TFs) regulates the rate of transcription. Whether they enhance or block transcription, TFs are considered as activators or repressors (**Figure 8**). Activators may help the recruitment and assembly of the transcription machinery to ensure efficient gene expression, while repressors impede their binding and inhibit gene transcription. The interplay between various TFs and gene promotors impacts the overall pattern of gene expression driving cell fate at specific developmental stages and in specific tissues (D'Alessio et al., 2009; Spitz and Furlong, 2012; Slattery et al., 2014).

CHROMATIN STATE: EUCHROMATIN VERSUS HETEROCHROMATIN

The expression of genes also depends on the local composition of chromatin. The compaction of chromatin inside the nucleus is mediated by the wrapping of DNA around a set of eight histones forming a scaffold unit, the nucleosome (van Holde, 1989; Kornberg, 1974; Arents and Moudrianakis, 1993) (**Figure 8**). Posttranslational modifications of histones, such as acetylation or methylation, serve as sites for specific protein binding which influence the degree of chromatin compaction (Berger, 2007; Rando and Chang, 2009) and control important functions as replication, transcription and DNA-repair (reviewed in (van Attikum and Gasser, 2005; Pandita and Richardson, 2009; Zhu and Wani, 2010; Lawrence et al., 2016). Those are considered as epigenetic marks.

Chromatin condensation is subdivided in two states referred as euchromatin and heterochromatin (**Figure 8**). The euchromatin is a relaxed and "open" configuration and associates mainly with active genes on chromosome arms. In contrast, the tightly packed heterochromatin is poor, even if not devoid of protein coding genes (Dimitri et al., 2003, 2009) and mainly contains DNA repeats. It is usually late-replicating and presents a high fluorescent signal when labelled with DNA intercalants in interphase - notably on polytene chromosomes. The heterochromatin constitutes 1/3 of the *Drosophila* genome and concerns nearly the whole Y chromosome, most of the 4 and telomeric and pericentric regions of the X and

autosomes. Heterochromatin covers 40% and 20% of the X and autosome chromosomes respectively (Smith et al., 2007). Due to its "close" configuration, heterochromatin and associated proteins are involved in gene silencing. Most epigenetic factors that favor the establishment and maintenance of euchromatin or heterochromatin were identified in screens for mutations that affect gene silencing due to position effect variegation (PEV) (detailed below). Thus, specific histone modifications are associated with different proteins that together will negatively or positively regulate gene expression.

Using genome-wide profiles of DNA-protein interactions, Filion and colleagues complexified this view and reported five types of chromatin state in *Drosophila*, named with colors: two euchromatin YELLOW and RED, two heterochromatin GREEN and BLUE, and one neutral BLACK (Filion et al., 2010). While the YELLOW chromatin corresponds to ubiquitously expressed genes, RED euchromatin present a more restricted expression pattern influenced by developmental stages and it is tissue specific. GREEN heterochromatin concerns constitutive heterochromatin, mainly on pericentric regions where it associates with the heterochromatin protein 1 (HP1). BLUE heterochromatin with associated proteins of the Polycomb Group (PcG) negatively regulates genes with developmental functions (Filion et al., 2010). Interestingly, it was previously shown that repressive marks PcG and HP1 heterochromatin do not overlap in the *Drosophila* genome (de Wit et al., 2007).

Position effect variegation. PEV is described as the stochastic silencing of a gene juxtaposed to heterochromatin regions. It occurs upon chromosome rearrangements, such as inversions or transpositions of DNA sequences containing genes that were initially located in euchromatin and that become near heterochromatin (reviewed in (Elgin and Reuter, 2013). The first evidence of PEV comes from studies on the *white* gene mutation that confers fly white eyes. After X-ray mutagenesis, Muller described a variegated phenotype in the fly eye color as it presented mosaicism of red and white patches (Muller, 1930). In screens analyzing this phenotypic variegation of reporter genes, hundreds of loci were identified and named Su(var) or E(var), for Suppressor or Enhancer of variegation, in which mutations result in the loss or increase of silencing, respectively (Sinclair et al., 1983; Birchler et al., 1994; Donaldson et al., 2002; Schotta et al., 2003; Schneiderman et al., 2010). Interestingly, similar mutations affecting coat color could be identified in mouse (Blewitt and Whitelaw, 2013).

3D ORGANIZATION: CHROMATIN FOLDING AND CHROMOSOME TERRITORIES

In addition to this linear view, epigenomic maps of histone modifications have shown that chromatin can also adopt 3D configurations and form regulatory domains that also affect gene expression patterns in *cis* and *trans*. This is possible by the activity and binding of specific proteins. For example, the insulators or chromatin boundaries fold the chromatin into loops and establish long-range contacts to ensure various functions (reviewed in (Hou et al., 2012)) (**Figure 8**). Insulators can block the spreading of heterochromatin and inhibits PEV (Roseman et al., 1993; Schwartz et al., 2012), shorten the distances and bring closer enhancers or TFs to distant promotors to enhance activation or repression (Cai and Shen, 2001; Muravyova et al., 2001; Li et al., 2011, 2013a) (**Figure 8**). Conversely, they can also separate epigenetic domains to inhibit their interactions (Holdridge and Dorsett, 1991; Kellum and Schedl, 1991, 1992; Geyer and Corces, 1992; Cai and Levine, 1995). Interestingly, insulators allow long-range contacts between regions of the same (Sexton et al., 2012) or in different chromosomes (Schoenfelder et al., 2015).

Chromatin organization is influenced by its position within the nucleus. For example, in the *Drosophila* embryo heterochromatin locates on one side of the nuclear periphery and this organization persists during development (Foe and Alberts, 1985). Such specific compartments may favor the repression capacity by concentrating repressive factors. Indeed, it was shown that PEV also occurs for distant genes that through 3D organization locates near heterochromatin masses. Microscopy studies indeed revealed the non-random positioning of certain loci within nucleus and chromosomal territories (Cremer et al., 2006; Parada et al., 2004) (**Figure 8**). Hi-C technologies that capture chromosome conformation further described the existence of physical domains called topologically associating domains in mammals (Hou et al., 2012; Sexton et al., 2012; Dixon et al., 2012; Nora et al., 2012).

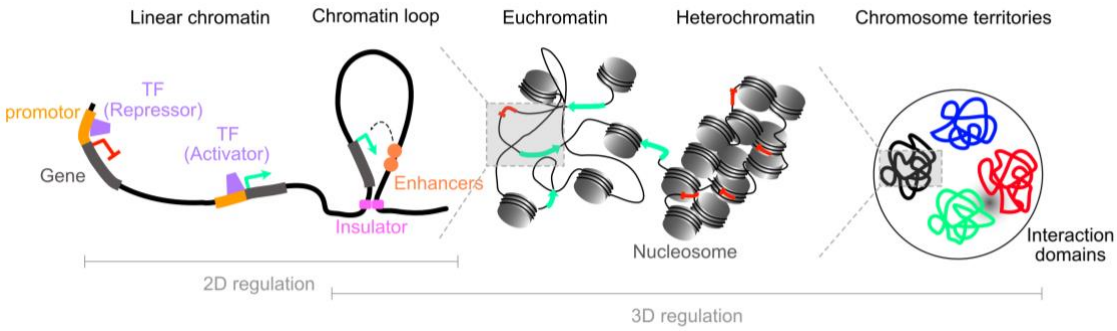

Figure 8. Different scales for chromatin organization. Schematic representation of chromatin organization and main actors controlling gene expression. TFs directly activate or repress gene expression through interaction with gene regulatory sequences such as promotors. Insulators fold chromatin into loops for linear long-range contacts between genes and enhancers for example. The chromatin wrapped into nucleosomes, presents different degree of compaction: the "open" conformation euchromatin favors gene expression (turquoise arrows) while highly compacted heterochromatin correlates with gene repression (red bars). Inside the nucleus, chromatin adopts a 3D conformation forming specific interaction domains and compartments as chromosome territories.

3.2. Epigenetic landscape establishment: from stem to differentiated state

3.2.1 The balance between proliferation and differentiation

All multicellular organisms originate from one unique totipotent cell, the fertilized egg. This single cell divides to generate a large number of cells that ultimately will acquire post-mitotic states with different specialized functions and populate different organs and tissues. These different cell types emerge from the establishment of specific developmental programs, through which cells acquire novel gene expression pattern driving changes in their morphology and function. Proliferation and differentiation are opposite as gradual process of differentiation inversely correlates with proliferation capacity. At terminal differentiation, cells permanently exit from the division cycle. The tune regulation of the temporal coupling of proliferation and differentiation is crucial for organ development but also for tissue homeostasis and regeneration. One regulator of this balance is the mode of cell division (**Figure 9**). In symmetric divisions, the two daughter cells will be identical, they will either remain stem cells and keep proliferating to increase stem cell pool or generate two more committed cells that either stop dividing and differentiate, or become a type of progenitor.

These transit-amplifying progenitors differentiate after few more divisions. In asymmetric division, the two daughters differ in fate, one remains a stem cell and continues to proliferate, the other enters a differentiation program. This latter allows the maintenance of the progenitor pool while generating differentiated cells (reviewed in (Morrison and Kimble, 2006)) (**Figure 9A**).

In the *Drosophila* larval brain, all NBs from the central brain (CB) and the optic lobe (OL) divide asymmetrically to generate more committed GMCs that will in turn, divide a few more times to give neurons and/or glia that will populate the brain (**Figure 9B**). This apico-basal polarity of NBs ensures the proper spindle orientation and consequently, the asymmetric inheritance of molecular factors that drive cell fate (reviewed in (Gonzalez, 2007; Gönczy, 2008; Chia et al., 2008; Knoblich, 2008)). Three major fate determinants, Numb, Brat and Prospero, act in suppressing proliferation and promoting differentiation (**Figure 9B**). For example, the TF Prospero promotes the activation of neuron-specific genes and specifies GMC identity, by the repression of NB-specific genes such as cell cycle genes (Li and Vaessin, 2000; Choksi et al., 2006). In embryos mutant for *prospero,* Cyclin E, Cyclin A and String/Cdc25 are upregulated, conversely ectopic *prospero* expression terminates the expression of those cell cycle genes (Li and Vaessin, 2000). In the *Drosophila* adult gut, resident intestinal stem cells (ISCs) participate to the normal turn over and regeneration upon injury or stress. Live-imaging analysis showed that ISCs can switch their mode of division for an adaptive response to food accessibility (O'Brien et al., 2011). In response to epithelial damage, ISCs asymmetrically divide to regenerate the tissue and many signaling pathways become activated to balance proliferation and differentiation (reviewed in (Jiang et al., 2016)). Interestingly, in a recent study mapping chromatin state, authors reported the control of ISC proliferation by epigenetic modifications, without affecting differentiation (Gervais et al., 2019).

Deregulation of this equilibrium has severe impact on tissue integrity as it can induce over-proliferation of stem cells and tumorigenesis. In the brain, defective asymmetric division induces the uncontrolled proliferation of NB-like cells and the concomitant loss of differentiated cells (**Figure 9C**), which lead to brain tumor formation in transplantation assays (Caussinus and Gonzalez, 2005) or directly *in situ* (reviewed in (Januschke and Gonzalez, 2008)).

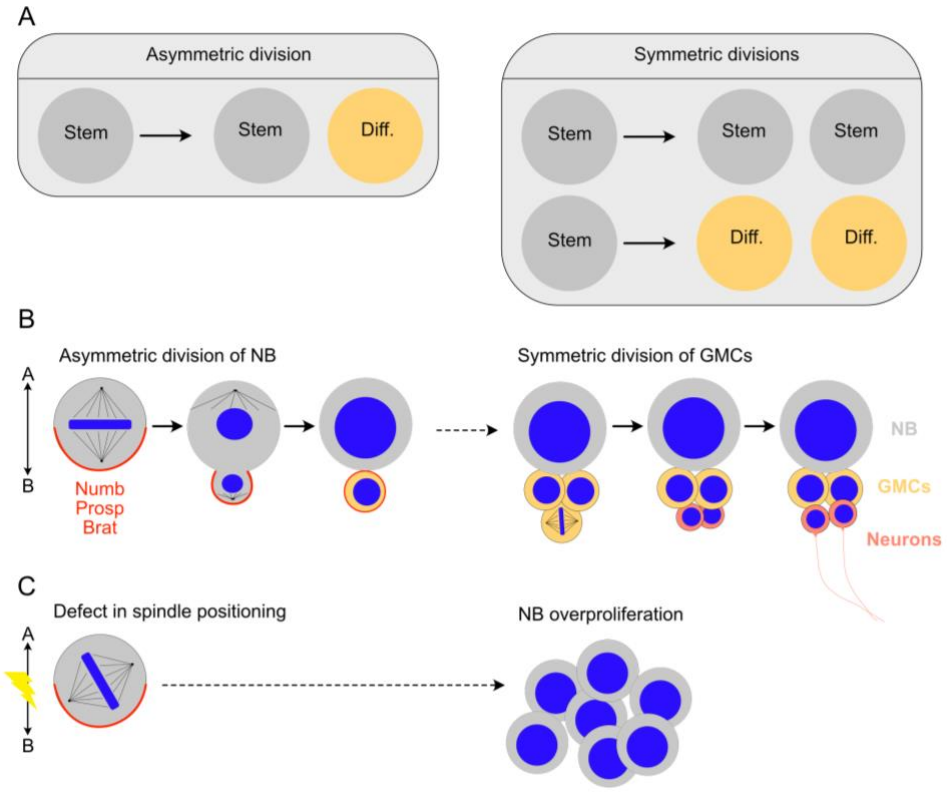

Figure 9. Different modes of cell division. Schematic representations of symmetric and asymmetric divisions. (A) Asymmetric division of stem cells generates daughter cells that differ in fate: one cell remains a stem cell and the other cell will undergo differentiation. In contrast, upon symmetric divisions, the two daughters are identical in fate. They can maintain stem cell fate and keep proliferating or enter the differentiation program. (B) NBs divide asymmetrically generating a new NB and a more committed GMC. This is allowed by asymmetric inheritance of specific fate determinants (Numb, Prospero and Brat for examples) due to the establishment of an apico-basal polarity in NB and the correct positioning of the mitotic spindle. Then GMCs divide one more time, before giving rise to terminally differentiated neurons and/or glia. (C) Defects in spindle positioning disrupt the inheritance of fate determinants and can lead to NB over-proliferation.

3.2.2. Gene expression pattern establishment

SPATIAL AND TEMPORAL PATTERNING OF NEURONAL DIFFERENTIATION.

The establishment of appropriate developmental programs are tightly controlled in space and in time. The temporal information is required for the timely regulation of progeny generation and differentiation. The first description of temporal patterning was related with embryonic NBs of the *Drosophila* central nervous system (CNS) (reviewed in (Doe, 2017)), through the discovery of the sequential expression of temporal TFs in parent NBs and inherited by their progeny (Kambadur et al., 1998; Brody and Odenwald, 2000; Isshiki et al., 2001; Novotny et

al., 2002; Pearson and Doe, 2003; Grosskortenhaus et al., 2005, 2006; Baumgardt et al., 2009; Benito-Sipos et al., 2010). Interestingly, perturbing a given TF does not affect temporal series progression but only results in the loss of one temporal identity (Brody and Odenwald, 2000; Isshiki et al., 2001; Grosskortenhaus et al., 2006; Maurange et al., 2008; Tran and Doe, 2008). In addition, NBs can share the same temporal series of certain TFs. Thus, combination of temporal and spatial axes of NBs specify progeny fate and explain the wide variety of neurons (reviewed in (Maurange, 2012)). The positional information of all NBs of the CB and ventral nerve cord (VNC) is established at the embryonic stage (Doe, 1992; Doe and Technau, 1993; Broadus and Doe, 1995; Bossing et al., 1996; Schmidt et al., 1997; Urbach and Technau, 2003). Importantly, temporal and spatial specification continues in post-embryonic neurogenesis, in the CB (Maurange et al., 2008) and OL (Li et al., 2013d; Erclik et al., 2017). The OL, responsible for the development of the visual system of the fly, is a striking example. The integration of temporal patterning (Li et al., 2013d; Suzuki et al., 2013) that drives the cascade of a variety of TFs with spatial cues (Erclik et al., 2017) (**Figure 10**) continuously produce an enormous diversity of neurons (60,000 neurons per lobe and around 200 morphologically distinct neuronal types) reviewed in (Holguera and Desplan, 2018)).

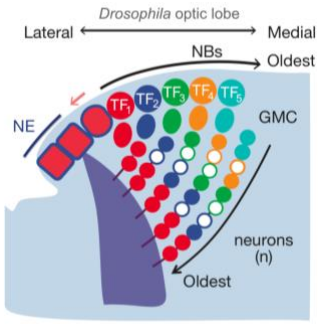

Figure 10. Temporal patterning of *Drosophila* NBs in the OL. Schematic and simplistic representation of the temporal patterning responsible for neuronal diversity of the *Drosophila* visual nervous system. Proliferative NBs of the OL sequentially express different TFs that, inherited by daughters will drive neuron specificity. (NE: neuroepithelium; TF: Transcription factor; NB: Neuroblast and GMC: Ganglion mother cell). (adapted from (Li et al., 2013d).

CHROMATIN REMODELING DURING DEVELOPMENT AND AGING

Differentiation programs are not only achieved by TFs but are also accompanied by concomitant changes in chromatin state. The first evidence of chromatin remodelling comes from imaging of heterochromatin and its differential distribution in post-mitotic cells (Francastel et al., 2000; Le Gros et al., 2016). The genome-wide chromatin mapping revealed that specification was associated with chromatin restriction during development. Analysis of several systems reported a more accessible chromatin in pluripotent embryonic stem cells

(ESCs) that become more compacted in committed cells (Francastel et al., 2000; Arney and Fisher, 2004; Meshorer et al., 2006; Meshorer and Misteli, 2006; Zhu et al., 2013). This “open” chromatin configuration reported in ESCs may reflect a permissive state allowing the rapid establishment of any of the multiple differentiation programs (discussed in (Gaspar-Maia et al., 2011). Chromatin immunoprecipitation followed by sequencing (ChIP-seq) (Mikkelsen et al., 2007), and Hi-C technics (Dixon et al., 2015) confirmed that upon developmental processes, chromatin faces changes in its composition (histone modifications) and 3D architecture, respectively. To further investigate chromatin states and identify “open” regions, several assays for chromatin accessibility were developed, based on analysis of nucleosome-free and unprotected DNA for examples (reviewed in (Tsompana and Buck, 2014)).

In *Drosophila*, chromatin accessibility and protein-DNA binding-profiles have been used to map chromatin landscape variations across developmental stages and among cell types in embryo (Ye et al., 2017) and larval stages (Marshall and Brand, 2017; Aughey et al., 2018). Marshall and colleagues reported a large-scale remodelling of the chromatin across *Drosophila* neural cell lineages (NBs, GMCs, immature and mature neurons), by analysing the redistribution of chromatin remodelers that characterise the five chromatin types. Interestingly, authors showed that repressive marks differ depending on the cell type. In neurons, HP1 silences genes involved in NSC identity, while Thritorax group (TrxG) or Black chromatin turn off genes essential for neuronal fates in NBs. PcG, in turn, was shown to regulate the lineage specific transcription factors of the spatial and temporal patterning in the OL (Marshall and Brand, 2017). Another chromatin accessibility profiling *in vivo* confirmed this dynamic chromatin remodeling across development stages in the *Drosophila* CNS, which also occurs in gut lineages. In addition, they confirmed that in stem cells the chromatin accessibility is globally increased and identified cell type specific enhancers and regulator elements that influence their accessibility (Aughey et al., 2018). As a complementary study, authors performed a ChIP-seq in *Drosophila* NC lineages to obtain histone modification profiling (Abdusselamoglu et al., 2019). At adulthood, chromatin remodelling also occurs and was shown to be linked to aging (reviewed in (Abdul Halim et al., 2020) . Changes in the regulation of histone methylation and heterochromatin affect *Drosophila* lifespan. For example, an increase in HP1 levels slowers senescence, while HP1 reduction and thus, decrease in heterochromatin levels is associated with aging (Larson et al., 2012). In addition, depletion of

histone demethylases also negatively influence fly longevity as it was shown to activate certain anti-aging genes (Lorbeck et al., 2010). Changes in deposition of histones modifications, binding and function of chromatin remodelers and consequent chromatin accessibility may drive a certain level of chromatin plasticity essential during development but also throughout life.

3.3. Cellular memory: Epigenetic stability versus plasticity

In terminally differentiated cells, establishment of novel and proper epigenetic marks stably install gene expression patterns, necessary for cell function and integrity. In proliferative cells epigenetic marks also establish and can be inherited and maintained over cycles. The maintenance of cell potential in absence of initial signals is crucial. The propagation of epigenetic programs throughout development and life is known as cellular memory. It requires regulation by the TrxG and PcG complexes that recognize chromosomal elements, the Cellular Memory Modules (CMMs) (Moehrle and Paro, 1994; Simon and Tamkun, 2002; Ringrose and Paro, 2007; Steffen and Ringrose, 2014). The first example of cellular memory comes from *Drosophila* embryogenesis, when expression of segmentation genes initiates and spatially restricts the expression pattern of developmental regulators, as the homeotic genes (Ingham and Martinez Arias, 1992). Later, the signal turns over and this transcriptional memory is maintained by TrxG and PcG proteins (reviewed in (Francis and Kingston, 2001). This cellular memory is not restricted to embryonic development but also freezes developmental decisions and pattern in larval wing discs for example (Maurange and Paro, 2002). Inheritance of epigenetic marks over generations requires mechanisms that propagate their signal through replication and mitosis. For example, PcG proteins spread using their DNA-binding factors and the loss of the DNA sequence elements induces the loss of PcG-dependent gene silencing in a few divisions (Coleman and Struhl, 2017; Laprell et al., 2017).

In contrast, there are also examples of epigenetic instability, as in *Drosophila* follicle stem cells. Skora and Spradling observed variegation of GFP intensity driven by the GAL4/UAS and showed that daughter cells randomly acquire changes in transgene programming. Interestingly, authors demonstrated that epigenetic stability increases with differentiation and correlates with S-phase length (Skora and Spradling, 2010). Certain levels of epigenetic

flexibility and plasticity in progenitors may favor reprogramming and adaptability to environmental stress for example.

The impact of environmental stimuli on epigenetic landscape was highlighted by the change in PEV silencing depending on the temperature of fly development. Indeed, high developmental temperature (25°C) suppresses variegation, while lower temperatures (14°C or 19°C) increase silencing (Hartmann-Goldstein, 1967). Using a reporter gene system, I also confirmed the environmental influence on gene expression pattern in *Drosophila* larval brain (*Chapter 2 - Results – Section B*;(Goupil et al., 2020b)). Interestingly, phenotypic variability deriving from environmentally-induced epigenetic variations can be transgenerational inherited. Toxic challenges upon fly development induced epigenetic changes and phenotypic variations that may reflect increased tolerance to stress (Stern et al., 2012). Heat- and osmotic shock of the *Drosophila* embryo strongly disrupts heterochromatic formation by phosphorylation of the yeast homolog of activation transcription factor-2 (dATF-2), involved in heterochromatin maintenance (Seong et al., 2011). In both studies, stress-induced epigenetic events (Seong et al., 2011) and phenotypic variability (Stern et al., 2012) were transmitted to following generations. In addition, the paternal diet was shown to reprogram epigenetic marks, notably histone modifications, and induced obesity propensity in the offspring (Öst et al., 2014). These data confirmed the importance of epigenetic plasticity for adaptability that can subsist across generations. However, even though several studies linked environment to epigenetic regulation, understanding the impact of multifactorial exposure remains challenging.

Chapter 2 – Results

Chapter 2 - Results – *Section A*

Article – Goupil, Nano et al. 2020 - Journal of Cell Biology

"Chromosomes function as a barrier to mitotic spindle bipolarity in polyploid cells"

JCB Journal of Cell Biology

ARTICLE

Chromosomes function as a barrier to mitotic spindle bipolarity in polyploid cells

Alix Goupil*[1], Maddalena Nano*[1], Gaëlle Letort[2], Simon Gemble[1], Frances Edwards[1], Oumou Goundiam[1,3], Delphine Gogendeau[1], Carole Pennetier[1], and Renata Basto[1]

Ploidy variations such as genome doubling are frequent in human tumors and have been associated with genetic instability favoring tumor progression. How polyploid cells deal with increased centrosome numbers and DNA content remains unknown. Using *Drosophila* neuroblasts and human cancer cells to study mitotic spindle assembly in polyploid cells, we found that most polyploid cells divide in a multipolar manner. We show that even if an initial centrosome clustering step can occur at mitotic entry, the establishment of kinetochore-microtubule attachments leads to spatial chromosome configurations, whereby the final coalescence of supernumerary poles into a bipolar array is inhibited. Using in silico approaches and various spindle and DNA perturbations, we show that chromosomes act as a physical barrier blocking spindle pole coalescence and bipolarity. Importantly, microtubule stabilization suppressed multipolarity by improving both centrosome clustering and pole coalescence. This work identifies inhibitors of bipolar division in polyploid cells and provides a rationale to understand chromosome instability typical of polyploid cancer cells.

Introduction

Polyploidy is a condition in which the entire duplicated chromosome set is maintained within a single cell (Frawley and Orr-Weaver, 2015). Polyploidy can be programmed and regulated. It is a strategy normally employed during development to increase metabolic potential through endoreplication (Orr-Weaver, 2015). Further, the increase in cell size through polyploidization can confer barrier functions essential during organogenesis (Unhavaithaya and Orr-Weaver, 2012). In these contexts, however, polyploid cells have limited proliferative capacity. In what appears somewhat paradoxical, events of unscheduled polyploidization, such as whole genome duplications (WGDs), have been identified in a variety of tumors and have been associated with chromosome instability (CIN) and poor prognosis (Bielski et al., 2018; Zack et al., 2013). Importantly, polyploid cells generated through cytokinesis failure give rise to tumors when transplanted subcutaneously into nude mice (Fujiwara et al., 2005), highlighting the transformation capacity of polyploid cells.

Concerning polyploidization through cytokinesis failure, it is important to take into account the increase in centrosome number. Each centrosome is composed of two centrioles surrounded by pericentriolar material (PCM), which is the site of microtubule (MT) nucleation (Conduit et al., 2015). Centrosomes are normally duplicated only once during each cell cycle. This ensures that during mitosis, two centrosomes localized at opposite poles can sustain bipolar spindle assembly. In cells with supernumerary centrosomes, bipolar spindles can assemble thanks to centrosome clustering, an active process by which supernumerary centrosomes gather to form a single microtubule organizing center (MTOC; Basto et al., 2008; Ganem et al., 2009; Godinho et al., 2014; Kwon et al., 2008; Marthiens et al., 2012; Quintyne et al., 2005; Rhys et al., 2018; Silkworth et al., 2009). However, little is still known about centrosome clustering in cells that also contain increased DNA content (Dewhurst et al., 2014; Duncan et al., 2010; Fox et al., 2010; Storchova and Pellman, 2004).

Here we have characterized mitosis in polyploid cells generated through cytokinesis failure. We found that the accumulation of extra centrosomes and chromosomes leads to multipolarity in the majority of cases. Using genetic manipulations, laser ablation, and in silico approaches, we identified parameters that lead to multipolarity in polyploid cells. Interestingly, our work identifies MT stabilization as a suppressor of multipolarity, which might have important implications during tumorigenesis.

[1]Institut Curie, Paris Science et Lettres Research University, Centre National de la Recherche Scientifique, Unité Mixte de Recherche UMR144, Biology of Centrosomes and Genetic Instability Laboratory, Paris, France; [2]Center for Interdisciplinary Research in Biology, Collège de France, UMR7241/U1050, Paris, France; [3]Department of Translational Research, Institut Curie, PSL University, Paris, France.

*A. Goupil and M. Nano contributed equally to this paper; Correspondence to Renata Basto: renata.basto@curie.fr; Maddalena Nano: mnano@ucsb.edu; M. Nano's present address is Molecular, Cellular, and Developmental Biology Department, University of California, Santa Barbara, Santa Barbara, CA.

Results

Polyploid mitoses are multipolar

Polyploidy can have important physiological roles in many animals and plants (Frawley and Orr-Weaver, 2015). It can be generated through different means such as endoreplication or endomitosis (Orr-Weaver, 2015). Here we focus our analysis of polyploid cells generated through cytokinesis failure. To characterize cell division in polyploid cells, we chose to use an in vivo model system that is permissive to cytokinesis failure, the *Drosophila* neural stem cells of the developing larval brain, also called neuroblasts (NBs; Gatti and Baker, 1989; Somma et al., 2002; Straight et al., 2005). We induced cytokinesis failure through Pavarotti (Pav; the *Drosophila* homologue of MKLP1; Adams et al., 1998) knock-down (KD) by inducible RNAi. Pav^{KD} third instar brains revealed the presence of NBs of various sizes, indicative of different degrees of polyploidy, containing large amounts of DNA and increased centrosome numbers (Fig. 1, A–C). In this way, we generated polyploidy through cytokinesis failure in cells that are normally diploid. To facilitate comprehension, Pav^{KD} NBs will be referred simply as polyploid NBs.

To characterize mitosis by time-lapse microscopy, we used fly lines expressing transgenes encoding α-tubulin tagged with GFP (tubulin-GFP) and Histone H2Av variant tagged with RFP (histone-RFP). These allowed us to monitor spindle MTs and chromosomes, respectively. Control (Ctrl) diploid NBs divided asymmetrically, as described previously (Homem and Knoblich, 2012; Ikeshima-Kataoka et al., 1997; Fig. 1 D and Video 1). In polyploid NBs, several active MT-nucleating centrosomes were identified, and their number was increased in larger polyploid NBs (compare Fig. 1, E and F; and Video 1). Polyploid NBs presented multiple nuclei that entered mitosis in an asynchronous manner, as described using other genetic means of inducing polyploidy (Nano et al., 2019). After nuclear envelope breakdown (NEBD), extra centrosomes clustered in more than two groups, while chromosomes condensed and adopted a multilobed arrangement within a multipolar spindle, frequently centered within the cytoplasm. These multipolar configurations were never resolved into bipolar configurations, because multiple spindle poles failed to coalesce and were maintained as active MTOCs. Importantly, most polyploid anaphases were multipolar and generated several nuclei at mitotic exit (Fig. 1, E–G; and Video 1). These results are surprising, since in diploid NBs with centrosome amplification, induced through Sak, the PLK4 homologue, overexpression (SakOE), extra centrosomes always clustered in two major poles, and NBs invariably divided in a bipolar manner (Basto et al., 2006). The coalescence of spindle poles has been shown to favor the conversion of multipolar spindles into pseudo-bipolar or bipolar spindles in cancer cells (not polyploid) with extra centrosomes (Ganem et al., 2009; Silkworth et al., 2009). Together, our results suggest that bipolar spindle assembly in polyploid NBs, which requires a final step in spindle pole coalescence, is inhibited by the presence of extra DNA.

Characterization of polyploid mitosis

The analysis of polyploid NBs described above suggested a possible correlation between cell size and the degree of polyploidy. This was indeed the case, as DNA area correlated with cell area in polyploid NBs (Fig. 2 A). We next analyzed mitotic duration, defined as the time elapsed between NEBD and anaphase onset. We found that the large majority of polyploid NBs took more time to divide than Ctrl NBs (Fig. 2 B). Interestingly, this increased mitotic duration did not necessarily correlate with the degree of polyploidy. Small polyploid cells could take longer than larger cells to divide (Fig. 1, E and F; and Fig. 2 C). The increase in mitotic timing is a known feature of cells with extra centrosomes (Basto et al., 2008; Kwon et al., 2008), where it reflects a delay in satisfying the spindle assembly checkpoint (SAC), which monitors kinetochore-MT attachments (Musacchio, 2015). The observations reported here suggest that in polyploid cells, achieving accurate kinetochore-MT attachments takes longer than in diploid cells, independently of the degree of polyploidy.

We then wanted to assess the outcome of polyploid mitosis. While canonical cell division results in the separation of one nucleus in two daughter nuclei, polyploid mitosis frequently began with, and generated, multiple nuclei. To quantitatively assess the outcome of mitosis, we defined a parameter that we called nuclear index (NI). The NI was calculated as the ratio between the number of nuclei at anaphase and the number of nuclei at mitotic entry, divided by the number of daughter cells (see Materials and methods for details; Fig. 2 D). This allows us to distinguish between polyploid (only one daughter cell in our experimental setup) and diploid cells (two daughter cells). In diploid NBs, the NI was always 1, as NBs with one nucleus gave rise to two daughter NBs with one nucleus each after bipolar divisions. In contrast, in polyploid NBs that always started mitosis with at least two nuclei (generated through cytokinesis failure), the NI values spread between <1 and 4. A NI <1 or NI = 1 reflected a reduction or maintenance in the number of nuclei at anaphase when compared with mitotic entry. However, the vast majority of cells displayed a NI >1, showing that, in a given cell, the number of nuclei increased at mitotic exit (Fig. 2, D and E). Interestingly, we noticed a positive correlation between the number of nuclei at mitotic exit and cell area (Fig. 2 F). Very large cells (>4,000 μm^2), which contained more centrosomes and chromosomes than smaller polyploid cells, generated a higher number of nuclei at mitotic exit than smaller polyploids. These results suggest that the degree of polyploidy impacts the outcome of nuclear divisions, with more nuclei being generated at each cell cycle.

Probing the contribution of individual MT nucleation pathways to multipolarity in polyploid NBs

At least three pathways contribute to MT nucleation during mitosis in animal cells (Hayward et al., 2014; Prosser and Pelletier, 2017). We hypothesized that the multipolar outcome typical of polyploid NB mitosis could result from an excess of MTs nucleated from extra centrosomes, chromosomes, or pre-existing MTs. We tested their contribution by decreasing the expression of key players in each pathway individually.

We first ascertained the contribution of the centrosomal pathway. To reduce centrosome-dependent MT-nucleation, we used a mutation in the *sas-4* gene (Centrosomal P4.1-associated protein in humans), which encodes an essential centriole duplication gene (Basto et al., 2006; Kirkham et al., 2003). Small to medium size polyploid, $sas4^{mut}$ NBs started by assembling an amorphous MT-structure around the DNA. Surprisingly, this structure evolved into an almost perfect bipolar spindle, forming an array similar to the

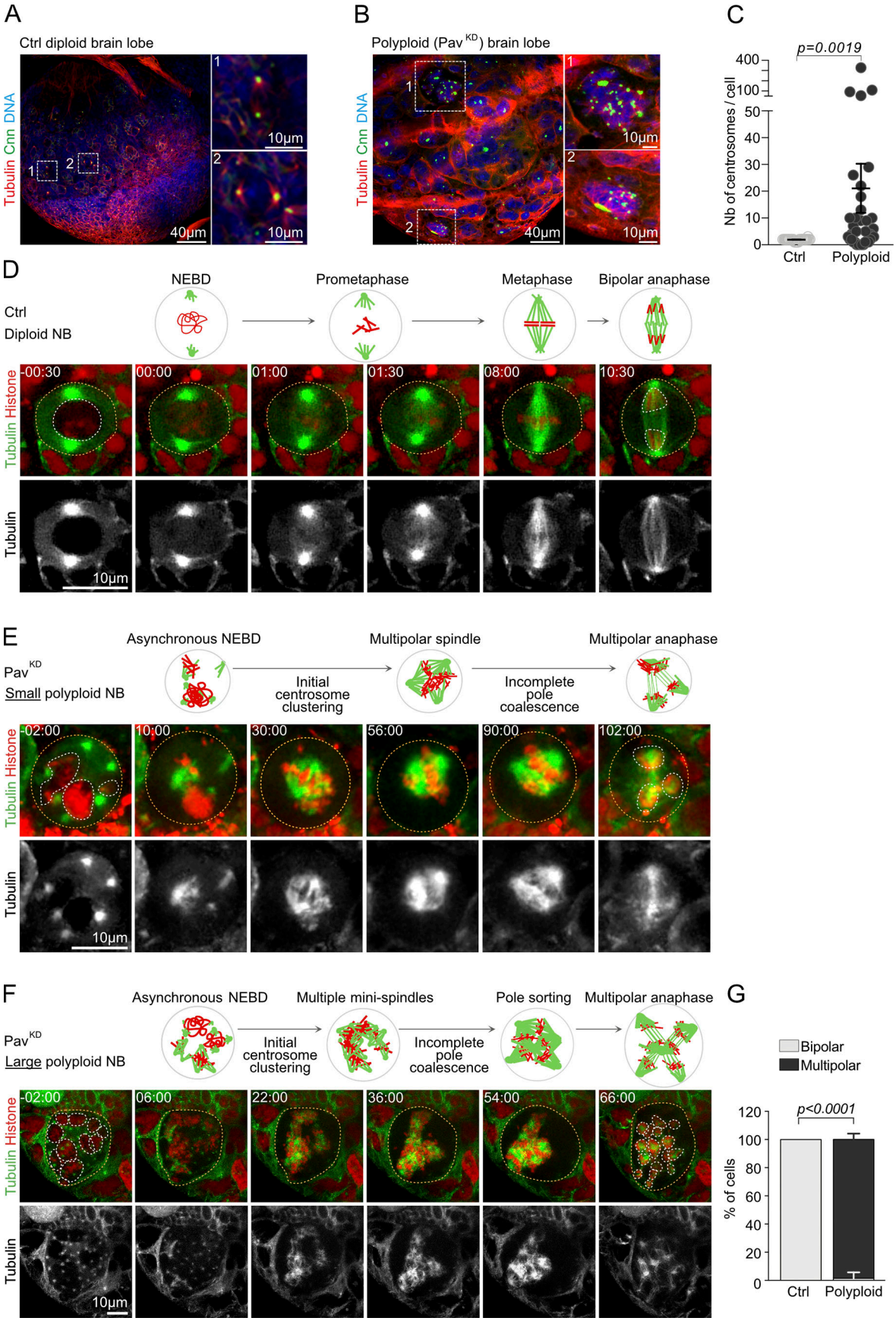

Figure 1. **Polyploid NBs undergo multipolar mitosis. (A and B)** Images of whole mount diploid (A) and polyploid (B) brain lobes (BL) and NBs (insets) labeled with antibodies against α-tubulin (red) and Cnn (green). DNA in blue. **(C)** Dot plot of centrosome number (Nb) per Ctrl (n = 30 NBs from 4 BL) and polyploid (n = 38 NBs from 10 BL) NBs. Statistical significance was determined using a t test. **(D–F)** Stills of time-lapse videos of mitotic NBs expressing tubulin-GFP (green and gray in the bottom insets) and histone-RFP (red). Orange and white dotted circles surround cells and nuclei, respectively. Time of mitosis is indicated in minutes:seconds. Time 00:00 corresponds to NEBD. Schematic representations above the stills. **(D–F)** Ctrl diploid (D), small (E), and large (F) polyploid NBs. **(G)** Percentage of cells in each category in Ctrl (n = 34 NBs from 2 BL) and polyploid NBs (n = 107 NBs from 37 BL). Statistical significance by a multiple t test. Error bars represent the mean ± SD and p the P value.

one observed in diploid, *sas4*^{mut} NBs, albeit larger (Fig. 3 A, Fig. S1 A, and Video 2). However, the ability of centrosome loss to sustain bipolar spindle assembly was limited by cell size. Medium or large polyploid, *sas4*^{mut} NBs divided in a multipolar manner even in the absence of centrosomes or when centrosome number was highly reduced (Fig. 3, B and C; and Video 2). Mitotic timing was decreased in polyploid, *sas4*^{mut} NBs when compared with polyploid NBs (Fig. 3 D and Table S1). Consistent with a decrease in multipolarity, the number of nuclei generated at anaphase was lower but still correlated with cell area (Fig. 3 E). Further, polyploid, *sas4*^{mut} NBs presented a high proportion of cells with a NI ≤ 1 (Fig. 3 F), confirming that a reduction in centrosome number in polyploid cells promotes the generation of fewer nuclei at mitotic exit. We concluded that MT nucleation from the centrosomes contributes to the assembly of multipolar spindles in polyploid NBs.

In contrast to the centrosomal pathway, reducing the Augmin or chromatin-mediated MT-nucleation pathways (CMP) did not reduce multipolarity. We used previously validated RNAi tools to deplete Mars and the Augmin Dgt2 subunit (Goshima et al., 2008; Hayward et al., 2014). Polyploid, Mars^{KD} and polyploid, Aug^{KD} NBs always divided in a multipolar fashion, while respective diploid conditions always divided in a bipolar manner (Fig. S1, B–F; and Videos 3 and 4). Manipulation of either of these pathways did not reduce the NI in polyploid NBs but impacted the mitotic timing in opposite directions. The mitotic timing was reduced in polyploid, Mars^{KD}, while it increased in polyploid, Aug^{KD} (Fig. S1, G–I). Interestingly, in certain polyploid, Mars^{KD} NBs and polyploid, Aug^{KD} NBs, we noticed the presence of several individual spindles that assembled between the main spindle and the cell cortex (Fig. S1, C and E, white arrows). These

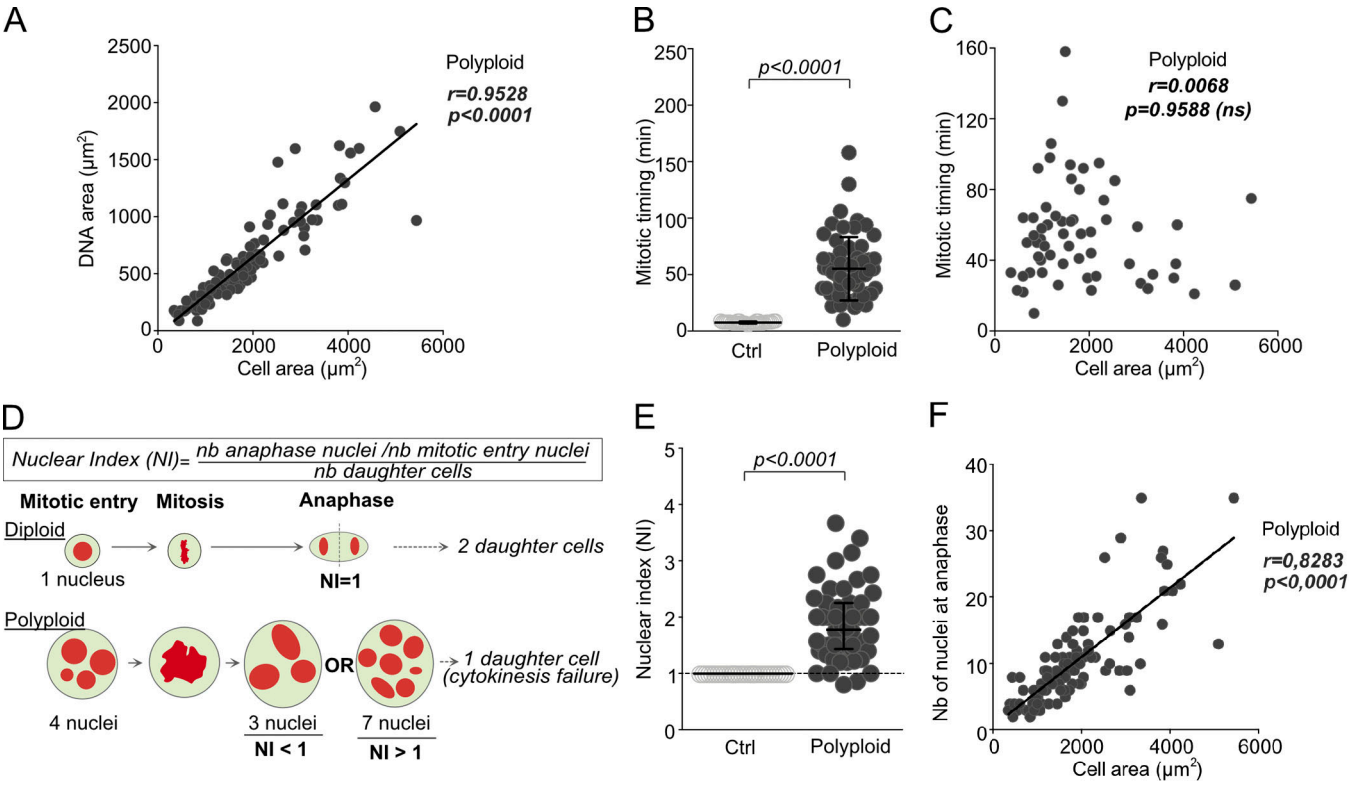

Figure 2. **Characterization of polyploid mitosis in *Drosophila* NBs. (A)** XY plot representing DNA and cell area in polyploid NBs (n = 112 NBs from 37 BL). **(B)** Dot plot showing the time spent in mitosis for Ctrl (n = 34 NBs from 2 BL) and polyploid (n = 60 NBs from 31 BL) NBs. **(C)** XY plot representing the mitotic timing and cell area (n = 60 NBs from 31 BL). **(D)** Schematic representation of NI calculation. **(E)** Dot plot of NI in Ctrl (n = 34 NBs from 2 BL) and polyploid NBs (n = 54 NBs from 28 BL). **(F)** XY plot of nuclei at anaphase and cell area (n = 107 NBs from 37 BL). **(B and E)** Statistical significance by a Mann-Whitney test. Error bars represent the mean ± SD (B) and the median ± interquartile range (E). **(A, C, and F)** Statistical significance of the correlation by a Spearman r test. ns, not significant; p, P value; r, correlation coefficient; Nb, number.

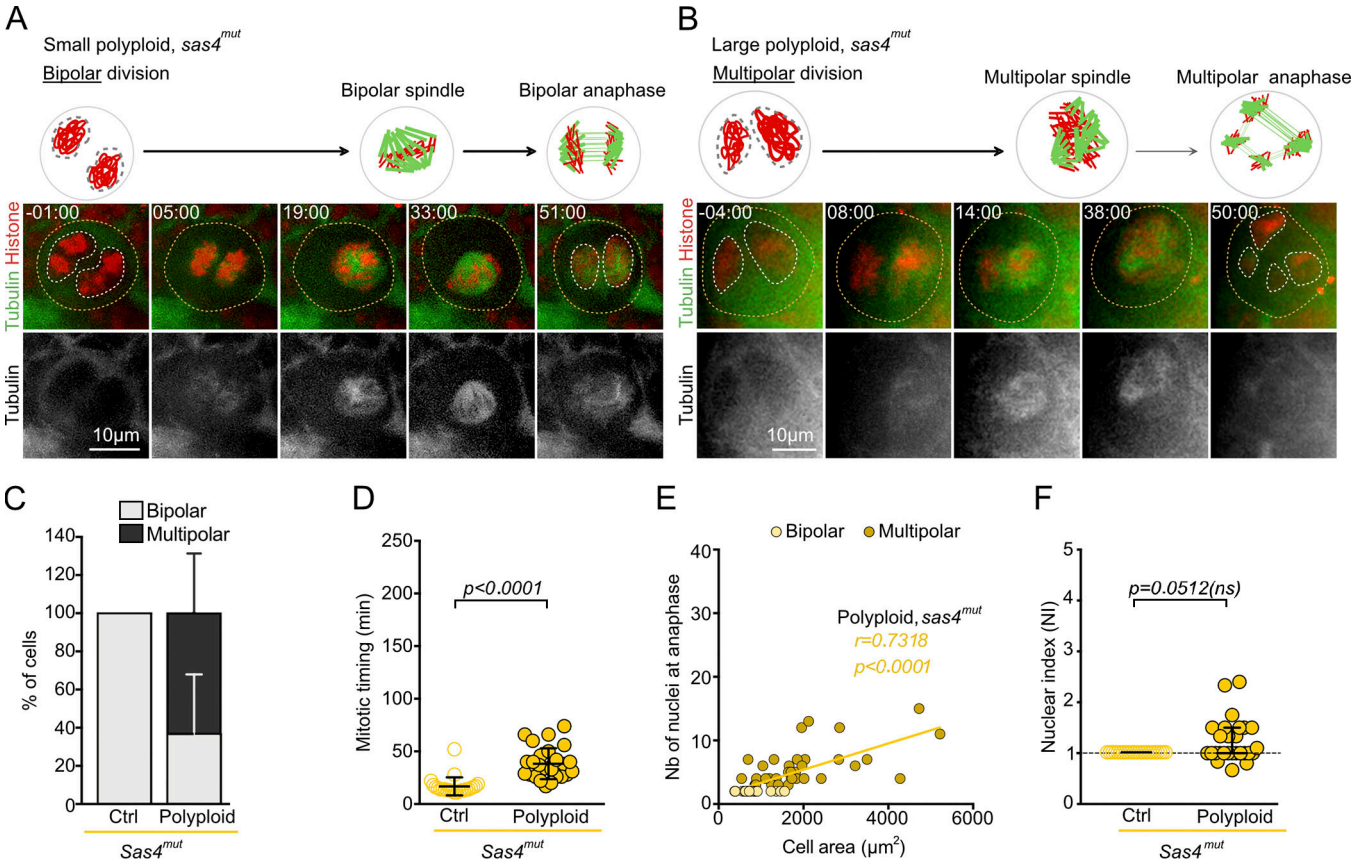

Figure 3. **Small polyploid NBs without centrosomes divide bipolarly. (A and B)** Stills of time-lapse videos of mitotic small (A) and large (B) polyploid, *sas4*^{mut} NBs expressing tubulin-GFP (green and gray in the bottom insets) and histone-RFP (red). Orange and white dotted circles surround cells and nuclei, respectively. Time of mitosis is indicated in minutes:seconds. Time 00:00 corresponds to NEBD. Schematic representations of mitosis above the stills. **(C)** Graph bars showing the percentage of cells in each category in Ctrl, *sas4*^{mut} (n = 23 NBs from 5 BL), and polyploid, *sas4*^{mut} (n = 56 NBs from 22 BL) NBs. **(D)** Dot plot showing the time spent in mitosis for Ctrl, *sas4*^{mut} (n = 23 NBs from 5 BL), and polyploid, *sas4*^{mut} (n = 28 NBs from 14 BL) NBs. **(E)** XY plot of nuclei at anaphase and cell area (n = 56 NBs from 22 BL). Statistical significance of the correlation by a Spearman r test, r corresponds to the correlation coefficient. **(F)** Dot plot of NI in Ctrl, *sas4*^{mut} (n = 23 NBs from 5 BL), and polyploid, *sas4*^{mut} (n = 28 NBs from 14 BL) NBs. **(D and F)** Statistical significance by a Mann-Whitney test. Error bars represent the mean ± SD (D) and the median ± interquartile range (F), p the P value. ns, not significant.

results show that the centrosomal pathway is the major contributor to multipolarity in polyploid mitosis.

Centrosome clustering takes place in polyploid mitosis, but it is not sufficient to promote bipolar spindle assembly

In cells with extra centrosomes, the minus-end directed kinesin Ncd (*Drosophila* orthologue of HSET/ KIFC1) plays an essential role in centrosome clustering (Basto et al., 2008; Kwon et al., 2008; Rhys et al., 2018). We induced polyploidy in *ncd* mutants (*ncd*^{mut}; Endow and Komma, 1998) and readily noticed that after NEBD, in polyploid, *ncd*^{mut} NBs, centrosomes did not cluster. Instead, they formed individual and independent poles, leading to the formation of a network of multiple mini-spindles, which remained connected to each other. As cells progressed through mitosis, this multipolar status was maintained, and nuclear divisions were always multipolar, while mitoses were always bipolar in diploid, *ncd*^{mut} NBs (Fig. S2, A, B, and E; and Videos 3 and 4). Although mitotic duration was increased in polyploid, *ncd*^{mut} NBs compared with diploid, *ncd*^{mut}, it was similar to polyploid NBs (Fig. S2 F and Table S1), suggesting that failure in the initial centrosome clustering step does not delay mitotic progression.

We reasoned that, in polyploid NBs, Ncd might be a limiting factor precluding pole coalescence into two main MTOCs. To test this possibility, we overexpressed Ncd (NcdOE). Diploid, NcdOE cells divided normally (Fig. S2 C and Video 3). However, multipolarity was maintained in polyploid, NcdOE NBs (Fig. S2, D and E; and Video 4). In both polyploid, *ncd*^{mut} and polyploid, NcdOE NBs, the number of nuclei at anaphase correlated with cell size. Importantly, a higher number of nuclei at anaphase was noticed in polyploid, *ncd*^{mut} NBs when compared with polyploid NBs even for cells of the same size (Fig. S2 G and Fig. 2 F), confirming the increase in multipolarity when Ncd is absent. Importantly, the NI in polyploid, *ncd*^{mut} NBs and polyploid, NcdOE was mostly >1 (Fig. S2 H). These results suggest that Ncd plays an essential role in the initial centrosome clustering step in polyploid mitosis. Further, they suggest that the second step of spindle pole coalescence is not limited by insufficient Ncd levels.

Centrosome number, DNA content, and chromosome shape influence the final step of spindle pole coalescence in polyploid cells

To further characterize spindle pole coalescence in polyploid NBs, we used Plp and Cnn to label centrioles and PCM. Mitotic

polyploid NBs contained condensed chromosomes arranged in a multilobed configuration separating large spindle poles, which could be visualized as large Cnn structures containing multiple Plp-positive dots (Fig. 4, A and B). We filmed brains expressing Histone-RFP and Spd2-GFP to label centrosomes. At mitotic entry, several centrosomes clustered in multiple poles, consistent with our previous observation that, by late prometaphase, each pole contained several clustered centrosomes. However, these poles did not coalesce, but remained separated by condensed chromosomes until anaphase onset, which was always multipolar (Fig. 4, C and D; and Video 5).

To identify the contributors of multipolarity and lack of spindle pole coalescence in polyploid cells, we established an in silico approach. We designed simulations using Cytosim, a cytoskeleton-dedicated agent-based software package (Nedelec and Foethke, 2007; see Materials and methods and Table S2 for details). Mitotic cells were considered as circular shapes (2D) with confined MTs, DNA, and motors. With the aim of validating the in silico approach, we configured a system where the number of centrosomes, modeled as asters nucleating MTs radially, was increased in conditions of fixed DNA content, modeled as mobile beads clustered as nuclei. At the start of the simulations, centrosomes were randomly positioned while DNA clusters were slightly centered. In the presence of a constant and high DNA level, simulations containing 10 centrosomes were mostly resolved in a bipolar spindle. However, an increase in centrosome number above a certain threshold highly reduced the bipolar outcome in favor of multipolar spindles (Fig. 4, E and F; and Video 6). This is in line with our observations in polyploid, *sas4*^{mut} NBs, as a decrease in centrosome number favored the formation of bipolar spindles. Next, we tested the consequences of DNA levels variation to a polyploid-like status (from 9 to 41 DNA beads), in conditions of high (30) centrosome number. In simulations containing ≤17 beads, spindles were mostly bipolar. However, mitotic spindles became multipolar just by increasing the number of beads (Fig. 4, G and H; and Video 6). These results can be compared with what has been described in SakOE (Basto et al., 2008) and polyploid NBs (this work): increase in DNA content in the presence of extra centrosomes results in multipolar divisions, while centrosome amplification is permissive to bipolar divisions if the DNA levels are not considerably increased.

We then calculated the DNA shape aspect ratio (defined as the ratio between width and length of the chromosomes plate at the end of the simulation) and found that DNA beads could be organized in classic "metaphase-like" shapes (aspect ratio closer to 0) or "cross-like" shapes (aspect ratio closer to 1). Interestingly, the increase in the DNA shape aspect ratio correlated with multipolarity (Fig. 4 I). This result prompted us to test if abnormal DNA configurations, such as the metaphase-like figures seen in vivo in polyploid NBs (Fig. 1, E and F; and Fig. 4, B and D), influence spindle multipolarity. We used a minimalist system where the DNA is represented as immobile metaphase-like plates displaying different morphologies. While centrosomes clustered into two main poles when the DNA shape corresponded to a classical metaphase plate, simulations with more complex DNA shapes always resulted in multipolar spindles (Fig. 4, J and K; and Video 6). These observations suggest that DNA content, and in particular the chromosome configurations, influences spindle pole coalescence and leads to multipolarity in silico.

Since the simulations exposed a contribution of extra DNA to inhibit spindle pole coalescence, we turned to in vivo experiments to confirm these findings. We tried to reduce DNA content of polyploid NBs using DNase treatment or laser ablation. Unfortunately, these were highly toxic (data not shown). To overcome this drawback, we designed an alternative strategy to induce multipolarity independently of polyploidy. We used a combination of SakOE with mutations in the *mad2* gene. Mad2 is a member of the SAC (Musacchio and Hardwick, 2002), and a fraction of SakOE, *mad2*^{mut} NBs divide multipolarly and generate aneuploid daughter cells due to defects in centrosome clustering (Basto et al., 2008; Gogendeau et al., 2015; Kwon et al., 2008). Analysis of mitotic SakOE, *mad2*^{mut} NBs by time-lapse microscopy revealed that in certain NBs, chromosomes were positioned in a way that seemed to prevent centrosome clustering and pole coalescence (Fig. S3, A–E). When the DNA was ultimately repositioned toward the metaphase plate, a bipolar spindle was assembled. A complete or partial lack of spindle pole coalescence was observed if one or multiple chromosomes were maintained between two poles. These observations strengthen our hypothesis and support a model in which chromosomes act as a barrier to spindle pole coalescence. They also suggest that the barrier size might ultimately determine whether spindle poles will coalesce or not.

Chromosomes act as a barrier to spindle pole coalescence in human cancer cells

The results obtained in *Drosophila* NBs showed that extra DNA of polyploid cells can act as a barrier to spindle bipolarity. We wanted to test if this was also the case in the ovarian cancer cell line OVCAR-8, since multipolar divisions might have deleterious consequences on genetic stability. We generated doxycycline (Dox)-inducible OVCAR-8 cell lines that overexpress the Sak homologue, PLK4 (hence referred to as PLK4OE cells), and stably express the H2B-RFP to test their clustering capacity. Characterization of the OVCAR-8 PLK4OE cell line showed that at least 56% of the cells contained extra centrosomes (Fig. S4, A and B). Importantly, these cells, incubated with SiR-tubulin to follow the spindle, by time-lapse microscopy, divide bipolarly (Fig. 5, A–C; and Video 7). Even if chromosome barriers were noticed, these appear rather small and were resolved during progression through prometaphase, allowing spindle pole coalescence (Fig. 5 B, white arrowhead and arrows).

To generate polyploid OVCAR-8 cells, we inhibited cytokinesis in a population of asynchronous cells using a short (1-h) pulse of Latrunculin B (LatB), an actin polymerization inhibitor. Cells were then released for 24 h before analysis. Immunostaining of Ctrl (EtOH-treated) or polyploid (LatB-treated) OVCAR-8 cells clearly showed an enrichment of multipolar and pseudo-bipolar spindles containing a DNA barrier (Fig. 6, A and B). Interestingly, we observed that certain spindle poles in these cells contained more than one centrosome (Fig. 6 B), showing that in polyploid OVCAR-8 cells, similarly to

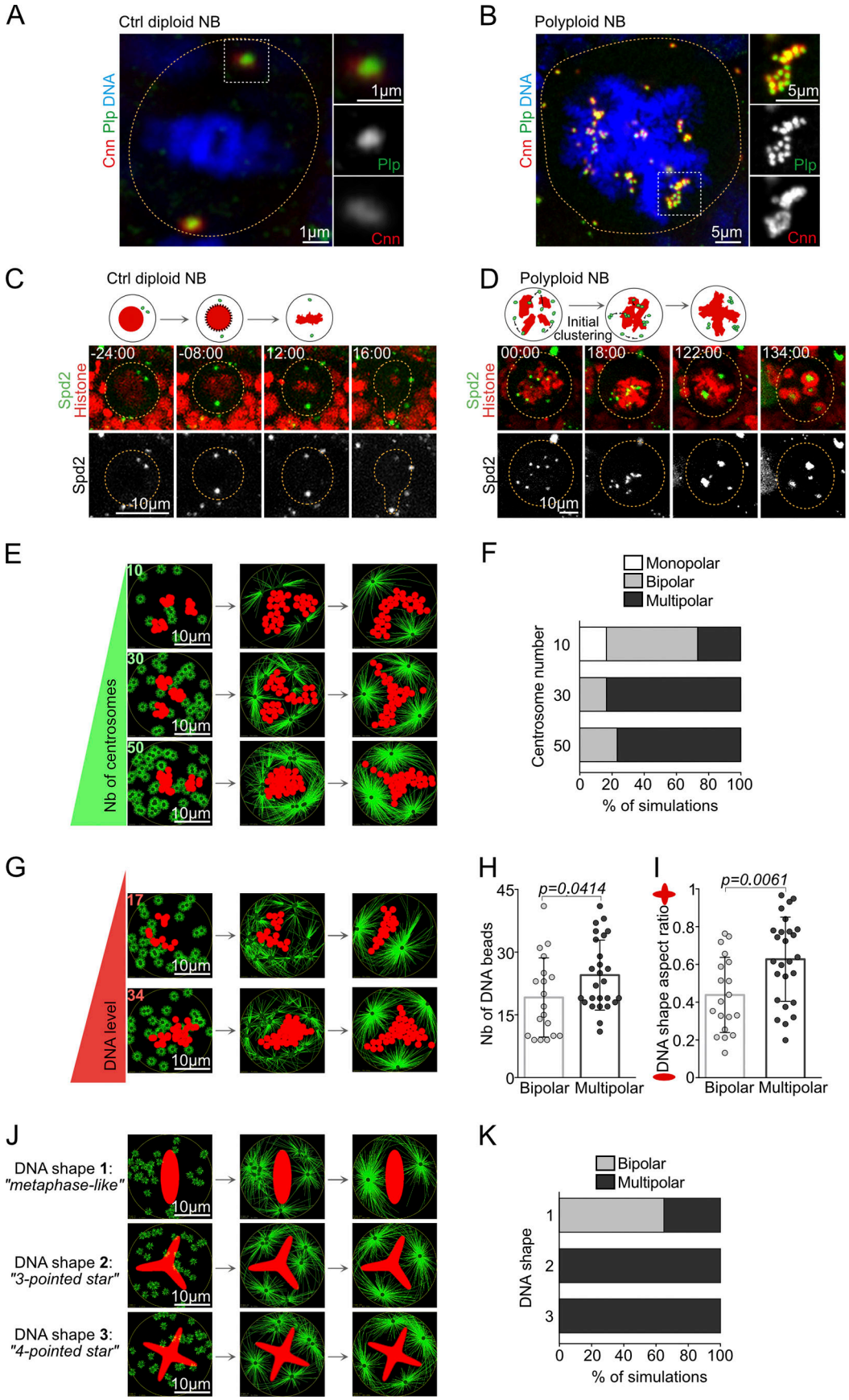

Figure 4. **Centrosome number, DNA content, and shape influence mitotic spindle assembly. (A and B)** Images of diploid (A) and polyploid (B) NBs labeled with Plp (green and gray) and Cnn (red and gray) antibodies. DNA in blue. **(C and D)** Stills of time-lapse videos of mitotic diploid (C) and polyploid (D) NBs expressing Histone 2B-RFP (red) and Spd2-GFP (green and gray in the bottom insets), corresponding to DNA and centrosomes. Time of mitosis is represented in minutes:seconds. Time 00:00 corresponds to NEBD. Schematic representations of mitosis above the stills. **(A–D)** Orange circles highlight NBs. **(E, G, and J)** Representative images of Cytosim-based simulations of spindle assembly around the DNA represented as mobile beads (E and G) or immobile plate (J). DNA is in red; MTs, green lines; and centrosomes, green circles. **(E)** Simulations with fixed DNA content and variable number of centrosomes. **(F)** Graph bars showing the percentage of simulations in each category (n = 30 simulations/condition). **(G)** Simulations with fixed number of 30 centrosomes and increasing number of mobile DNA beads. **(H and I)** Dot plots representing the number of DNA beads (H) and DNA shape aspect ratio (I) in simulations with bipolar or multipolar status (n = 45 simulations). Statistical significance was determined using a Mann-Whitney test. Error bars represent the mean ± SD and p the P value. **(J)** Simulations with fixed number of 30 centrosomes and different DNA shape configurations. **(K)** Graph bars of the percentage of simulations in each category (n = 20 simulations/condition).

Drosophila polyploid NBs, centrosome clustering can take place, but not spindle pole coalescence. To explore the dynamics of cell division in this system by time-lapse microscopy, we generated cell lines stably expressing H2B-GFP that were incubated with SiR-tubulin, allowing us to follow chromosomes and spindles, respectively. Strikingly, the presence of chromosomes lingering between two spindle poles was readily observed in polyploid cells. Importantly, these cells mostly divided in a multipolar fashion (Fig. 6, C–E; and Video 7). Interestingly, when we measured the area of chromosome barriers before

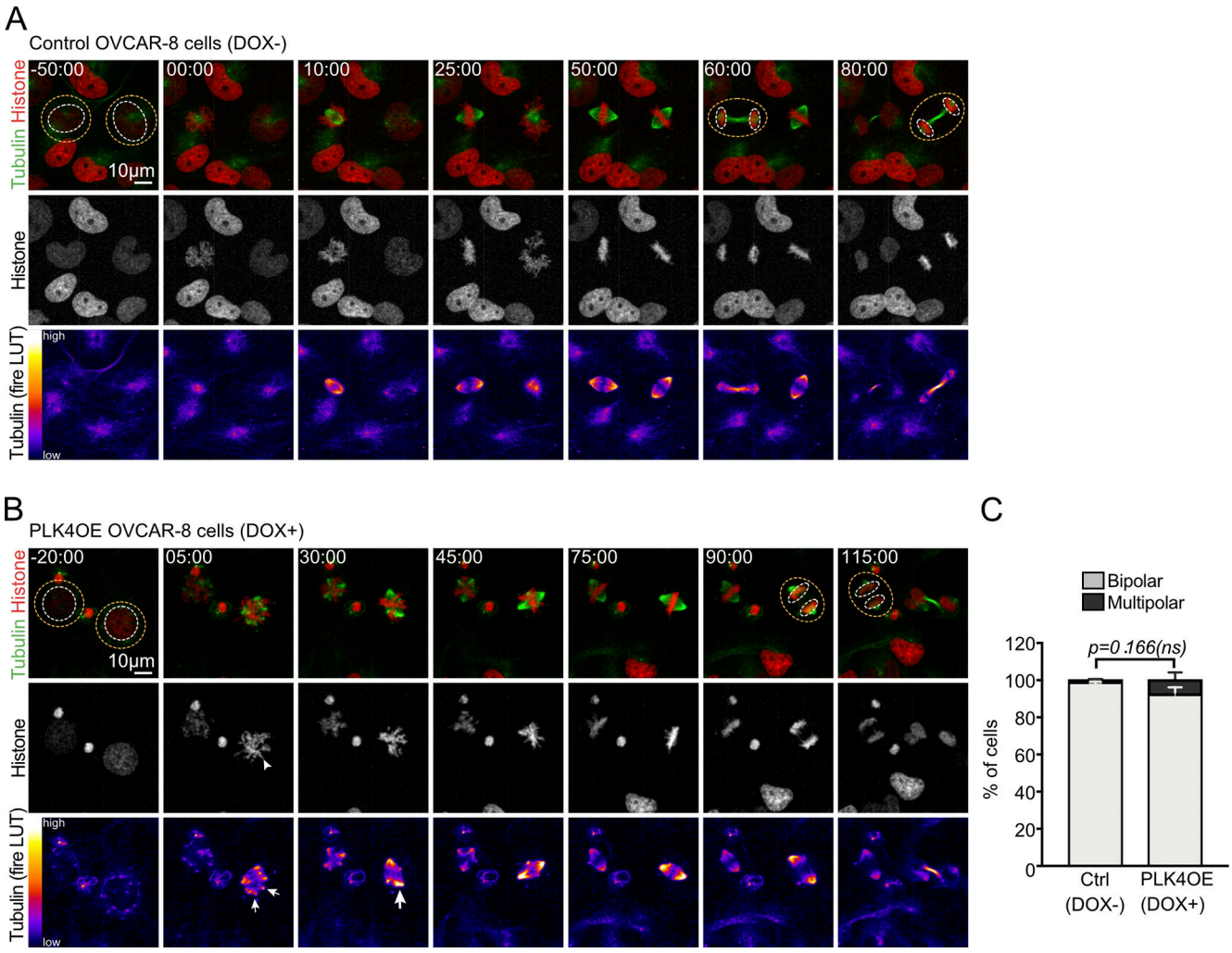

Figure 5. **OVCAR-8 cells are proficient for centrosome clustering. (A and B)** Stills of time-lapse videos of mitotic Ctrl (DOX-; A) and centrosome amplified PLK4OE (DOX+; B) OVCAR-8 cells expressing Histone 2B-RFP (red and gray in the middle insets) and incubated with SiR-tubulin (green and fire lookup table; LUT in the bottom insets). Orange and white dotted circles surround cells and nuclei, respectively. Time of mitosis is represented in minutes:seconds. Time 00:00 corresponds to the first NEBD. **(C)** Graph bars showing the percentage of cells in Ctrl (n = 149 cells from two independent experiments) and PLK4OE (n = 161 cells from two independent experiments) OVCAR-8 cells. Statistical significance by a multiple t test. Error bars represent the mean ± SD, p the P value; ns, not significant.

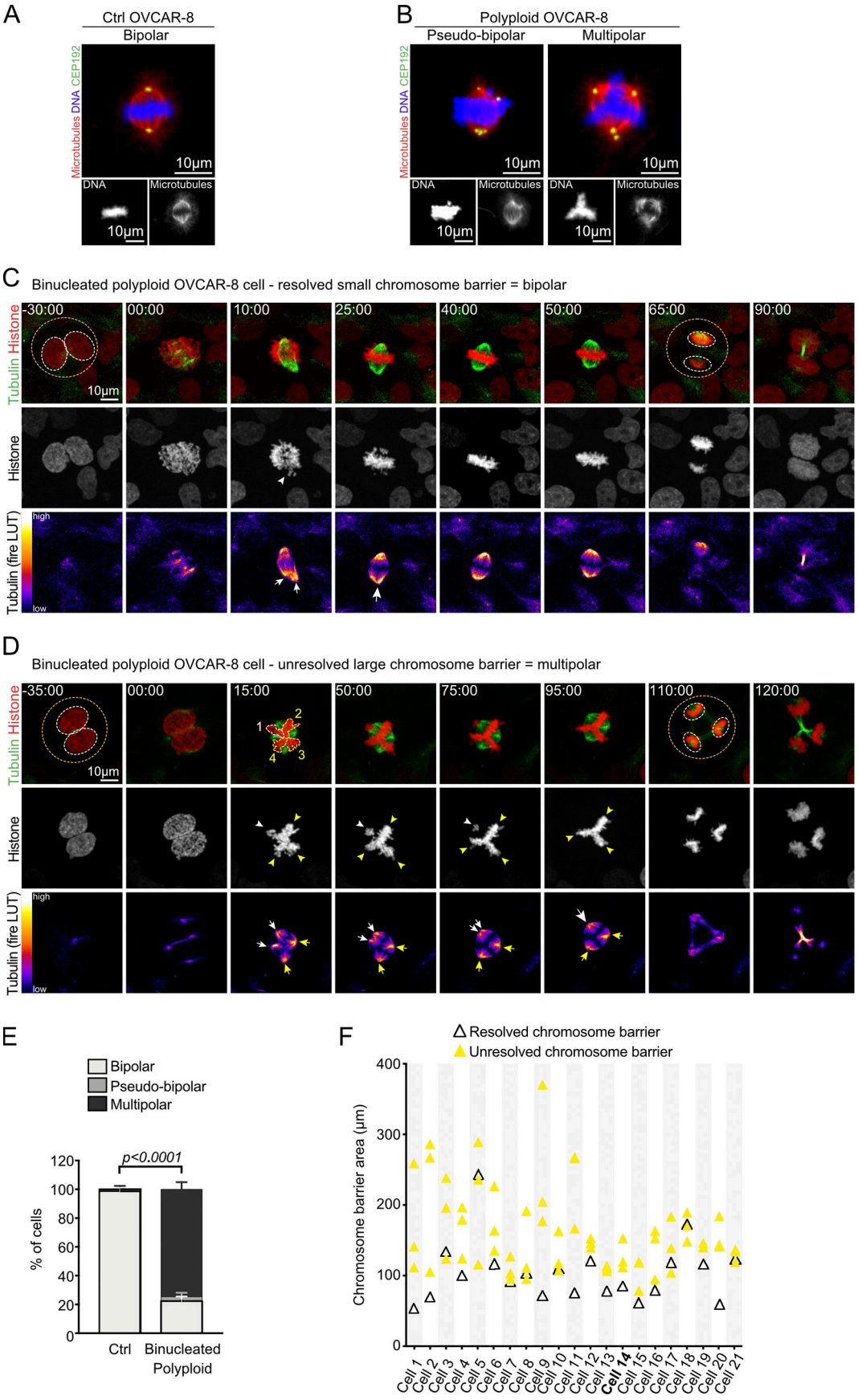

Figure 6. **Polyploid OVCAR-8 cells also divide multipolarly and fail spindle pole coalescence. (A and B)** Images of Ctrl (A) and polyploid (B) OVCAR-8 cells labeled with antibodies against α-tubulin (red and gray) and CEP192 (green) to label the mitotic spindle and the PCM, respectively. DNA in blue and gray. **(C and D)** Stills of time-lapse videos of mitotic binucleated polyploid OVCAR-8 cells expressing Histone 2B-GFP (red and gray in the middle insets) and incubated with SiR-tubulin (green and fire LUT in the bottom insets). Orange and white dotted circles surround cells and nuclei, respectively. Time of mitosis is represented in minutes:seconds. Time 00:00 corresponds to NEBD. **(E)** Graph bars of the percentage of cells in each category in Ctrl (n = 142 cells from three independent experiments) and binucleated polyploid OVCAR-8 cells (n = 101 cells from three independent experiments). Statistical significance by a multiple t test. Error bars represent the mean ± SD and p the P value between "multipolar" populations. **(F)** Dot plot showing the area of revolved (white) and unresolved (yellow) chromosome barriers in 21 polyploid OVCAR-8 cells. Stills of cell 14 (bold) shown in D.

spindle pole coalescence, we noticed that in most cases, the barrier displaying the smallest area was the one resolved, while the remaining larger DNA barriers represented obstacles to coalescence (Fig. 6, C, D, and F, white and yellow arrowheads).

To directly demonstrate the function of chromosome barriers in inhibiting spindle pole coalescence, we used laser ablation to remove chromosome(s) that were positioned between two poles. Remarkably, this led to the coalescence of spindle poles previously separated by the chromosome barrier in 53% of the cases (n = 39/74 cells; Fig. 7, A, B, and E; and Video 8). We also observed that in 47% of the cases that did not coalesce (n = 35/74 cells), this was explained in 19% of the cases (n = 14/35 cells) by the remodeling of the chromosomes within the abnormal prometaphase plate, which generated a second chromosome barrier (Fig. 7 C). In the remaining 28% (n = 21/35 cells), no further chromosome barriers were formed after ablation. However, we noticed that unclustered poles were positioned far away from each other (Fig. 7 D). Recently, it has been shown that HSET/KIFC1, the human Ncd homologue, requires a minimal pole distance to trigger efficient clustering (Rhys et al., 2018). Therefore, we measured pole-to-pole distance just before laser ablation. Interestingly, a lack of coalescence was noticed in conditions with large pole-to-pole distances (8.11 ± 2.36 µm). In contrast, this distance was smaller in situations where coalescence occurred (6.02 ± 1.72 µm; P = 0.0002; Fig. 7 F). These results suggest that chromosomes can indeed act as a barrier to spindle pole coalescence. If this barrier is removed, a permissive HSET/KIFC1 working distance between the two poles must be reached to generate efficient coalescence.

Mononucleated polyploid cells also divide multipolarly

So far, our work showed that binucleated OVCAR-8 cells and multinucleated polyploid *Drosophila* NBs assemble multipolar spindles, since centrosomes and poles fail to cluster due to the presence of chromosome barriers. To test if chromosome barriers and subsequent multipolarity are less likely to be formed when a single nucleus was present at mitotic entry, we generated simulations where the 30 DNA beads were distributed in one or three groups (representing nuclei) in the presence of 30 centrosomes. In either case, the percentage of multipolarity was comparable (Fig. 8, A and B; and Video 9), suggesting that extra DNA (rather than its organization in multiple nuclei) favors the formation of chromosome barriers.

We next attempted to generate *Drosophila* mononucleated polyploid NBs through endoreplication. Unfortunately, these cells only rarely entered mitosis, precluding the analysis of mitotic progression (data not shown). Thus, we generated mononucleated polyploid OVCAR-8 cells through the combination of Eg5 and MPS1 inhibition. Inhibition of Eg5 with monastrol generates monopolar spindles that arrest in a prometaphase-like state (Kapoor et al., 2000). MPS1 inhibition relieves the SAC and forces arrested cells to exit mitosis even without anaphase (Santaguida et al., 2010), generating a high frequency of polyploid mononucleated cells through mitotic slippage. Importantly, analysis of these cells in their following mitosis revealed that a large majority divided in a multipolar manner after assembling multipolar spindles. In these spindles, similarly to binucleated polyploid OVCAR-8 cells, chromosomes formed barriers to spindle pole coalescence (Fig. 8, C and D; and Video 9). We concluded that chromosome barriers in polyploid cells are not necessarily a by-product of multinucleation.

MT stabilization suppresses multipolarity in polyploid cells

We next investigated whether MT stabilization influenced cell division in polyploid conditions. Motivated by the findings that MT stabilization in simulations (obtained by decreasing their catastrophe rate by 25%) showed a clear improvement in centrosome and pole clustering (Fig. 9, A and B; and Video 10), we further tested this possibility in OVCAR-8 cells, using the depletion of the MT-depolymerizing kinesin mitotic centromere-associated kinesin (MCAK). Using small interefering RNAs for 72 h (siMCAK), MCAK levels were reduced (Fig. S4 C), which led to MT stabilization as shown previously (Desai et al., 1999; Gemble et al., 2019) and an increase in astral MT length easily noticeable in prometaphase cells (Fig. S4, D and E). Strikingly, MT stabilization resulted in a considerable improvement in spindle bipolarity, and the large majority of polyploid cells divided in a bipolar manner (Fig. 9, C and E; and Video 10). Interestingly, this improvement occurred through distinct mechanisms. First, a clear improvement in centrosome clustering was apparent at the beginning of mitosis in ~40.0% of the cells. In this case, extra centrosomes rapidly clustered in two main poles (Fig. 9, C, E, and F), and the spindle maintained a bipolar status throughout mitosis. Second, in cells where the initial centrosome clustering was not fully efficient and instead of generating two poles, generated three, spindle pole coalescence took place, culminating with bipolar spindle assembly (Fig. 9, D–F). We also analyzed the siMCAK polyploid OVCAR-8 cells that failed to assemble a bipolar spindle (Fig. S4 F). In this case, the chromosome condensation and achievement of a stable chromosome-MT configuration blocked spindle pole coalescence, inhibiting bipolar spindle assembly. These results show that MT stabilization in polyploid cells can favor centrosome clustering and/or spindle pole coalescence generating bipolar spindles.

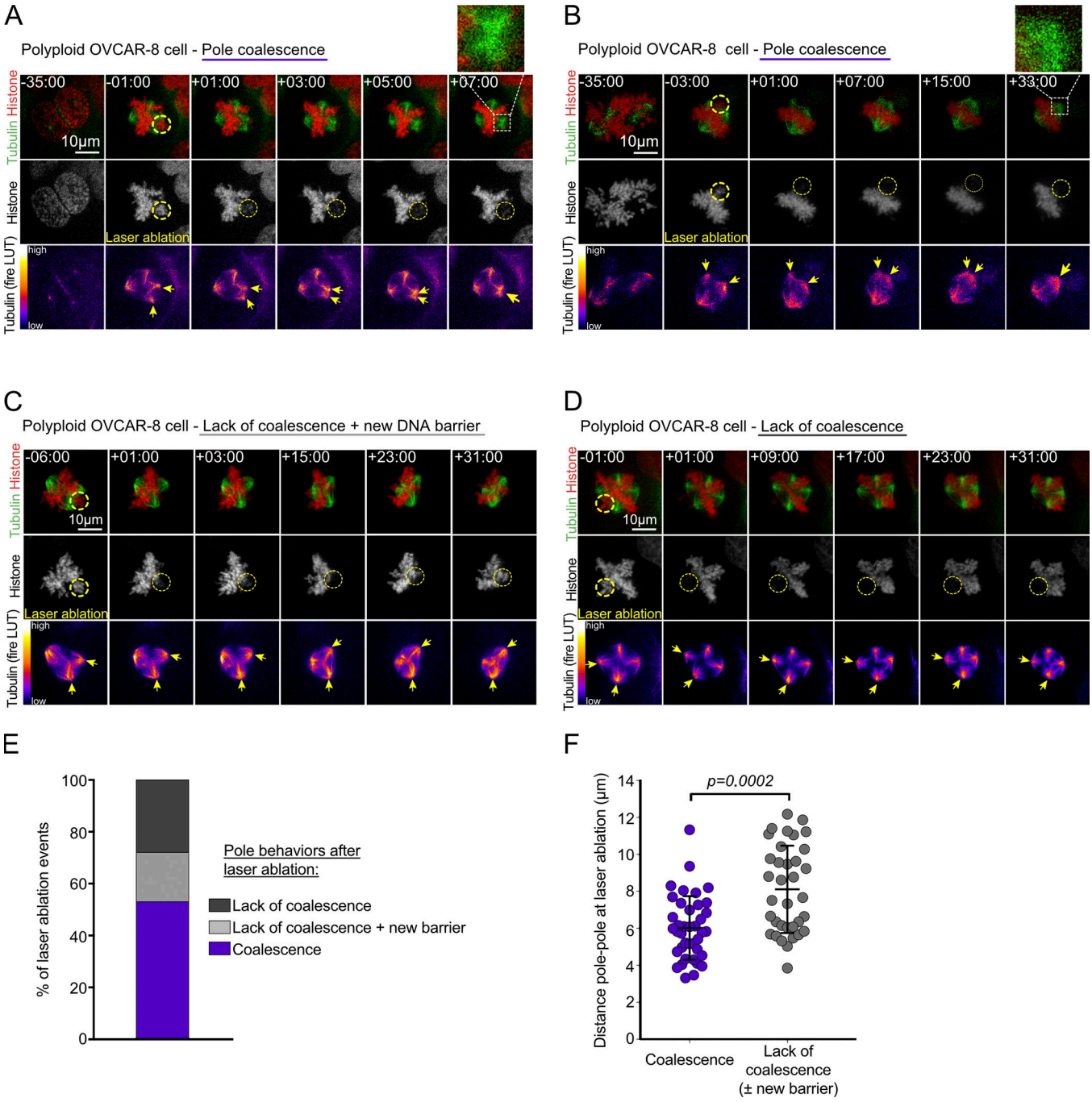

Figure 7. **Chromosome laser ablation allows spindle pole coalescence in polyploid OVCAR-8 cells. (A–D)** Stills of time-lapse videos of mitotic binucleated polyploid OVCAR-8 cells expressing histone 2B-GFP (red and gray in the middle insets) and incubated with SiR-tubulin (green and fire LUT in the bottom insets). Yellow dotted circles surround the laser ablated area. Time of mitosis is represented in minutes:seconds. Time 00:00 corresponds to the time of laser ablation. **(E)** Graph bars representing the percentage of laser ablation events leading to the indicated behaviors (n = 74 cells from six independent experiments). **(F)** Dot plot representing the distance between the two poles on both sides of laser ablated DNA in polyploid OVCAR-8 cells (n = 74 cells). Statistical significance by a Mann-Whitney test. Error bars represent the mean ± SD and p the P value.

Discussion

Here we have analyzed polyploid mitosis in three different model systems: *Drosophila* NBs, in silico simulations, and the OVCAR-8 cancer cell line. In all cases, an increase in centrosome number, accompanied by increased DNA content, resulted in multipolar spindle assembly and multipolar divisions. We observed that in polyploid mitosis, an initial centrosome clustering step gathers multiple centrosomes in multiple spindle poles. These poles are maintained, separated from each other throughout mitosis, since a second step that should trigger their coalescence into two main poles of a bipolar spindle fails (Fig. 10). Importantly, lack of spindle pole coalescence after

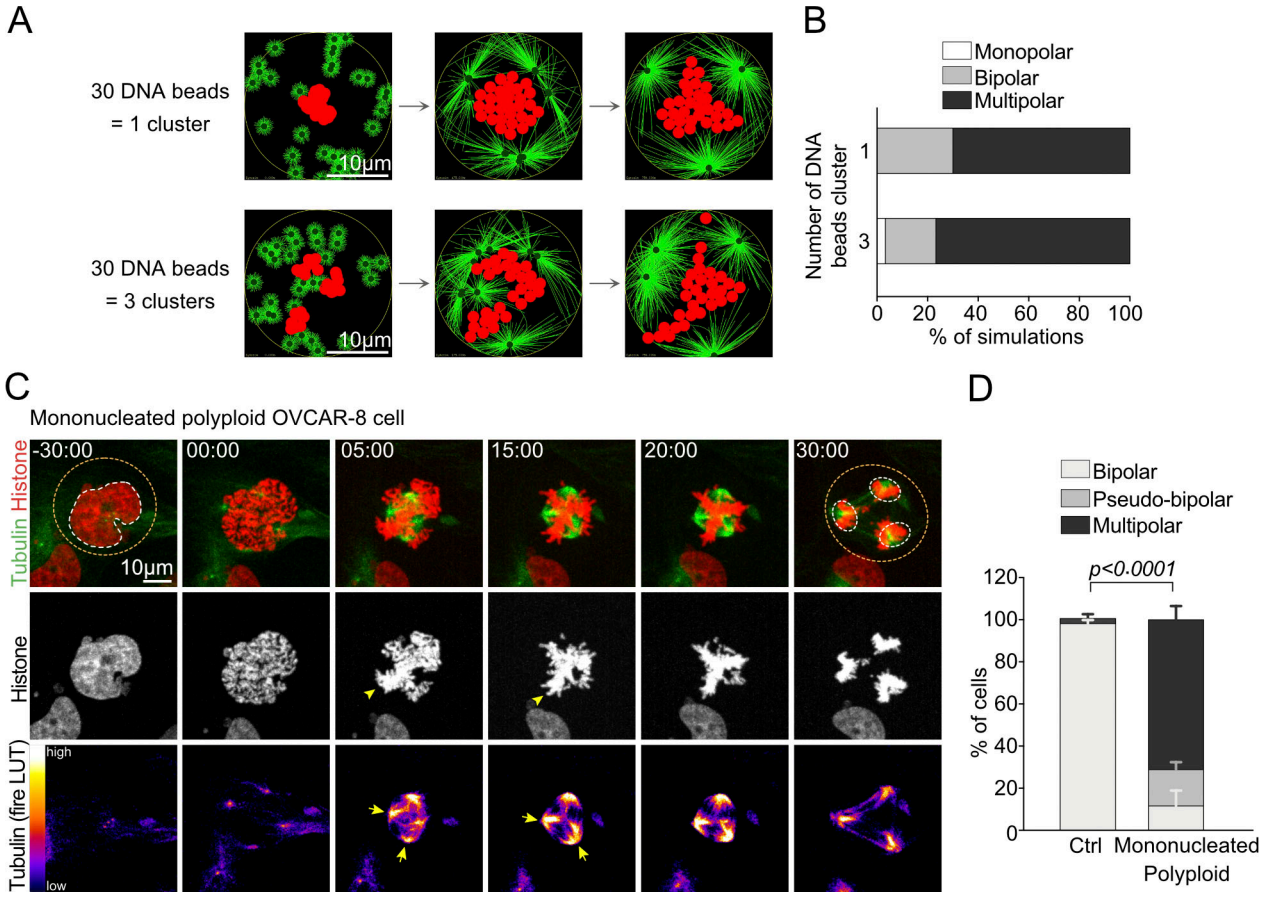

Figure 8. **Polyploid OVCAR-8 cells undergo multipolar divisions regardless the number of nuclei at mitotic entry. (A)** Representative images of Cytosim-based simulations of spindle formation. **(B)** Graph bars of the percentage of simulations in each category (n = 30 simulations/condition). **(C)** Stills of time-lapse video of mitotic mononucleated polyploid OVCAR-8 cell expressing histone 2B-GFP (red and gray in the middle insets) and incubated with SiR-tubulin (green and fire LUT in the bottom insets). Orange and white dotted circles surround cells and nuclei, respectively. Time of mitosis is represented in minutes:seconds. Time 00:00 corresponds to NEBD. **(D)** Graph bars of the percentage of cells in each category in Ctrl (n = 152 cells from three independent experiments) and mononucleated polyploid OVCAR-8 cells (n = 178 cells from three independent experiments). Statistical significance by a multiple t test. Error bars represent the mean ± SD and p the P value between "multipolar" populations.

initial centrosome clustering was also seen in polyploid cells containing a single nucleus. Taking into consideration the fact that bipolar or pseudo-bipolar spindles are assembled in cells that have been manipulated to amplify centrosomes, but not their DNA content (Kwon et al., 2008; Basto et al., 2008; Ganem et al., 2009; Silkworth et al., 2009), our results suggest that extra chromosomes hinder spindle pole coalescence and contribute to the establishment of multipolarity.

It is important to consider that as polyploid cells progress through mitosis and kinetochore-MT attachments become stabilized, abnormal chromosome configurations emerge. It is possible that in this situation, bipolar attachments of chromosomes prevent evolution of the spindle into a bipolar array. In other words, the spatial chromosome configuration achieved through local bipolar attachments using MTs emanating from several MTOCs might generate geometries with stable chromosome barriers that block spindle pole coalescence. Once the SAC has been satisfied, cells can then transit into anaphase in a multipolar manner.

An interesting question raised by this work relates to the equilibrium between chromosome number and bipolar spindle assembly. Eukaryotes, despite extreme differences in genome size, segregate chromosomes using bipolar arrays established, at least during mitosis, by two centrosomes or equivalent organelles. Polyploidization and increased centrosome numbers challenge bipolarity both in cell types that contain small chromosome numbers like in *Drosophila* (haploid genome, four chromosomes) or human cells (haploid genome, 23 chromosomes, although OVCAR-8 are not diploid cells). Interestingly, we found that even in aneuploid SakOE, *mad2* NBs, small chromosome barriers led to multipolarity. In contrast, in OVCAR-8 cells, small chromosome barriers were resolved while large barriers blocked spindle pole coalescence. It is tempting to speculate the existence of a DNA increase threshold that can ultimately influence spindle polarity if extra centrosomes are present.

The CMP and the Augmin pathways did not appear to be major contributors to spindle multipolarity in *Drosophila* polyploid NBs. Moreover, and in contrast with what has been reported for the large number of MTOCs in mouse oocytes (Watanabe et al., 2016), Augmin did not influence the initial step

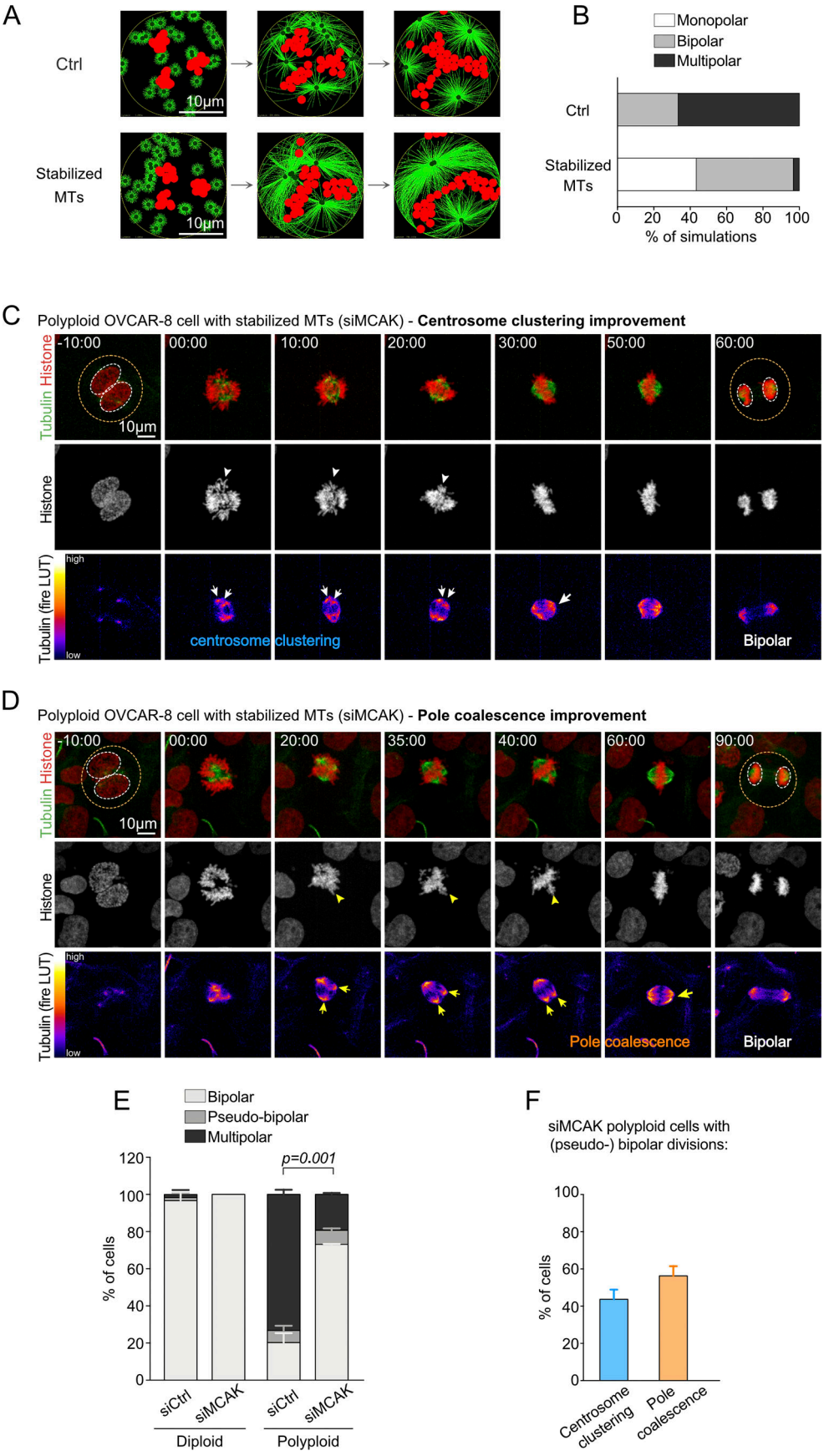

Figure 9. **Increased MT stability/length rescues bipolar spindle formation in polyploid OVCAR-8 cells. (A)** Representative images of Cytosim-based simulations of spindle formation. **(B)** Graph bars of the percentage of simulations in each category (n = 30 simulations/condition). **(C and D)** Stills of time-lapse videos of mitotic polyploid OVCAR-8 cells with stabilized MTs (siMCAK) expressing histone 2B-GFP (red and gray in the middle insets) and incubated with SiR-tubulin (green and fire LUT in the bottom insets). Orange and white dotted circles surround cells and nuclei, respectively. Time of mitosis is represented in minutes:seconds. Time 00:00 corresponds to NEBD. **(E)** Graph bars showing the percentage of cells in each category in Ctrl, siCtrl (n = 96 cells from two independent experiments), Ctrl, siMCAK (n = 100 cells from two independent experiments), polyploid, siCtrl (n = 81 cells from two independent experiments), and polyploid, siMCAK (n = 109 cells from two independent experiments) OVCAR-8 cells. Statistical significance by a multiple t test. p represents the P value between "multipolar" populations. **(F)** Graph bars showing the percentage of (pseudo-)bipolar siMCAK, polyploid OVCAR-eight cells presenting an improvement of centrosome clustering or spindle pole coalescence. Error bars represent the mean ± SD.

of centrosome clustering in *Drosophila* NBs. Together, these results show cell- and tissue-specific requirements for these pathways in promoting spindle bipolarization. Interestingly, a recent study performed in tetraploid acentriolar mouse oocytes reported the presence of two individual spindles assembled independently around each nucleus (Paim and FitzHarris, 2019), which is not the case in the polyploid cells analyzed here. In contrast to CMP and Augmin, removing centrosomes from small- to medium-sized polyploid NBs generated bipolar spindles that segregated large chromosome masses into two poles. One single bipolar spindle was assembled around polyploid DNA content. However, increased DNA content, typical of large polyploids, did not allow bipolar spindle assembly, revealing an unknown threshold of DNA content (and most likely cell volume or area) permissive to bipolar spindle assembly in the absence of centrosomes. Future work will be required to dissect the limiting factors that condition bipolar spindle assembly in acentriolar polyploid mitosis.

Our work in *Drosophila* polyploid NBs also confirmed an essential role of the minus-end directed motor Ncd/HSET in the initial centrosome clustering step. However, even if required during early mitosis, the final spindle pole coalescence phase, which is blocked in polyploid cells, does not seem to fail because of limiting Ncd levels, since its overexpression did not lead to any reduction of multipolarity. Surprisingly, however, increased MT stability was sufficient to improve bipolarity. This suggests that longer MTs that promote clustering at mitotic entry and/or spindle pole coalescence later on allow Ncd/HSET to promote bipolarization (Fig. 10).

WGDs are found in a variety of tumors and are associated with CIN and poor tumor prognosis (Bielski et al., 2018; Zack et al., 2013). The tendency to divide multipolarly in polyploid cells does not seem to depend on the number of nuclei at mitotic entry, suggesting that multiple conditions that lead to increased DNA content such as cytokinesis failure, mitotic slippage, and most likely endoreplication can lead to CIN. Here, we show that

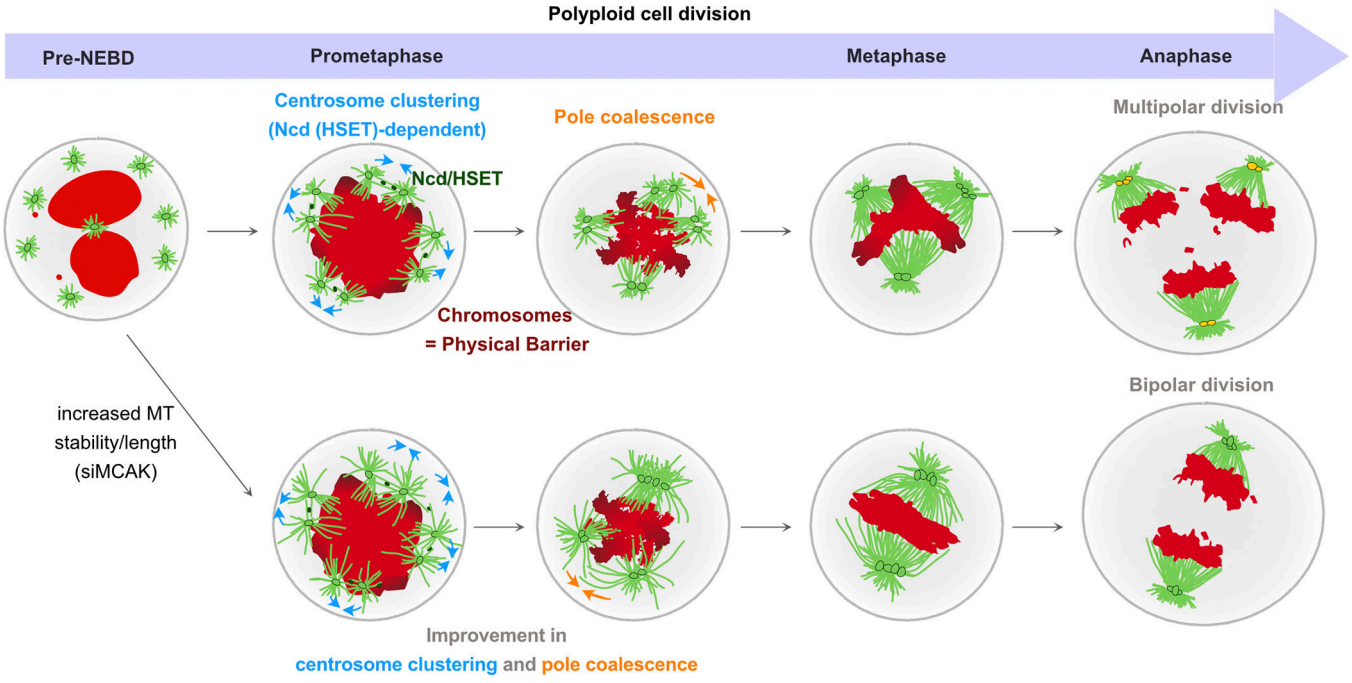

Figure 10. **Model of polyploid mitotic division containing multiple centrosomes and nuclei.** Top: When a cell with two nuclei (red dots) undergoes NEBD, an Ncd/HSET-dependent clustering step gathers extra centrosomes in multiple active MTOCs. As kinetochore-MT attachments become stabilized, chromosomes can be positioned between two spindle poles and inhibit their coalescence, acting as a physical barrier to bipolarity. At anaphase, chromosomes are segregated into multipolar arrays, giving rise to more than two nuclei. Bottom: In the presence of increased MT stability, centrosomes and spindle poles cluster and coalesce more efficiently, giving rise to bipolar spindles.

error-prone mitosis in polyploid cells results from the incapacity of these cells to fully coalesce spindle poles containing extra centrosomes due to the presence of chromosome barriers. It is important to take into account the suppression of multipolarity in polyploid cells with increased MT stability. This treatment not only improved centrosome clustering but also permitted spindle pole coalesce into a bipolar configuration. MT polymers, even if stiff, are unlikely to break through condensed mitotic DNA (Ganem and Pellman, 2012; Houchmandzadeh et al., 1997). Thus, the improvement in spindle pole coalescence seems to be explained by increased MT length, allowing the DNA barrier to be surrounded (Fig. 10). Multipolar cell divisions are poorly tolerated, and cancer cells should minimize the generation of unviable daughter cells (Ganem et al., 2009; Kwon et al., 2008). In light of our findings and knowing that WGDs are frequent in cancer, it is possible that clonal expansion of polyploid cancer cells is favored in conditions of increased MT stability.

Materials and methods

Experimental models

Fly husbandry and fly stocks

Flies were raised in plastic vials or bottles containing homemade *Drosophila* culture medium (0.75% agar, 3.5% organic wheat flour, 5% yeast, 5.5% sugar, 2.5% nipagin, 1% penicillin-streptomycin, and 0.4% propanic acid). Fly stocks were conserved at 18°C. For temporal activation of RNAi, crosses were kept at 18°C and switched to 29°C for 24–48 h. Other experimental crosses were maintained at 25°C. Most fly stocks were obtained from Bloomington *Drosophila* Stock Center or described in Endow and Komma (1998); Basto et al. (2006); Zhu et al. (2006); and Gogendeau et al.(2015).

Human cell lines

Cell culture conditions. Cells were maintained at 37°C in a 5% CO_2 atmosphere. OVCAR-8 (female) and human embryonic kidney (HEK; female) cells were grown in DMEM F12 containing 10% fetal bovine serum, 100 U/ml penicillin, and 100 U/ml streptomycin.

Cells were routinely checked for mycoplasma and underwent cell authentication by short tandem repeat analysis processed at the Genomics Platform (Department of Translational Research, Institut Curie).

Generation of OVCAR-8 PLK4OE stable cell line. To generate PLK4 inducible stable cell lines from OVCAR-8 cells, we used a Dox-inducible PLK4 lentiviral expression system (Holland et al., 2012). Viruses were produced in HEK cells, cotransfected with pMD2.G and psPAX2 plasmids using lipofectamine 2000. Viral particles were then used to infect OVCAR-8 cells for 24 h. Infected cells were selected using bleomycin (50 µg/ml) for 15 d.

Generation of OVCAR-8 H2B-GFP and OVCAR-8 PLK4OE H2B-RFP stable cell lines. To produce viral particles, HEK cells were transfected with psPAX2, pMD2.G, and pHR_dSV40-H2B-GFP or pHR_dSV40-H2B-RFP plasmids using FuGENE HD Transfection Reagent or PEI MAX in OptiMEM medium, respectively. Cells were incubated at 37°C in a 5% CO_2 atmosphere for 16 h. The growth media were removed and replaced by 5 ml fresh OptiMEM. The day after, viral particles were isolated by filtering the medium containing the viral particles through a 0.45-µm filter. Then, OVCAR-8 or OVCAR-8 PLK4OE cells were incubated with viral particles in the presence of polybrene 8 µg/ml for 24 h. OVCAR-8 GFP-positive and OVCAR-8 PLK4OE RFP-positive cells were then collected using BD FACS Aria IIIu (BD FACSDiva Software Version 8.0.1). To preserve inherent OVCAR-8 heterogeneity, a bulk population of GFP-positive and RFP-positive cells has been sorted.

Drug treatments for human cell lines

To induce centrosome amplification, OVCAR-8 PLK4OE H2B-RFP cells were plated at the appropriate confluence and treated for 96 h with Dox (1 µg/ml) or DMSO (drug diluent 0.0001%) for control before immunofluorescence and live imaging.

OVCAR-8 H2B-GFP cells were plated 24 h before drug treatment at the appropriate confluence. To induce cytokinesis failure, cells were treated for 1 h at 37°C with latrunculin B (5 µM) or ethanol (drug diluent, 0.015%) for control and then washed in PBS. The efficiency of the drug treatment was assessed by cell rounding and was considered as time 0. To induce mitotic slippage, cells were treated overnight (O/N) with the combination of MPI-0479605 (MPS1 inhibitor, 0.5 µM) and monastrol (Eg5 inhibitor, 50 µM) or DMSO (drug diluent 0.15%) for control. Drugs were washed out 3× in PBS. Immunofluorescence and live imaging were performed 24 h or 12 h after drugs washout in proliferative medium. 4 h before live imaging, cells were treated with SiR-tubulin (33 nM) and Verapamil (1 nM).

MCAK depletion in human cell lines

To deplete MCAK, OVCAR-8 H2B-GFP cells were plated at the appropriate confluence and treated for 72 h with 10 nM of siMCAK or control siRNAs (siCtrl). siRNA mixes were prepared using the jetPRIME kit and following the manufacturer's protocol. Reagents and materials are listed in Table S3.

Methods and microscope image acquisition

Live imaging of Drosophila *larval brains*

Mid third-instar larval (L3) brains were dissected in Schneider's *Drosophila* medium supplemented with 10% heat-inactivated fetal bovine serum, penicillin (100 U/ml), and streptomycin (100 µg/ml). Several brains were placed on a glass-bottom dish with near 10 µl of medium, covered with a permeable membrane, and sealed around the membrane borders with oil 10 S Voltalef. Images were acquired with 60× oil objective (NA 1.4) on two microscopes: an Inverted Spinning Disk Confocal Roper/Nikon (a Yokagawa CSU-X1 spinning head mounted on a Nikon Ti-E inverted microscope equipped with a camera EMCCD 512 × 512 Evolve; Photometrics) and the wide-field Inverted Spinning Disk Confocal Gattaca/Nikon (a Yokagawa CSU-W1 spinning head mounted on a Nikon Ti-E inverted microscope equipped with a camera complementary metal-oxide semiconductor 1,200 × 1,200 Prime95B; Photometrics), controlled by Metamorph software. For both microscopes, images were acquired at time intervals spanning from 30 s (diploid conditions) to 2 min (polyploid conditions) and 30 to 50 Z-stacks of 1–1.5 µm.

Immunofluorescence of Drosophila *larval squashed brains*

L3 brains were dissected in PBS and fixed for 20–40 min at RT in 4% formaldehyde diluted in PBS. After fixation, brains were transferred in a drop of 45% acetic acid on a coverslip for 15 s and then immediately moved in a drop of 60% acetic acid. Acetic acid was diluted in water. A slide was then placed on top of the coverslip, and brains were squashed with a pencil until the tissue appeared transparent. The slide was rapidly flash frozen in liquid nitrogen before the removal of the coverslip using a sharp blade. Slides were incubated 7 min in −20°C methanol, washed, and permeabilized three times for 10 min in PBST 0.1% solution (PBS, 0.1% Triton X-100, and 0.02% sodium azide) at RT. Slides were dried at RT before incubation with 10 µl of primary antibodies diluted in PBST 0.1% and covered with a coverslip in a humid chamber at 4°C O/N. After removal of the coverslips, slides were washed 3x for 10 min in PBST 0.1% at RT. 10 µl of secondary antibody dilution was added to the slides, and slides were covered with coverslips in a dark, humid chamber and incubated 3 h at 25°C. Slides were washed 3x for 10 min in PBST 0.1% and incubated in 0.5 µg/ml Hoechst for 15 min at RT. Slides were mounted using a 22 × 22 mm coverslip using 10 µl of mounting medium (1.25% n-propyl gallate, 75% glycerol, 25% H_2O). Images were acquired with 40× (NA 1.25), 63× (NA 1.32), or 100× (NA 1.4) oil objectives on an Epifluorescent Upright microscope Leica DM6000 equipped with a camera CCD, 1,392 × 1,040 CoolSnap HQ (Photometrics). Intervals for Z-stack acquisitions were set to 0.3 to 1 µm using Metamorph software.

Immunofluorescence of Drosophila *larval whole mount brains*

L3 brains were dissected in PBS and fixed for 30 min at RT in 4% paraformaldehyde diluted in PBS. After fixation, brains were washed and permeabilized three times for 10 min in PBST 0.3% (PBS, 0.3% Triton X-100, and 0.02% sodium azide). Brains were then incubated in primary antibodies diluted in PBST 0.3%, at 4°C O/N in a humid chamber. After 3× 10 min washes in PBST 0.3%, brains were incubated in secondary antibodies and DAPI dilution (in PBST 0.3%), either for several hours at 25°C or O/N at 4°C, protected from light in a humid chamber. After three washes for 10 min in PBST 0.3%, brains were rinsed in PBS and mounted using 12-mm coverslips with 5 µl of mounting medium (1.25% n-propyl gallate, 75% glycerol, 25% H_2O). Images were acquired on a confocal Nikon A1R Ti-E inverted microscope with a 60× (NA 1.4) oil objective. The interval for Z-stack acquisitions was set up with 0.3 µm using the NIS Element software.

Immunofluorescent staining of human cells

Cells were plated on coverslips in 12-well plates and treated with the indicated drugs. The day of the immunofluorescence, cells were fixed using cold methanol (7 min at −20°C). Cells were washed three times using PBST (PBS 1× + 0.1% Triton X-100 + 0.02% sodium azide) and incubated with PBST + BSA 0.5% for 30 min at RT. After three washes with PBST, primary and secondary antibodies (1:250 concentration) were incubated in PBST + BSA 0.5% for 1 h and 30 min at RT, respectively. Nuclear DNA was detected by incubating with DAPI diluted in PBS, and slides were mounted with mounting medium (1.25% n-propyl gallate, 75% glycerol, and 25% H_2O). Images were acquired on an upright widefield microscope (DM6B, Leica Systems) equipped with a motorized XY and a 40× objective (HCX PL APO 100×/1.40-0.70 Oil from Leica). Acquisitions were performed using Metamorph software and a sCMOS camera (Flash 4V2, Hamamatsu). Stacks of conventional fluorescence images were collected automatically at a Z-distance of 0.2 µm (Metamorph software). Images are presented as maximum intensity projections generated with ImageJ software, from stacks deconvolved with an extension of Metamorph software.

Live imaging of human cells and laser ablation

Cells were plated on a dish and treated with the indicated drug. For live imaging, images were acquired on a spinning disk microscope (Gataca Systems). Based on a CSU-W1 (Yokogawa), the spinning head was mounted on an inverted Eclipse Ti2 microscope equipped with a motorized XY Stage (Nikon). Images were acquired through a 40× 1.4 NA Plan-Apo objective, with a sCMOS camera (Prime95B, Photometrics). Optical sectioning was achieved using a piezo stage (Nano-z series, Mad City Lab). Gataca Systems' laser bench was equipped with 405-, 491-, and 561-nm laser diodes, delivering 150 mW each, coupled to the spinning disk head through a single mode fiber. Multidimensional acquisitions were performed using Metamorph 7.10.1 software. Stacks of conventional fluorescence images were collected automatically at a Z-distance of 1.5 µm (Metamorph software). Images are presented as maximum intensity projections generated with ImageJ software, from stacks deconvolved with an extension of Metamorph software. For laser ablation experiments, images were acquired on an Inverted Eclipse Ti-E (Nikon) + Spinning disk CSU-X1 (Yokogawa) integrated in Metamorph software by Gataca Systems. Images were acquired through a 100× 1.3 NA Plan Fluor (UV) objective with a sCMOS camera (Prie BSI, Photometrics). Optical sectioning was achieved using a piezo stage (Nano-z series, Mad City Lab). Gataca Systems' laser bench was equipped with 405-, 488-, 561-, and 633-nm laser diodes, delivering 100 mW, 70 mW, 60 mW, and 35 mW, respectively. Laser ablation was performed with a Photoablation module ILAS2 (Gataca Systems) equipped with a pulsed laser at 355 nM for nanoablation. Laser ablation was performed with spot length of 100 nm of UV laser, between two time points of acquisition.

Western blot siMCAK OVCAR-8 cells

Cells were lysed in the lysis buffer composed of 8 M urea, 50 mM Tris HCl, pH 7.5, and 150 mM β-mercaptoethanol, sonicated and heated at 95°C for 10 min. Samples were subjected to electrophoresis in NuPAGE Novex 4–12% Bis-Tris precast gels. Protein fractions from the gel were electrophoretically transferred to polyvinylidene fluoride membranes. After 1 h saturation in PBS containing 5% dry nonfat milk and 0.5% Tween 20, the membranes were incubated with primary antibody against MCAK or α-tubulin (for control) diluted in PBS containing 5% dry nonfat milk and 0.5% Tween 20 for 1 h. After three 10-min washes with PBS 0.5% Tween 20, membranes were incubated for 45 min with peroxidase-conjugated antibodies. Membranes were then washed three times with PBS containing 0.5% Tween 20, and the reaction was developed according to the manufacturer's specifications using ECL reagent.

Computer simulations

Simulations were performed using Cytosim considering mitotic cells as spherical entities (Letort et al., 2016). We confined the MTs and motors in a circular shape (2D). Centrosomes were modeled as asters nucleating MTs radially. They were initially randomly placed inside the cell, corresponding to the experimental situations just after NEBD. MTs were considered as flexible polymers with static minus ends and dynamic plus ends that could grow and shrink according to the dynamic instability model (Gittes et al., 1993; Dogterom and Yurke, 1997; Gallaud et al., 2014). The kinesin motors Ncd were represented as entities composed of two separate MT-binding "heads," one static (corresponding to the nonmotor domain) and one that could move toward the MT minus ends (Howard et al., 1989; Oladipo et al., 2007; Rupp and Nédélec, 2012; Letort et al., 2019). Ncd was shown to bind and slide anti-parallel MTs and cross-link parallel MTs (Fink et al., 2009). Here, as we were interested in the clustering effect (which depends on anti-parallel sliding), we constrained Ncd-like entities to bind exclusively to anti-parallel MTs. This reduces the amount of entities to simulate. Finally, we used two different representations of the chromatin: (1) the metaphase plate was simulated as a static obstacle (an area of a defined shape) that MTs cannot cross nor deform based on Houchmandzadeh et al. (1997), and (2) the chromatin was simulated as mobile beads (without intrinsic motion) that could be pushed by the MTs (Letort et al., 2019). In condition 1, MTs and the initial position of the centrosomes were excluded from this area. In condition 2, the DNA beads were initially placed in two to five groups (mimicking the nuclei number at NEBD) of 0–50 DNA beads each, randomly distributed within a disk of radius slightly smaller than the cell radius (so that the cluster will not be blocked against the cortex). In both conditions, we did not consider MT nucleation from the plate/beads to simplify the model. MTs were prevented from sliding on the surface of the plate/beads by the presence of plus-end tracking entities (mimicking chromokinesins present on chromosomes or capture by prometaphase kinetochores) similar to simulations from Lacroix et al., (2018). Parameters in the simulations were chosen to match the experimental conditions when measurable or from the literature when available. Note that values of these parameters were adjusted to check that the numerical conclusions were not greatly affected by this choice. All parameters are detailed in Table S2.

To further test our interpretation of DNA acting as a physical barrier to centrosome clustering, we took advantage of the flexibility of the simulations and explored numerically different scenarios, changing only one parameter at a time. In our previous simulations (condition 2), we kept a constant number of 30 centrosomes and varied the DNA content, from 9 to 41 DNA beads distributed in two to five initial groups (approximate nuclei at NEBD). Conversely, we varied the number of centrosome (10, 30, or 50 centrosomes), keeping a constant but high DNA content (30 beads of DNA, initially distributed in three randomly placed clusters). Then we tested the effect of the initial geometry of the DNA by varying the number of initial beads group (1 or 3), keeping a constant number of beads (30) and centrosomes (30). Finally, the stability of MTs was increased by decreasing by 25% their catastrophe rate in our default condition (30 centrosomes, 30 beads of DNA in three initial clusters), in order to increase their length.

Image quantification and statistical analysis

Image analysis and quantifications were performed using Fiji software. Centrosomes were manually counted and identified as the colocalization of Cnn (Lucas and Raff, 2007) and Plp (Martinez-Campos et al., 2004) markers on *Drosophila* whole mount brains. Centrioles were manually counted and identified as the colocalization of Centrin 3 dots and CEP192 (Vargas-Hurtado et al., 2019) for OVCAR-8 cells delimitated with the membrane marker N-cadherin. The bipolar/multipolar state of the mitotic spindle, the number of nuclei, the cell and DNA area, and the mitotic timing were assessed on live-imaging data. For all *Drosophila* polyploid NBs, quantifications were done on cells with an area inferior to 6,000 μm^2 to be able to compare all genetic conditions. To calculate the nuclear index (number of nuclei at mitotic exit over mitotic entry relative to the number of daughter cells), the number of nuclei was manually counted for all Z-stacks at preNEBD and at anaphase, when nuclei are individualized, before chromosome decondensation. This ratio was then normalized by the number of cells generated after anaphase, two in diploid conditions and one in polyploid conditions (cytokinesis failure). Knowing the time intervals between acquired frames, the mitotic timing was calculated from NEBD to anaphase onset. The cell or DNA area was calculated using the "Freehand selection" tool in Fiji software to draw cell or DNA contour of *Drosophila* NBs in metaphase. In polyploid LatB-treated OVCAR-8 cells that presented four poles in prometaphase, the four chromosome barriers were measured using the "Freehand selection" tool. We analyzed cells that then evolve into a tripolar spindle configuration.

In siCtrl/siMCAK polyploid OVCAR-8 cells, the length of astral MTs was manually measured using the "Freehand selection" tool in Fiji software. We measured the two to four longest MTs for each pole of eight to eleven prometaphase cells.

All statistical analyses were performed in Prism software (see figure legends for details). For all the analysis of the correlation between the number of nuclei at anaphase or mitotic timing or DNA area and NB area, the correlation coefficient r measures the strength of the relationship between the two variables, while the regression slope represents the rate of change. In other words, the slope indicates to what extent the number of nuclei increases with cell area. For the figures, images were processed on Photoshop and Affinity Photo, and mounted using Illustrator and Affinity Designer.

Fly genetic crosses

Crosses for Fig. 1

Fixed analysis. Control: wt[118]. Line maintained at 25°C. Polyploid: Pav^{RNAi}/Cyo-GFP x Act-GAL4-$GAL80^{ts}$/Cyo-GFP. Crosses were maintained at 18°C after egg laying until reaching first/second instar stages and then switched to 29°C for 24–48 h.

Live imaging. Control: Tub-GFP, Hist-RFP/Cyo-GFP; Actin-GAL4-$GAL80^{ts}$/TM6,Tb.. Pav^{KD}: Pav^{RNAi}/Cyo-GFP x Tub-GFP,

Hist-RFP/Cyo-GFP; Act-GAL4-GAL80^{ts}/TM6,Tb. Crosses were maintained at 18°C after egg laying until reaching first/second instar stages and then switched to 29°C for 24–48 h.

Crosses for Fig. 3

Live imaging. Polyploid, *sas4^{mut}*: Pav^{RNAi},Hist-RFP/Cyo-GFP; *DSas4$^{mut(S2214)}$*/TM6,Tb x Ase-GAL4,Tub-GFP/Cyo-GFP; *DSas4$^{mut(S2214)}$*/TM6,Tb. Fly crosses were maintained at 25°C.

Crosses for Fig. 4

Fixed analysis. Control: wt[118]. Line maintained at 25°C. Polyploid: Pav^{RNAi}/Cyo-GFP x Act-GAL4-GAL80^{ts}/Cyo-GFP. Crosses were maintained at 18°C after egg laying until reaching first/second instar stages and then switched to 29°C for 24–48 h.

Live imaging. Diploid: Spd2-GFP,Hist-GFP/Cyo-GFP. Polyploid: Pav^{RNAi}/Cyo-GFP x Spd2-GFP,Hist-RFP/Cyo-GFP; Act-GAL4-GAL80^{ts}/TM6,Tb. Crosses were maintained at 18°C after egg laying until reaching first/second instar stages and then switched to 29°C for 24–48 h.

Crosses for Fig. S1

Live imaging. Diploid, *sas4^{mut}*: Tub-GFP,Hist-RFP/Cyo-GFP; *DSas4$^{mut(S2214)}$*/TM6,Tb.. Diploid, Mars^{KD}: Tub-GFP,Hist-RFP/Cyo-GFP; mars^{RNAi}/TM6,Tb x Act-GAL4-GAL80^{ts}/TM6,Tb. Polyploid, Mars^{KD}: Pav^{RNAi}/Cyo-GFP; mars^{RNAi}/TM6,Tb x Tub-GFP,Hist-RFP/Cyo-GFP; Act-GAL4-GAL80^{ts}/TM6,Tb. Diploid, Aug^{KD}: Tub-GFP,Hist-RFP/Cyo-GFP; dgt2^{RNAi}/TM6,Tb x Act-GAL4-GAL80^{ts}/TM6, Tb. Polyploid, Aug^{KD}: Pav^{RNAi}/Cyo-GFP; dgt2^{RNAi}/TM6,Tb x Tub-GFP,Hist-RFP/Cyo-GFP; Act-GAL4-GAL80^{ts}/TM6,Tb. Crosses were maintained at 18°C after egg laying and until reaching first/second instar stages and then switched to 29°C for 24–48 h.

Crosses for Fig. S2

Live imaging. Diploid, *ncd^{mut}*: Tub-GFP,Hist-RFP/Cyo-GFP; *ncd^{1}*/TM6,Tb. Polyploid, *ncd^{mut}*: Pav^{RNAi}, Hist-RFP/Cyo-GFP; *ncd^{1}*/TM6,Tb x Asense-GAL4,Tub-GFP/Cyo-GFP; *ncd^{1}*/TM6,Tb. Diploid, Ncd-GFP: Ncd-GFP/Cyo-GFP; Ncd-GFP, *ncd^{1}, cand*/TM6,Tb. Crosses were maintained at 25°C.. Polyploid Ncd-GFP: Pav^{RNAi}, Hist-RFP/Cyo-GFP; Ncd-GFP, *ncd^{1}, cand*/TM6,Tb x Ncd-GFP/Cyo-GFP; Act-GAL4-GAL80^{ts}/TM6, Tb. Crosses were maintained at 18°C after egg laying until reaching first/second instar stages and then switched to 29°C for 24–48 h.

Crosses for Fig. S3

Live imaging. SakOE, *mad2^{mut}*: pUbqSak-#68, *mad2^{mut}*/TM6,Tb. X Tub-GFP,Hist-RFP/Cyo-GFP; *mad2^{mut}*/TM6,Tb. Crosses were maintained at 25°C.

Online supplemental material

Fig. S1 shows that diploid and polyploid NBs depleted for MT-nucleating pathways undergo bipolar and multipolar divisions. Fig. S2 shows that centrosome clustering takes place in polyploid mitosis, but it is not sufficient to promote bipolar spindle assembly. Fig. S3 shows that chromosomes as physical barriers can perturb centrosome clustering in NBs with centrosome amplification. Fig. S4 shows that PLK4OE and MCAK depletion, respectively, induce centrosome amplification and increase astral MT length. Table S1 summarizes all mitotic parameters calculated in the different diploid and polyploid conditions. Table S2 and Table S3 present the lists of computer simulations parameters and of materials and reagents, respectively. Videos 1, 2, 3, and 4 show mitotic divisions in diploid, small, and large polyploid NBs (Video 1), in diploid, *sas4^{mut}*, small and large polyploid, *sas4^{mut}* NBs (Video 2), in diploid Mars^{KD}, diploid Aug^{KD}, diploid *ncd^{mut}*, and diploid NcdOE NBs (Video 3), or in polyploid Mars^{KD}, polyploid Aug^{KD}, polyploid *ncd^{mut}*, and polyploid NcdOE NBs (Video 4). Video 5 shows centrosome clustering in polyploid NBs. Video 6 shows computer simulations of spindle assembly according to centrosome number, DNA content, and DNA shape. Video 7 shows Ctrl, PLK4OE, and polyploid OVCAR-8 cells mitotic division. Video 8 shows experiments of laser ablation in polyploid OVCAR-8 cells. Videos 9 and 10 show experimental and simulated mitotic divisions in mononucleated polyploid cells (Video 9) or polyploid cells with increased MT stability (Video 10).

Acknowledgments

We thank the Plateforme d'Imagerie Cellulaire et Tissulaire (PiCT)-Infrastructure en Biologie Santé et Agronomie (IBiSA) platform and Nikon Imaging Center at Institut Curie for microscopy and V. Fraisier for outstanding help with image acquisition and advice. We thank V. Marthiens, D. Vargas-Hurtado, D. Fachinetti, and S. Passemard for helpful discussion and/or comments on the manuscript. We thank A. Holland (Johns Hopkins School of Medicine, Baltimore, MD) for providing the PLK4 plasmid.

This work was supported by a European Research Council consolidator grant (ChromoNumber LS3, ERC-2016-COG), Institut Curie, and Centre National de la Recherche Scientifique. M. Nano was funded by La Ligue Nationale Contre le Cancer and Fondation pour la Recherche Medicale (FRM; FDT20160435352) grants and A. Goupil by an FRM (ECO20170637529) fellowship. G. Letort was funded by ANR (Agence Nationale de la Recherche,ANR-16-CE13 to M.-E. Terret, College de France, Paris, France). The Basto laboratory is a member of the Labex CelTisPhyBio (ANR-11-LABX-0038 and ANR-10-IDEX-0001-02).

The authors declare no competing financial interests.

Author contributions: A. Goupil performed the large majority of the experiments, analyzed the data, and generated the figures and videos. M. Nano conceived the project, performed the initial experiments, and established the majority of *Drosophila* lines and tools. G. Letort generated the simulation models and contributed to the discussions. S. Gemble generated human OVCAR-8 cell lines, performed some experiments, and contributed to the discussions. F. Edwards and O. Goundiam generated the PLK4OE OVCAR-8 cell line and contributed to the discussions. D. Gogendeau contributed with part of the SakOE, mad2 analysis, and C. Pennetier generated certain antibodies and helped with fly pushing. R. Basto conceived the project, wrote the manuscript, and supervised the project. A. Goupil, M. Nano, and R. Basto interpreted the data, which was discussed between all authors during the preparation of the manuscript.

Submitted: 1 August 2019
Revised: 13 December 2019
Accepted: 24 January 2020

References

Adams, R.R., A.A. Tavares, A. Salzberg, H.J. Bellen, and D.M. Glover. 1998. pavarotti encodes a kinesin-like protein required to organize the central spindle and contractile ring for cytokinesis. *Genes Dev.* 12:1483–1494. https://doi.org/10.1101/gad.12.10.1483

Basto, R., J. Lau, T. Vinogradova, A. Gardiol, C.G. Woods, A. Khodjakov, and J.W. Raff. 2006. Flies without centrioles. *Cell.* 125:1375–1386. https://doi.org/10.1016/j.cell.2006.05.025

Basto, R., K. Brunk, T. Vinadogrova, N. Peel, A. Franz, A. Khodjakov, and J.W. Raff. 2008. Centrosome amplification can initiate tumorigenesis in flies. *Cell.* 133:1032–1042. https://doi.org/10.1016/j.cell.2008.05.039

Bielski, C.M., A. Zehir, A.V. Penson, M.T.A. Donoghue, W. Chatila, J. Armenia, M.T. Chang, A.M. Schram, P. Jonsson, C. Bandlamudi, et al. 2018. Genome doubling shapes the evolution and prognosis of advanced cancers. *Nat. Genet.* 50:1189–1195. https://doi.org/10.1038/s41588-018-0165-1

Conduit, P.T., A. Wainman, and J.W. Raff. 2015. Centrosome function and assembly in animal cells. *Nat. Rev. Mol. Cell Biol.* 16:611–624. https://doi.org/10.1038/nrm4062

Desai, A., S. Verma, T.J. Mitchison, and C.E. Walczak. 1999. Kin I kinesins are microtubule-destabilizing enzymes. *Cell.* 96:69–78. https://doi.org/10.1016/S0092-8674(00)80960-5

Dewhurst, S.M., N. McGranahan, R.A. Burrell, A.J. Rowan, E. Grönroos, D. Endesfelder, T. Joshi, D. Mouradov, P. Gibbs, R.L. Ward, et al. 2014. Tolerance of whole-genome doubling propagates chromosomal instability and accelerates cancer genome evolution. *Cancer Discov.* 4:175–185. https://doi.org/10.1158/2159-8290.CD-13-0285

Dogterom, M., and B. Yurke. 1997. Measurement of the force-velocity relation for growing microtubules. *Science.* 278:856–860. https://doi.org/10.1126/science.278.5339.856

Duncan, A.W., M.H. Taylor, R.D. Hickey, A.E. Hanlon Newell, M.L. Lenzi, S.B. Olson, M.J. Finegold, and M. Grompe. 2010. The ploidy conveyor of mature hepatocytes as a source of genetic variation. *Nature.* 467:707–710. https://doi.org/10.1038/nature09414

Endow, S.A., and D.J. Komma. 1998. Assembly and dynamics of an anastral: astral spindle: the meiosis II spindle of Drosophila oocytes. *J. Cell Sci.* 111:2487–2495.

Fink, G., L. Hajdo, K.J. Skowronek, C. Reuther, A.A. Kasprzak, and S. Diez. 2009. The mitotic kinesin-14 Ncd drives directional microtubule-microtubule sliding. *Nat. Cell Biol.* 11:717–723. https://doi.org/10.1038/ncb1877

Fox, D.T., J.G. Gall, and A.C. Spradling. 2010. Error-prone polyploid mitosis during normal Drosophila development. *Genes Dev.* 24:2294–2302. https://doi.org/10.1101/gad.1952710

Frawley, L.E., and T.L. Orr-Weaver. 2015. Polyploidy. *Curr. Biol.* 25:R353–R358. https://doi.org/10.1016/j.cub.2015.03.037

Fujiwara, T., M. Bandi, M. Nitta, E.V. Ivanova, R.T. Bronson, and D. Pellman. 2005. Cytokinesis failure generating tetraploids promotes tumorigenesis in p53-null cells. *Nature.* 437:1043–1047. https://doi.org/10.1038/nature04217

Gallaud, E., R. Caous, A. Pascal, F. Bazile, J.P. Gagné, S. Huet, G.G. Poirier, D. Chrétien, L. Richard-Parpaillon, and R. Giet. 2014. Ensconsin/Map7 promotes microtubule growth and centrosome separation in Drosophila neural stem cells. *J. Cell Biol.* 204:1111–1121. https://doi.org/10.1083/jcb.201311094

Ganem, N.J., and D. Pellman. 2012. Linking abnormal mitosis to the acquisition of DNA damage. *J. Cell Biol.* 199:871–881. https://doi.org/10.1083/jcb.201210040

Ganem, N.J., S.A. Godinho, and D. Pellman. 2009. A mechanism linking extra centrosomes to chromosomal instability. *Nature.* 460:278–282. https://doi.org/10.1038/nature08136

Gatti, M., and B.S. Baker. 1989. Genes controlling essential cell-cycle functions in Drosophila melanogaster. *Genes Dev.* 3:438–453. https://doi.org/10.1101/gad.3.4.438

Gemble, S., A. Simon, C. Pennetier, M. Dumont, S. Herve, F. Meitinger, K. Oegema, R. Rodriguez, G. Almouzni, D. Fachinetti, and R. Basto. 2019. Centromere Dysfunction Compromises Mitotic Spindle Pole Integrity. *Curr. Biol.* 29:3072–3080.e5. https://doi.org/10.1016/j.cub.2019.07.052

Gittes, F., B. Mickey, J. Nettleton, and J. Howard. 1993. Flexural rigidity of microtubules and actin filaments measured from thermal fluctuations in shape. *J. Cell Biol.* 120:923–934. https://doi.org/10.1083/jcb.120.4.923

Godinho, S.A., R. Picone, M. Burute, R. Dagher, Y. Su, C.T. Leung, K. Polyak, J.S. Brugge, M. Théry, and D. Pellman. 2014. Oncogene-like induction of cellular invasion from centrosome amplification. *Nature.* 510:167–171. https://doi.org/10.1038/nature13277

Gogendeau, D., K. Siudeja, D. Gambarotto, C. Pennetier, A.J. Bardin, and R. Basto. 2015. Aneuploidy causes premature differentiation of neural and intestinal stem cells. *Nat. Commun.* 6:8894. https://doi.org/10.1038/ncomms9894

Goshima, G., M. Mayer, N. Zhang, N. Stuurman, and R.D. Vale. 2008. Augmin: a protein complex required for centrosome-independent microtubule generation within the spindle. *J. Cell Biol.* 181:421–429. https://doi.org/10.1083/jcb.200711053

Hayward, D., J. Metz, C. Pellacani, and J.G. Wakefield. 2014. Synergy between multiple microtubule-generating pathways confers robustness to centrosome-driven mitotic spindle formation. *Dev. Cell.* 28:81–93. https://doi.org/10.1016/j.devcel.2013.12.001

Holland, A.J., D. Fachinetti, Q. Zhu, M. Bauer, I.M. Verma, E.A. Nigg, and D.W. Cleveland. 2012. The autoregulated instability of Polo-like kinase 4 limits centrosome duplication to once per cell cycle. *Genes Dev.* 26:2684–2689. https://doi.org/10.1101/gad.207027.112

Homem, C.C., and J.A. Knoblich. 2012. Drosophila neuroblasts: a model for stem cell biology. *Development.* 139:4297–4310. https://doi.org/10.1242/dev.080515

Houchmandzadeh, B., J.F. Marko, D. Chatenay, and A. Libchaber. 1997. Elasticity and structure of eukaryote chromosomes studied by micromanipulation and micropipette aspiration. *J. Cell Biol.* 139:1–12. https://doi.org/10.1083/jcb.139.1.1

Howard, J., A.J. Hudspeth, and R.D. Vale. 1989. Movement of microtubules by single kinesin molecules. *Nature.* 342:154–158. https://doi.org/10.1038/342154a0

Ikeshima-Kataoka, H., J.B. Skeath, Y. Nabeshima, C.Q. Doe, and F. Matsuzaki. 1997. Miranda directs Prospero to a daughter cell during Drosophila asymmetric divisions. *Nature.* 390:625–629. https://doi.org/10.1038/37641

Kapoor, T.M., T.U. Mayer, M.L. Coughlin, and T.J. Mitchison. 2000. Probing spindle assembly mechanisms with monastrol, a small molecule inhibitor of the mitotic kinesin, Eg5. *J. Cell Biol.* 150:975–988. https://doi.org/10.1083/jcb.150.5.975

Kirkham, M., T. Müller-Reichert, K. Oegema, S. Grill, and A.A. Hyman. 2003. SAS-4 is a C. elegans centriolar protein that controls centrosome size. *Cell.* 112:575–587. https://doi.org/10.1016/S0092-8674(03)00117-X

Kwon, M., S.A. Godinho, N.S. Chandhok, N.J. Ganem, A. Azioune, M. Thery, and D. Pellman. 2008. Mechanisms to suppress multipolar divisions in cancer cells with extra centrosomes. *Genes Dev.* 22:2189–2203. https://doi.org/10.1101/gad.1700908

Lacroix, B., G. Letort, L. Pitayu, J. Sallé, M. Stefanutti, G. Maton, A.M. Ladouceur, J.C. Canman, P.S. Maddox, A.S. Maddox, et al. 2018. Microtubule Dynamics Scale with Cell Size to Set Spindle Length and Assembly Timing. *Dev. Cell.* 45:496–511.e6. https://doi.org/10.1016/j.devcel.2018.04.022

Letort, G., F. Nedelec, L. Blanchoin, and M. Théry. 2016. Centrosome centering and decentering by microtubule network rearrangement. *Mol. Biol. Cell.* 27:2833–2843. https://doi.org/10.1091/mbc.e16-06-0395

Letort, G., I. Bennabi, S. Dmitrieff, F. Nedelec, M.H. Verlhac, and M.E. Terret. 2019. A computational model of the early stages of acentriolar meiotic spindle assembly. *Mol. Biol. Cell.* 30:863–875. https://doi.org/10.1091/mbc.E18-10-0644

Lucas, E.P., and J.W. Raff. 2007. Maintaining the proper connection between the centrioles and the pericentriolar matrix requires Drosophila centrosomin. *J. Cell Biol.* 178:725–732. https://doi.org/10.1083/jcb.200704081

Marthiens, V., M. Piel, and R. Basto. 2012. Never tear us apart--the importance of centrosome clustering. *J. Cell Sci.* 125:3281–3292. https://doi.org/10.1242/jcs.094797

Martinez-Campos, M., R. Basto, J. Baker, M. Kernan, and J.W. Raff. 2004. The Drosophila pericentrin-like protein is essential for cilia/flagella function, but appears to be dispensable for mitosis. *J. Cell Biol.* 165:673–683. https://doi.org/10.1083/jcb.200402130

Musacchio, A. 2015. The Molecular Biology of Spindle Assembly Checkpoint Signaling Dynamics. *Curr. Biol.* 25:R1002–R1018. https://doi.org/10.1016/j.cub.2015.08.051

Musacchio, A., and K.G. Hardwick. 2002. The spindle checkpoint: structural insights into dynamic signalling. *Nat. Rev. Mol. Cell Biol.* 3:731–741. https://doi.org/10.1038/nrm929

Nano, M., S. Gemble, A. Simon, C. Pennetier, V. Fraisier, V. Marthiens, and R. Basto. 2019. Cell-Cycle Asynchrony Generates DNA Damage at Mitotic Entry in Polyploid Cells. *Curr. Biol.* 29:3937–3945.e7. https://doi.org/10.1016/j.cub.2019.09.041

Nedelec, F., and D. Foethke. 2007. Collective Langevin dynamics of flexible cytoskeletal fibers. *New J. Phys.* 9:427. https://doi.org/10.1088/1367-2630/9/11/427

Oladipo, A., A. Cowan, and V. Rodionov. 2007. Microtubule motor Ncd induces sliding of microtubules in vivo. *Mol. Biol. Cell.* 18:3601–3606. https://doi.org/10.1091/mbc.e06-12-1085

Orr-Weaver, T.L. 2015. When bigger is better: the role of polyploidy in organogenesis. *Trends Genet.* 31:307–315. https://doi.org/10.1016/j.tig.2015.03.011

Paim, L.M.G., and G. FitzHarris. 2019. Tetraploidy causes chromosomal instability in acentriolar mouse embryos. *Nat. Commun.* 10:4834. https://doi.org/10.1038/s41467-019-12772-8

Prosser, S.L., and L. Pelletier. 2017. Mitotic spindle assembly in animal cells: a fine balancing act. *Nat. Rev. Mol. Cell Biol.* 18:187–201. https://doi.org/10.1038/nrm.2016.162

Quintyne, N.J., J.E. Reing, D.R. Hoffelder, S.M. Gollin, and W.S. Saunders. 2005. Spindle multipolarity is prevented by centrosomal clustering. *Science.* 307:127–129. https://doi.org/10.1126/science.1104905

Rhys, A.D., P. Monteiro, C. Smith, M. Vaghela, T. Arnandis, T. Kato, B. Leitinger, E. Sahai, A. McAinsh, G. Charras, and S.A. Godinho. 2018. Loss of E-cadherin provides tolerance to centrosome amplification in epithelial cancer cells. *J. Cell Biol.* 217:195–209. https://doi.org/10.1083/jcb.201704102

Rupp, B., and F. Nédélec. 2012. Patterns of molecular motors that guide and sort filaments. *Lab Chip.* 12:4903–4910. https://doi.org/10.1039/c2lc40250e

Santaguida, S., A. Tighe, A.M. D'Alise, S.S. Taylor, and A. Musacchio. 2010. Dissecting the role of MPS1 in chromosome biorientation and the spindle checkpoint through the small molecule inhibitor reversine. *J. Cell Biol.* 190:73–87. https://doi.org/10.1083/jcb.201001036

Silkworth, W.T., I.K. Nardi, L.M. Scholl, and D. Cimini. 2009. Multipolar spindle pole coalescence is a major source of kinetochore mis-attachment and chromosome mis-segregation in cancer cells. *PLoS One.* 4:e6564. https://doi.org/10.1371/journal.pone.0006564

Somma, M.P., B. Fasulo, G. Cenci, E. Cundari, and M. Gatti. 2002. Molecular dissection of cytokinesis by RNA interference in Drosophila cultured cells. *Mol. Biol. Cell.* 13:2448–2460. https://doi.org/10.1091/mbc.01-12-0589

Storchova, Z., and D. Pellman. 2004. From polyploidy to aneuploidy, genome instability and cancer. *Nat. Rev. Mol. Cell Biol.* 5:45–54. https://doi.org/10.1038/nrm1276

Straight, A.F., C.M. Field, and T.J. Mitchison. 2005. Anillin binds nonmuscle myosin II and regulates the contractile ring. *Mol. Biol. Cell.* 16:193–201. https://doi.org/10.1091/mbc.e04-08-0758

Unhavaithaya, Y., and T.L. Orr-Weaver. 2012. Polyploidization of glia in neural development links tissue growth to blood-brain barrier integrity. *Genes Dev.* 26:31–36. https://doi.org/10.1101/gad.177436.111

Vargas-Hurtado, D., J.B. Brault, T. Piolot, L. Leconte, N. Da Silva, C. Pennetier, A. Baffet, V. Marthiens, and R. Basto. 2019. Differences in Mitotic Spindle Architecture in Mammalian Neural Stem Cells Influence Mitotic Accuracy during Brain Development. *Curr. Biol.* 29:2993–3005.e9. https://doi.org/10.1016/j.cub.2019.07.061

Watanabe, S., G. Shioi, Y. Furuta, and G. Goshima. 2016. Intra-spindle Microtubule Assembly Regulates Clustering of Microtubule-Organizing Centers during Early Mouse Development. *Cell Reports.* 15:54–60. https://doi.org/10.1016/j.celrep.2016.02.087

Zack, T.I., S.E. Schumacher, S.L. Carter, A.D. Cherniack, G. Saksena, B. Tabak, M.S. Lawrence, C.Z. Zhsng, J. Wala, C.H. Mermel, et al. 2013. Pan-cancer patterns of somatic copy number alteration. *Nat. Genet.* 45:1134–1140. https://doi.org/10.1038/ng.2760

Zhu, S., S. Lin, C.F. Kao, T. Awasaki, A.S. Chiang, and T. Lee. 2006. Gradients of the Drosophila Chinmo BTB-zinc finger protein govern neuronal temporal identity. *Cell.* 127:409–422. https://doi.org/10.1016/j.cell.2006.08.045

Supplemental material

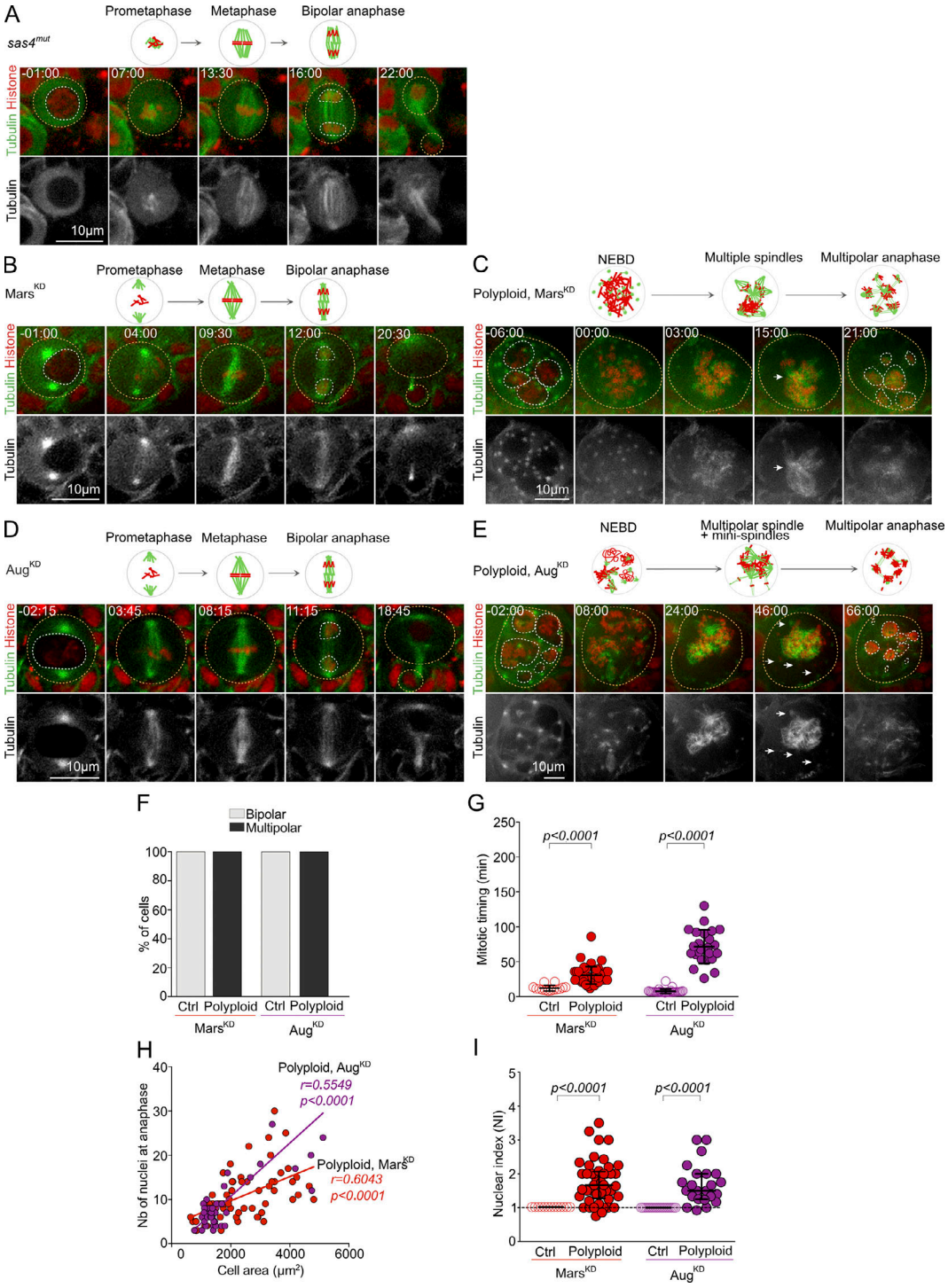

Figure S1. **Diploid and polyploid NBs depleted for MT-nucleating pathways undergo bipolar and multipolar divisions. (A–E)** Stills of time-lapse videos of mitotic NBs expressing histone-RFP (red) and tubulin-GFP (green and gray in the bottom insets). Orange and white dotted circles surround cells and nuclei, respectively. Time of mitosis is represented in minutes:seconds, and time 00:00 corresponds to NEBD. Schematic representations of mitosis are shown above the stills. Diploid *sas4*^{mut} (A) Diploid, Mars^{KD} (B), polyploid, Mars^{KD} (C), diploid, Aug^{KD} (D), and polyploid, Aug^{KD} (E) NBs. **(F)** Graph bars showing the percentage of cells presenting bipolar and multipolar mitosis in Ctrl, Mars^{KD} (n = 13 NBs from 1 BL), polyploid, Mars^{KD} (n = 63 NBs from 36 BL), Ctrl, Aug^{KD} (n = 30 NBs from 3 BL), and polyploid, Aug^{KD} (n = 45 NBs from 15 BL) NBs. **(G)** Dot plot showing the time spent in mitosis for Ctrl, Mars^{KD} (n = 13 NBs from 1 BL), polyploid, Mars^{KD} (n = 63 NBs from 36 BL), Ctrl, Aug^{KD} (n = 30 NBs from 3 BL) and polyploid, Aug^{KD} (n = 24 NBs from 10 BL) NBs. **(H)** XY plot and corresponding linear regression between the number of nuclei generated at anaphase and cell area of polyploid, Mars^{KD} (n = 63 NBs from 36 BL), and polyploid Aug^{KD} (n = 45 NBs from 15 BL) NBs. Statistical significance of the correlation was determined by a Spearman r test. r corresponds to the correlation coefficient. **(I)** Dot plot showing the NI in Ctrl, Mars^{KD} (n = 13 NBs from 1 BL), polyploid, Mars^{KD} (n = 44 NBs from 26 brains), Ctrl, Aug^{KD} (n = 30 NBs from 3 BL), and polyploid, Aug^{KD} (n = 24 NBs from 10 brains) NBs. **(G and I)** Statistical significance was determined using a Mann-Whitney test. Error bars represent the mean ± SD (G) and the median ± interquartile range (I). p corresponds to the P value.

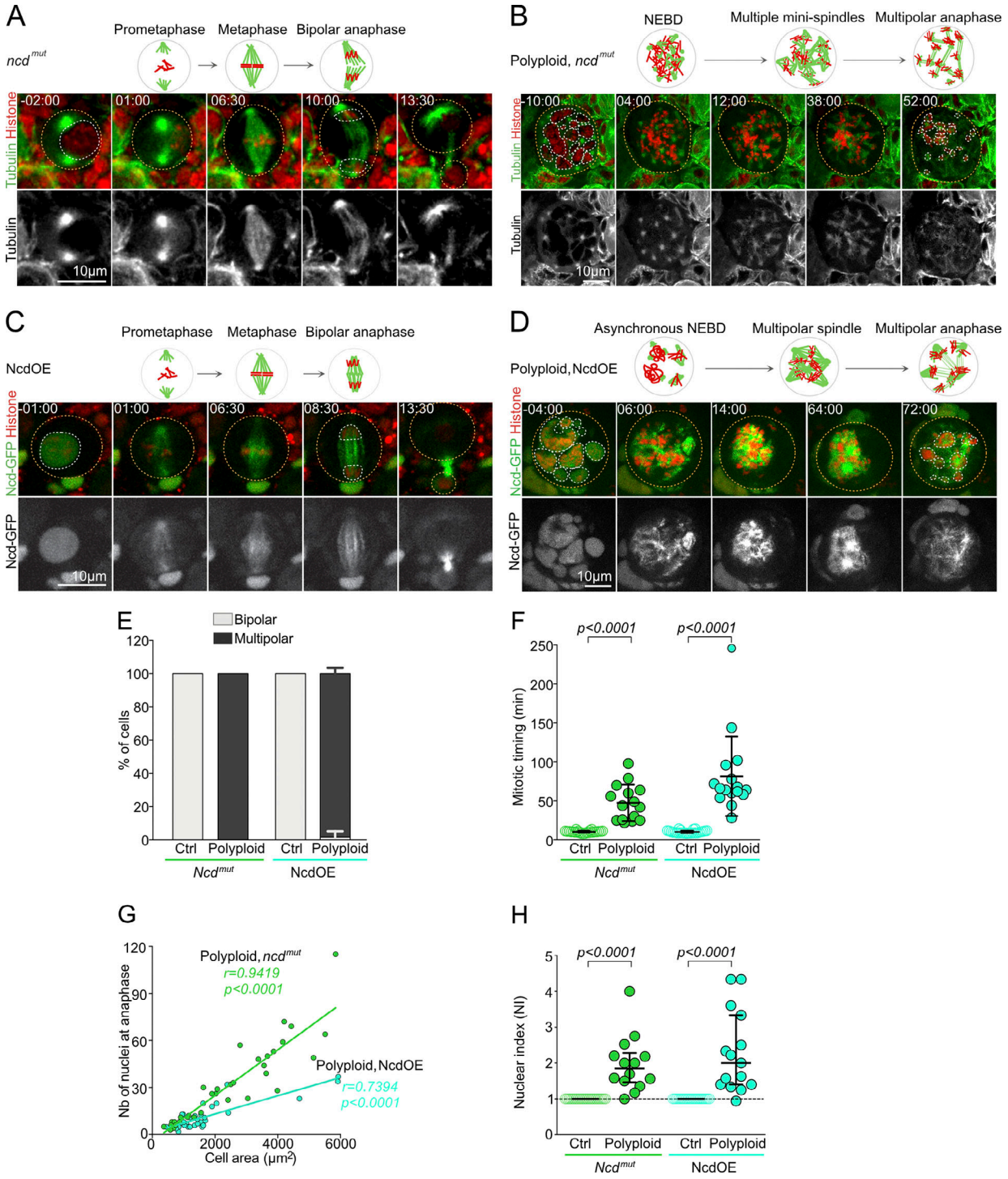

Figure S2. **Centrosome clustering takes place in polyploid mitosis, but it is not sufficient to promote bipolar spindle assembly. (A–D)** Stills of time-lapse videos of mitotic NBs expressing histone-RFP (red) and tubulin-GFP (A and B) or Ncd-GFP (C and D; green). Orange and white dotted circles surround cells and nuclei, respectively. Time of mitosis is represented in minutes:seconds, and time 00:00 corresponds to NEBD. Schematic representations of mitosis are shown above the stills. Ctrl, *ncd*^{mut} (A), polyploid, *ncd*^{mut} (B), Ctrl, NcdOE (C), and polyploid, NcdOE (D) NBs. **(E)** Graph bars showing the percentage of cells undergoing bipolar and multipolar mitosis in Ctrl, *ncd*^{mut} (n = 23 NBs from 3 BL), polyploid, *ncd*^{mut} (n = 34 NBs from 20 BL), Ctrl, NcdOE (n = 25 from 2 BL), and polyploid, NcdOE (n = 35 from 6 BL) NBs. **(F)** Dot plot showing the time spent in mitosis for Ctrl, *ncd*^{mut} (n = 24 NBs from 3 BL), polyploid, *ncd*^{mut} (n = 15 NBs from 12 BL), Ctrl, NcdOE (n = 25 NBs from 2 BL), and polyploid, NcdOE (n = 16 NBs from 5 BL) NBs. **(G)** XY plot and corresponding linear regression between the number of nuclei generated at anaphase and cell area for polyploid, *ncd*^{mut} (n = 34 NBs from 20 BL) and polyploid, NcdOE (n = 35 NBs from 6 BL) NBs. Statistical significance of the correlation was determined by a Spearman r test. r corresponds to the correlation coefficient. **(H)** Dot plot showing the NI for Ctrl, *ncd*^{mut} (n = 24 NBs from 3 BL), polyploid, *ncd*^{mut} (n = 14 NBs from 11 BL), Ctrl, NcdOE (n = 25 NBs from 2 BL), and polyploid NcdOE (n = 15 NBs from 4 BL) NBs. **(F and H)** Statistical significance was determined using a Mann-Whitney test. Error bars represent the mean ± SD (F) and the median ± interquartile range (H). p corresponds to the P value.

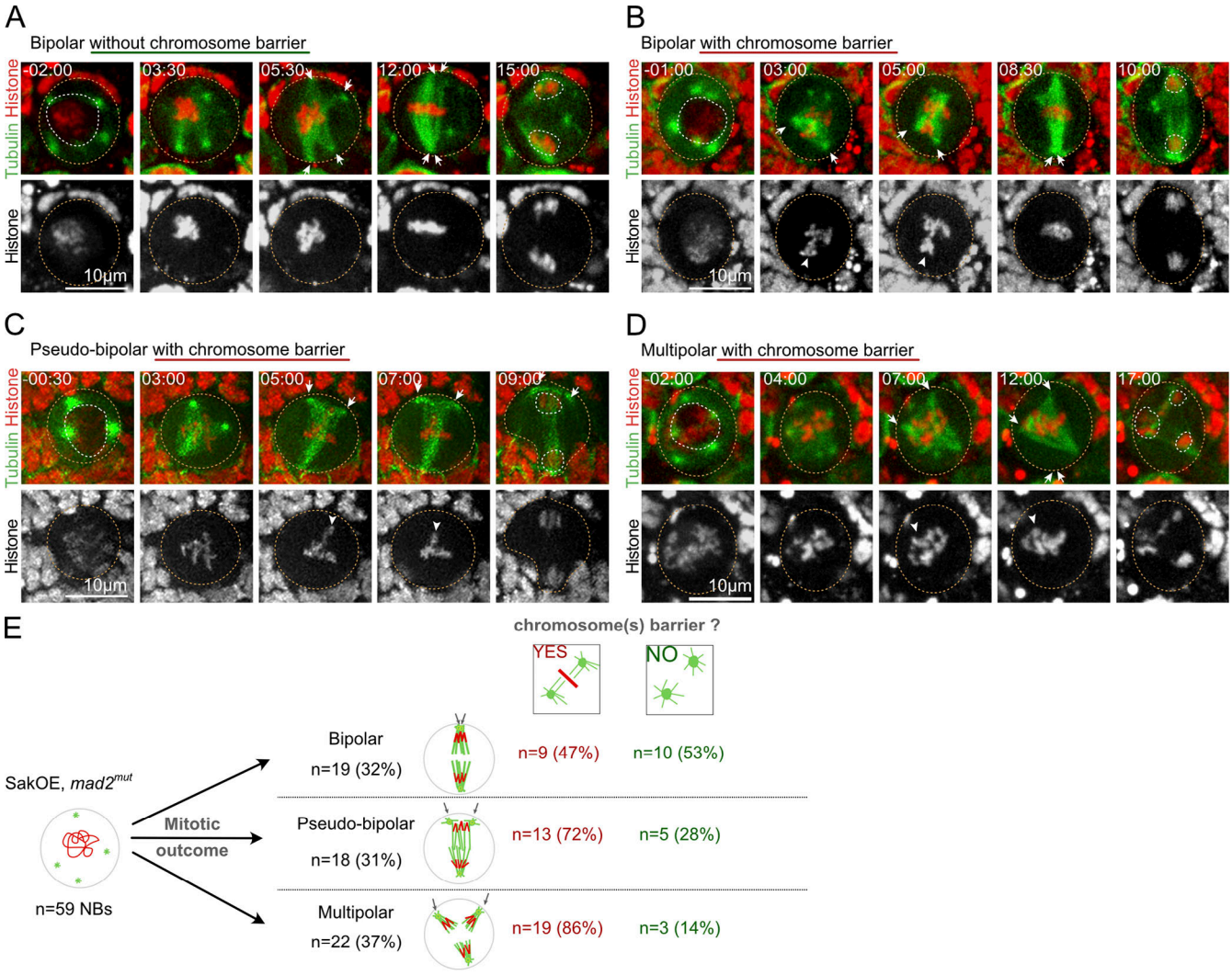

Figure S3. **Chromosomes as physical barrier can perturb centrosome clustering in diploid cells with centrosome amplification. (A–D)** Stills of time-lapse videos of mitotic SakOE, *mad2*^{mut} NBs expressing tubulin-GFP (green) and histone-RFP (red and gray in the bottom insets). Orange and white dotted circles surround cells and nuclei, respectively. Time of mitosis is indicated in minutes:seconds, and time 00:00 corresponds to NEBD. **(A)** SakOE, *mad2*^{mut} NB with several MT-nucleating sites builds up a bipolar spindle as centrosomes (arrows) are not blocked by a DNA barrier. **(B)** SakOE, *mad2*^{mut} NB presents several MT-nucleating sites and assembles a tripolar spindle containing DNA (arrowhead) between two poles (arrows). As mitosis proceeds, the DNA is pushed toward the metaphase plate, and the spindle becomes bipolar. **(C)** SakOE, *mad2*^{mut} NB with several MT-nucleating sites assembles first a tripolar spindle. A DNA mass acts as a barrier blocking the clustering of two poles (arrows). At anaphase onset, a pseudo-bipolar spindle, resulting from partial centrosome clustering, generates two nuclei. **(D)** SakOE, *mad2*^{mut} NB with several MT-nucleating sites displays multipolar division, as unresolved DNA barrier inhibits pole coalescence. **(E)** Table showing the number and the percentage of cells in each indicated category in SakOE, *mad2*^{mut} NBs (n = 59 NBs).

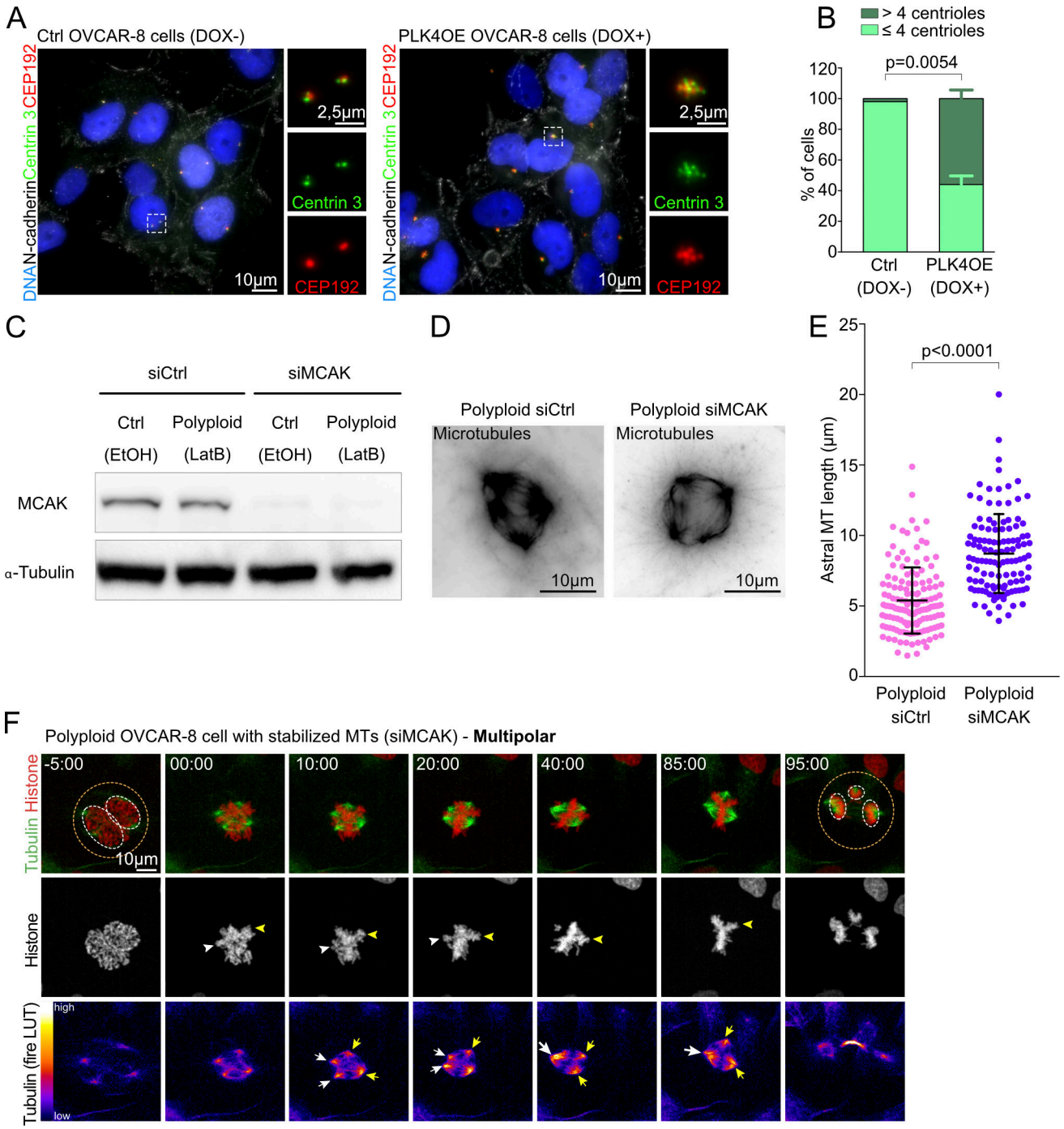

Figure S4. **PLK4OE and MCAK depletion, respectively, induce centrosome amplification and increased astral MT length. (A)** Pictures of Ctrl (DOX-) and PLK4OE (DOX+) OVCAR-8 cells labeled with antibodies against CEP192 and Centrin 3 to label the centrosomes and against the membrane marker N-cadherin. **(B)** Graph bars showing the percentage of Ctrl (DOX-; *n* = 488 cells from two independent experiments) and PLK4OE (DOX+; *n* = 410 cells from two independent experiments) OVCAR-8 cells presenting four or fewer or more than four centrioles. Statistical significance was determined using a multiple *t* test. **(C)** Western blot of siCtrl and siMCAK, OVCAR-8 cells. **(D)** Pictures of siCtrl polyploid and siMCAK polyploid OVCAR-8 cells labeled with antibodies against α-tubulin. **(E)** Dot plot showing the length of astral MTs in siCtrl, polyploid (*n* = 140 MTs from 11 cells) and siMCAK, polyploid (*n* = 118 MTs from eight cells) OVCAR-8 cells. Statistical significance was determined using a Mann-Whitney test. **(F)** Stills of time-lapse video of mitotic polyploid OVCAR-8 cell with stabilized MTs (siMCAK) expressing histone 2B-GFP (red and gray in the middle insets) and incubated with SiR-tubulin (green and fire LUT in the bottom insets). Orange and white dotted circles surround cells and nuclei, respectively. Time of mitosis is represented in minutes:seconds, and time 00:00 corresponds to the NEBD. Error bars represent the mean ± SD. p corresponds to the P value.

Video 1. **Mitosis in diploid and small and large polyploid NBs.** NBs expressing tubulin-GFP (green) and histone-RFP (red). Time of mitosis is indicated in minutes:seconds and hours:minutes:seconds for Ctrl and PavKD NBs, respectively. Frame rate speed of six frames per second. Time 00:00 and 00:00:00 correspond to NEBD. Still images from this video shown in Fig. 1.

Video 2. **Mitosis in diploid, sas4^{mut} and small and large polyploid, sas4^{mut} NBs.** NBs expressing tubulin-GFP (green) and histone-RFP (red). Time of mitosis is indicated in minutes:seconds and hours:minutes:seconds for Ctrl and PavKD NBs, respectively. Frame rate speed of six frames per second. Time 00:00 and 00:00:00 correspond to NEBD. Still images from this video shown in Fig. 3 and Fig. S1.

Video 3. **Mitosis in diploid, Mars^{KD}, diploid, Aug^{KD}, diploid, ncd^{mut}, and diploid, NcdOE NBs.** NBs expressing histone-RFP (red) and tubulin-GFP (green) or Ncd-GFP (green). Time of mitosis is indicated in minutes:seconds, and time 00:00 corresponds to NEBD. Frame rate speed of six frames per second. Still images from this video shown in Figs. S1 and 2.

Video 4. **Mitosis in polyploid, Mars^{KD}, polyploid, Aug^{KD}, polyploid, ncd^{mut}, and polyploid, NcdOE NBs.** NBs expressing histone-RFP (red) and yubulin-GFP (green) or Ncd-GFP (green). Time of mitosis is indicated in hours:minutes:seconds, and time 00:00:00 corresponds to NEBD. Frame rate speed of six frames per second. Still images from this video shown in Figs. S1 and 2.

Video 5. **Centrosome clustering in polyploid NBs. NBs expressing Spd2-GFP (green) and histone-RFP (red).** Time of mitosis is indicated in hours:minutes:seconds. Time 00:00:00 corresponds to NEBD. Frame rate speed of six frames per second. Still images from this video are shown in Fig. 4.

Video 6. **Computer simulations of spindle assembly according to centrosome number, DNA content, and DNA shape.** MTs are represented as green lines, centrosomes as green circles, and DNA as red dots or red plates. Computer simulations of spindle behavior run with low and high number of centrosomes, DNA beads, and different DNA shapes. Frame rate speed of six frames per second. Still images from this video shown in Fig. 4.

Video 7. **Mitosis in Ctrl, PLK4OE and polyploid OVCAR-8 cells.** Mitotic cells expressing histone 2B-GFP (red) and incubated with SiR-tubulin (green). Time of mitosis is indicated in hours:minutes:seconds, and time 00:00:00 corresponds to NEBD. Frame rate speed of six frames per second. Still images from this video shown in Figs. 5 and 6.

Video 8. **Laser ablation in polyploid OVCAR-8 cells.** Mitotic cells expressing histone 2B-GFP (red) and incubated with SiR-tubulin (green), presenting or failing spindle pole coalescence after laser ablation. Time of mitosis is indicated in hours:minutes:seconds, and time 00:00:00 corresponds to time of laser ablation. Yellow dotted circles represent laser ablation area. Frame rate speed of six frames per second. Still images from this video shown in Fig. 7.

Video 9. **Mitosis in mononucleated polyploid cells.** Computer simulations of spindle assembly in conditions of one or multiple DNA bead clusters and mitosis of mononucleated polyploid OVCAR-8 cells expressing histone 2B-GFP (red) and incubated with SiR-tubulin (green). Time of mitosis is indicated in hours:minutes:seconds, and time 00:00:00 corresponds to NEBD. Frame rate speed of six frames per second. Still images from this video shown in Fig. 8.

Video 10. **Mitosis in polyploid cells with increased MT stability.** Computer simulations of spindle assembly in conditions of Ctrl and increased MT stability and mitosis of polyploid OVCAR-8 cells expressing histone 2B-GFP (red) and incubated with SiR-tubulin (green) with siCtrl or siMCAK. Time of mitosis is indicated in hours:minutes:seconds, and time 00:00:00 corresponds to NEBD. Frame rate speed of six frames per second. Still images from this video shown in Fig. 9.

Provided online are three supplemental tables in Excel format. Table S1 shows the different parameters of mitotic NBs in diploid and polyploid conditions characterized in this study. The mitotic timing corresponds to the time elapsed from NEBD to anaphase onset in minutes. The NI is calculated as the ratio between the number of nuclei at anaphase over the number of nuclei at mitotic entry relative to the number of daughter cells. The slope of the linear regression between the number of nuclei generated at anaphase and polyploid cell area is determined using the equation of the linear regression line. Values correspond to the mean ± SD or percentage, and the statistical significances are related to diploid or polyploid controls. Statistical significances have been determined by Mann-Whitney tests for mitotic timing and NI and by linear regression for the slope lines. ND, not determined; ns, not significant; p, P value. Table S2 lists computer simulation parameters. Table S3 lists materials.

Chapter 2 - Results – *Section B*

Article - Goupil et al. 2021 – preprint version on BioRxiv

"Drosophila neural stem cells show a unique dynamic pattern of gene expression that is influenced by environmental factors"

Alix Goupil, Carole Pennetier, Anthony Simon, Patricia Skorski, Allison Bardin and Renata Basto

Abstract

With the aim of developing a sensor for chromosome loss *in vivo*, we used the well-established GAL4/GAL80 system combined with a visual GFP marker in *Drosophila*. We show a low frequency of green cells in most *Drosophila* tissues, suggesting low aneuploidy levels. Unexpectedly, in the brain, GFP positive cells are more frequent, but in this case, they do not represent chromosome loss. Using genetic manipulations, RNA FISH and time-lapse microscopy, we uncovered a dynamic and reversible silencing of *GAL80* that occurs in *Drosophila* neural stem cells. Further, we showed that this novel gene expression regulation is influenced by environmental changes such as temperature variations or food composition. These results have important implications for the *Drosophila* community, namely the possible interpretation of false positive cells in clonal experiments. Additionally, they also highlight a level of mosaicism and plasticity in the brain, consistent with possible epigenetic regulation of fly chromosomes, which is different from other organs and tissues.

Introduction

All multicellular organisms originate from one unique totipotent cell, the zygote. This single cell divides to generate a high number of different cell types in different organs. Frequently, different cell lineages can adopt different morphologies which might be related with their function (Prasad and Alizadeh, 2019). The balance between proliferation and differentiation has to be finely tune in order to allow, during development, accurate gene expression patterns, which ensure cell fate determination (Rué and Martinez Arias, 2015). The establishment of appropriate developmental programs are tightly controlled in space and in time, such as in the optic lobe of the *Drosophila* larval brain where the combination of temporal and spatial axes in a set of neural stem cells generates highly complex neuronal diversity (Isshiki et al., 2001; Li et al., 2013; Suzuki et al., 2013; Erclik et al., 2017). Patterns of gene expression can be established by epigenetic modifications in proliferating cells, which can then be inherited by daughter cells and stably maintained over time. Genome plasticity such as the control of gene expression in response to environmental changes also influences tissue and organ behavior and development with important consequences in organism fitness (Tian and Marsit, 2018).

Most cells of a given organism present the same genetic information, which is transmitted throughout generations to maintain genetic stability. Defects in chromosome segregation result in deviations to the normal diploid chromosome content (Siegel and Amon, 2012; Bakhoum et al., 2014) In this case, cells are aneuploid, which can impact several processes such as proliferation capacity, protein homeostasis, chromosome and genetic instability (Pfau et al., 2016). Interestingly, aneuploid cells might also have different fates. In *Drosophila*, for example aneuploid wing disc cells are eliminated by apoptosis (Dekanty et al., 2012), while neural stem cells in the brain seem to lose proliferative capacity and undergo premature differentiation (Gogendeau et al., 2015). In humans, whole organism aneuploidies are frequently inviable. Developmental diseases such Down and Turner syndromes are associated with mental retardation (Lippe, 1991; Antonarakis et al., 2004). In cancer, complex aneuploidies have been described which are thought to contribute to tumour initiation and evolution (Harris and Boveri, 2008; Sansregret and Swanton, 2017; Bakhoum and Landau, 2017).

While multiple studies have addressed the mechanisms by which aneuploid cells are generated, we still lack knowledge concerning their genesis in wild type (WT) organisms. Additionally, the factors that contribute to the maintenance of aneuploid cells in tissues or that influence their fate and outcome remain to be explored. To overcome this caveat, we have established an *in vivo* method to analyse chromosome loss in a multicellular organism. This system is based on the bipartite GAL4/UAS for detection of green nuclear fluorescent protein (GFP) combined with the repressor GAL80 inserted at specific chromosome sites in *Drosophila melanogaster*. Analysis of 20 different GAL80 fly lines corresponding to different chromosome locations across the X, II and III chromosomes revealed only the presence of a low number of GFP positive cells, consistent with low levels of aneuploidy in WT proliferative epithelial tissues such as the wing disc. Strikingly however, in developing brains a large number of green cells was noticed. Using a variety of methods, including FISH and live imaging analysis, we show that, unexpectedly these cells are not aneuploid. Instead, they seem to result from a dynamic plastic gene regulation specific of the *Drosophila* brain that we further show it is influenced by environmental outputs such as food intake and temperature variations.

Results

A novel strategy to monitor chromosome loss based on the GAL4/GAL80 system

With the aim of developing a chromosome loss sensor in *Drosophila melanogaster* we designed a genetic tool based the principle of the loss of heterozygosity using the well-established GAL4/UAS/GAL80 system (Suster et al. 2004; Siudeja et al. 2015; Szabad, Bellen, and Venken 2012) and the expression of a fluorescent tag- green fluorescent protein (GFP fused to a nuclear localization signal (GFP-NLS). The *GFP-NLS* expression is driven by the Upstream Activating Sequence (UAS), which is a regulatory sequence activated by the transcriptional factor GAL4 (Brand and Perrimon, 1993). In the presence of the repressor GAL80, the GAL4 transcriptional activity is inhibited (Lee and Luo, 1999; Suster et al., 2004) and thus represses *GFP-NLS* expression. In this case all nuclei should appear black since they are GFP negative (GFP^-). However, upon the loss of the chromosome carrying the *GAL80* sequence, *GFP-NLS* expression should be noticed through the appearance of green fluorescence, GFP positive (GFP^+) nuclei (Figure 1A). We wanted to develop this system to monitor random chromosome loss of any of the major autosomes (chromosomes II and III) and the X chromosome.

Because chromosome loss is known to occur after chromosome mis-segregation in mitotically active cells (Levine and Holland, 2018), we focused on two *Drosophila* tissues known to be highly proliferative at third instar larvae (L3): the brain lobes, which make part of the fly central nervous system and epithelial wing discs, which are the primordial fly wings (Figure 1B).

Using meiotic recombination in the female germline, we established an *Act-GAL4, GFP-NLS Drosophila* recombinant line carrying on chromosome II the *UAS-stinger* sequence (Stable insulated nuclear eGFP) (Barolo et al., 2000) and the *GAL4* gene controlled by the ubiquitous *Actin5C* promotor (Struhl and Basler, 1993; Ito et al., 1997). Importantly, we confirmed that *Act-GAL4, GFP-NLS* expressing larvae show GFP^+ nuclei in both brain lobes and wing discs (Figure 1C). For the establishment of the *GAL80* lines, we designed a new vector expressing a *GAL80* version which has been optimized for *Drosophila* codon usage (Pfeiffer et al., 2010) under the control of the ubiquitous *Tubulin 1α* promotor – *Tub-GAL80* (O'Donnell et al., 1994; Lee and Luo, 1999). Even though this GAL80 optimized codon was shown to have a higher GAL4 suppression capacity (Pfeiffer et al., 2010), it is known that the chromosomal

environment and so its insertion site impacts transgene expression (Elgin and Reuter, 2013). To ensure the best optimal *Tub-GAL80* expression conditions, we generated a total of 20 *Drosophila* lines. Each line carried one copy of the *Tub-GAL80* transgene inserted at one specific site and it will be referred to as *Tub-GAL80* followed by the insertion site in superscript. As an example, the *Tub-GAL80* insertion at the 5B8 location on the X chromosome will be referred as *Tub-GAL80$^{X\text{-}5B8}$*. We obtained lines with *Tub-GAL80* insertions at different locations on chromosomes X, II and III. A list summarizing the insertion sites and their position relative to the centromere can be found in Figure 1D.

The large majority of wing disc cells are GFP negative

As a proof of concept, we screened all *Tub-GAL80* stocks for their capacity to repress the *Act-GAL4, GFP-NLS* driver. We analysed by immunofluorescence 7 to 20 wing discs per *Tub-GAL80* insertion. For all lines, the vast majority of wing discs were GFP$^-$ (361/369 in total) (Figure 1E-F). In 5 out of the 8 wing discs that contained GFP$^+$ cells, these cells were restricted to only a few cells within the whole GFP$^-$ tissue (5 wing discs from 5 different *Tub-GAL80* constructs) (Supplementary Figure 1A). Interestingly, only one single *Tub-GAL80* line- *Tub-GAL80$^{III\text{-}82A1}$*- had a high number of GFP$^+$ cells (Supplementary Figure 1B). Importantly, however, this only occurred in 3 out of 12 wing discs analysed for this line (Figure 1F). This suggests that in the wing disc, most *Tub-GAL80* expressing flies, can repress *GFP-NLS* expression. The same observation, namely the absence of GFP signal, was obtained after the analysis of other imaginal discs (Supplementary Figure 1C). Overall these results showed that for 19 out of 20 lines, the system is functional with GAL80 repressing GAL4 activity in epithelial larval discs.

The brain presents a high number of GFP$^+$ cells

The larval brain lobe can be divided in two main regions, the central brain and the optic lobe. The central brain is composed of the neural stem cells, also called neuroblasts (NBs) that divide asymmetrically to self-renew and give rise to smaller and more committed progenitors, the ganglion mother cells (GMCs). Two populations of larval NBs have been identified. Type I NBs, which divide asymmetrically to give rise to GMCs that will divide once more before undergoing differentiation to generate either glia or neurons. Type II NBs generate intermediate progenitors through asymmetric cell division, which will then generate GMCs

followed by differentiation (Bello et al., 2008; Boone and Doe, 2008; Homem and Knoblich, 2012). The optic lobe comprises two proliferative centers, the inner and the outer, which correspond to a pseudo-stratified epithelium called the neuroepithelium (NE). NE cells give rise to neurons necessary for the development of the visual system of the fly. Further, perineural and sub-perineural glial cells with large nuclei are found at the superficial layer of the brain (Pereanu et al., 2005). Interestingly, all these cell types are easily distinguishable by their morphology, position within the tissue and expression markers (Figure 2A-E).

As described above, we screened the *Tub-GAL80* lines for their capacity to repress GAL4 and thus the expression of *GFP-NLS*. Interestingly and in contrast with the results obtained for wing discs, brain lobes frequently contained GFP^+ cells. Moreover, the morphology of the GFP^+ cells was different among the various *Tub-GAL80* lines, suggesting that GFP^+ cells belong to different cell populations (Figure 2B-E). The different cell types that populate the brain lobes are morphologically distinguishable and recognised through DNA labelling (DAPI) and by their spatial position within the brain (Figure 2A). Using specific markers, we confirmed by immunofluorescence the various identities of GFP^+ cells. Indeed, Dpn^+ NBs in the central brain occupy the first layers of the tissue, just below the surface and have large nuclei. Dpn^-/$Propero^{weak}$ GMCs are small nuclei juxtaposed to NBs (Figure 2A-B and Supplementary 2A). The individual $Elav^+$ neurons recognised by the small-sized nuclei are dispersed in the central brain and localised deeper in the tissue (Figure 2C and Supplementary 2B). The NE, which is recognizable by the actin organization of this pseudo-stratified epithelium, is localised in the optic lobe region and NE cells contain highly arranged and small nuclei (Figure 2D and Supplementary 2C). Finally, $Repo^+$ glial cells are located at the periphery of the lobes and have large nuclei (Figure 2E and Supplementary 2D). Interestingly, some brain lobes presented a mix population of GFP^+ cells, while in others these cells were absent (Supplementary Figure 2E-F).

To obtain a quantitative view of the population of GFP^+ cells, we counted and categorized GFP^+ cells into the following subtypes: 1) GFP^+ clusters which included NBs and associated GMCs (independently of their number); 2) GFP^+ clusters for NE cells and 3) individual GFP^+ cells for differentiated neurons and glia. We represented with a colour code the number of GFP^+ cells/clusters, taken as independent groups. Interestingly, analysis of 459 brain lobes from all the *Tub-GAL80* lines (minimum of 14 brain lobes per *Tub-GAL80* insertion line) revealed that the number and identity of GFP^+ cells varied between different *Tub-GAL80*

lines and even more surprisingly within the same *Tub-GAL80* line (Supplementary Figure 3). For example, *Tub-GAL80$^{X\text{-}5B8}$* on the X chromosome presented a high number of green NBs and associated GMCs, but no green neurons or glial cells were detected and only very few green NE cells were observed. (Supplementary Figure 2A and Supplementary Figure 3A). In contrast, *Tub-GAL80$^{III\text{-}82A1}$* on chromosome III, showed a high number of green neurons and glia and only a low number of green NBs/GMCs (Supplementary Figure 3E), while *Tub-GAL80$^{II\text{-}22A}$* (chromosome II) displayed only a few green cells in each category (Supplementary Figure 2F and Supplementary Figure 3B).

To be able to compare the frequency and identity of green cells, we plotted the mean value of each group category (cell identity) for all the *Tub-GAL80* lines (Figure 2F). Strikingly, this analysis showed that green cells were highly frequent in the central brain of all the *Tub-GAL80* lines, with the highest incidence in the NB and GMC cell population. It is important to mention that we did not find a trend in the position or spatial arrangement of GFP$^+$ NBs or even other cell types within the different brain lobes analysed. These observations suggest that there is no particular stereotype or spatial pattern of the cells expressing *GFP-NLS*, but rather that they are randomly positioned.

To use an alternative means of quantifying the frequency of GFP$^+$ cells in the brain, we measured the area of the GFP signal and express it as the percentage of coverage per brain lobe area (Supplementary Figure 4A). As expected, the high frequency revealed by the colour code correlated with highest coverage values (Figure 2F and Supplementary Figure 4B). We conclude that a high number of GFP$^+$ cells including NBs, GMCs, NE cells, glia and neurons are present, independently of the *Tub-GAL80* insertion site. This result highly contrasts with the findings in wing discs using the same *Tub-GAL80* lines.

GFP positive cells in the brain are not the by-product of chromosome loss

We next focused our analysis on understanding the origin of the difference in the frequency of GFP$^+$ cells between wing discs and brains. An obvious hypothesis to explain the high incidence of GFP$^+$ cells in the brain was aneuploidy due to the loss of the *GAL80* containing chromosome (Figure 1A). We reasoned that if this was the case, GFP$^+$ cells should be aneuploid in contrast to diploid GFP$^-$ surrounding cells. To assess the ploidy of the GFP$^+$ cells, we used a Fluorescent *In Situ* Hybridization (FISH) protocol using probes against the chromosome carrying the *Tub-GAL80* insertion. As reported previously, dotty FISH signals can

be easily noticed ranging from 1 to 4 structures, which correspond most likely to different degrees of chromosome pairing and unpairing (Joyce et al., 2012). While this limitation precluded the use of FISH signals for precise ploidy assessment, we did notice that the FISH signals were similar between GFP^+ and GFP^- cells (Figure 3). Thus, this argues against the GFP^+ cells being aneuploid via chromosome loss, which would predict an overall decrease in the number of FISH signal dots. Additionally, to avoid possible mis-interpretation due to chromosome pairing, typical of *Drosophila* cells, we examined FISH signals in mitotic NBs which facilitates the analysis of FISH probes combined with individual chromosomes (Gatti et al., 1994). We confirmed that GFP^+ cells were not aneuploid as they presented the same number of FISH dots (Figure 3B) than control GFP^- NBs. These results suggest that the high frequency of green cells observed across different *Tub-GAL80* lines do not result from chromosome loss.

Mitotic recombination does not account for the presence of GFP positive cells in the brain

Non-sister chromatids can exchange chromosome pieces by cross-over in somatic cells, an event called mitotic recombination. Such event has been previously described in *Drosophila* (Stern, 1936; Kaplan, 1953; Siudeja et al., 2015; Siudeja and Bardin, 2017). We hypothesised that after replication, mitotic recombination might explain the loss of *Tub-GAL80* heterozygosity. In light of this scenario after cell division one daughter cell should be homozygous for *Tub-GAL80* (GFP^-) and its sister cell should lack the *Tub-GAL80* sequence (GFP^+) (Supplementary Figure 5A). We first tested this hypothesis considering the X inserted GAL80 line – $Tub\text{-}GAL80^{X\text{-}5B8}$. We compared GFP-NLS signals between males and females as mitotic recombination cannot occur between non-homologous X and Y chromosomes. Interestingly, both male and female larval brains presented similar levels of GFP^+ cells (Supplementary Figure 2A and Supplementary Figure 5B and H), suggesting that at least for the X chromosome mitotic recombination does not account for loss of the repressor GAL80. We next tested other genetic conditions where mitotic recombination was inhibited by the use of balancer chromosomes. Balancer chromosomes contain chromosomal inversions that supress crossing over with the homologous chromosome (Novitski and Braver, 1954). We used FM7, CyO and TM6 fly lines, which are specific balancers for the X, II and III chromosomes, respectively. Interestingly, the frequency of brain lobes presenting GFP^+ cells was unchanged using any of the balancer chromosomes when compared to controls (Supplementary Figure

5C-H). Additionally, we did not observe an obvious decrease in the GFP coverage when mitotic recombination was inhibited, as values were highly variable between and within conditions as in control experiments (Supplementary Figure 5I and Supplementary Figure 3). Altogether, this suggests that the presence of GFP$^+$ cells and thus, the expression of *GFP-NLS* specifically in the brain does not result from mitotic recombination.

Analysis of frequently used *Tub-GAL80* lines confirms the lack of GAL80 inhibition in *Drosophila* NBs and alert on its use for MARCM analysis

Our results so far suggest that the high incidence of green cells found in *Drosophila* brains cannot be explained by chromosome loss or mitotic recombination. Thus, we hypothesised that in GFP$^+$ cells, the *Tub-GAL80* sequence was still present but likely not expressed. One trivial explanation for our results was that the *Tub-GAL80* sequences generated and used in this study may contain a particular feature that precludes its use in the brain. To test this possibility, we analysed *GAL80 Drosophila* lines with different origins and established by other labs available from the Bloomington *Drosophila* Stock Center. We first tested three different lines containing one copy of *Tub-GAL80* inserted on the X chromosome (#5132-*Tub-GAL80$^{X\text{-}1C2}$*) and chromosome III (#5191-*Tub-GAL80$^{III\text{-}75E1}$* and #9490-*Tub-GAL80^{III}*). Interestingly, similar to our *Tub-GAL80* lines, the large majority of brain lobes presented high levels of GFP$^+$ cells in contrast to the absence or low levels of GFP-NLS signals in the wing discs (Figure 4A-D and G). These results suggest that like our *Tub-GAL80* lines described above, the *Tub-GAL80* lines available from other labs cannot inhibit GAL4 activity in the brain, arguing against a specific effect of our lines.

In the experiments described so far, *GAL4* and *GAL80* expression are under the control of different promoters, even if both are strong and ubiquitous - actin and tubulin, respectively. We decided to test if differences in the promoters could contribute to inefficient repression of GAL4 as previously reported (Pfeiffer et al., 2010). Strikingly, this was indeed the case as very few GFP$^+$ cells were noticed in the *Drosophila* line carrying the *GAL80* sequence under the control of an *Actin* promotor - *Act-GAL80* (#67092) (Figure 4E-G). It is important to notice that in contrast to the other *Tub-GAL80* lines inserted on chromosomes X and III and used in this study, the *Act-GAL80* sequence is located at position 25C6 on chromosome II. This position might also impact *GAL80* expression levels and explain the efficiency in GAL4 inhibition and thus, *GFP-NLS* repression. This suggests that both the chromosomal insertion and the use of

the same promoters in repression/activation experiments accounts for stoichiometry between *GAL4* and *GAL80* expression levels.

The GAL4/GAL80 system is widely and routinely used by the *Drosophila* community to control gene expression. Importantly, this system has been used in MARCM experiments for neuronal lineage tracing in the developing *Drosophila* brain (Lee and Luo, 1999; Ren et al., 2016). This is based on the loss of heterozygosity (LOH) after mitotic recombination by the heat-induced FLP recombinase at specific FRT sites. LOH generates labelled mutant clones that lack the *GAL80* sequence and unlabelled wild type cells homozygous for *GAL80* (Figure 4H). We wanted to ensure that GFP$^+$ clones generated in the MARCM experiment was only due to LOH and not *GAL80* repression as we described above in the larval brain. We used *heat-shock FLP;; FRT^{82B}sas4^{mut}* expressing flies crossed with *UAS-GFP-NLS; Tub-GAL4, FRT^{82B}, Tub-GAL80.* The *sas-4* gene encodes for a protein essential for centriole duplication and *sas4* mutant cells lack centrosomes (Basto et al., 2006). Heat-shock at 37**°**C for 1H was used to induce FLP mediated recombination. We analysed GFP$^+$ clones in L3 brains and wing discs. As expected, we observed GFP$^+$ mutant clones without centrosomes (Figure 4I). Surprisingly, we also observed GFP$^+$ clones containing centriolar staining of Sas-4 protein, indicating that the WT sas4 gene was present (Figure 4J). Most likely, these latter clones were not generated through *GAL80* sequence loss upon FLP/FRT-mediated LOH, but they rather represent GFP$^+$ cells arising in the manner described above. Interestingly, and as a control, we also analysed brains that were not heat-shocked and again observed GFP$^+$ clones, even if at lower frequencies (Supplementary Figure 6A-B). Importantly, however in the wing discs in contrast to the brains, we only observed GFP$^+$ clones after heat-shock induction and these clones were *sas-4* negative (Figure 4K and Supplementary Figure 6C).

Importantly in this set of experiments, we found false positive cells using the MARCM system in the larval brain as it presents a mix population of GFP$^+$ clones generated both by the loss of *GAL80* sequence or by the loss of *GAL80* expression. To our knowledge, a brain-specific *GAL80* expression regulation has never been described before.

Increasing *Tub-GAL80* levels at certain chromosome locations efficiently inhibits GAL4 activity in the brain

It has been shown that one limitation of the GAL4/GAL80 system results from the stoichiometry in the system, since if both activator and repressor are expressed at the same

levels, one copy of *GAL80* might not be sufficient to repress GAL4 (Pfeiffer et al., 2010). In our experimental set up, *Act-GAL4* and *Tub-GAL80* are both ubiquitously expressed with strong actin and tubulin promoters, respectively. In principle, one copy of *Tub-GAL80* should be sufficient, especially because it has been optimized for *Drosophila* codon usage. However, the high frequency of GFP$^+$ cells observed in brain lobes and described above raise the question whether increased levels of GAL80 would favour GAL4 inhibition in the brain.

We built 5 different *Drosophila* recombinant lines harbouring two copies of *Tub-GAL80* inserted at two different and distant loci of the same chromosome and will be referred to as *2xTub-GAL80* (Supplementary Figure 7A). Interestingly, all brain lobes (n=50) from two lines containing *2xTub-GAL80* insertions on chromosomes II (*2xTub-GAL80$^{II\text{-}22A,53B2}$*) and III (*2xTub-GAL80x2$^{III\text{-}62E1,96F3}$*) were GFP$^-$ (Figure 5A and D-E). Surprisingly, however, the two other lines for the same chromosomes (*2xTub-GAL80$^{II\text{-}25A3,59D3}$* and *2xTub-GAL80$^{III\text{-}65B2,99F}$*) presented GFP$^+$ cells, though with a highly reduced frequency (Figure 5D-E and Supplementary Figure 7B-C). These results suggested that the addition of one extra-copy of *Tub-GAL80* on chromosomes II and III increased the capacity of GAL80 to inhibit GAL4 activity. Moreover, they also show that the position of the *Tub-GAL80* insertion influences its capacity to supress *GFP-NLS* expression, or in other words that *GAL80* expression might be conditioned by its position within the genome.

We next analysed brains containing the recombinant *2xTub-GAL80* insertions on the X chromosome - *2xTub-GAL80$^{X\text{-}5B8,19E7}$*, also confirmed by PCR (Supplementary Figure 7D). Strikingly, a high number of GFP$^+$ NBs and GMCs was noticed in this condition, either in the presence of two copies (*2xTub-GAL80$^{X\text{-}5B8,19E7}$* heterozygous) or even four copies (*2xTub-GAL80$^{X\text{-}5B8,19E7}$* homozygous) (Figure 5C-E). Importantly, the vast majority of wing discs were still GFP$^-$ (Supplementary Figure 7E and Figure 5E). To test if a NB specific promoter resulted in the change of GFP$^+$ NBs frequency in the *2xTub-GAL80$^{X\text{-}5B8,19E7}$* we used the NB specific promotor *Worniu* to drive *GAL4* expression. However, even in this condition, GFP$^+$ cells were very frequent (Supplementary Figure 7F).

Taken together our results show that increasing GAL80 levels results in a more effective inhibition of GAL4 in the brain for certain chromosomes and chromosome territories with the X chromosome representing an exception. Interestingly, our work revealed that *GAL80* insertions on the X chromosome behave quite differently from other lines, suggesting that this chromosome is somehow differently regulated in neural stem cells. We next focus

this study on the analysis of *2xTub-GAL80$^{X\text{-}5B8,19E7}$* line to understand why these *GAL80* insertions do not allow for complete GAL4 repression even if present at higher doses.

2xTub-GAL80$^{X\text{-}5B8,19E7}$ is not expressed in green *Drosophila* NBs

The results described above suggest a specific-brain failure of GAL80 to inhibit GAL4. To obtain more information about *GAL80* expression, we designed FISH probes that recognised *GAL80* mRNAs. The probes were tagged with a red fluophore (Methods). Analysis of *2xTub-GAL80$^{X\text{-}5B8,19E7}$* larval brains revealed that GFP^{+} NBs lack *GAL80* RNAs FISH signals, which was not the case for GFP^{-} NBs and surrounding cells that clearly presented red fluorescent dots (Figure 6A). These results suggest that *2xTub-GAL80$^{X\text{-}5B8,19E7}$* expression is indeed abolished in GFP^{+} NBs. The divisions of the NBs are highly stereotyped and daughter GMCs are always generated at the same location. Thus, as the NB continues to cycle, the older daughter GMCs become more distant and placed away from the NB (Homem and Knoblich, 2012). We noticed that in some NB/GMCs clusters, localised within the central brain, the GFP-NLS signal became weaker in the GMCs placed further away from the NB. Interestingly, GMCs displaying weak GFP fluorescence were positive for *GAL80* RNAs FISH signals (Figure 6A - above the red dotted line). This observation suggests that *Tub-GAL80* expression might have been re-activated in the oldest GMCs.

2xTub-GAL80$^{X\text{-}5B8,19E7}$ expression is dynamic and reversible

To obtain a dynamic view of the *Tub-GAL80* expression, we combined the same system - *Act-GAL4, GFP-NLS/2xTub-GAL80$^{X\text{-}5B8,19E7}$* - with the expression of histone H2Av variant tagged with RFP to follow chromosome behaviour. We performed time-lapse microscopy of larval brains for up to 48hrs, which represents roughly two thirds of the total proliferative window of the central nervous system during third instar larvae-72hrs. We analysed 168 NBs from 17 brain lobes and using our imaging set up we could identify mitotic entry and exit even after long periods of laser exposure at the end of the filming period. We also did not detect nuclear fragmentation, which is a sign of apoptosis. Together, we concluded that NBs were not being subjected to deleterious phototoxicity in our imaging conditions (see methods for details).

At the start of the movie several green clusters of NBs and GMCs could be easily noticed and interestingly, showed different green fluorescent intensities. We could also

identify non-fluorescent NBs as in the fixed preparations, confirming on one hand the concomitant presence of the two populations (GFP^+ and GFP^- NBs), but also possibly suggesting different birth timings revealed by the intensity of the GFP signal (Figure 6B-C). As the green NBs underwent consecutive mitosis, we noticed that the daughter GMC generated at each cell division was always green. Interestingly, we also observed that in some of the "oldest" GMCs the intensity of the green fluorescence was decreased. These results are consistent with the results of mRNA *GAL80* FISH described above and suggest that *GAL80* expression might be re-established in older GMCs. They also suggest that the young GMCs might inherit GFP-NLS through mitosis as the signal diffuses through the cytoplasm. This type of behaviour, maintenance of GFP in the NB and inheritance by the daughter GMC was observed in the large majority of all NBs presenting GFP signals at the start of the movie (n=158 out of 168 NBs) (Figure 6D-E).

In NBs that were initially non-fluorescent and so presumably expressing *GAL80*, we noticed the transient rise in GFP signal, which was also transmitted upon mitosis to the GMCs (Figure 6F). This was a much less common event as only a small proportion (1,2%, n=2 out of 168 NBs) of third instar NBs behaved in this way (Figure 6D). Importantly, these observations show that at this stage of development, while some NBs have already lost *Tub-GAL80* expression and thus accumulated a high level of GFP-NLS fluorescence, other NBs switch from a *Tub-GAL80* expressing to a *Tub-GAL80* repressive status.

Finally, a third type of behaviour was also noticed. In this case, GFP-NLS fluorescence disappeared from NBs (n=8 out of 168 NBs, Figure 6G). Interestingly, the lack of signal was maintained for many hours suggesting the maintenance of the expression of *Tub-GAL80* during this period of time. Altogether, time-lapse analysis of GFP-NLS in third instar larval brains reveals that *Tub-GAL80* expression in NBs from X- double inserted line, undergoes dynamic and to lower extend reversible changes resulting in GAL4 activity and GFP expression.

2xTub-GAL80$^{X\text{-}5B8,19E7}$ expression is influenced by environmental changes.

The dynamics and specificity of *GAL80* expression in NBs suggested a possible epigenetic regulation, specific to the brain during *Drosophila* development. This appears particular important in respect to the X chromosome since the presence of two *GAL80* copies resulted in the expression of GFP-NLS at a high frequency (Figure 5D-E). Epigenetic regulation is often used during development to provide adaptability to different environmental

conditions (Friedrich et al., 2019). We tested if different stresses could influence the system using the *2xTub-GAL80*$^{X\text{-}5B8,19E7}$ as a reporter of modifications in gene expression pattern. We controlled three parameters: (1) the food composition, (2) the abundance of parent flies and (3) the temperature of incubation and we assessed GFP signal frequency in L3 brain lobes. Importantly, each parameter was tested separately, however all conditions within each experiment were performed at the same time to allow comparison.

In all of our experimental set ups described so far, fly crosses were composed of about 20-30 parents and cultured at 25°C on a protein-rich medium, which are the standards used in *Drosophila* culture. We first altered food composition and cultured flies in a protein-poor medium made of cornmeal and low yeast content. Surprisingly, the number of GFP$^+$ clusters was significantly reduced in this latter condition when compared to standard rich medium (Figure 7A). Then, as a way to influence food accessibility, we varied the number of parent flies to induce different larval crowding. The addition of <5, ±30 or >100 parents did not change GFP signal frequency (Figure 7B). Finally, we switched the temperature of larval incubation varying from 18°C to 29°C. Temperature variations strongly impacted the frequency of GFP$^+$ cells. Interestingly, this was in a dose-dependent manner as the frequency gradually decreased as temperature increased (Figure 7C). Although we confirmed that change in environment conditions influences the system, it is important to mention that whatever the condition (Figure 7), the GFP signal was highly variable within a define experimental set up, as we described above (Figure 2 and Supplementary Figure 3). This suggests that abundant and yet unknown parameters influence the system.

Together, these results suggest that NBs of the *Drosophila* developing larval brain undergo a novel gene expression regulation mode that appears to be dynamic, reversible and capable of being influenced by different environmental conditions. It will be interesting to investigate if the findings described here also apply to other more complex central nervous systems.

Figure 1

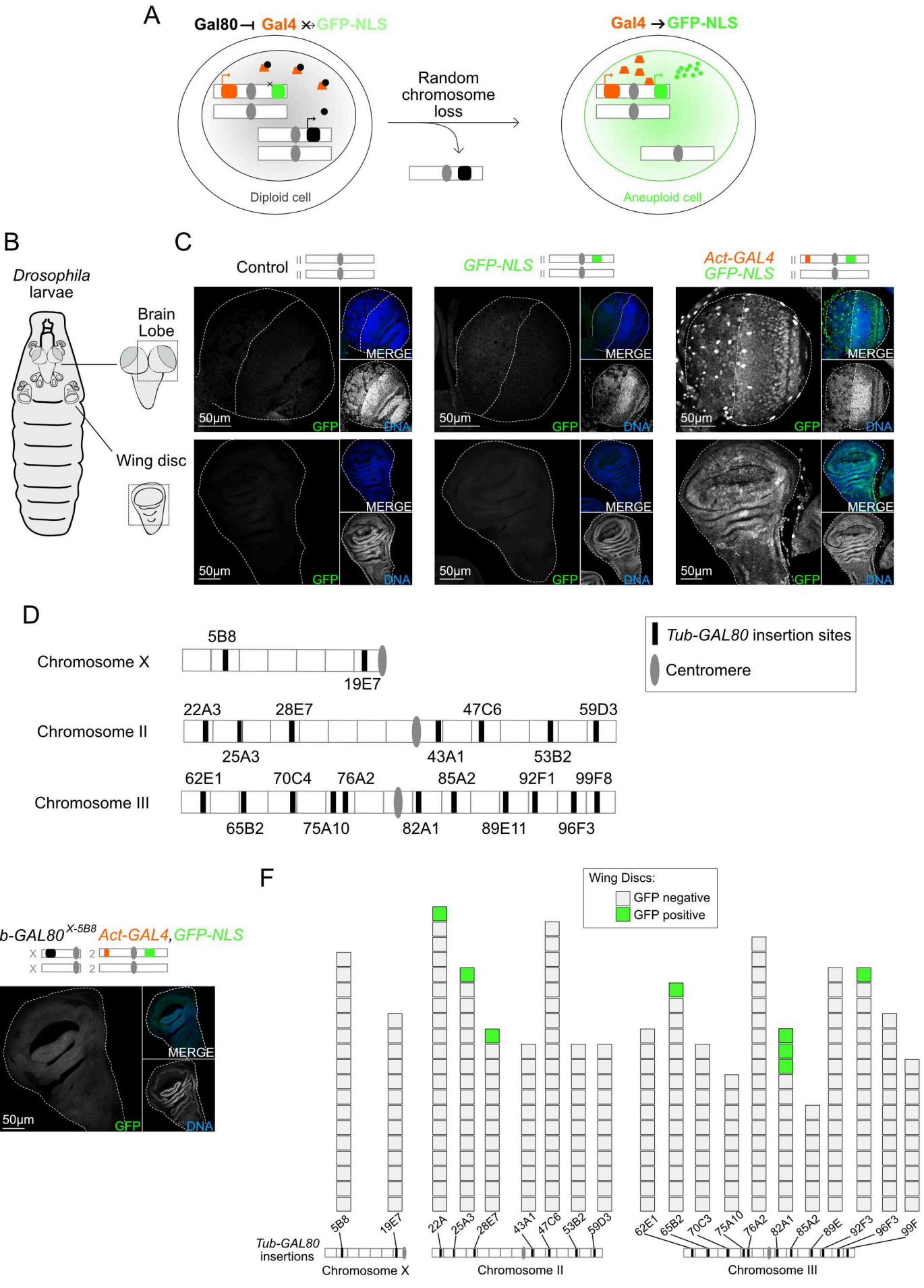
A
Gal80 ⊣ Gal4 → GFP-NLS
Gal4 → GFP-NLS
Random chromosome loss
Diploid cell
Aneuploid cell
B
Drosophila larvae
Brain Lobe
Wing disc
C
Control
GFP-NLS
Act-GAL4 GFP-NLS
MERGE
GFP
DNA
50µm
D
Tub-GAL80 insertion sites
Centromere
Chromosome X
5B8
19E7
Chromosome II
22A3
28E7
47C6
59D3
25A3
43A1
53B2
Chromosome III
62E1
70C4
76A2
85A2
92F1
99F8
65B2
75A10
82A1
89E11
96F3
E
Tub-GAL80X-5B8 Act-GAL4,GFP-NLS
F
Wing Discs:
GFP negative
GFP positive
Tub-GAL80 insertions
Chromosome X
Chromosome II
Chromosome III

Figure 2

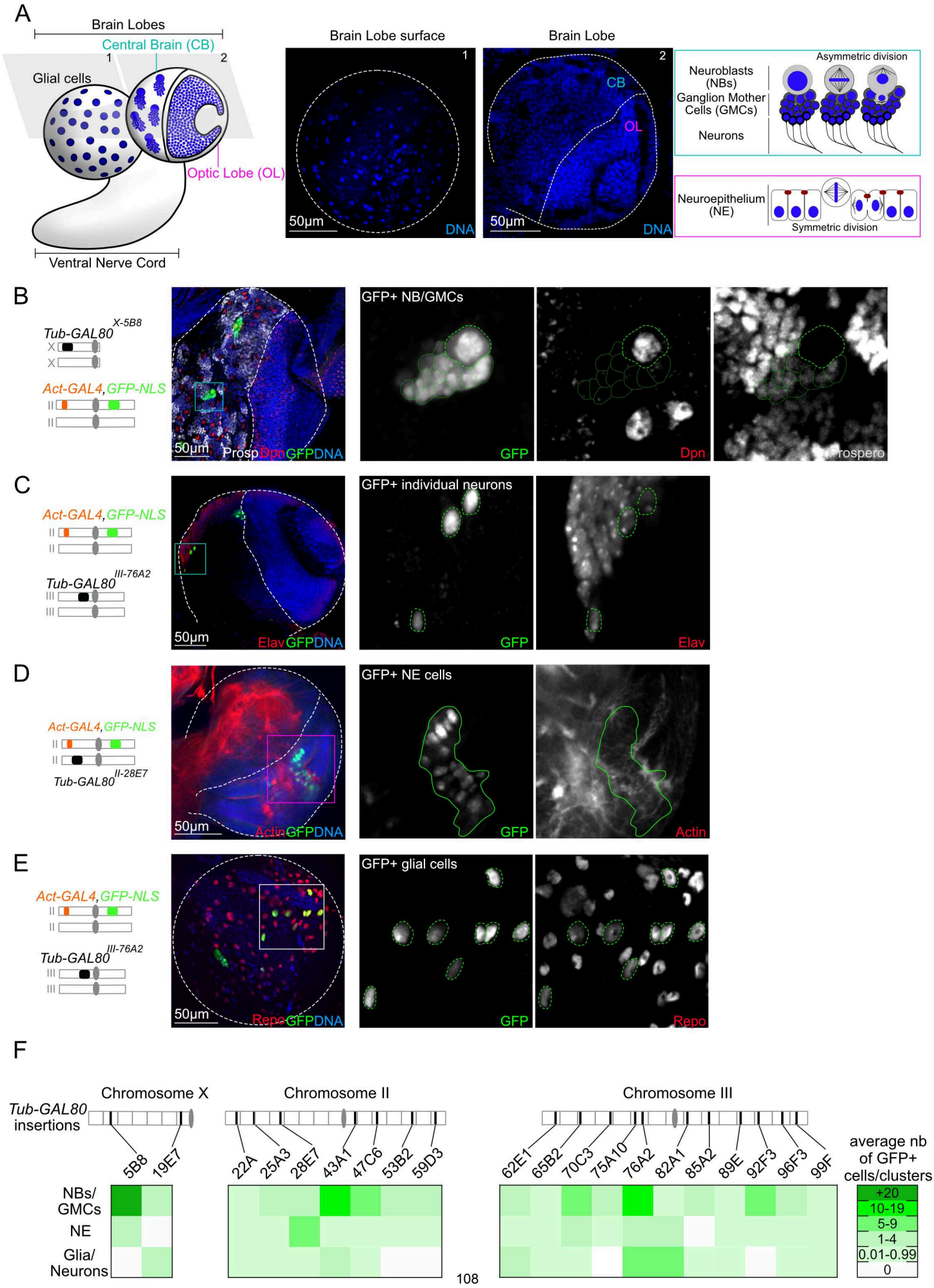
A
Brain Lobes
Central Brain (CB)
1
2
Glial cells
Optic Lobe (OL)
Ventral Nerve Cord
Brain Lobe surface
Brain Lobe
50µm
DNA
CB
OL
Neuroblasts (NBs)
Ganglion Mother Cells (GMCs)
Neurons
Asymmetric division
Neuroepithelium (NE)
Symmetric division
B
Tub-GAL80 X-5B8
Act-GAL4, GFP-NLS
Prosp Dpn GFP DNA
GFP+ NB/GMCs
GFP
Dpn
Prospero
C
Act-GAL4, GFP-NLS
Tub-GAL80 III-76A2
Elav GFP DNA
GFP+ individual neurons
Elav
D
Act-GAL4, GFP-NLS
Tub-GAL80 II-28E7
Actin GFP DNA
GFP+ NE cells
Actin
E
Act-GAL4, GFP-NLS
Tub-GAL80 III-76A2
Repo GFP DNA
GFP+ glial cells
Repo
F
Chromosome X
Chromosome II
Chromosome III
Tub-GAL80 insertions
5B8
19E7
22A
25A3
28E7
43A1
47C6
53B2
59D3
62E1
65B2
70C3
75A10
76A2
82A1
85A2
89E
92F3
96F3
99F
NBs/ GMCs
NE
Glia/ Neurons
average nb of GFP+ cells/clusters
+20
10-19
5-9
1-4
0.01-0.99
0

Figure 3

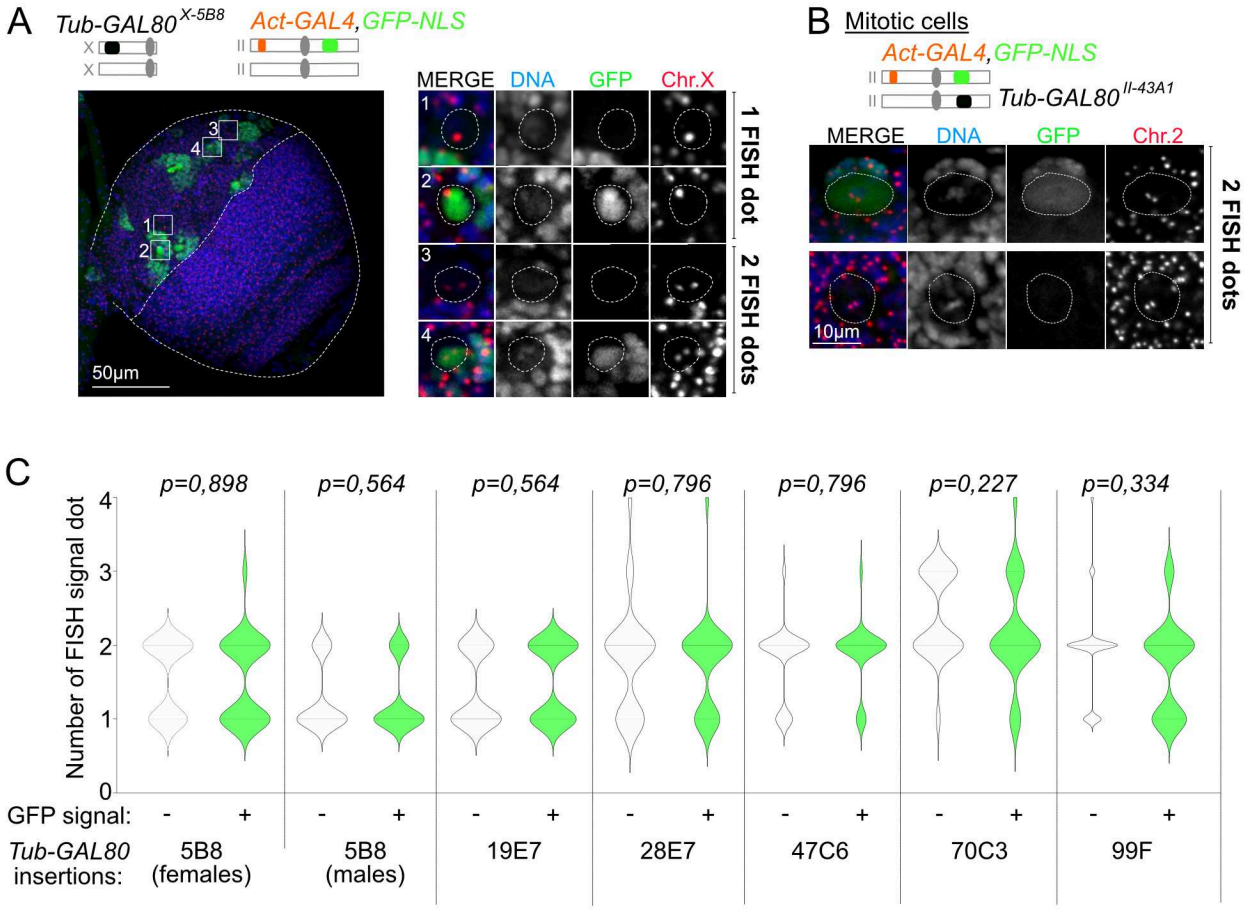
A
Tub-GAL80X-5B8
Act-GAL4,GFP-NLS
MERGE
DNA
GFP
Chr.X
1 FISH dot
2 FISH dots
50µm
B
Mitotic cells
Act-GAL4,GFP-NLS
Tub-GAL80II-43A1
MERGE
DNA
GFP
Chr.2
2 FISH dots
10µm
C
Number of FISH signal dot
p=0,898
p=0,564
p=0,564
p=0,796
p=0,796
p=0,227
p=0,334
GFP signal:
Tub-GAL80 insertions:
5B8 (females)
5B8 (males)
19E7
28E7
47C6
70C3
99F

Figure 4

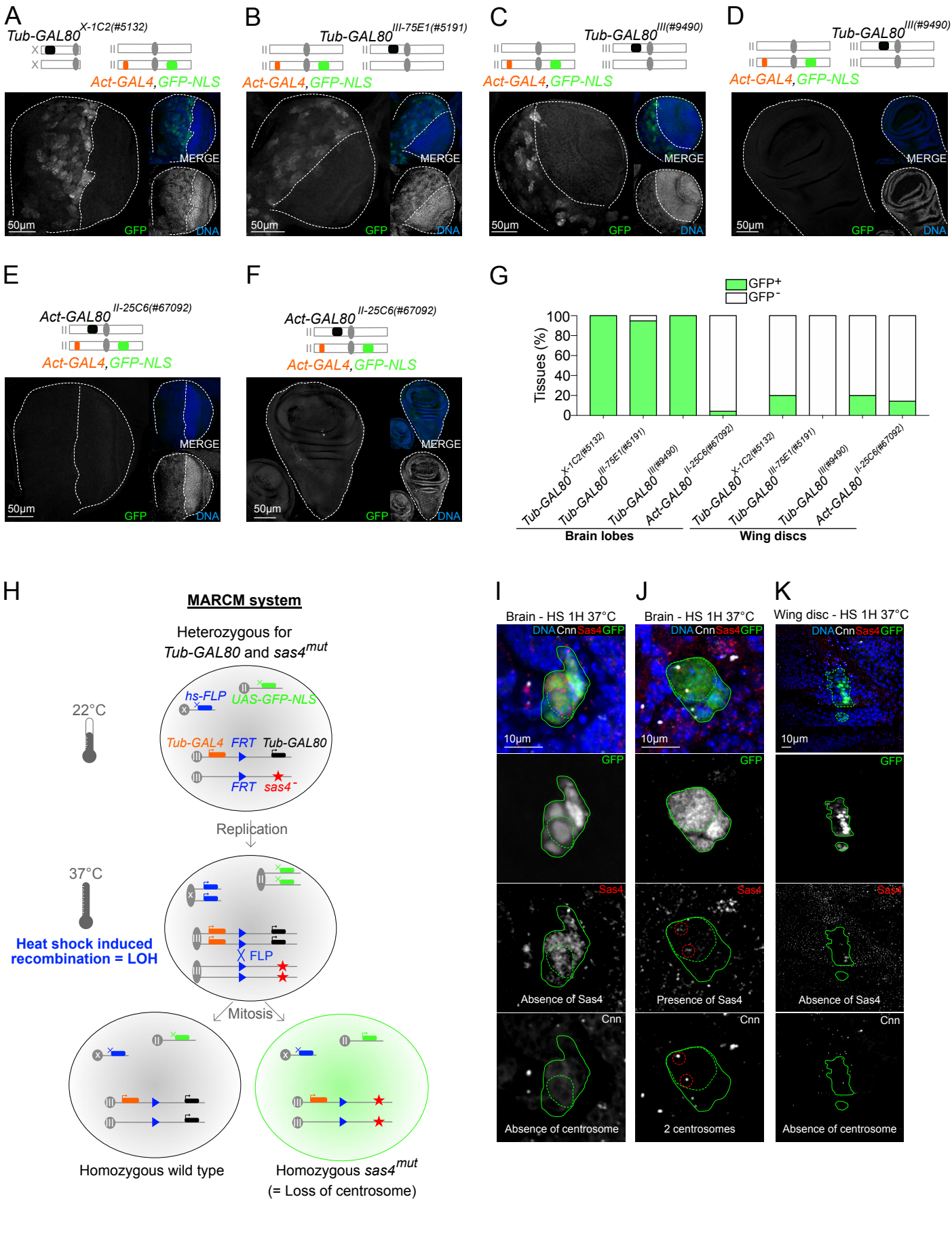
A
Tub-GAL80 X-1C2(#5132)
Act-GAL4,GFP-NLS
B
Tub-GAL80 III-75E1(#5191)
Act-GAL4,GFP-NLS
C
Tub-GAL80 III(#9490)
Act-GAL4,GFP-NLS
D
Tub-GAL80 III(#9490)
Act-GAL4,GFP-NLS
MERGE
50µm
GFP
DNA
E
Act-GAL80 II-25C6(#67092)
Act-GAL4,GFP-NLS
F
Act-GAL80 II-25C6(#67092)
Act-GAL4,GFP-NLS
G
GFP+
GFP-
Tissues (%)
100
80
60
40
20
0
Tub-GAL80 X-1C2(#5132)
Tub-GAL80 III-75E1(#5191)
Tub-GAL80 III(#9490)
Act-GAL80 II-25C6(#67092)
Brain lobes
Wing discs
H
MARCM system
Heterozygous for
Tub-GAL80 and sas4mut
22°C
hs-FLP UAS-GFP-NLS
Tub-GAL4 FRT Tub-GAL80
FRT sas4-
Replication
37°C
Heat shock induced
recombination = LOH
FLP
Mitosis
Homozygous wild type
Homozygous sas4mut
(= Loss of centrosome)
I
Brain - HS 1H 37°C
J
Brain - HS 1H 37°C
K
Wing disc - HS 1H 37°C
DNA Cnn Sas4 GFP
10µm
GFP
Sas4
Absence of Sas4
Presence of Sas4
Absence of Sas4
Cnn
Absence of centrosome
2 centrosomes
Absence of centrosome

Figure 5

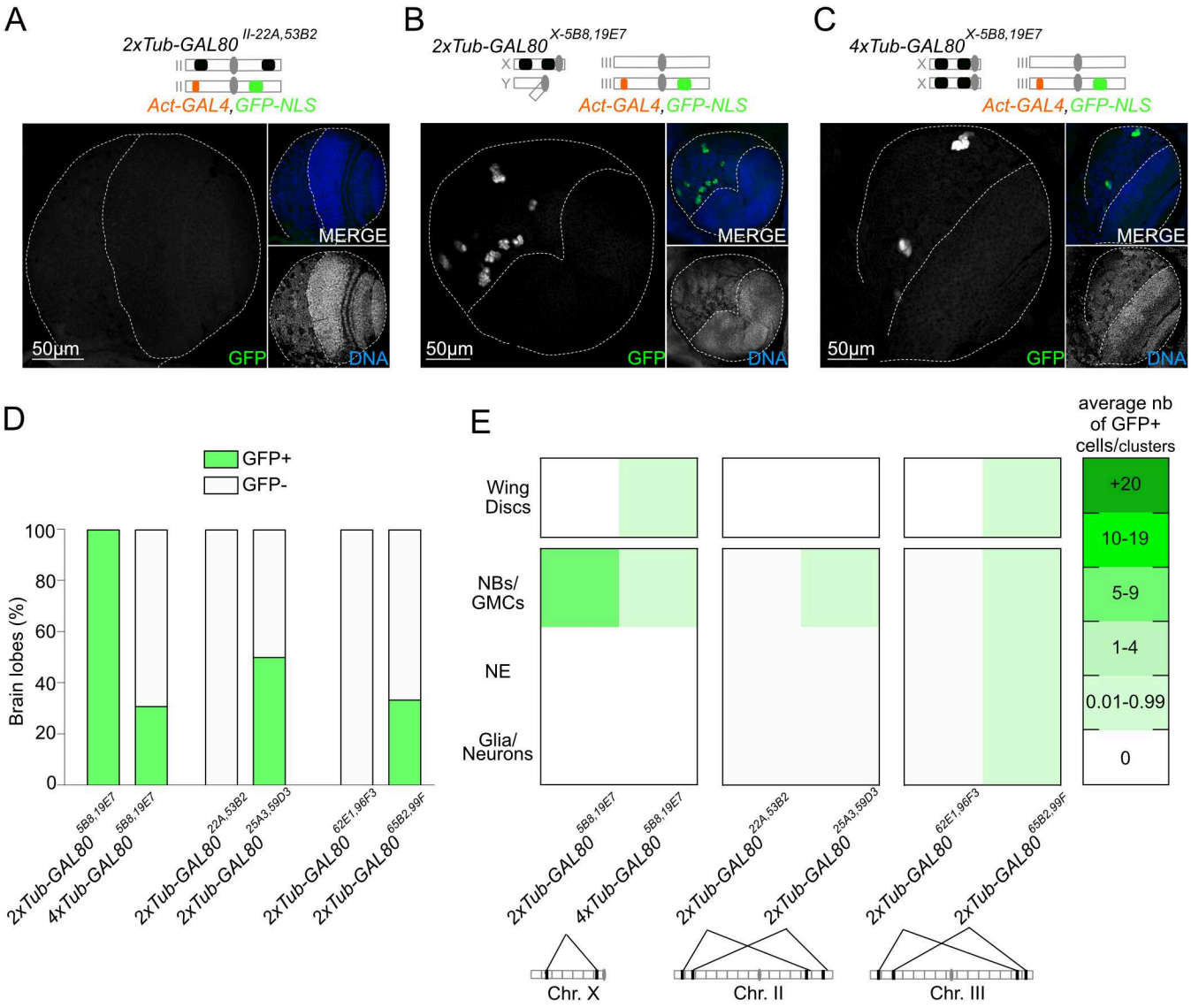
A
2xTub-GAL80 II-22A,53B2
Act-GAL4, GFP-NLS
MERGE
50µm
GFP
DNA
B
2xTub-GAL80 X-5B8,19E7
Act-GAL4, GFP-NLS
MERGE
50µm
GFP
DNA
C
4xTub-GAL80 X-5B8,19E7
Act-GAL4, GFP-NLS
MERGE
50µm
GFP
DNA
D
GFP+
GFP-
Brain lobes (%)
100
80
60
40
20
0
5B8,19E7
5B8,19E7
22A,53B2
25A3,59D3
62E1,96F3
65B2,99F
2xTub-GAL80
4xTub-GAL80
2xTub-GAL80
2xTub-GAL80
2xTub-GAL80
2xTub-GAL80
E
Wing Discs
NBs/ GMCs
NE
Glia/ Neurons
average nb of GFP+ cells/clusters
+20
10-19
5-9
1-4
0.01-0.99
0
5B8,19E7
5B8,19E7
22A,53B2
25A3,59D3
62E1,96F3
65B2,99F
2xTub-GAL80
4xTub-GAL80
2xTub-GAL80
2xTub-GAL80
2xTub-GAL80
2xTub-GAL80
Chr. X
Chr. II
Chr. III

Figure 6

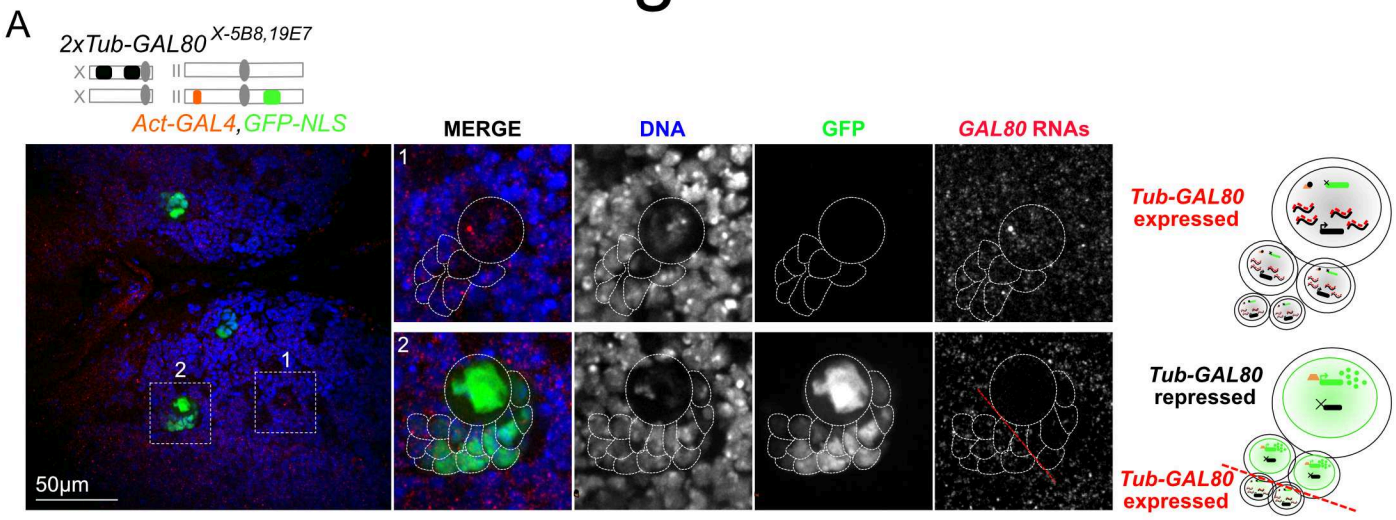
A
2xTub-GAL80 X-5B8,19E7
Act-GAL4, GFP-NLS
MERGE
DNA
GFP
GAL80 RNAs
50µm
Tub-GAL80 expressed
Tub-GAL80 repressed
Tub-GAL80 expressed

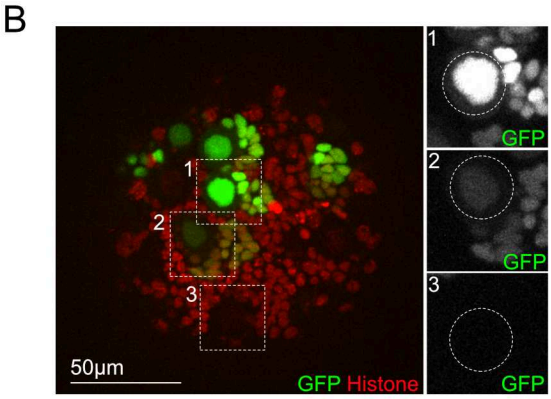
B
GFP
GFP Histone
50µm

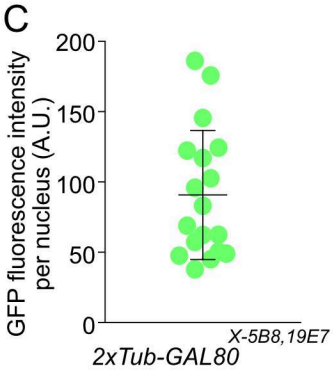
C
GFP fluorescence intensity per nucleus (A.U.)
200
150
100
50
0
X-5B8,19E7
2xTub-GAL80

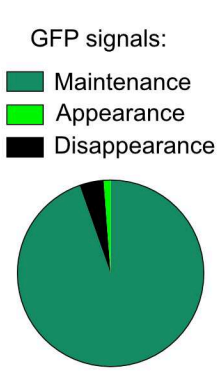
D
GFP signals:
Maintenance
Appearance
Disappearance

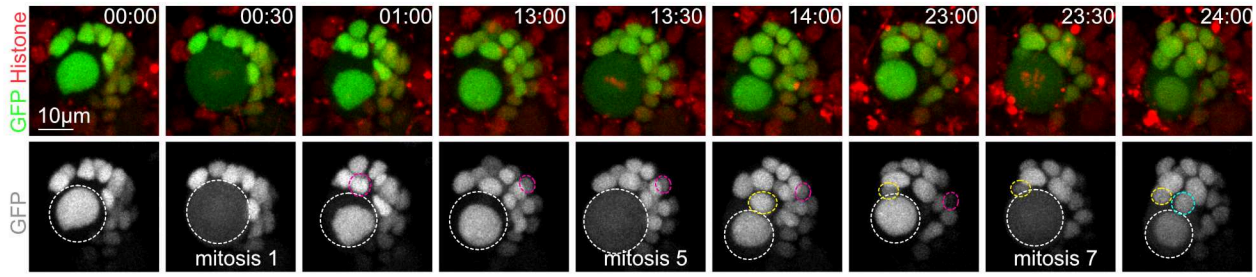
E
Maintenance and clonal expansion of the GFP signal
GFP Histone
GFP
10µm
00:00
00:30
01:00
13:00
13:30
14:00
23:00
23:30
24:00
mitosis 1
mitosis 5
mitosis 7

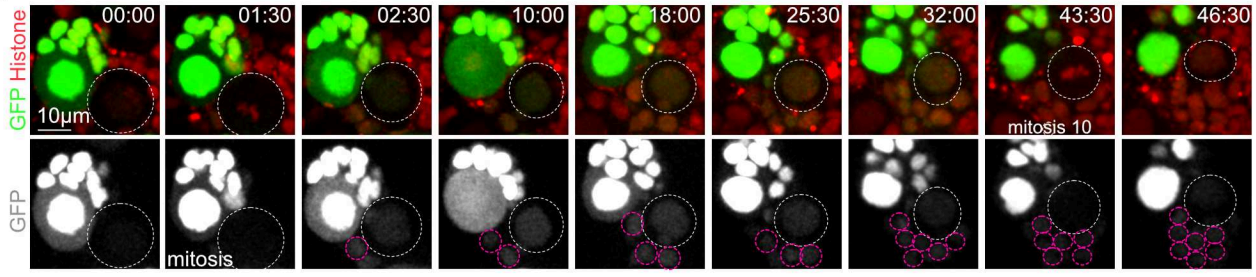
F
Transient appearance of the GFP signal
GFP Histone
GFP
10µm
00:00
01:30
02:30
10:00
18:00
25:30
32:00
43:30
46:30
mitosis
mitosis 10

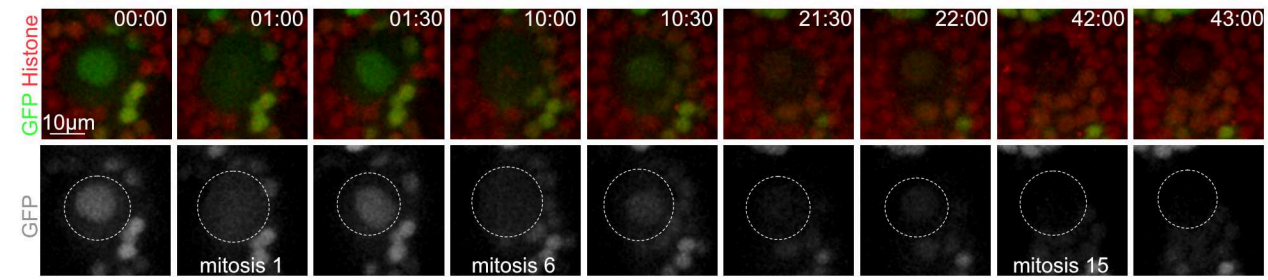
G
Disappearance of the GFP signal
GFP Histone
GFP
10µm
00:00
01:00
01:30
10:00
10:30
21:30
22:00
42:00
43:00
mitosis 1
mitosis 6
mitosis 15

Figure 7

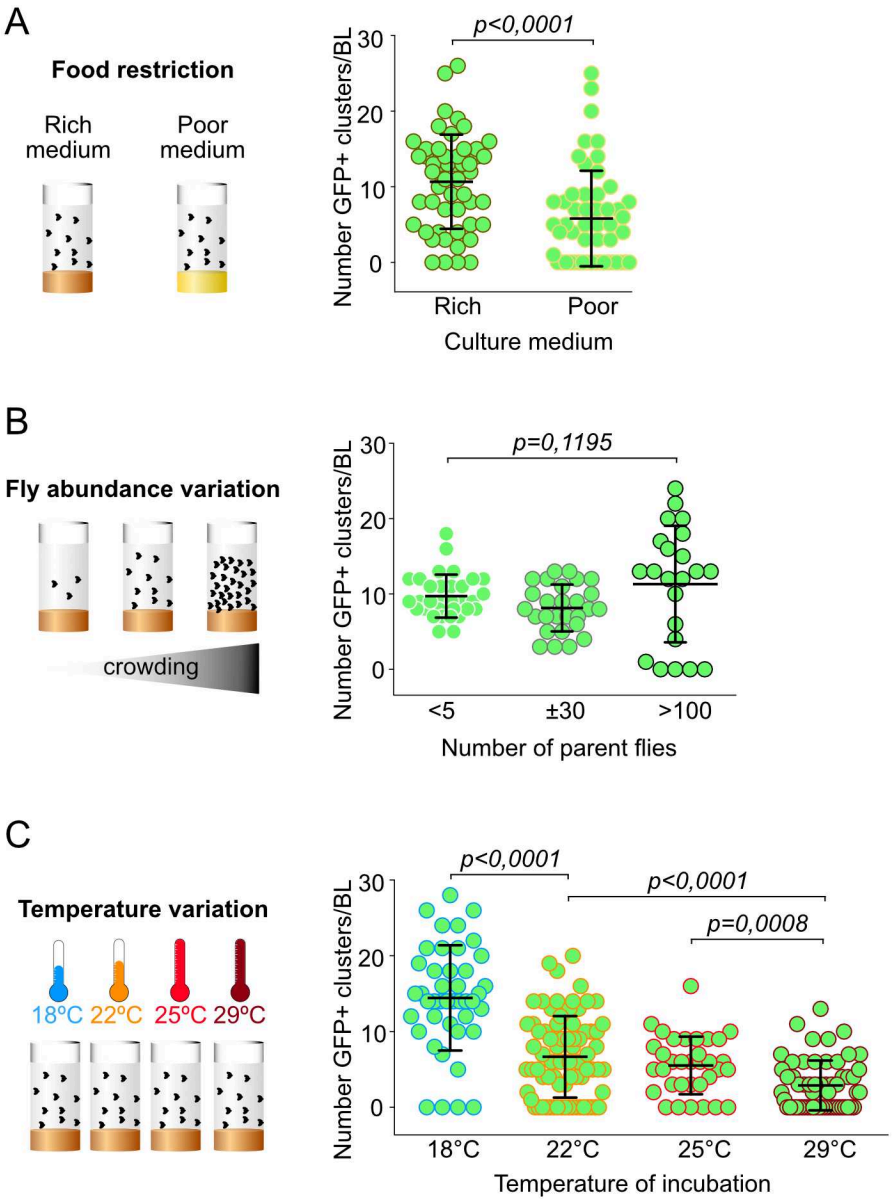
A
Food restriction
Rich medium
Poor medium
p<0,0001
Number GFP+ clusters/BL
30
20
10
0
Rich
Poor
Culture medium
B
Fly abundance variation
crowding
p=0,1195
Number GFP+ clusters/BL
30
20
10
0
<5
±30
>100
Number of parent flies
C
Temperature variation
18°C 22°C 25°C 29°C
p<0,0001
p<0,0001
p=0,0008
Number GFP+ clusters/BL
30
20
10
0
18°C
22°C
25°C
29°C
Temperature of incubation

Supplementary Figure 1

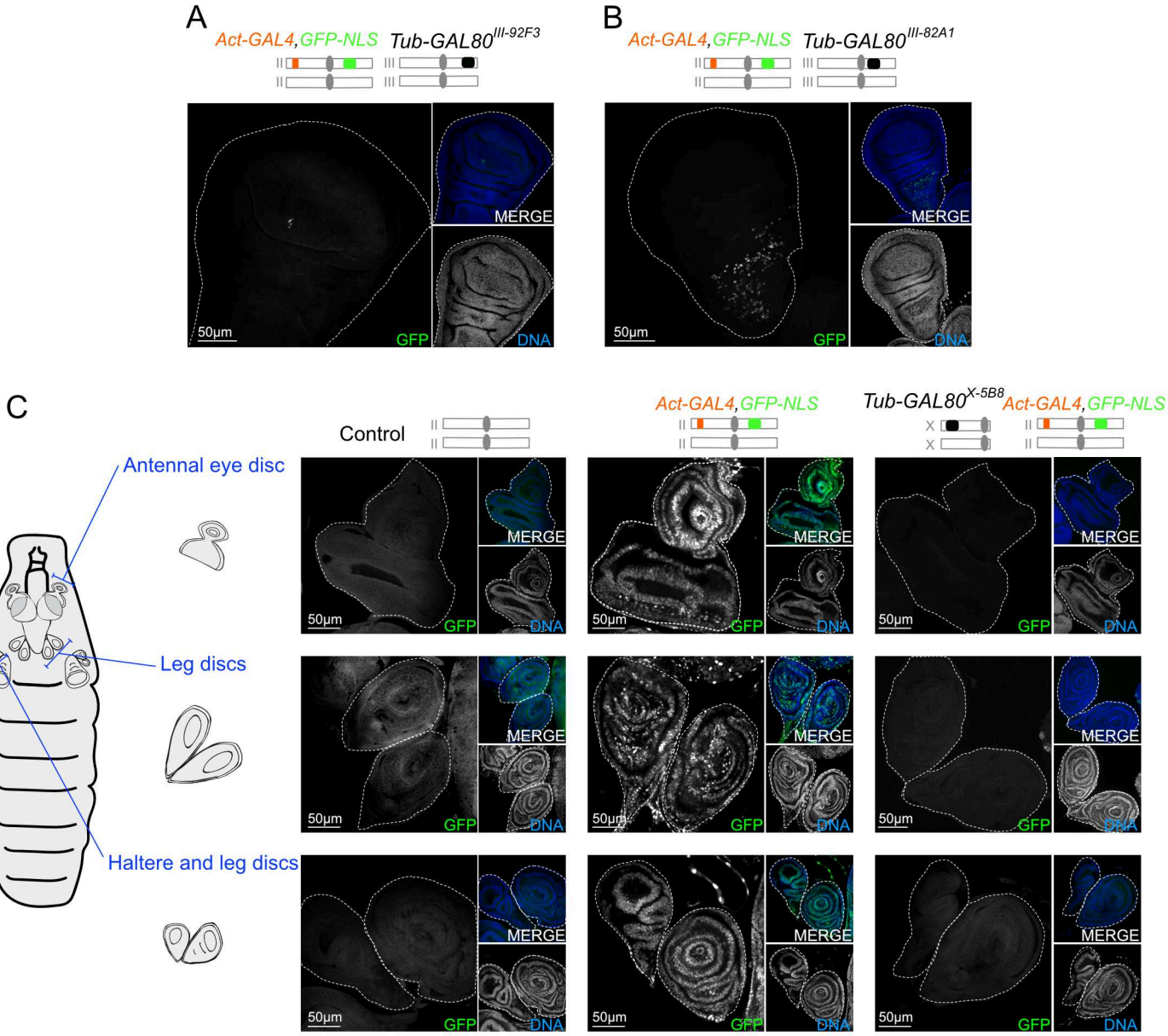

Supplementary Figure 2

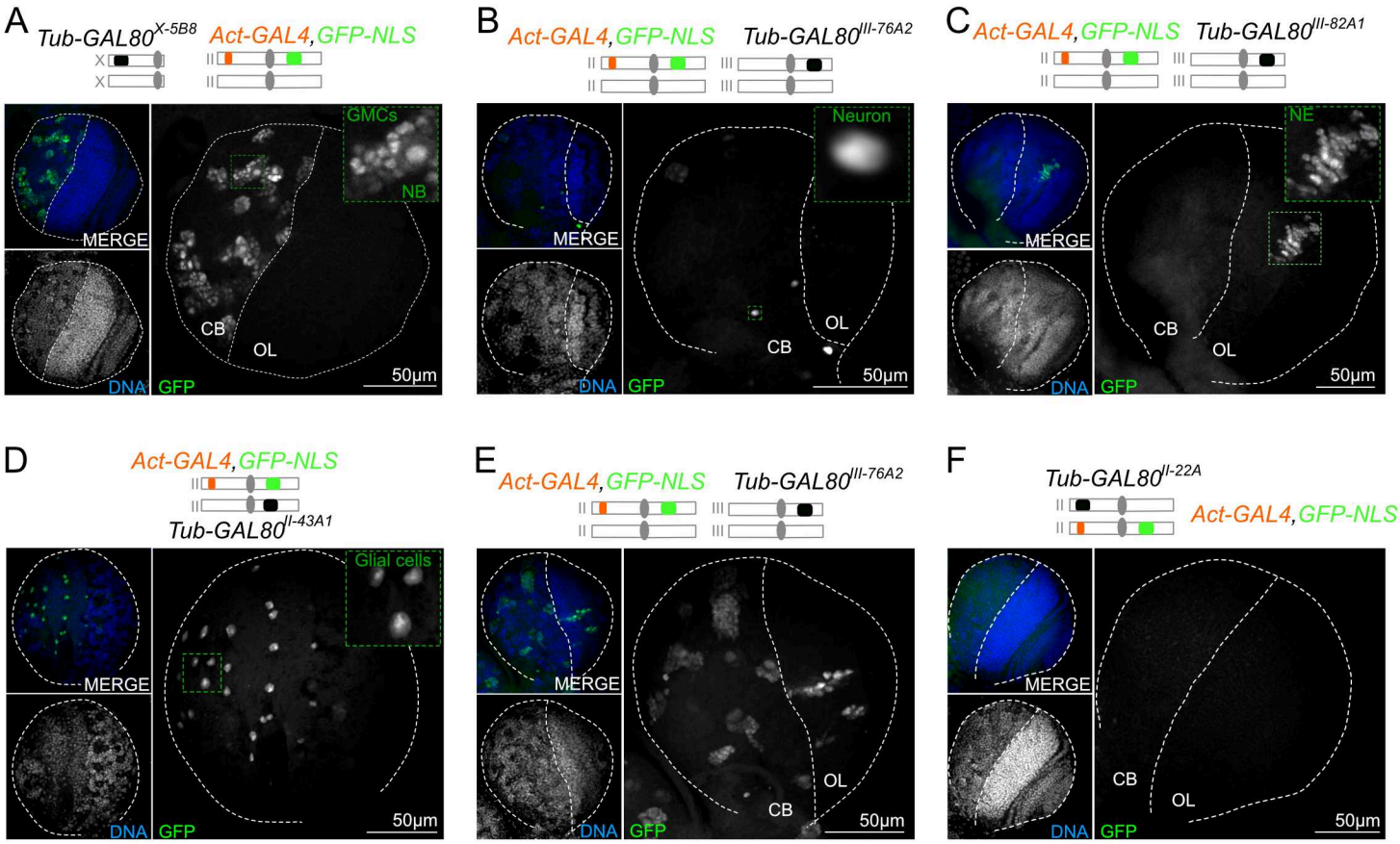

Supplementary Figure 3

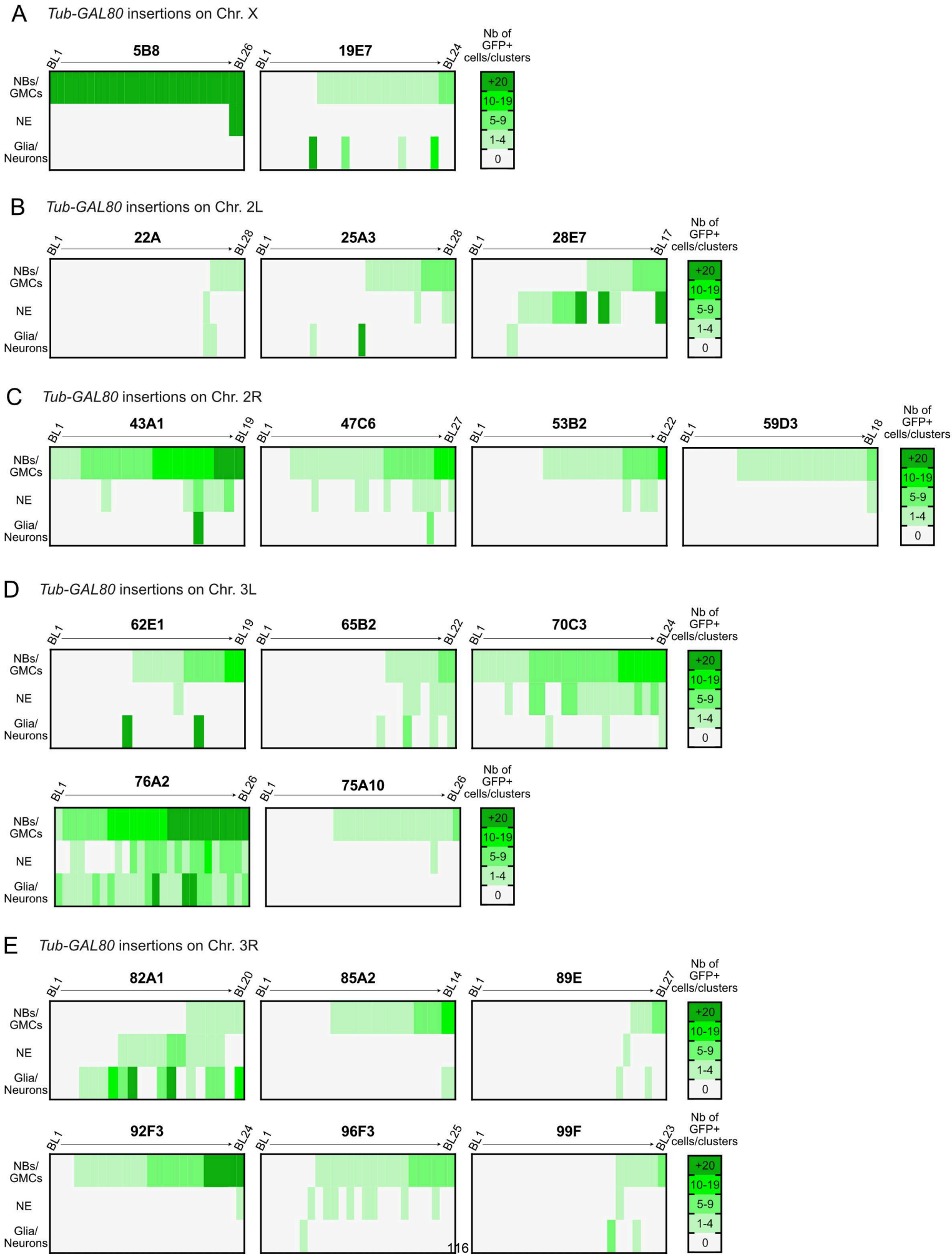

Supplementary Figure 4

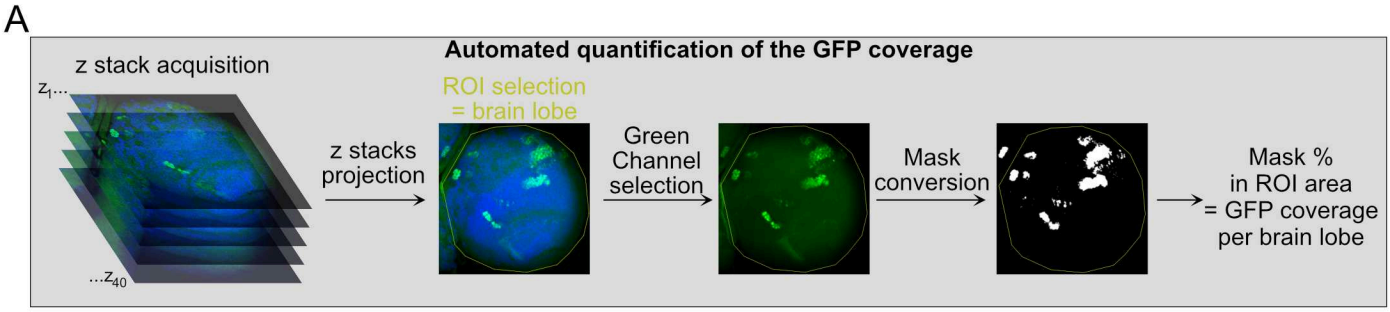

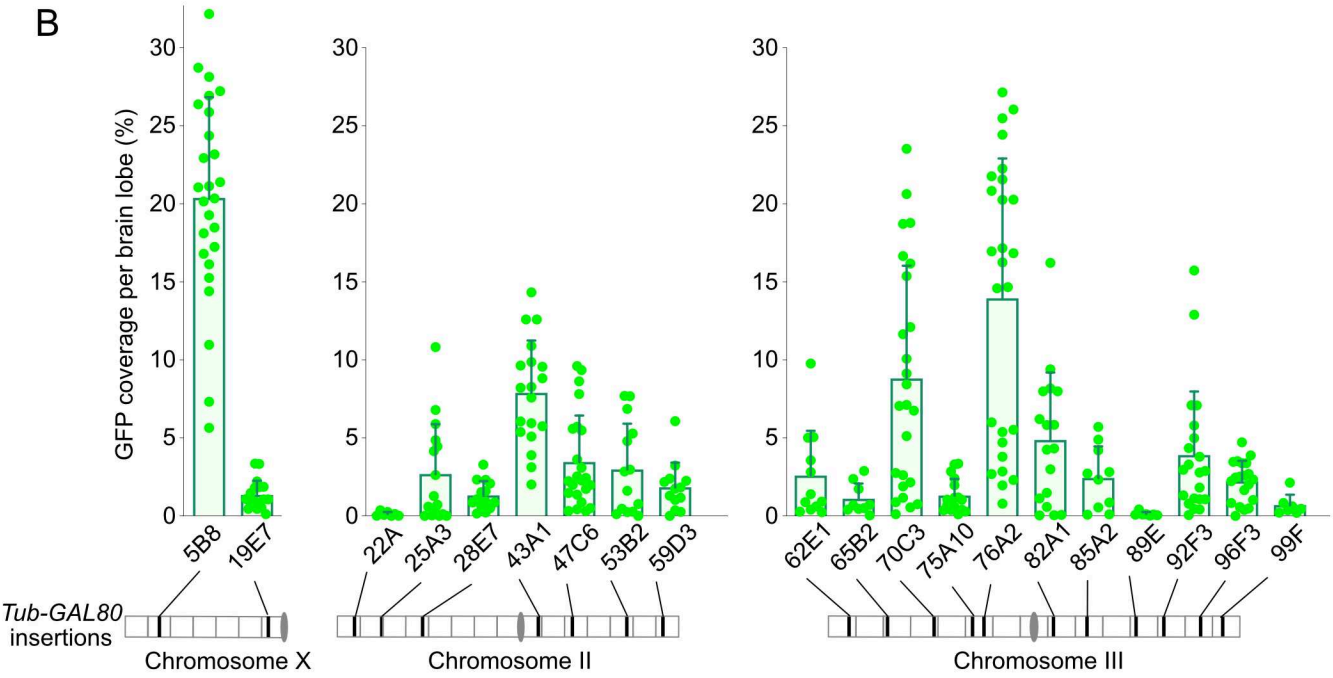

Supplementary Figure 5

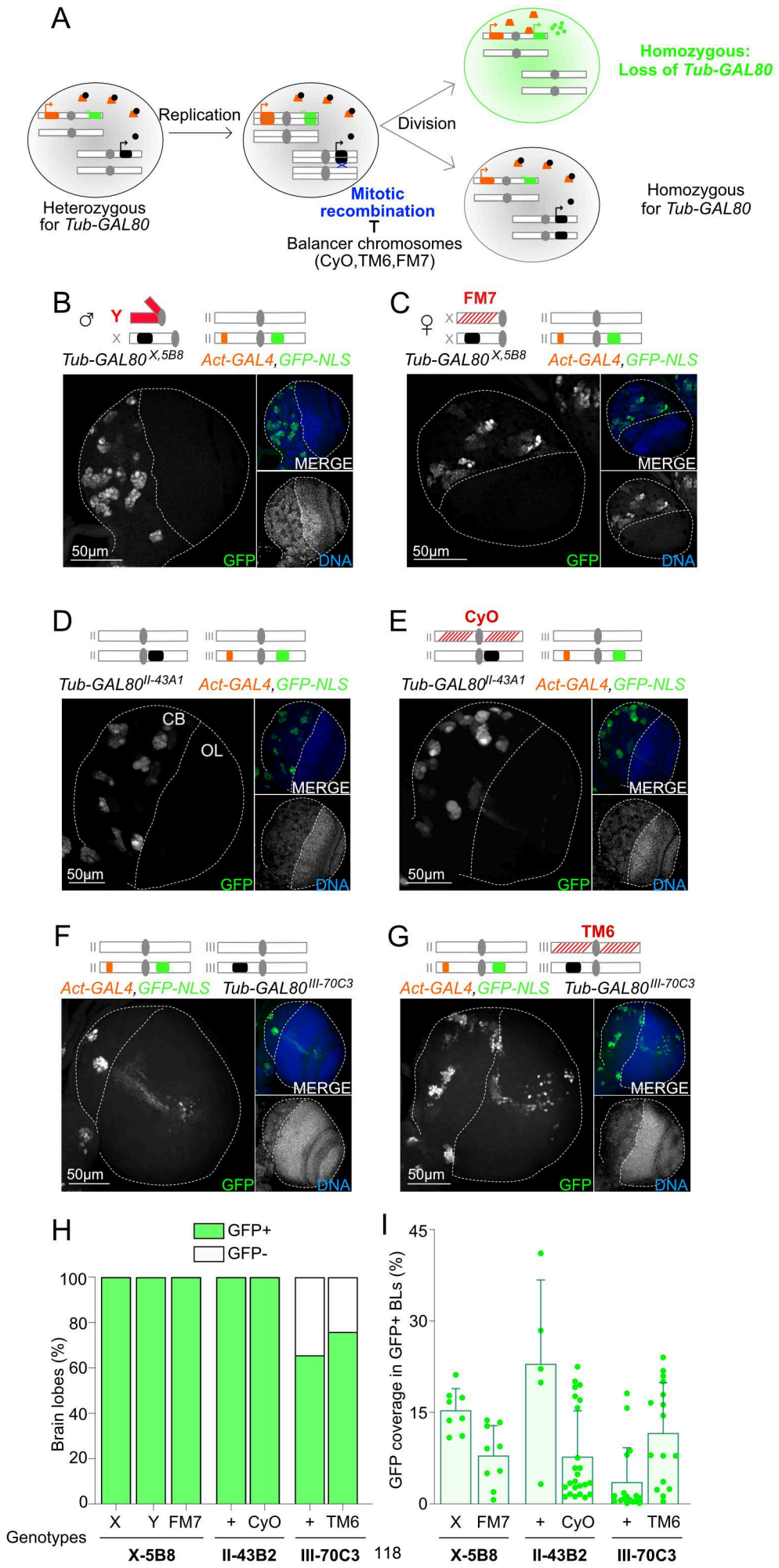

Supplementary Figure 6

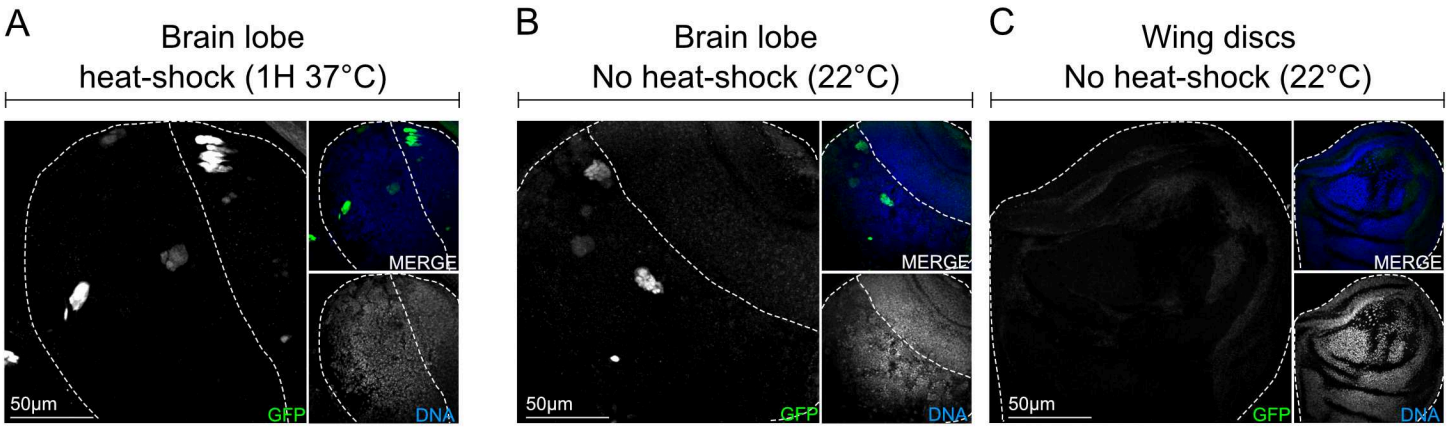

Supplementary Figure 7

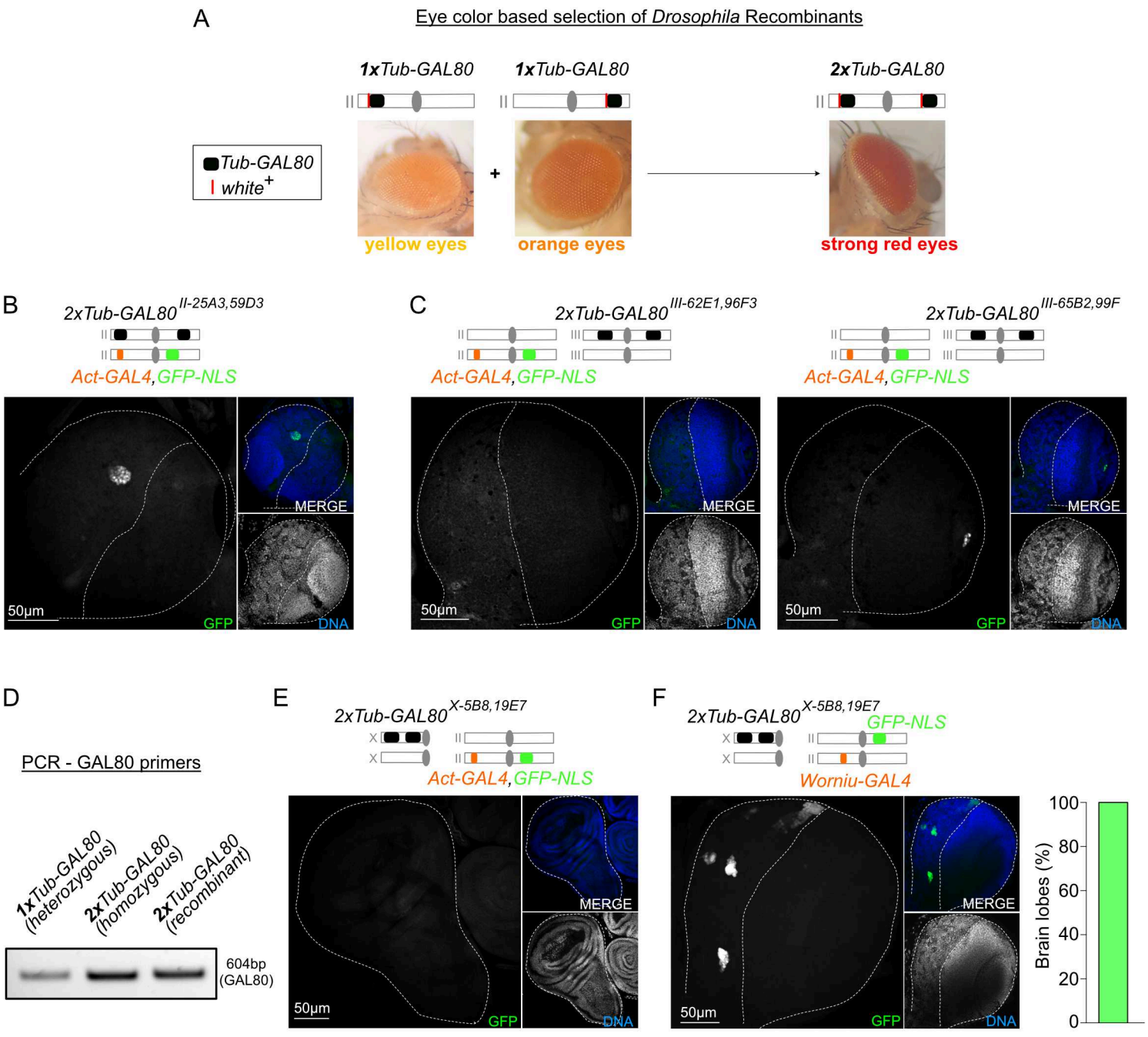

Figure 1: A novel strategy to monitor chromosome loss based on the GAL4/GAL80 system which is functional in *Drosophila* larval wing discs.

(A) Schematic representation of the genetic system to monitor chromosome loss in *Drosophila* cells. On the left- the presence of Gal80 inhibits Gal4 and so the nuclei are black. On the right- Upon random loss of the *GAL80* containing chromosome, Gal4 is released from Gal80 repression and promotes *GFP-NLS* expression. Thus, aneuploid cells appear with green nuclei. (B) Schematic representation of the brain and imaginal discs of the *Drosophila* L3 larvae. (C) Images of whole mount brain lobes and wing discs labeled with GFP booster (grey and green in large and small insets, respectively) and DAPI for DNA (grey and blue in small insets). Control and GFP-NLS tissues present no GFP signal. In the presence of the activator Gal4, *GFP-NLS* is expressed and all cells present GFP positive (GFP^+) nuclei. Schematic representation of the genotypes is shown above the images: *GFP-NLS* and *Act-GAL4* sequences are represented with green and orange rectangles on white chromosomes, respectively. White dotted lines delimitate tissues. (D) Representative map of the *Tub-GAL80* insertion sites on *Drosophila* chromosomes X, II and III used in this study. (E) Images of whole mount wing disc labeled with GFP booster (grey and green in large and small insets, respectively) and DAPI for DNA (grey and blue in small insets). In the presence of Gal80, Gal4 is repressed and all cells are GFP negative (GFP^-). Schematic representation of the genotype is shown above the images: *GFP-NLS, Act-GAL4* and *Tub-GAL80* sequences are represented with green, orange and black rectangles on white chromosomes, respectively. White dotted line delimitates the wing disc. (F) Graph summarizing the results from the screen of all *Drosophila* lines carrying one copy of the *Tub-GAL80* cassette on the chromosomes X, II and III. Insertion sites are represented in the scheme bellow. Each square of the graph represents one wing disc that presented no GFP signal (grey) or at least one GFP^+ cell (green) (n=7 to 20 wing discs /GAL80 condition).

Figure 2: GFP positive cells correspond to different cell types in the larval brain and their frequency is variable.

(A) Schematic representation of the *Drosophila* larval brain and its different cell types. Representative images of different z stacks of the brain lobes are shown with DNA in blue. Glial cells with large nuclei are present at the surface of the brain lobe (image 1). The core of the brain lobe is divided in two parts, the central brain (CB) and the optic lobe (OL) (image 2). The CB is composed of neuroblasts (NBs) that divide asymmetrically to generate ganglion

mother cells (GMCs) that will then give rise to neurons. The OL is composed of neuroepithelial (NE) cells that divide symmetrically. (B-E) Images of whole mount brain lobes labeled for GFP (grey and green) and for specific markers of the different cell types (red and grey). DNA is shown in blue. Schematic representation of the genotypes is shown next to the images. Zoom insets are highlighted by colored squares. White dotted lines delimitate brain lobes and separate CB and OL. Green dotted and continuous lines surround GFP^+ cells and clusters, respectively. GFP^+ cells are (B) Dpn^+ NBs with Dpn^-/$Prospero^{weak}$ GMCs, (C) individual $Elav^+$ neurons, (D) cells of the NE which is distinguishable by the specific F-actin organization, and (E) $Repo^+$ glial cells. (F) Heat map showing the average number of GFP^+ cells/clusters (green color code) for each cell type of the brain lobe and per GAL80 condition. The absence of any green cell is represented in white, while the presence of 1 to 4 cells/clusters, 5 to 9 cells/clusters, 10 to 19 cells/clusters and more than 20 cells/clusters were represented in increased shades of green. The map of *Tub-GAL80* insertion sites is schematized above the graph.

Figure 3: GFP positive cells are not aneuploid in the larval brain.

(A-B) Fluorescent *in situ* hybridization with probes for the (A) X chromosome or (B) chromosome II (red and grey in zoom insets) combined with labeling with GFP booster (green and grey in zoom insets) and DAPI for DNA (blue and grey in zoom insets) of the brain lobe. The number of FISH signal dot is similar between GFP^+ and GFP^- (A) interphase and (B) mitotic NBs. Schematic representation of the genotypes is shown above the images. White dotted lines surround brain lobe and NBs in large and zoom insets, respectively. (C) Violin plot representing the number of FISH signal dots between GFP^+ and GFP^- cells. FISH signals correspond to the chromosomes X, II or III for conditions where *Tub-GAL80* was inserted at positions 5B8 (n=43 cells for females and n=50 cells for males) and 19E7 (n=47 cells), 28E7 (n=50 cells) and 47C6 (n=50 cells) or 70C3 (n=47 cells) and 99F (n=60 cells), respectively. FISH signals are variable between conditions but similar between GFP^+ (green) and GFP^- (white) cells from the same condition. Statistical non-significance was determined by a Mann-Whitney test and p corresponds to the p-value.

Figure 4: The *Tub-GAL80* expression is not sufficient to induce a complete GAL4 repression, precluding its use in MARCM analysis.

(A-F) Images of whole mount (A-C and E) brains lobes or (D and F) wing discs labeled with GFP booster (grey and green in large and small insets, respectively) and DAPI for DNA (grey and blue in small insets). White dotted lines delimitate tissues. Schematic representation of the genotypes is shown above the images. (G) Graph bar showing the percentage of tissues without (white) and with GFP signal (green). (H) Schematic representation of the MARCM system. In principle, after recombination of FRT sites by the heat-induced FLP recombinase, the daughter cells lose their heterozygosity. One cell becomes homozygous mutant and labeled with GFP due to the concomitant loss of the *Tub-GAL80* sequence. The other cell becomes homozygous wild type and it is unlabeled. (I-K) Images of GFP^+ clones in (I-J) brain lobes and (K) wing disc of *hs-FLP/+, UAS-GFP-NLS/+; Tub-GAL4,FRT82B,Tub-GAL80/FRT82B,sas4^{mut}* flies heat-shocked at 37ºC for 1 hour. Green dotted and continuous lines surround GFP^+ NBs and clones, respectively. (I) *Sas4* mutant GFP^+ NB without centrosome. (K) Wild type GFP^+ NB with two centrosomes. (K) *Sas4* mutant GFP^+ clones in the WD.

Figure 5: The *GAL80* levels partially explain GFP signal appearance.

(A-C) Images of whole mount brain lobes labeled with GFP booster (grey and green in large and small insets, respectively) and DAPI for DNA (grey and blue in small insets). White dotted lines delimitate brain lobes. Schematic representation of the genotypes is shown above the images. (D) Graph bar showing the percentage of brain lobes without (white) and with GFP signal (green) (n=22 to 26 brain lobes/condition). (E) Heat map summarizing the average number of GFP^+ cells/clusters per GAL80 condition in wing discs (n=7 to 18 wing discs/condition) and for each cell type in brain lobes (n=22 to 26 brain lobes/condition). The *Tub-GAL80* insertions map is schematized above the graph.

Figure 6: 2x*Tub-GAL80$^{X\text{-}5B8,19E7}$* expression is dynamic and reversible.

(A) Images of whole mount brain lobes from RNA FISH experiment with probes against the GAL80 RNAs (red and grey in zoom insets) and labeled with GFP booster (green and grey in zoom insets) and DAPI for DNA (blue and grey in zoom insets). Schematic representation of cells is shown next to the images. White dotted lines surround NBs and GMCs clusters. (B) Single still from a time-lapse movie of a brain lobe (large inset) and NBs (zoom insets) expressing *2xTub-GAL80$^{X\text{-}5B8,19E7}$, Act-GAL4,GFP-NLS* (green) and *histone-RFP* (red). Several

NBs from the same brain lobe present different levels of GFP intensity. (C) Dot plot showing the GFP intensity (A.U.) of NBs at the beginning of movies (n=18 NBs from 3 brains). (D) Pie chart of the different GFP dynamics (n=168 NBs from 17 brain lobes). (E-G) Stills of time-lapse movies of mitotic NBs expressing *2xTub-GAL80$^{X\text{-}5B8,19E7}$, Act-GAL4,GFP-NLS* (green) and *histone-RFP* (red) to monitor GFP and chromosome dynamics. White and colored dotted circles surround NBs and daughter GMCs, respectively. GFP signal present different dynamics: (E) maintenance and clonal expansion, (F) the transient appearance and (G) the disappearance of the GFP signal.

Figure 7: Environmental changes influence the expression/repression of *Tub-GAL80*

(A-C) Schematic representation of the different environmental stresses and dot plot showing the number of GFP$^+$ clusters/brain lobe in larvae (A) raised on different culture media- protein-rich (n=70 BLs from 35 brains) or -poor medium (n=62 BLs from 31 brains), in tubes (B) containing <5 (n=32 BLs from 16 brains), ±30 (n=137BLs from 14 brains) or >100 (n=22 BLs from 11 brains) parent flies and (C) incubated at different temperatures- 18ºC (n=43 BLs from 22 brains), 22ºC (n=76 BLs from 38 brains), 25ºC (n=34 BLs from 17 brains) or 29ºC (n=58 BLs from 29 brains). Statistical significance was determined by a Mann-Whitney test and p corresponds to the p-value.

Supplementary Figure 1: The GAL4/GAL80 system is functional in imaginal discs of the *Drosophila* larvae.

(A-C) Images of whole mount imaginal discs labeled with GFP booster (grey and green in large and small insets, respectively) and DAPI for DNA (blue and grey in small insets). White dotted lines surround discs. Schematic representation of the genotypes is shown above the images. Few wing discs presented low (A) or high (B) levels of GFP$^+$ cells. (C) Schematic representation of imaginal discs in *Drosophila* larvae. Control discs present no GFP signal. In the presence of the activator GAL4, *GFP-NLS* is expressed and all cells present GFP$^+$ nuclei. GAL80 efficiently inhibits GAL4 and thus, cells are GFP negative.

Supplementary Figure 2: The GFP-NLS signal is sufficient to distinguish all cell types.

(A-F) Images of whole mount brain lobes labeled with GFP booster (grey and green in large and small insets, respectively) and DAPI for DNA (grey and blue in small insets). Schematic

representation of the genotypes is shown above the images. White dotted lines delimitate brain lobes and separate CB and OL. GFP^+ cells are (A) NBs with GMCs, (B) individual neurons, (C) NE cells, (D) glial cells, or (E) a mix population of different cell types. (F) Very few brain lobes presented an absence of GFP signal.

Supplementary Figure 3: The majority of the brains present GFP signals which show variable frequency.

(A-E) Heat map showing the number of GFP^+ (green color code) cells for glial cells and individual neurons and GFP^+ clusters for NBs with GMCs and NE cells. All brain lobes analyzed are numerated ($BL_1 \rightarrow BL_n$) and the *Tub-GAL80* insertion sites are indicated above the graphs. The cell type and the number of GFP^+ cells/clusters are highly variable between all conditions with *Tub-GAL80* inserted on the (A) X chromosome, on the (B) left and (C) right arms of the chromosome II and on the (D) left and (E) right arms of the chromosome III (n=14 to 28 BLs/ condition). Representative images are shown in Figure 2 and Supplementary Figure 2.

Supplementary Figure 4: The coverage of the GFP signals is variable between all GAL80 conditions.

(A) Schematic representation of the automated quantification of the GFP coverage. ROI corresponds to "Region Of Interest". (B) Scatter plot with bars showing the GFP coverage per brain lobe for each GAL80 condition (n=7 to 26 GFP^+ brain lobes/condition).

Supplementary Figure 5: Mitotic recombination does not account for GFP appearance.

(A) Schematic representation of mitotic recombination inducing loss of *Tub-GAL80* heterozygosity and GFP appearance. (B-G) Images of whole mount brain lobes labeled with GFP booster (grey and green in large and small insets, respectively) and DAPI for DNA (blue and grey in small insets). White dotted lines surround brain lobes and delimitate CB and OL. Schematic representation of the genotypes is shown above the images. (H) Graph bar showing the percentage of brain lobes without (white) and with GFP signal (green) (n=6 to 32 brain lobes/condition). (I) Scatter plot with bars showing the GFP coverage per brain lobe for each condition (n=5 to 33 GFP^+ brain lobes/condition).

Supplementary Figure 6: GFP$^+$ NB/GMCs clones are formed in MARCM flies in absence of heat shock.

(A-C) Images of whole mount *hs-FLP/+, UAS-GFP-NLS/+; Tub-GAL4, FRT82B, Tub-GAL80/FRT82B, sas4^{mut}* brain lobes (A-B) or wing disc (C) labeled with antibodies against GFP (grey and green in large and small insets, respectively) and DAPI for DNA (grey and blue in small insets). White dotted lines delimitate tissues. (A) Presence of GFP$^+$ clones in brain lobes of flies heat-shocked at 37ºC for 1 hour. (B-C) In the absence of heat-shock, (B) brain lobes present GFP$^+$ clones, in contrast to (C) wing discs that are GFP$^-$.

Supplementary Figure 7: Double insertions of *Tub-GAL80* decrease GFP frequency.

(A) Pictures of *Drosophila* recombinant selection to obtain lines carrying two copies of the *Tub-GAL80* cassette (black boxes) based on eyes color (white$^+$ transgene - red lines). (B-C) Brain lobes labeled with GFP booster (grey and green in large and small inserts, respectively) and DAPI for DNA (blue and grey in small insets). White dotted lines surround brain lobes. Schematic representation of the genotypes is shown above the images. (D) PCR analysis of *Drosophila* lines using primers recognizing the two extremities of the *GAL80* sequence (604 base pairs). The recombinant flies (*2xTub-GAL80$^{X\text{-}5B8,19E7}$*) present a similar or stronger band than flies carrying a single *Tub-GAL80* copy in homozygous (*2xTub-GAL80$^{II\text{-}53B2}$*) or heterozygous (*1xTub-GAL80$^{II\text{-}53B2}$*) state, respectively. (E) Wing disc and (F) brain lobe labeled with GFP booster (grey and green in large and small inserts, respectively) and DAPI for DNA (blue and grey in small insets) and graph bar showing the percentage of brain lobes presenting GFP$^+$ cells in flies expressing *2xTub-GAL80$^{X\text{-}5B8,19E7}$; worniu-GAL4/UAS-GFP-NLS* (n=30 brain lobes).

Discussion

Here we sought to develop a new probe to monitor chromosome loss. Using the bipartite UAS-GAL4 reporter system in combination with the GAL80 repressor, we reasoned that loss of the *GAL80* containing chromosome would be translated by the appearance of nuclear GFP signals. While this reasoning appears to apply to some larval tissues, including imaginal discs, it appears nonfunctional in the brain. Quite surprisingly, however this study revealed an unexpected level of regulation of gene expression in the larval brain.

The UAS-GAL4/GAL80 system is widely used among the *Drosophila* community to spatially and temporally control gene expression (McGuire et al., 2003). It was therefore difficult to predict the results obtained in the *Drosophila* developing brain and described here. Our findings on the lack of *GAL80* expression highlights a weakness of the system and precludes, or at least alerts, its use in the *Drosophila* developing brain for MARCM or "gypsy-trap" analysis that are based on the *GAL80* sequence loss after heat-induced mitotic recombination (Lee and Luo, 1999) or on the gypsy dependent *GAL80* repression (Li et al., 2013) .

One of the most surprising result was related with the variability of cell types becoming GFP^+ according to the *GAL80* insertion position on each chromosome. For instance, while in lines *Tub-GAL80$^{X\text{-}5B8}$* or *Tub-GAL80$^{III\text{-}92F3}$* the majority of green cells were NBs and GMCs, in line *Tub-GAL80$^{III\text{-}82A1}$* we mainly detected green neurons or green glial cells. These results suggest that different chromosome regions within the fly genome might be subjected to particular rules of gene regulation in a cell type (brain specific)- dependent manner, as already suggested for heterochromatin-mediated silencing during larval development (Lu et al., 1996). Additionally, it is important to consider that for the same line, the position of green cells was also quite variable. For example, in line *Tub-GAL80$^{III\text{-}70C3}$*, green NBs were positioned at different regions of the central brain, in different brain lobes. These results, combine with the results obtained by time-lapse microscopy suggest a certain randomness or stochasticity of the system.

The lack of repression capacity found for most *GAL80* insertions in different chromosome locations for the X, II and III chromosomes suggest however that one single *GAL80* copy is not sufficient to inhibit GAL4 activity. These results can be explained by an imbalance in terms of GAL4/GAL80 stoichiometry (Pfeiffer et al., 2010). Generally, the

strength of gene expression relies on the strength of its promoter. The stoichiometry imbalance can thus be explained by the different promoters used in this study. Indeed, the lines used here: *Tub-GAL80* and *Act-GAL4*, even if considered as ubiquitous and containing strong promoters seem to be rather different. The differences in promoter strength seem to be supported by our findings showing that when both *GAL4* and *GAL80* sequences were under the same actin promoter, the frequency of GFP$^+$ cells was drastically reduced in the brain. However, even if plausible, this explanation might also be quite simplistic and does not explain all our results. While lines *2xTub-GAL80$^{II\text{-}22A,53B2}$* and *2xTub-GAL80$^{III\text{-}62E1,96F3}$*, which contained two copies of *Tub-GAL80* did repress GAL4 activity and represent good candidates as probes for chromosome loss, lines *2xTub-GAL80$^{X\text{-}5B9,19E7}$*, *2xTub-GAL80$^{II\text{-}25A3,59D3}$* and *2xTub-GAL80$^{III\text{-}65B2,99F}$* did not suppress all GFP$^+$ cells. This was even more obvious in line *2xTub-GAL80$^{X\text{-}5B9,19E7}$*, on the X chromosome, which suggests that the chromosome X might be subjected to an even more particular and yet unknown gene regulation process.

From all the lines analysed in this study, the X chromosome appears as a particular chromosome in terms of gene regulation specifically in NBs. The presence of two or four *Tub-GAL80* copies did not repress GFP expression. GFP was inherited by the daughter GMCs during mitosis, suggesting a dynamic behavior. Importantly, older GMCs from a NB/GMCs cluster were frequently less green than younger GMCs or even the mother NB. Together with the RNA FISH analysis showing *GAL80* mRNAs signals in GMCs away from the NB, these results suggest that *GAL80* expression might be re-installed as GMCs age and become more differentiated. These observations indicate therefore that the particular and most likely random gene regulation of the X chromosome is associated with neural stem cell identity.

The findings that different *Tub-GAL80* lines generate different GFP$^+$ patterns exclusive in the brain suggest a specific regulation at the chromatin level most likely dependent on epigenetic marks that might allow adaptation in adverse situations. The plasticity of the system seems to be partially supported by our observations of different green cell frequency in response to different environmental changes. For example, the difference in the frequency of GFP$^+$ NBs observed at lower temperature might also reflect a safeguard mechanism that closes chromatin (less GAL80) to slow down neurogenesis. In agreement, it has been proposed that neurogenesis requires a certain neuroblast plasticity and competence to generate different types of neurons (Pearson and Doe, 2003; Cleary and Doe, 2006). This plasticity at the scale of an organ like the brain can positively serve adaptation and evolution. In light of

this possibility, the epigenetic plasticity, inherent and specific to the brain might allow a rapid adaptation to stress and environmental changes.

Acknowledgments

We acknowledge the PiCT-IBiSA platform and Nikon Imaging Center at Institut Curie for image set up. We thank V. Marthiens, S. Gemble, M. Bud zyk, F. Leulier, J. Merlet, P. Tran and the Bardin team for helpful discussion and/or comments on the manuscript. This work was supported by an ERC CoG (ChromoNumber - LS3, ERC-2016-COG), Institut Curie and the CNRS. A.G was funded by FRM (ECO20170637529) and LLCC (IP/SC-16533) fellowships.

Author contribution:

A.G performed all experiments, analyzed the data, generated the figures and wrote the paper. C.P generated certain tools and A.S helped for some experiments. C.P and A.S helped with fly pushing. P.S generated the *Tub-GAL80* plasmid. R.B conceived and supervised the project. A.G, R.B and A.B interpreted the data which was discussed between all authors during the preparation of the manuscript.

Materials and Methods

Fly husbandry and fly stocks

For most experiments, flies were raised in plastic vials containing homemade standard *Drosophila* rich culture medium (0.75% agar, 3.5% organic wheat flour, 5% yeast, 5.5% sugar, 2.5% nipagin, 1% penicillin-streptomycin (Gibco #15140), and 0.4% propanic acid). Fly stocks were maintained at 22ºC and experimental crosses at 25ºC. For food restriction experiment, flies were raised on homemade protein-poor medium (0.75% agar, 7% cornmeal, 1.4% yeast, 5.2% sugar, 1.4% nipagin) at 22ºC and compared to flies raised on homemade standard rich medium at 22ºC. For temperature variation experiment, flies were laying eggs for 24hours and tubes containing progeny were maintained at 18ºC, 22ºC, 25ºC or 29ºC for 7, 5, 5 or 4 days, prior dissection, respectively. For the MARCM experiment, fly crosses were kept at 22ºC. L2 progenies were heat-shocked 1hour at 37 ºC in a water bath and maintained at 22ºC for 30hours before dissection. Fly stocks are summarized in Supplementary Table 1.

GAL80 Drosophila lines establishment

The plasmid containing codon-optimized *GAL80* sequence driven by a tubulin promoter is a gift from Allison Bardin and corresponds to the combination of pattB-tubP-SV40 - generated by Lee and Luo (Lee and Luo, 1999)- with the codon optimized GAL80 sequence from pBPGAL80Uw-6 - a gift from Gerald Rubin (Addgene plasmid #26236, http://n2t.net/addgene:26236 ; RRID:Addgene_26236) (Pfeiffer et al., 2010). Then, the plasmid was inserted in a P[acman] vector and send to Bestgene® company to integrate it into the *Drosophila* genome at specific insertion sites using PhiC31 integrase-mediated transgenesis system.

To obtain *Drosophila* recombinants carrying two copies of *Tub-GAL80* on the same chromosome, we used female meiotic recombination and selected recombination events based on the fly eyes colour, a method widely used to generate *Drosophila* recombinants. Indeed, all *Tub-GAL80* are associated with the white^{+} transgene expressing marker, which is used as a marker for efficient transgene insertion as it confers yellow to red eye colour. Simply, in the presence of two copies, as for efficient recombination, fly eyes display a strong red colour.

IMMUNOFLUORESCENCE OF *DROSOPHILA* LARVAL WHOLE MOUNT TISSUES

Mid third-instar larval (L3) brains and imaginal discs were dissected in fresh Phosphate-Buffered Saline 10X (PBS, VWR #L182-10) and fixed for 30 minutes (min) at room temperature (RT) in 4% paraformaldehyde (EMS # 15710) diluted in PBS. Fixed tissues were washed and permeabilized three times 15 min in PBST3 or PBST1 (PBS, 0,3% or 0,1% Triton X-100, Euromedex #2000-C). For antibody staining, larval tissues were incubated in primary antibodies diluted in PBST3 or PBST1 overnight at 4ºC in a humid chamber. After 3x15 min washes in PBST3 or PBST1, tissues were incubated in secondary antibodies diluted in PBST3 or PBST1, O/N at 4ºC and protected from light in a humid chamber. Tissues were then washed 3x15 min in PBST3 or PBST1, rinsed in PBS and mounted between slides (Thermo Fisher Scientific #AA00008232E00MNT10) and 12-mm circular cover glasses (Marienfield Superior #0111520) with 5µl of homemade mounting medium (1,25% n-propyl gallate, 75% glycerol, 25% H_2O).

Primary antibodies used in this study are: chicken (chk) anti-GFP (1:1000, Abcam #ab13970), guinea pig (GP) anti-Deadpan (Dpn) (1:1000, J. Skeath), mouse anti-Prospero (1:500, MR1A, DSHB), rat anti-Elav (1:100, 7EA10, DSHB), mouse anti-Repo (1:500, 8D15, DSHB), rabbit (Rb) anti-Sas4 (1:500, Basto et al 2006), GP anti-Centrosomin (Cnn) (1:1000, E. Lucas and J.W.R.).

Secondary antibodies (1:250) used in this study are: chk-488 (Thermo Fisher Scientific #A-11039), Rat-546 (Thermo Fisher Scientific #A-11081), Rb-568 (Thermo Fisher Scientific #A-10042), mouse-546 (Thermo Fisher Scientific #A-11030) and GP-647 (Thermo Fisher Scientific #A-21450).

For GFP screening of larval brains and imaginal discs, one step of O/N incubation at 4ºC with GFP booster (1:250, Alexa Fluor ® 488 Chromotek #gb2AF488), Phalloidin-647 (1:250, Thermo Fisher Scientific #A-22287) and DAPI (1:1000, Thermo Fisher Scientific #62248) were performed followed by 3x15 min washes in PBST3, a rinse in PBS and mounting.

Images were acquired with 40x (NA 1.25), 63x (NA 1.32) or 100x (NA 1.4) oil objectives on a wide-field Inverted Spinning Disk Confocal Gattaca/Nikon (a Yokagawa CSU-W1 spinning head mounted on a Nikon Ti-E inverted microscope equipped with a camera complementary metal-oxide semiconductor 1.200 x 1.200 Prime95B; Photometrics). Intervals for z-stack acquisitions were set to 0.5 to 1.5µm using Metamorph software.

LIVE IMAGING OF *DROSOPHILA* LARVAL BRAINS

Mid second-instar larval (L2) brains were dissected in Schneider's *Drosophila* medium (Gibco #21720024) supplemented with 10% heat-inactivated fetal bovine serum (Gibco #10500), penicillin (100 U/ml) and streptomycin (100 µg/ml). Several brains were placed in 10µl of medium on a glass-bottom dish (Dutcher #627870), covered with a permeable membrane (Standard YSI), and sealed around the membrane borders with oil 10 S Voltalef (VWR Chemicals). Images were acquired with 60x oil objective (NA 1.4) on two microscopes: an Inverted Spinning Disk Confocal Roper/Nikon (a Yokagawa CSU-X1 spinning head mounted on a Nikon Ti-E inverted microscope equipped with a camera EMCCD 512 x 512 Evolve; Photometrics) and the wide-field Inverted Spinning Disk Confocal Gattaca/Nikon (a Yokagawa CSU-W1 spinning head mounted on a Nikon Ti-E inverted microscope equipped with a camera complementary metal-oxide semiconductor 1.200 x 1.200 Prime95B; Photometrics), controlled by Metamorph software. For both microscopes, images were acquired at time intervals spanning 30 min and 50 z-stacks of 1.5 µm.

DNA FLUORESCENT *IN SITU* HYBRIDIZATION

After fixation, permeabilization and O/N incubation with GFP booster (description below), brains were washed 3x15min in PBT3 and fixed a second time 30 min in 4%PFA. Then, brains were rinse 3x in PBS, washed 1x5 min in 2xSSCT (2X Saline Sodium Citrate (Euromedex #EU0300-A) 0,1% Tween-20 (Sigma Aldrich #P1379) diluted in water), 1x5 min in 2xSSCT/50% formamide (Sigma Aldrich #47671), transferred in pre-warmed 2xSSCT/50% formamide and pre-hybridized 3 min at 92°C. In the meantime, DNA probes diluted in the Hybridization Buffer (20%dextransulfate (Sigma Aldrich #D8906), 2xSSCT, 50%formamide, 0,5mg/ml salmon DNA sperm (Sigma Aldrich #D1626)) were denature at 92°C. After removal of the supernatant, brains were incubated in the probes solutions and hybridize 5 min at 92°C and O/N at 37°C.

Brains were then rinse at RT, washed 1x10 min at 60°C and 1x5 min at RT in 2xSSCT. Finally, after a rinse in PBS brains were mounted as described below.

DNA probes used in this study were against chromosomes X (80ng/µl), II (40ng/µl) and III (80ng/µl).

RNA Fluorescent *in situ* hybridization

L3 brains were dissected in fresh PBS, fixed 30 min in 4% formaldehyde (EMS # 15686) and washed and permeabilized in PBSTw (PBS 0,3% Tween-20). Brains were incubated with GFP booster and Phalloidin diluted in PBSTw, O/N at 4°C in a humid chamber. After 3x15 min washes PBSTw, RNA hybridization was performed as described by Yang and colleagues (Yang et al., 2017). RNA probes against *GAL80* were designed by the biosearchtech® technical support team (https://www.biosearchtech.com/) and labeled with quasar 570.

Polymerase Chain Reaction (PCR) of *Drosophila* lines

Good quality genomic DNA was extracted according to the protocol provided by the Vienna Drosophila Resource Center from flies heterozygous for *Tub-GAL80*$^{II\text{-}53B2}$ (one *GAL80* copy), homozygous for *Tub-GAL80*$^{II\text{-}53B2}$ (two *GAL80* copies) and heterozygous recombinant *2xTub-GAL80*^{X5B8,19E7} (two *GAL80* copies). PCR analysis was performed using the following primers: *GAL80* forward (5' CGGTGCCGAATGCTGCTCCCA 3') and *GAL80* reverse (5' CCGAACGTGGTGGTCACCAGA 3').

Table 1 - List of *Drosophila* stocks

Stock Name	Genotype	Chromosomal location	Origins
WT	w[118]		RRID:BDSC_5905
Tub-GAL80	alphaTub84B-GAL80	X-5B8	This study
Tub-GAL80	alphaTub84B-GAL80	X-19E7	This study
Tub-GAL80	alphaTub84B-GAL80	2L-22A3	Bardin lab
Tub-GAL80	alphaTub84B-GAL80	2L-25A3	This study
Tub-GAL80	alphaTub84B-GAL80	2L-28E7	Bardin lab
Tub-GAL80	alphaTub84B-GAL80	2R-43A1	This study
Tub-GAL80	alphaTub84B-GAL80	2R-47C6	This study
Tub-GAL80	alphaTub84B-GAL80	2R-53B2	This study
Tub-GAL80	alphaTub84B-GAL80	2R-59D3	This study
Tub-GAL80	alphaTub84B-GAL80	3L-62E1	This study
Tub-GAL80	alphaTub84B-GAL80	3L-65B2	This study
Tub-GAL80	alphaTub84B-GAL80	3L-70C4	This study
Tub-GAL80	alphaTub84B-GAL80	3L-75A10	This study
Tub-GAL80	alphaTub84B-GAL80	3L-76A2	This study
Tub-GAL80	alphaTub84B-GAL80	3R-82A1	This study
Tub-GAL80	alphaTub84B-GAL80	3R-85A2	This study
Tub-GAL80	alphaTub84B-GAL80	3R-89E11	Bardin lab
Tub-GAL80	alphaTub84B-GAL80	3R-92F1	This study
Tub-GAL80	alphaTub84B-GAL80	3R-96F3	This study
Tub-GAL80	alphaTub84B-GAL80	3R-99F8	Bardin lab
Act-GAL4	Actin5C-GAL4	2	RRID:BDSC_4414
Act-GAL4	Actin5C-GAL4	3	RRID:BDSC_3954
GFP-NLS	UAS-GFP-NLS	3	RRID:BDSC_4776
GFP-NLS	UAS-stinger	2	RRID:BDSC_84277
Tub-GAL80	hsFLP,alphaTub84B-GAL80,FRT19A	X-1C2	RRID:BDSC_5132
Tub-GAL80	alphaTub84B-GAL80,FRT80B	3L-75E1	RRID:BDSC_5191
Tub-GAL80	alphaTub84B-GAL80	3	RRID:BDSC_9490
Act-GAL80	Actin5C(loxP.GAL80.stop)loxA::p65	2-25C6	RRID:BDSC_67092
Tub-GAL4,FRT82B,Tub-GAl80	alphaTub84B-GAL4,FRT82B,alphaTub84B-GAL80	3-79A2,82B2	RRID:BDSC_30036
hsFLP	Hsp70-FLP	X	N/A
FRT82B,sas4mut	FRT82B, sas4mut	3	Raff lab
Histone-RFP	HistoneH2Av-mRFP	2	RRID:BDSC_23651
Act-GAL4,GFP-NLS/CyoGFP		2	This study
Act-GAL4,GFP-NLS/TM6,Tb		3	This study
Act-GAL4,GFP-NLS,Histone-RFP/CyoGFP		2	This study
GFP-NLS;Tub-GAL4,FRT82B,Tub-GAL80		2;3	This study
hsFLP/FM7,kr;;FRT82B,sas4mut/TM6,Tb		X;;3	This study
2xTub-GAL80		X-5B8,19E7	This study
2xTub-GAL80		2-22A,53B2	This study
2xTub-GAL80		2-25A3,59D3	This study
2xTub-GAL80		3-62E1,96F3	This study
2xTub-GAL80		3-65B2,99F8	This study
2xTub-GAL80;;Act-GAL4,GFP-NLS		X-5B8,19E7;;3	This study

Chapter 3 – Discussion and Perspectives

Main findings of my two projects are separately discussed in specific sub-parts of the previous chapter (*Chapter 2 – Results*). Here, I will summarize all major discoveries, provide multiple perspectives and discuss additional questions and concepts raised by the data provided in this manuscript.

Multipolar divisions in polyploid cells: a problem of scaling?

In the context of cytokinesis failure, the resulting cell doubles its genome but also all components of its cytoplasm which includes proteins or organelles. This is accompanied by an increase in cell size. Thus, one would expect that all cellular machineries would scale accordingly. Notably, the mitotic spindle and MT dynamics were shown to adapt and scale with cell size for example (Dumont and Mitchison, 2009; Lacroix et al., 2018). Using live-cell imaging of polyploid *Drosophila* NBs and cancer cells, I found that polyploid mitoses largely associate with multipolarity. To understand the major contributor of this multipolarity, I combined *in sillico* approaches of spindle modelling and perturbations of spindle and DNA. The increase in centrosome number - as a result of cytokinesis failure - does explain on its own spindle multipolarity. I found that polyploid mitotic chromosomes adopt abnormal configurations and do not properly align. Consequently, the presence of extra-DNA masses between spindle poles physically blocks their coalescence and leads to a multipolar division. This finding provides a mechanistic link between polyploidy and associated multipolarity which together can fuel cancer genome evolution. Interestingly, bipolarity was restored when MT-stability was increased strengthening the idea that polyploid mitotic spindle properties do not scale for the need of bipolarity. In agreement, we have shown in the lab that some nuclei in these multinucleated polyploid cells presented a delay in cell cycle progression, generating high levels of DNA damage when forced to enter mitosis (Nano et al., 2019). Altogether, these findings in unscheduled polyploidy questioned about the lack of proper scaling of cell machineries to sustain essential functions such as cell cycle progression and cell division. It appears somehow paradoxical that polyploidy is broadly found in various tissues in physiological contexts where it favours cell fitness and tissue homeostasis. Thus, understanding the differences between unscheduled and programmed polyploidy on cell homeostasis will help dissecting the link between genome doubling and GIN. Those are questions currently developed in the lab.

Low frequency of chromosome loss in WT tissues: not happening or not tolerated?

In contrast to polyploidy, the presence of aneuploid cells in normal conditions remains a long-term debate. In a second part of my thesis, I aimed to assess aneuploidy frequency in *Drosophila* tissues. For that, I developed a novel tool to monitor chromosome loss based on the widely used inhibitor/activator system GAL80/GAL4/UAS combined with a GFP reporter. By analysing the appearance of green aneuploid cells – due to GAL80-containing chromosome loss – I found that aneuploidy is extremely infrequent in most *Drosophila* tissues. Importantly, due to the probe design I follow the loss of only one copy of one chromosome at a time, thus aneuploidy frequency is under-estimated. However, even considering all chromosomes, this rate of chromosome loss in WT tissues would remain extremely low. This finding raises the question whether this low level represents low frequency of errors or intolerance of aneuploid cells that were eliminated prior detection. In fly wing discs, it is known that aneuploid cells are eliminated from the tissue by apoptosis (Dekanty et al., 2012; Sabino et al., 2015). In the brain aneuploid cells prematurely differentiate and thus remain within the tissue as aneuploid neurons (Gogendeau et al., 2015). It is important to mention that most studies investigating aneuploidy in WT or aneuploid-mutant flies mainly reported chromosome gain while here, the probe used exclusively monitors chromosome loss. Knowing that the *Drosophila* genome only contains four pairs of chromosomes, it is possible that losing a significant part of the genome does not have similar consequences when compared to chromosome gain. Interestingly, this in light with the fact that gain of whole chromosome sets is tolerated in NBs of the *Drosophila* brain, despite abnormal divisions and high DNA-damage (Nano et al., 2019; Goupil et al., 2020a). However, this remains an assumption and further investigation on the consequences of different degrees of chromosome copy number variations on cell fitness will be useful. For example, the use of this probe in several conditions that are permissive for aneuploidy, in combination with fluorescent markers probing cell components for live-imaging, will help deciphering the mechanisms behind aneuploidy generation and outcome *in vivo*.

Genetic and epigenetic regulations: why is the brain so different?

While generating the GAL80/GAL4/GFP tool, I observed an unexpected proportion of green brain cells that was not a by-product of chromosome loss. Instead, I found an unknown dysregulation of the GAL4/GAL80 system. Through the analysis of *GAL80* expression by FISH and long-term live-imaging, I found that GAL80 was silenced in certain NBs randomly

dispersed within the brain central region. Interestingly, I observed this *GAL80* silencing exclusively in the brain when compared to other tissues, such as imaginal discs and furthermore, this was influenced by environmental changes. These findings highlight a certain degree of epigenetic plasticity in the brain that differs from other organs and that seems to adapt to external cues. The mapping of the different epigenetic marks and regulators in these cells, and comparison with surrounding cells and other tissues will be required to understand the mechanisms behind this epigenetic instability specific to the brain.

My work gathered with data from literature suggest that the all types of genome regulation - aneuploidy, polyploidy and epigenetics - differ between brain and other tissues. I will discuss hypothesis that would justify why the brain is so permissive to (epi)genetic instability.

Brain specificity: lack of control for rapid development?

During the short-course of development, larval tissues extensively expends in size. While some tissues use polyploidization as a way of rapid growth, epithelial cells of the wing disc and neural stem cells of the brain proliferate extremely fast. However, the mode of division differs between both tissues. Wing disc cells symmetrical divide giving rise to two daughters that will in turn symmetrically divide, allowing rapid exponential growth. In contrast, in the brain, asymmetric division occurs, maintaining NBs pool and generating a more committed cell that divides only once and thus, poorly participates to brain growth. Most likely to circumvent this, the NB cell cycle is extremely short, around 1,5 hours compared to about 10 hours for epithelial wing disc cells (analysis performed in the lab). Consequently, tolerance for instable karyotypes or epigenetic instability might reflect a leakiness of quality controls in a tissue where fast division is the priority to reach a certain size. Notably, concerning gene expression pattern in NBs, it is possible that epigenetic marks do not have enough time to be properly established and are thus randomly positioned. Thus, if we consider the hypothesis of lack of control, instability in the establishment of epigenetic marks would change gene expression pattern at each cycle and the GFP signal would present an on/off fluctuation over time. However, this is not the case, as once established - due to *GAL80* silencing - the GFP signal remains extremely stable over time. This means that even though the epigenetic landscape is highly variable between cells of the same type - here, NBs - random acquisition or loss of

certain marks is maintained over time. Analysis of the consequences following perturbations in the mode of division or cell cycle speed might contribute to understand the mechanisms at stake.

Brain specificity: plasticity for variability and adaptability?

As shown for embryonic stem cells, usually stemness correlates with more open chromatin and indeed, repression marks as heterochromatin were shown to increase with differentiation (Francastel et al., 2000; Arney and Fisher, 2004; Meshorer et al., 2006; Meshorer and Misteli, 2006; Zhu et al., 2013). This was believed to represent a permissive state that would allow the rapid establishment of diverse differentiation programs (Gaspar-Maia et al., 2011) and NBs produce an enormous variety of neurons. Thus, *GAL80* repression in *Drosophila* NBs is very surprising and suggests that the establishment of epigenetic marks differs in the brain compared to other tissues.

Studies already described epigenetic landscape transitions between the different cell types of NB and gut lineages (Marshall and Brand, 2017; Aughey et al., 2018). However, my work demonstrates that over the inter-cell type, an intra-cell type variability needs to be considered. Analysis at the single cell level will be require to precisely dissect this regulation of gene expression. Using the GAL80 system described in *Chapter 2 - Results – Section B* comparison between GFP+ and GFP- cells at the transcriptome level might be very informative.

Interestingly, NBs that repress *GAL80* did not present any pattern as they were randomly positioned within the central brain. It suggests that this control is independent of the epigenetic regulation occurring during the spatial and temporal patterning driving neuronal lineage production in the central brain and optic lobe (Maurange et al., 2008; Li et al., 2013c; Erclik et al., 2017), which is in contrast highly stereotyped and stable. This possibly reflects a certain level of epigenetic plasticity in the brain necessary for such diversity that occurs in no other tissue. Another study in *Drosophila* follicles, found that epigenetic stability was increasing with differentiation and importantly with S-phase length (Skora and Spradling, 2010). Thus, this plasticity described in fast-cycling NBs fits with the idea of epigenetic instability favouring rapid reprogramming, diversity and adaptability.

Epigenetics is known to respond to environment modifications to adjust accordingly. Interestingly, by changing several parameters of fly culture, I found that the GAL80/GAL4

system was affected by environmental challenges. This set of data suggests that NBs are able to adapt their gene expression pattern in response to external cues as temperature or food composition. Interestingly, this plasticity of epigenetic regulation for adaptability or flexibility is not specific to the *Drosophila* brain but most likely inherent to the brain itself. Indeed, it was shown that the retrotransposon LINE-1 in mammalian and human brains favours mosaicism in the neuronal genome and consequently neural diversity (reviewed in (Bodea et al., 2018)). Further, this (epi)genetic plasticity of the brain would represent a mechanism that allows rapid evolution of brain functions, essential for survival.

Bibliography

Abdul Halim, M., F.H.P. Tan, A. Azlan, I.I. Rasyid, N. Rosli, S. Shamsuddin, and G. Azzam. 2020. Ageing, Drosophila melanogaster and Epigenetics. *Malaysian J. Med. Sci.* 27:7–19.

Abdusselamoglu, M.D., L. Landskron, S.K. Bowman, E. Eroglu, T. Burkard, R.E. Kingston, and J.A. Knoblich. 2019. Dynamics of activating and repressive histone modifications in Drosophila neural stem cell lineages and brain tumors. *Dev.* 146.

Abmayr, S.M., and G.K. Pavlath. 2012. Myoblast fusion: Lessons from flies and mice. *Development*. 139:641–656.

Adams, M.D., S.E. Celniker, R.A. Holt, C.A. Evans, J.D. Gocayne, P.G. Amanatides, S.E. Scherer, P.W. Li, R.A. Hoskins, R.F. Galle, R.A. George, S.E. Lewis, S. Richards, M. Ashburner, S.N. Henderson, G.G. Sutton, J.R. Wortman, M.D. Yandell, Q. Zhang, L.X. Chen, R.C. Brandon, Y.H.C. Rogers, R.G. Blazej, M. Champe, B.D. Pfeiffer, K.H. Wan, C. Doyle, E.G. Baxter, G. Helt, C.R. Nelson, G.L. Gabor Miklos, J.F. Abril, A. Agbayani, H.J. An, C. Andrews-Pfannkoch, D. Baldwin, R.M. Ballew, A. Basu, J. Baxendale, L. Bayraktaroglu, E.M. Beasley, K.Y. Beeson, P. V. Benos, B.P. Berman, D. Bhandari, S. Bolshakov, D. Borkova, M.R. Botchan, J. Bouck, P. Brokstein, P. Brottier, K.C. Burtis, D.A. Busam, H. Butler, E. Cadieu, A. Center, I. Chandra, J. Michael Cherry, S. Cawley, C. Dahlke, L.B. Davenport, P. Davies, B. de Pablos, A. Delcher, Z. Deng, A. Deslattes Mays, I. Dew, S.M. Dietz, K. Dodson, L.E. Doup, M. Downes, S. Dugan-Rocha, B.C. Dunkov, P. Dunn, K.J. Durbin, C.C. Evangelista, C. Ferraz, S. Ferriera, W. Fleischmann, C. Fosler, A.E. Gabrielian, N.S. Garg, W.M. Gelbart, K. Glasser, A. Glodek, F. Gong, J. Harley Gorrell, Z. Gu, P. Guan, M. Harris, N.L. Harris, D. Harvey, T.J. Heiman, J.R. Hernandez, J. Houck, D. Hostin, K.A. Houston, T.J. Howland, et al. 2000. The genome sequence of Drosophila melanogaster. *Science (80-.).* 287:2185–2195.

Adams, R.R., A.A. Tavares, A. Salzberg, H.J. Bellen, and D.M. Glover. 1998. pavarotti encodes a kinesin-like protein required to organize the central spindle and contractile ring for cytokinesis. *Genes Dev*. 12:1483–1494.

Akhmanova, A., and C.C. Hoogenraad. 2015. Microtubule minus-end-targeting proteins. *Curr. Biol.* 25:R162–R171.

De Almeida, B.P., A.F. Vieira, J. Paredes, M. Bettencourt-Dias, and N.L. Barbosa-Morais. 2019. Pan-cancer association of a centrosome amplification gene expression signature with genomic alterations and clinical outcome. 15. 1–31 pp.

Andersen, J.S., C.J. Wilkinson, T. Mayor, P. Mortensen, E.A. Nigg, and M. Mann. 2003. Proteomic characterization of the human centrosome by protein correlation profiling. *Nature*. 426:570–574.

Anderson, C.T., and T. Stearns. 2009. Centriole Age Underlies Asynchronous Primary Cilium Growth in Mammalian Cells. *Curr. Biol.* 19:1498–1502.

Andreassen, P.R., O.D. Lohez, F.B. Lacroix, and R.L. Margolis. 2001. Tetraploid state induces p53-dependent arrest of nontransformed mammalian cells in G1. *Mol. Biol. Cell*. 12:1315–1328.

Andreassen, P.R., S.N. Martineau, and R.L. Margolis. 1996. Chemical induction of mitotic checkpoint override in mammalian cells results in aneuploidy following a transient

tetraploid state. *Mutat. Res. - Fundam. Mol. Mech. Mutagen.* 372:181–194.

Andrews, P.D., Y. Ovechkina, N. Morrice, M. Wagenbach, K. Duncan, L. Wordeman, and J.R. Swedlow. 2004. Aurora B regulates MCAK at the mitotic centromere. *Dev. Cell*. 6:253–268.

Andriani, G.A., J. Vijg, and C. Montagna. 2017. Mechanisms and consequences of aneuploidy and chromosome instability in the aging brain. *Mech. Ageing Dev.* 161:19–36.

Antonarakis, S.E., R. Lyle, E.T. Dermitzakis, A. Reymond, and S. Deutsch. 2004. Chromosome 21 and Down syndrome: From genomics to pathophysiology. *Nat. Rev. Genet.* 5:725–738.

Arents, G., and E.N. Moudrianakis. 1993. Topography of the histone octamer surface: repeating structural motifs utilized in the docking of nucleosomal DNA. *Proc. Natl. Acad. Sci. U. S. A.* 90:10489–10493.

Arney, K.L., and A.G. Fisher. 2004. Epigenetic aspects of differentiation. *J. Cell Sci.* 117:4355–4363.

Askjaer, P., V. Galy, E. Hannak, and I.W. Mattaj. 2002. Ran GTPase cycle and importins alpha and beta are essential for spindle formation and nuclear envelope assembly in living Caenorhabditis elegans embryos. *Mol. Biol. Cell*. 13:4355–4370.

van Attikum, H., and S.M. Gasser. 2005. The histone code at DNA breaks: a guide to repair? *Nat. Rev. Mol. Cell Biol.* 6:757–765.

Aughey, G.N., A. Estacio Gomez, J. Thomson, H. Yin, and T.D. Southall. 2018. CATaDa reveals global remodelling of chromatin accessibility during stem cell differentiation in vivo. *Elife*. 7:1–22.

Babu, J.R., K.B. Jeganathan, D.J. Baker, X. Wu, N. Kang-Decker, and J.M. Van Deursen. 2003. Rae1 is an essential mitotic checkpoint regulator that cooperates with Bub3 to prevent chromosome missegregation. *J. Cell Biol.* 160:341–353.

Baines, K.J., and S.J. Renaud. 2017. Transcription Factors That Regulate Trophoblast Development and Function. 145. 1st ed. Elsevier Inc. 39–88 pp.

Baker, D.J., M.M. Dawlaty, T. Wijshake, K.B. Jeganathan, L. Malureanu, J.H. Van Ree, R. Crespo-Diaz, S. Reyes, L. Seaburg, V. Shapiro, A. Behfar, A. Terzic, B. Van De Sluis, and J.M. Van Deursen. 2013. Increased expression of BubR1 protects against aneuploidy and cancer and extends healthy lifespan. *Nat. Cell Biol.* 15:96–102.

Bakhoum, S.F., and D.A. Landau. 2017. Chromosomal instability as a driver of tumor heterogeneity and evolution. *Cold Spring Harb. Perspect. Med.* 7:1–14.

Bakhoum, S.F., W.T. Silkworth, I.K. Nardi, J.M. Nicholson, D.A. Compton, and D. Cimini. 2014. The mitotic origin of chromosomal instability. 24. Elsevier.

Bakhoum, S.F., S.L. Thompson, A.L. Manning, and D.A. Compton. 2009. Genome stability is ensured by temporal control of kinetochore-microtubule dynamics. *Nat. Cell Biol.* 11:27–35.

Bakker, B., H. van den Bos, P.M. Lansdorp, and F. Foijer. 2015. How to count chromosomes in a cell: An overview of current and novel technologies. *BioEssays*. 37:570–577.

Bamba, C., Y. Bobinnec, M. Fukuda, and E. Nishida. 2002. The GTpase Ran regulates chromosome positioning and nuclear envelope assembly in vivo. *Curr. Biol.* 12:503–507.

Barisic, M., P. Aguiar, S. Geley, and H. Maiato. 2014. Kinetochore motors drive congression of peripheral polar chromosomes by overcoming random arm-ejection forces. *Nat. Cell Biol.* 16:1249–1256.

Barlow, P.W., and M.I. Sherman. 1974. Cytological studies on the organization of DNA in giant trophoblast nuclei of the mouse and the rat. *Chromosoma*. 47:119–131.

Barnum, K.J., and M.J. O'Connell. 2014. Cell cycle regulation by checkpoints. *Methods Mol. Biol.* 1170:29–40.

Barolo, S., L.A. Carver, and J.W. Posakony. 2000. GFP and β-Galactosidase Transformation Vectors for Promoter/Enhancer Analysis in Drosophila. *Biotechniques*. 29:726–732.

Basto, R., K. Brunk, and T. Vinadogrova. 2008. Centrosome amplification can initiate tumorigenesis in flies. *Chemtracts*. 21:111–113.

Basto, R., J. Lau, T. Vinogradova, A. Gardiol, C.G. Woods, A. Khodjakov, and J.W. Raff. 2006. Flies without centrioles. *Cell*. 125:1375–1386.

Bastock, R., and D. St Johnston. 2008. Drosophila oogenesis. *Curr. Biol.* 18:1082–1087.

Batty, P., and D.W. Gerlich. 2019. Mitotic Chromosome Mechanics: How Cells Segregate Their Genome. *Trends Cell Biol.* 29:717–726.

Bauer, M., F. Cubizolles, A. Schmidt, and E.A. Nigg. 2016. Quantitative analysis of human centrosome architecture by targeted proteomics and fluorescence imaging. *EMBO J.* 35:2152–2166.

Baumgardt, M., D. Karlsson, J. Terriente, F.J. Díaz-Benjumea, and S. Thor. 2009. Neuronal subtype specification within a lineage by opposing temporal feed-forward loops. *Cell*. 139:969–982.

Baumgart, J., M. Kirchner, S. Redemann, J. Woodruff, J.M. Verbavatz, F. Jülicher, A.A. Hyman, T. Müller-Reichert, and J. Brugués. 2019. Soluble tubulin is locally enriched at mitotic centrosomes in C. elegans. *bioRxiv*. 218:3977–3985.

Bazzi, H., and K. V. Anderson. 2014. Acentriolar mitosis activates a p53-dependent apoptosis pathway in the mouse embryo. *Proc. Natl. Acad. Sci. U. S. A.* 111.

Bello, B.C., N. Izergina, E. Caussinus, and H. Reichert. 2008. Amplification of neural stem cell proliferation by intermediate progenitor cells in Drosophila brain development. *Neural Dev.* 3:5.

Ben-David, U., G. Arad, U. Weissbein, B. Mandefro, A. Maimon, T. Golan-Lev, K. Narwani, A.T. Clark, P.W. Andrews, N. Benvenisty, and J. Carlos Biancotti. 2014. Aneuploidy induces profound changes in gene expression, proliferation and tumorigenicity of human pluripotent stem cells. *Nat. Commun.* 5:1–11.

Benito-Sipos, J., A. Estacio-Gómez, M. Moris-Sanz, M. Baumgardt, S. Thor, and F.J. Díaz-Benjumea. 2010. A genetic cascade involving klumpfuss, nab and castor specifies the abdominal leucokinergic neurons in the Drosophila CNS. *Development*. 137:3327–3336.

Bennabi, I., M.E. Terret, and M.H. Verlhac. 2016. Meiotic spindle assembly and chromosome segregation in oocytes. *J. Cell Biol.* 215:611–619.

Bennett, M.D., and J.B. Smith. 1976. Nuclear dna amounts in angiosperms. *Philos. Trans. R. Soc. London. Ser. B, Biol. Sci.* 274:227–274.

Bergen, L.G., R. Kuriyama, and G.G. Borisy. 1980. Polarity of microtubules nucleated by

centrosomes and chromosomes of chinese hamster ovary cells in vitro. *J. Cell Biol.* 84:151–159.

Berger, S.L. 2007. The complex language of chromatin regulation during transcription. *Nature*. 447:407–412.

Beroukhim, R., C.H. Mermel, D. Porter, G. Wei, S. Raychaudhuri, J. Donovan, J. Barretina, J.S. Boehm, J. Dobson, M. Urashima, K.T. McHenry, R.M. Pinchback, A.H. Ligon, Y.J. Cho, L. Haery, H. Greulich, M. Reich, W. Winckler, M.S. Lawrence, B.A. Weir, K.E. Tanaka, D.Y. Chiang, A.J. Bass, A. Loo, C. Hoffman, J. Prensner, T. Liefeld, Q. Gao, D. Yecies, S. Signoretti, E. Maher, F.J. Kaye, H. Sasaki, J.E. Tepper, J.A. Fletcher, J. Tabernero, J. Baselga, M.S. Tsao, F. Demichelis, M.A. Rubin, P.A. Janne, M.J. Daly, C. Nucera, R.L. Levine, B.L. Ebert, S. Gabrie, A.K. Rustgi, C.R. Antonescu, M. Ladanyi, A. Letai, L.A. Garraway, M. Loda, D.G. Beer, L.D. True, A. Okamoto, S.L. Pomeroy, S. Singer, T.R. Golub, E.S. Lander, G. Getz, W.R. Sellers, and M. Meyerson. 2010. The landscape of somatic copy-number alteration across human cancers. *Nature*. 463:899–905.

Bettencourt-Dias, M., A. Rodrigues-Martins, L. Carpenter, M. Riparbelli, L. Lehmann, M.K. Gatt, N. Carmo, F. Balloux, G. Callaini, and D.M. Glover. 2005. SAK/PLK4 Is Required for Centriole Duplication and Flagella Development. *Curr. Biol.* 15:2199–2207.

Biggins, S., and A.W. Murray. 2001. The budding yeast protein kinase Ipl1/Aurora allows the absence of tension to activate the spindle checkpoint. *Genes Dev.* 15:3118–3129.

Biggins, S., F.F. Severin, N. Bhalla, I. Sassoon, A.A. Hyman, and A.W. Murray. 1999. The conserved protein kinase Ipl1 regulates microtubule binding to kinetochores in budding yeast. *Genes Dev.* 13:532–544.

Birchler, J.A., U. Bhadra, L. Rabinow, R. Linsk, and A.T. Nguyen-Huynh. 1994. Weakener of white (Wow), a gene that modifies the expression of the white eye color locus and that suppresses position effect variegation in Drosophila melanogaster. *Genetics*. 137:1057–1070.

Blakely, C.M., T.B.K. Watkins, W. Wu, B. Gini, J.J. Chabon, C.E. McCoach, N. McGranahan, G.A. Wilson, N.J. Birkbak, V.R. Olivas, J. Rotow, A. Maynard, V. Wang, M.A. Gubens, K.C. Banks, R.B. Lanman, A.F. Caulin, J. St John, A.R. Cordero, P. Giannikopoulos, A.D. Simmons, P.C. MacK, D.R. Gandara, H. Husain, R.C. Doebele, J.W. Riess, M. Diehn, C. Swanton, and T.G. Bivona. 2017. Evolution and clinical impact of co-occurring genetic alterations in advanced-stage EGFR-mutant lung cancers. *Nat. Genet.* 49:1693–1704.

Blewitt, M., and E. Whitelaw. 2013. The use of mouse models to study epigenetics. *Cold Spring Harb. Perspect. Biol.* 5:a017939.

Bodakuntla, S., A.S. Jijumon, C. Villablanca, C. Gonzalez-Billault, and C. Janke. 2019. Microtubule-Associated Proteins: Structuring the Cytoskeleton. *Trends Cell Biol.* 29:804–819.

Bodea, G.O., E.G.Z. McKelvey, and G.J. Faulkner. 2018. Retrotransposon-induced mosaicism in the neural genome. *R. Soc. Open Sci.* 8.

Boone, J.Q., and C.Q. Doe. 2008. Identification of Drosophila type II neuroblast lineages containing transit amplifying ganglion mother cells. *Dev. Neurobiol.* 68:1185–1195.

Borisy, G.G., and E.W. Taylor. 1967. The mechanism of action of colchicine. Colchicine binding to sea urchin eggs and the mitotic apparatus. *J. Cell Biol.* 34:535–548.

Bornens, M. 2002. Centrosome composition and microtubule anchoring mechanisms. *Curr. Opin. Cell Biol.* 14:25–34.

van den Bos, H., D.C.J. Spierings, A.S. Taudt, B. Bakker, D. Porubský, E. Falconer, C. Novoa, N. Halsema, H.G. Kazemier, K. Hoekstra-Wakker, V. Guryev, W.F.A. den Dunnen, F. Foijer, M.C. Tatché, H.W.G.M. Boddeke, P.M. Lansdorp, D. Porubsky, E. Falconer, C. Novoa, N. Halsema, H.G. Kazemier, K. Hoekstra-Wakker, V. Guryev, W.F.A. den Dunnen, F. Foijer, M.C. Tatche, H.W.G.M. Boddeke, and P.M. Lansdorp. 2016. Single-cell whole genome sequencing reveals no evidence for common aneuploidy in normal and Alzheimer's disease neurons. *Genome Biol.* 17:1–9.

Bosco, G., P. Campbell, J.T. Leiva-Neto, and T.A. Markow. 2007. Analysis of Drosophila species genome size and satellite DNA content reveals significant differences among strains as well as between species. *Genetics*. 177:1277–1290.

Bossing, T., G. Udolph, C.Q. Doe, and G.M. Technau. 1996. The Embryonic Central Nervous System Lineages ofDrosophila melanogaster: I. Neuroblast Lineages Derived from the Ventral Half of the Neuroectoderm. *Dev. Biol.* 179:41–64.

Boveri, T. 1887. Ueber den Antheil des Spermatozoon an der Theilung des Eies. Gesellschaft für Morphologie und Physiologie zu München.

Boveri, T. 1902. Uber mehrpolige mitosen als mittle zur analyse des zellkerns. *Verhandl Phys-med Ges NF*. 35:67–90.

De Brabander, M., G. Geuens, R. Nuydens, R. Willebrords, and J. De Mey. 1981. Taxol induces the assembly of free microtubules in living cells and blocks the organizing capacity of the centrosomes and kinetochores. *Proc. Natl. Acad. Sci. U. S. A.* 78:5608–5612.

Brand, A.H., and N. Perrimon. 1993. Targeted gene expression as a means of altering cell fates and generating dominant phenotypes. *Development*. 118:401–415.

Bridges, C.B. 1921a. PROOF OF NON-DISJUNCTION FOR THE FOURTH CHROMOSOME OF DROSOPHILA MELANOGASTER. *Science*. 53:308.

Bridges, C.B. 1921b. Genetical and Cytological Proof of Non-disjunction of the Fourth Chromosome of Drosophila Melanogaster. *Proc. Natl. Acad. Sci. U. S. A.* 7:186–192.

Bridges, C.B. 1935. SALIVARY CHROMOSOME MAPS: With a Key to the Banding of the Chromosomes of Drosophila Melanogaster. *J. Hered.* 26:60–64.

Brinkley, B.R. 2001. Managing the centrosome numbers game: from chaos to stability in cancer cell division. *Trends Cell Biol.* 11:18–21.

Brito, D.A., and C.L. Rieder. 2006. Mitotic Checkpoint Slippage in Humans Occurs via Cyclin B Destruction in the Presence of an Active Checkpoint. *Curr. Biol.* 16:1194–1200.

Broadus, J., and C.Q. Doe. 1995. Evolution of neuroblast identity: Seven-up and prospero expression reveal homologous and divergent neuroblast fates in Drosophila and Schistocerca. *Development*. 121:3989–3996.

Brody, T., and W.F. Odenwald. 2000. Programmed transformations in neuroblast gene expression during Drosophila CNS lineage development. *Dev. Biol.* 226:34–44.

Brouhard, G.J., and A.J. Hunt. 2005. Microtubule movements on the arms of mitotic chromosomes: Polar ejection forces quantified in vitro. *Proc. Natl. Acad.*

Sci. U. S. A. 102:13903 LP – 13908.

Brown, K.E., M.A. Barnett, C. Burgtorf, P. Shaw, V.J. Buckle, and W.R.A. Brown. 1994. Dissecting the centromere of the human Y chromosome with cloned telomeric DNA. *Hum. Mol. Genet.* 3:1227–1237.

De Bruin, E.C., N. McGranahan, R. Mitter, M. Salm, D.C. Wedge, L. Yates, M. Jamal-Hanjani, S. Shafi, N. Murugaesu, A.J. Rowan, E. Grönroos, M.A. Muhammad, S. Horswell, M. Gerlinger, I. Varela, D. Jones, J. Marshall, T. Voet, P. Van Loo, D.M. Rassl, R.C. Rintoul, S.M. Janes, S.M. Lee, M. Forster, T. Ahmad, D. Lawrence, M. Falzon, A. Capitanio, T.T. Harkins, C.C. Lee, W. Tom, E. Teefe, S.C. Chen, S. Begum, A. Rabinowitz, B. Phillimore, B. Spencer-Dene, G. Stamp, Z. Szallasi, N. Matthews, A. Stewart, P. Campbell, and C. Swanton. 2014. Spatial and temporal diversity in genomic instability processes defines lung cancer evolution. *Science (80-.).* 346:251–256.

Brukman, N.G., B. Uygur, B. Podbilewicz, and L. V. Chernomordik. 2019. How cells fuse. *J. Cell Biol.* 218:1436–1451.

Brunet, S., T. Sardon, T. Zimmerman, T. Wittmann, R. Pepperkok, E. Karsenti, and I. Vernos. 2004. Characterization of the TPX2 Domains Involved in Microtubule Nucleation and Spindle Assembly in Xenopus nucleation around chromatin and functions in a network of other molecules , some of which also are regulated by. *Mol Biol Cell*. 15:5318–5328.

Brust-Mascher, I., and J.M. Scholey. 2007. Mitotic Spindle Dynamics in Drosophila. *Int. Rev. Cytol.* 259:139–172.

Bryan, J., and L. Wilson. 1971. Are cytoplasmic microtubules heteropolymers? *Proc. Natl. Acad. Sci. U. S. A.* 68:1762–1766.

Burbank, K.S., T.J. Mitchison, and D.S. Fisher. 2007. Slide-and-Cluster Models for Spindle Assembly. *Curr. Biol.* 17:1373–1383.

Cabernard, C. 2012. Cytokinesis in Drosophila melanogaster. *Cytoskeleton*. 69:791–809.

Cai, H., and M. Levine. 1995. Modulation of enhancer-promoter interactions by insulators in the Drosophila embryo. *Nature*. 376:533–536.

Cai, H.N., and P. Shen. 2001. Effects of cis arrangement of chromatin insulators on enhancer-blocking activity. *Science*. 291:493–495.

Cai, X., G.D. Evrony, H.S. Lehmann, P.C. Elhosary, B.K. Mehta, A. Poduri, and C.A. Walsh. 2014. Single-cell, genome-wide sequencing identifies clonal somatic copy-number variation in the human brain. *Cell Rep*. 8:1280–1289.

Callaini, G., W.G.F. Whitfield, and M.G. Riparbelli. 1997. Centriole and centrosome dynamics during the embryonic cell cycles that follow the formation of the cellular blastoderm in Drosophila. *Exp. Cell Res.* 234:183–190.

Calvi, B.R., M.A. Lilly, and A.C. Spradling. 1998. Cell cycle control of chorion gene amplification. *Genes Dev.* 12:734–744.

Cao, J., J. Wang, C.P. Jackman, A.H. Cox, M.A. Trembley, J.J. Balowski, B.D. Cox, A. De Simone, A.L. Dickson, S. Di Talia, E.M. Small, D.P. Kiehart, N. Bursac, and K.D. Poss. 2017. Tension Creates an Endoreplication Wavefront that Leads Regeneration of Epicardial Tissue. *Dev. Cell*. 42:600-615.e4.

Carter, S.L., K. Cibulskis, E. Helman, A. McKenna, H. Shen, T. Zack, P.W. Laird, R.C. Onofrio,

W. Winckler, B.A. Weir, R. Beroukhim, D. Pellman, D.A. Levine, E.S. Lander, M. Meyerson, and G. Getz. 2012. Absolute quantification of somatic DNA alterations in human cancer. *Nat. Biotechnol.* 30:413–421.

Carvajal, L.A., and J.J. Manfredi. 2013. Another fork in the road--life or death decisions by the tumour suppressor p53. *EMBO Rep.* 14:414–421.

Castellanos, E., P. Dominguez, and C. Gonzalez. 2008. Centrosome Dysfunction in Drosophila Neural Stem Cells Causes Tumors that Are Not Due to Genome Instability. *Curr. Biol.* 18:1209–1214.

De Castro, I.P., C. Aguirre-Portolés, G. Fernández-Miranda, M. Cañamero, D.O. Cowley, T. Van Dyke, and M. Malumbres. 2013. Requirements for Aurora-A in tissue regeneration and tumor development in adult mammals. *Cancer Res.* 73:6804–6815.

Caussinus, E., and C. Gonzalez. 2005. Induction of tumor growth by altered stem-cell asymmetric division in Drosophila melanogaster. *Nat. Genet.* 37:1125–1129.

Cavalli, G., and T. Misteli. 2013. Functional implications of genome topology. *Nat. Struct. Mol. Biol.* 20:290–299.

Cesario, J., and K.S. McKim. 2011. RanGTP is required for meiotic spindle organization and the initiation of embryonic development in Drosophila. *J. Cell Sci.* 124:3797–3810.

Chan, C.S.M., and D. Botstein. 1993. Isolation and characterization of chromosome-gain and increase-in-ploidy mutants in yeast. *Genetics*. 135:677–691.

Chan, J.Y. 2011. A Clinical Overview of Centrosome Amplification in Human Cancers. *Int. J. Biol. Sci.* 7:1122–1144.

Chavali, P.L., G. Chandrasekaran, A.R. Barr, P. Tatrai, C. Taylor, E.K. Papachristou, C.G. Woods, S. Chavali, and F. Gergely. 2016. A CEP215-HSET complex links centrosomes with spindle poles and drives centrosome clustering in cancer. *Nat Commun*. 7:11005.

Chen, G., W.D. Bradford, C.W. Seidel, and R. Li. 2012. Hsp90 stress potentiates rapid cellular adaptation through induction of aneuploidy. *Nature*. 482:246–250.

Chen, J.W.C., A.R. Barker, and J.G. Wakefield. 2015. The Ran Pathway in Drosophila melanogaster Mitosis. *Front. Cell Dev. Biol.* 3.

Chia, W., W.G. Somers, and H. Wang. 2008. Drosophila neuroblast asymmetric divisions: cell cycle regulators, asymmetric protein localization, and tumorigenesis. *J Cell Biol*. 180:267–272.

Choksi, S.P., T.D. Southall, T. Bossing, K. Edoff, E. de Wit, B.E.E. Fischer, B. van Steensel, G. Micklem, and A.H. Brand. 2006. Prospero Acts as a Binary Switch between Self-Renewal and Differentiation in Drosophila Neural Stem Cells. *Dev. Cell*. 11:775–789.

Church, K., and H.P.P. Lin. 1982. Meiosis in drosophila melanogaster. II. The prometaphase-l kinetochore microtubule bundle and kinetochore orientation in males. *J. Cell Biol.* 93:365–373.

Cimini, D., B. Howell, P. Maddox, A. Khodjakov, F. Degrassi, and E.D. Salmon. 2001. Merotelic kinetochore orientation is a major mechanism of aneuploidy in mitotic mammalian tissue cells. *J. Cell Biol.* 152:517–527.

Cimini, D., B. Moree, J.C. Canman, and E.D. Salmon. 2003. Merotelic kinetochore orientation occurs frequently during early mitosis in mammalian tissue cells and error correction is

achieved by two different mechanisms. *J. Cell Sci.* 116:4213–4225.

Cleary, M.D., and C.Q. Doe. 2006. Regulation of neuroblast competence: multiple temporal identity factors specify distinct neuronal fates within a single early competence window. *Genes Dev.* 20:429–434.

Cleveland, D.W., Y. Mao, and K.F. Sullivan. 2003. Centromeres and kinetochores: from epigenetics to mitotic checkpoint signaling. *Cell*. 112:407–421.

Coelho, P.A., L. Bury, M.N. Shahbazi, K. Liakath-Ali, P.H. Tate, S. Wormald, C.J. Hindley, M. Huch, J. Archer, W.C. Skarnes, M. Zernicka-Goetz, and D.M. Glover. 2015. Over-expression of Plk4 induces centrosome amplification, loss of primary cilia and associated tissue hyperplasia in the mouse. *Open Biol.* 5:150209.

Cohen-Fix, O., J.M. Peters, M.W. Kirschner, and D. Koshland. 1996. Anaphase initiation in saccharomyces cerevisiae is controlled by the APC-dependent degradation of the anaphase inhibitor Pds1p. *Genes Dev.* 10:3081–3093.

Cole, D.G., W.M. Saxtonlll, and K.B. Sheehann. 1994. A “Slow” Homotetrameric Kinesin-related Motor Protein Purified. 22913–22916.

Coleman, R.T., and G. Struhl. 2017. Causal role for inheritance of H3K27me3 in maintaining the off state of a Drosophila HOX gene. *Science (80-.).* 356.

Colombié, N., A.A. Głuszek, A.M. Meireles, and H. Ohkura. 2013. Meiosis-Specific Stable Binding of Augmin to Acentrosomal Spindle Poles Promotes Biased Microtubule Assembly in Oocytes. *PLoS Genet.* 9.

Conduit, P.T., Z. Feng, J.H. Richens, J. Baumbach, A. Wainman, S.D. Bakshi, J. Dobbelaere, S. Johnson, S.M. Lea, and J.W. Raff. 2014a. The centrosome-specific phosphorylation of Cnn by Polo/Plk1 drives Cnn scaffold assembly and centrosome maturation. *Dev Cell*. 28:659–669.

Conduit, P.T., J.H. Richens, A. Wainman, J. Holder, C.C. Vicente, M.B. Pratt, C.I. Dix, Z.A. Novak, I.M. Dobbie, L. Schermelleh, and J.W. Raff. 2014b. A molecular mechanism of mitotic centrosome assembly in Drosophila. *Elife*. 3:1–23.

Conduit, P.T., A. Wainman, and J.W. Raff. 2015. Centrosome function and assembly in animal cells. *Nat. Rev. Mol. Cell Biol.* 16:611–624.

Conery, A.R., and E. Harlow. 2010. High-throughput screens in diploid cells identify factors that contribute to the acquisition of chromosomal instability. *Proc. Natl. Acad. Sci. U. S. A.* 107:15455–15460.

Crasta, K., N.J. Ganem, R. Dagher, A.B. Lantermann, E. V. Ivanova, Y. Pan, L. Nezi, A. Protopopov, D. Chowdhury, and D. Pellman. 2012. DNA breaks and chromosome pulverization from errors in mitosis. *Nature*. 482:53–58.

Cremer, T., M. Cremer, S. Dietzel, S. Müller, I. Solovei, and S. Fakan. 2006. Chromosome territories--a functional nuclear landscape. *Curr. Opin. Cell Biol.* 18:307–316.

Crockford, A., L.P. Zalmas, E. Grönroos, S.M. Dewhurst, N. McGranahan, M.E. Cuomo, V. Encheva, A.P. Snijders, J. Begum, S. Purewal, J. Cerveira, H. Patel, M.J. Renshaw, and C. Swanton. 2017. Cyclin D mediates tolerance of genome-doubling in cancers with functional p53. *Ann. Oncol. Off. J. Eur. Soc. Med. Oncol.* 28:149–156.

Cross, F.R. 1988. DAF1, a mutant gene affecting size control, pheromone arrest, and cell

cycle kinetics of Saccharomyces cerevisiae. *Mol. Cell. Biol.* 8:4675–4684.

Cuddihy, A.R., and M.J. O'Connell. 2003. Cell-cycle responses to DNA damage in G2. *Int. Rev. Cytol.* 222:99–140.

Cui, Y., M.K. Borysova, J.O. Johnson, and T.M. Guadagno. 2010. Oncogenic B-RafV600E induces spindle abnormalities, supernumerary centrosomes, and aneuploidy in human melanocytic cells. *Cancer Res.* 70:675–684.

D'Alessio, J.A., K.J. Wright, and R. Tjian. 2009. Shifting Players and Paradigms in Cell-Specific Transcription. *Mol. Cell*. 36:924–931.

Darlington, C.D. 1937. Recent advances in cytology. J. & A. Churchill, Ltd., London. xvi + 671 pp. pp.

David, A.F., P. Roudot, W.R. Legant, E. Betzig, G. Danuser, and D.W. Gerlich. 2019. Augmin accumulation on long-lived microtubules drives amplification and kinetochore-directed growth. *J. Cell Biol.* 218:2150–2168.

Davoli, T., E.L. Denchi, and T. de Lange. 2010. Persistent Telomere Damage Induces Bypass of Mitosis and Tetraploidy. *Cell*. 141:81–93.

Davoli, T., and T. de Lange. 2012. Telomere-Driven Tetraploidization Occurs in Human Cells Undergoing Crisis and Promotes Transformation of Mouse Cells. *Cancer Cell*. 21:765–776.

Debec, A., C. Marcaillou, Y. Bobinnec, and C. Borot. 1999. The centrosome cycle in syncytial Drosophila embryos analyzed by energy filtering transmission electron microscopy. *Biol. cell*. 91:379–391.

Dej, K.J., and A.C. Spradling. 1999. The endocycle controls nurse cell polytene chromosome structure during Drosophila oogenesis. *Development*. 126:293–303.

Dekanty, A., L. Barrio, M. Muzzopappa, H. Auer, M. Milán, M. Milan, and M. Milán. 2012. Aneuploidy-induced delaminating cells drive tumorigenesis in Drosophila epithelia. *Proc. Natl. Acad. Sci. U. S. A.* 109:20549–20554.

Delattre, M., C. Canard, and P. Gönczy. 2006. Sequential protein recruitment in C. elegans centriole formation. *Curr. Biol.* 16:1844–1849.

Delidakis, C., and F.C. Kafatos. 1987. Amplification of a chorion gene cluster in Drosophila is subject to multiple cis-regulatory elements and to long-range position effects. *J. Mol. Biol.* 197:11–26.

Denchi, E.L., G. Celli, and T. De Lange. 2006. Hepatocytes with extensive telomere deprotection and fusion remain viable and regenerate liver mass through endoreduplication. *Genes Dev.* 20:2648–2653.

Deng, Q., Q. Zeng, Y. Qian, C. Li, and Y. Yang. 2007. Research on the Karyotype and Evolution of Drosophila melanogaster Species Group. *J. Genet. Genomics*. 34:196–213.

Deng, W.M., C. Althauser, and H. Ruohola-Baker. 2001. Notch-Delta signaling induces a transition from mitotic cell cycle to endocycle in Drosophila follicle cells. *Development*. 128:4737–4746.

Denu, R.A., and M.E. Burkard. 2020. Analysis of the "centrosome-ome" identifies MCPH1 deletion as a cause of centrosome amplification in human cancer. *Sci. Rep.* 10:11921.

Dephoure, N., S. Hwang, C. O'Sullivan, S.E. Dodgson, S.P. Gygi, A. Amon, and E.M. Torres.

2014. Quantitative proteomic analysis reveals posttranslational responses to aneuploidy in yeast. *Elife*. 3:1–27.

Desai, A., and T.J. Mitchison. 1997. Microtubule polymerization dynamics. *Annu. Rev. Cell Dev. Biol.* 13:83–117.

Desalvo, M.K., N. Mayer, F. Mayer, and R.J. Bainton. 2011. Physiologic and anatomic characterization of the brain surface glia barrier of Drosophila. *Glia*. 59:1322–1340.

Dewhurst, S.M., N. McGranahan, R.A. Burrell, A.J. Rowan, E. Gronroos, D. Endesfelder, T. Joshi, D. Mouradov, P. Gibbs, R.L. Ward, N.J. Hawkins, Z. Szallasi, O.M. Sieber, C. Swanton, E. Grönroos, D. Endesfelder, T. Joshi, D. Mouradov, P. Gibbs, R.L. Ward, N.J. Hawkins, Z. Szallasi, O.M. Sieber, and C. Swanton. 2014. Tolerance of whole- genome doubling propagates chromosomal instability and accelerates cancer genome evolution. *Cancer Discov.* 4:175–185.

Díaz-Valencia, J.D., M.M. Morelli, M. Bailey, D. Zhang, D.J. Sharp, and J.L. Ross. 2011. Drosophila katanin-60 depolymerizes and severs at microtubule defects. *Biophys. J.* 100:2440–2449.

Dickson, E., J.B. Boyd, and C.D. Laird. 1971. Sequence diversity of polytene chromosome DNA from Drosophila hydei. *J. Mol. Biol.* 61:615–627.

Didion, J.P., R.J. Buus, Z. Naghashfar, D.W. Threadgill, H.C. Morse, and F.P.M. de Villena. 2014. SNP array profiling of mouse cell lines identifies their strains of origin and reveals cross-contamination and widespread aneuploidy. *BMC Genomics*. 15.

Dimitri, P., R. Caizzi, E. Giordano, M. Carmela Accardo, G. Lattanzi, and G. Biamonti. 2009. Constitutive heterochromatin: a surprising variety of expressed sequences. *Chromosoma*. 118:419–435.

Dimitri, P., N. Corradini, F. Rossi, F. Vernì, G. Cenci, G. Belloni, I.F. Zhimulev, and D.E. Koryakov. 2003. Vital genes in the heterochromatin of chromosomes 2 and 3 of Drosophila melanogaster. *Genetica*. 117:209–215.

Dinarina, A., C. Pugieux, M.M. Corral, M. Loose, J. Spatz, E. Karsenti, and F. Nedelec. 2009. Chromatin shapes the mitotic spindle. *Cell*. 138:502–513.

Dix, C.I., and J.W. Raff. 2007. Drosophila Spd-2 Recruits PCM to the Sperm Centriole, but Is Dispensable for Centriole Duplication. *Curr. Biol.* 17:1759–1764.

Dixon, J.R., I. Jung, S. Selvaraj, Y. Shen, J.E. Antosiewicz-Bourget, A.Y. Lee, Z. Ye, A. Kim, N. Rajagopal, W. Xie, Y. Diao, J. Liang, H. Zhao, V. V. Lobanenkov, J.R. Ecker, J.A. Thomson, and B. Ren. 2015. Chromatin architecture reorganization during stem cell differentiation. *Nature*. 518:331–336.

Dixon, J.R., S. Selvaraj, F. Yue, A. Kim, Y. Li, Y. Shen, M. Hu, J.S. Liu, and B. Ren. 2012. Topological domains in mammalian genomes identified by analysis of chromatin interactions. *Nature*. 485:376–380.

Dobbelaere, J., F. Josué, S. Suijkerbuijk, B. Baum, N. Tapon, and J. Raff. 2008. A genome-wide RNAi screen to dissect centriole duplication and centrosome maturation in Drosophila. *PLoS Biol.* 6:1975–1990.

Doe, C.Q. 1992. Molecular markers for identified neuroblasts and ganglion mother cells in the Drosophila central nervous system. *Development*. 116:855–863.

Doe, C.Q. 2017. Temporal patterning in the drosophila CNS. *Annu. Rev. Cell Dev. Biol.* 33:219–240.

Doe, C.Q., and G.M. Technau. 1993. Identification and cell lineage of individual neural precursors in the Drosophila CNS. *Trends Neurosci.* 16:510–514.

Donaldson, K.M., A. Lui, and G.H. Karpen. 2002. Modifiers of terminal deficiency-associated position effect variegation in Drosophila. *Genetics*. 160:995–1009.

Donne, R., M. Saroul-Aïnama, P. Cordier, S. Celton-Morizur, and C. Desdouets. 2020. Polyploidy in liver development, homeostasis and disease. *Nat. Rev. Gastroenterol. Hepatol.* 17:391–405.

Douville, C., J.D. Cohen, J. Ptak, M. Popoli, and J. Schaefer. 2020. Assessing aneuploidy with repetitive element sequencing. 117:4858–4863.

Doxsey, S., D. McCollum, and W. Theurkauf. 2005. Centrosomes in cellular regulation. *Annu. Rev. Cell Dev. Biol.* 21:411–434.

Dumont, J., S. Petri, F. Pellegrin, M.E. Terret, M.T. Bohnsack, P. Rassinier, V. Georget, P. Kalab, O.J. Gruss, and M.H. Verlhac. 2007. A centriole- and RanGTP-independent spindle assembly pathway in meiosis I of vertebrate oocytes. *J. Cell Biol.* 176:295–305.

Dumont, S., and T.J. Mitchison. 2009. Compression Regulates Mitotic Spindle Length by a Mechanochemical Switch at the Poles. *Curr. Biol.* 19:1086–1095.

Duncan, A.W. 2013. Aneuploidy, polyploidy and ploidy reversal in the liver. *Semin. Cell Dev. Biol.* 24:347–356.

Duncan, A.W., A.E. Hanlon Newell, W. Bi, M.J. Finegold, S.B. Olson, A.L. Beaudet, and M. Grompe. 2012. Aneuploidy as a mechanism for stress-induced liver adaptation. *J. Clin. Invest.* 122:3307–3315.

Duncan, A.W., M.H. Taylor, R.D. Hickey, A.E. Hanlon Newell, M.L. Lenzi, S.B. Olson, M.J. Finegold, and M. Grompe. 2010. The ploidy conveyor of mature hepatocytes as a source of genetic variation. *Nature*. 467:707–710.

Duronio, R.J., A. Brook, N. Dyson, and P.H. O'Farrell. 1996. E2F-induced S phase requires cyclin E. *Genes Dev.* 10:2505–2513.

Dyban, A.P., and V.S. Baranov. 1987. Cytogenetics of mammalian embryonic development. Clarendon Press ; Oxford University Press, Oxford; Oxford; New York.

Dzhindzhev, N.S., G. Tzolovsky, Z. Lipinszki, S. Schneider, R. Lattao, J. Fu, J. Debski, M. Dadlez, and D.M. Glover. 2014. Plk4 phosphorylates ana2 to trigger SAS6 recruitment and procentriole formation. *Curr. Biol.* 24:2526–2532.

Dzhindzhev, N.S., Q.D. Yu, K. Weiskopf, G. Tzolovsky, I. Cunha-Ferreira, M. Riparbelli, A. Rodrigues-Martins, M. Bettencourt-Dias, G. Callaini, and D.M. Glover. 2010. Asterless is a scaffold for the onset of centriole assembly. *Nature*. 467:714–718.

Earnshaw, W.C., B. Halligan, C.A. Cooke, M.M.S. Heck, and L.F. Liu. 1985. Topoisomerase II is a structural component of mitotic chromosome scaffolds. *J. Cell Biol.* 100:1706–1715.

Earnshaw, W.C., and U.K. Laemmli. 1983. Architecture of metaphase chromosomes and chromosome scaffolds. *J. Cell Biol.* 96:84–93.

Earnshaw, W.C., and N. Rothfield. 1985. Identification of a family of human centromere proteins using autoimmune sera from patients with scleroderma. *Chromosoma*.

91:313–321.

Edgar, B.A. 2006. How flies get their size: Genetics meets physiology. *Nat. Rev. Genet.* 7:907–916.

Edgar, B.A., and T.L. Orr-Weaver. 2001. Endoreplication cell cycles: More for less. *Cell*. 105:297–306.

Eggert, U.S., A.A. Kiger, C. Richter, Z.E. Perlman, N. Perrimon, T.J. Mitchison, and C.M. Field. 2004. Parallel chemical genetic and genome-wide RNAi screens identify cytokinesis inhibitors and targets. *PLoS Biol.* 2.

Elgin, S.C.R.R., and G. Reuter. 2013. Position-effect variegation, heterochromatin formation, and gene silencing in Drosophila. *Cold Spring Harb. Perspect. Biol.* 5:1–26.

Endow, S.A., R. Chandra, D.J. Komma, A.H. Yamamoto, and E.D. Salmon. 1994. Mutants of the Drosophila ncd microtubule motor protein cause centrosomal and spindle pole defects in mitosis. *J. Cell Sci.* 107:859–867.

Erclik, T., X. Li, M. Courgeon, C. Bertet, Z. Chen, R. Baumert, J. Ng, C. Koo, U. Arain, R. Behnia, A. Del Valle Rodriguez, L. Senderowicz, N. Negre, K.P. White, and C. Desplan. 2017. Integration of temporal and spatial patterning generates neural diversity. *Nature*. 541:365–370.

Estrada, J.C., Y. Torres, A. Benguría, A. Dopazo, E. Roche, L. Carrera-Quintanar, R.A. Pérez, J.A. Enríquez, R. Torres, J.C. Ramírez, E. Samper, and A. Bernad. 2013. Human mesenchymal stem cell-replicative senescence and oxidative stress are closely linked to aneuploidy. *Cell Death Dis.* 4.

Evans, T., E.T. Rosenthal, J. Youngblom, D. Distel, and T. Hunt. 1983. Cyclin: A protein specified by maternal mRNA in sea urchin eggs that is destroyed at each cleavage division. *Cell*. 33:389–396.

Faggioli, F., P. Vezzoni, and C. Montagna. 2011a. Single-cell analysis of ploidy and centrosomes underscores the peculiarity of normal hepatocytes. *PLoS One*. 6.

Faggioli, F., J. Vijg, and C. Montagna. 2011b. Chromosomal aneuploidy in the aging brain. *Mech. Ageing Dev.* 132:429–436.

Faggioli, F., T. Wang, J. Vijg, and C. Montagna. 2012. Chromosome-specific accumulation of aneuploidy in the aging mouse brain. *Hum. Mol. Genet.* 21:5246–5253.

Faktor, V.M., and I. V Uryvaeva. 1975. [Progressive polyploidy in mouse liver following repeated hepatectomy]. *Tsitologiia*. 17:909–916.

Farr, C.J., R.A.L. Bayne, D. Kipling, W. Mills, R. Critcher, and H.J. Cooke. 1995. Generation of a human X-derived minichromosome using telomere-associated chromosome fragmentation. *EMBO J.* 14:5444–5454.

Feit, H., L. Slusarek, and M.L. Shelanski. 1971. Heterogeneity of tubulin subunits. *Proc. Natl. Acad. Sci. U. S. A.* 68:2028–2031.

Field, C.M., M. Coughlin, S. Doberstein, T. Marty, and W. Sullivan. 2005. Characterization of anillin mutants reveals essential roles in septin localization and plasma membrane integrity. *Development*. 132:2849–2860.

Filion, G.J., J.G. van Bemmel, U. Braunschweig, W. Talhout, J. Kind, L.D. Ward, W. Brugman, I.J. de Castro, R.M. Kerkhoven, H.J. Bussemaker, and B. van Steensel. 2010. Systematic

Protein Location Mapping Reveals Five Principal Chromatin Types in Drosophila Cells. *Cell*. 143:212–224.

Flemming, W. 1880. Beiträge zur Kenntniss der Zelle und Ihrer Lebenserscheinungen. *Arch. für mikroskopische Anat.* 18:151–259.

Flemming, W. 1882. Zellsubstanz, Kern und Zelltheilung. Vogel, Leipzig.

Foe, V.E., and B.M. Alberts. 1985. Reversible chromosome condensation induced in Drosophila embryos by anoxia: visualization of interphase nuclear organization. *J. Cell Biol.* 100:1623–1636.

Follette, P.J., R.J. Duronio, and P.H. O'Farrell. 1998. Fluctuations in cyclin E levels are required for multiple rounds of endocycle S phase in Drosophila. *Curr. Biol.* 8:235–238.

Foster, D.A., P. Yellen, L. Xu, and M. Saqcena. 2010. Regulation of G1 cell cycle progression: Distinguishing the restriction point from a nutrient-sensing cell growth checkpoint(s). *Genes and Cancer*. 1:1124–1131.

Fox, D.T., J.G. Gall, and A.C. Spradling. 2010. Error-prone polyploid mitosis during normal Drosophila development. *Genes Dev.* 24:2294–2302.

Fox, D.T., D.E. Soltis, P.S. Soltis, T.L. Ashman, and Y. Van de Peer. 2020. Polyploidy: A Biological Force From Cells to Ecosystems. *Trends Cell Biol.* 30:688–694.

Francastel, C., D. Schübeler, D.I.K. Martin, and M. Groudine. 2000. Nuclear compartmentalization and gene activity. *Nat. Rev. Mol. Cell Biol.* 1:137–143.

Francis, N.J., and R.E. Kingston. 2001. Mechanisms of transcriptional memory. *Nat. Rev. Mol. Cell Biol.* 2:409–421.

Frawley, L.E., and T.L. Orr-Weaver. 2015. Polyploidy. *Curr. Biol.* 25:R353–R358.

Frenette, P., E. Haines, M. Loloyan, M. Kinal, P. Pakarian, and A. Piekny. 2012. An anillin-ect2 complex stabilizes central spindle microtubules at the cortex during cytokinesis. *PLoS One*. 7.

Friedrich, T., L. Faivre, I. Bäurle, and D. Schubert. 2019. Chromatin-based mechanisms of temperature memory in plants. 42.

Fu, J., and D.M. Glover. 2012. Structured illumination of the interface between centriole and peri-centriolar material. *Open Biol.* 2.

Fu, J., I.M. Hagan, and D.M. Glover. 2015. The Centrosome and Its Duplication Cycle. *Cold Spring Harb. Perspect. Biol.* 7.

Fu, J., Z. Lipinszki, H. Rangone, M. Min, C. Mykura, J. Chao-chu, S. Schneider, N.S. Dzhindzhev, M. Gottardo, G. Riparbelli, G. Callaini, and D.M. Glover. 2016. Conserved Molecular Interactions in Centriole-to-Centrosome Conversion. 18:87–99.

Fujiwara, T., M. Bandi, M. Nitta, E. V. Ivanova, R.T. Bronson, and D. Pellman. 2005. Cytokinesis failure generating tetraploids promotes tumorigenesis in p53-null cells. *Nature*. 437:1043–1047.

Gaetz, J., and T.M. Kapoor. 2004. Dynein/dynactin regulate metaphase spindle length by targeting depolymerizing activities to spindle poles. *J. Cell Biol.* 166:465–471.

Gall, J.G., E.H. Cohen, and M.L. Polan. 1971. Reptitive DNA sequences in drosophila. *Chromosoma*. 33:319–344.

Gandarillas, A., D. Davies, and J.M. Blanchard. 2000. Normal and c-Myc-promoted human keratinocyte differentiation both occur via a novel cell cycle involving cellular growth and endoreplication. *Oncogene*. 19:3278–3289.

Gandarillas, A., and A. Freije. 2014. Cycling up the epidermis: reconciling 100 years of debate. *Exp. Dermatol.* 23:87–91.

Ganem, N.J., H. Cornils, S.Y. Chiu, K.P. O'Rourke, J. Arnaud, D. Yimlamai, M. Théry, F.D. Camargo, and D. Pellman. 2014. Cytokinesis failure triggers hippo tumor suppressor pathway activation. *Cell*. 158:833–848.

Ganem, N.J., S.A. Godinho, and D. Pellman. 2009. A mechanism linking extra centrosomes to chromosomal instability. *Nature*. 460:278–282.

Ganem, N.J., and D. Pellman. 2007. Limiting the Proliferation of Polyploid Cells. *Cell*. 131:437–440.

Ganem, N.J., Z. Storchova, and D. Pellman. 2007. Tetraploidy, aneuploidy and cancer. *Curr Opin Genet Dev*. 17:157–162.

Gaspar-Maia, A., A. Alajem, E. Meshorer, and M. Ramalho-Santos. 2011. Open chromatin in pluripotency and reprogramming. *Nat. Rev. Mol. Cell Biol.* 12:36–47.

Gates, R.R. 1908. THE CHROMOSOMES OF OEligNOTHERA. *Science*. 27:193–195.

Gatti, M., and B.S. Baker. 1989. Genes controlling essential cell-cycle functions in Drosophila melanogaster. *Genes Dev.* 3:438–453.

Gatti, M., S. Bonaccorsi, and S. Pimpinelli. 1994. Looking at Drosophila Mitotic Chromosomes. *Methods Cell Biol.* 44:371–391.

Geigl, J.B., A.C. Obenauf, T. Schwarzbraun, and M.R. Speicher. 2008. Defining "chromosomal instability." *Trends Genet.* 24:64–69.

Gemble, S., and R. Basto. 2020. CHRONOCRISIS: When Cell Cycle Asynchrony Generates DNA Damage in Polyploid Cells. *BioEssays*. 42:1–12.

Gemble, S., A. Simon, C. Pennetier, M. Dumont, S. Hervé, F. Meitinger, K. Oegema, R. Rodriguez, G. Almouzni, D. Fachinetti, and R. Basto. 2019. Centromere Dysfunction Compromises Mitotic Spindle Pole Integrity. *Curr. Biol.* 29:3072-3080.e5.

Gentric, G., and C. Desdouets. 2014. Polyploidization in liver tissue. *Am. J. Pathol.* 184:322–331.

Gerlinger, M., A.J. Rowan, S. Horswell, J. Larkin, D. Endesfelder, E. Gronroos, P. Martinez, N. Matthews, A. Stewart, P. Tarpey, I. Varela, B. Phillimore, S. Begum, N.Q. McDonald, A. Butler, D. Jones, K. Raine, C. Latimer, C.R. Santos, M. Nohadani, A.C. Eklund, B. Spencer-Dene, G. Clark, L. Pickering, G. Stamp, M. Gore, Z. Szallasi, J. Downward, P.A. Futreal, and C. Swanton. 2012. Intratumor Heterogeneity and Branched Evolution Revealed by Multiregion Sequencing. *N. Engl. J. Med.* 366:883–892.

Gerlyng, P., A. Åbyholm, T. Grotmol, B. Erikstein, H.S. Huitfeldt, T. Stokke, and P.O. Seglen. 1993. Binucleation and polyploidization patterns in developmental and regenerative rat liver growth. *Cell Prolif.* 26:557–565.

Gervais, L., M. van den Beek, M. Josserand, J. Sallé, M. Stefanutti, C.N. Perdigoto, P. Skorski, K. Mazouni, O.J. Marshall, A.H. Brand, F. Schweisguth, and A.J. Bardin. 2019. Stem Cell Proliferation Is Kept in Check by the Chromatin Regulators Kismet/CHD7/CHD8 and

Trr/MLL3/4. *Dev. Cell*. 49:556-573.e6.

Geyer, P.K., and V.G. Corces. 1992. DNA position-specific repression of transcription by a Drosophila zinc finger protein. *Genes Dev.* 6:1865–1873.

Giansanti, M.G., E. Bucciarelli, S. Bonaccorsi, and M. Gatti. 2008. Drosophila SPD-2 Is an Essential Centriole Component Required for PCM Recruitment and Astral-Microtubule Nucleation. *Curr. Biol.* 18:303–309.

Giansanti, M.G., M. Gatti, and S. Bonaccorsi. 2001. The role of centrosomes and astral microtubules during asymmetric division of Drosophila neuroblasts. *Development*. 128:1137–1145.

Giehl, M., A. Fabarius, O. Frank, A. Hochhaus, M. Hafner, R. Hehlmann, and W. Seifarth. 2005. Centrosome aberrations in chronic myeloid leukemia correlate with stage of disease and chromosomal instability. *Leukemia*. 19:1192–1197.

Giet, R., and D.M. Glover. 2001. Drosophila aurora B kinase is required for histone H3 phosphorylation and condensin recruitment during chromosome condensation and to organize the central spindle during cytokinesis. *J. Cell Biol.* 152:669–681.

Giono, L.E., and J.J. Manfredi. 2006. The p53 tumor suppressor participates in multiple cell cycle checkpoints. *J. Cell. Physiol.* 209:13–20.

Girard, F., U. Strausfeld, A. Fernandez, and N.J.C. Lamb. 1991. Cyclin a is required for the onset of DNA replication in mammalian fibroblasts. *Cell*. 67:1169–1179.

Glotzer, M. 2009. The 3Ms of central spindle assembly: microtubules, motors and MAPs. *Nat. Rev. Mol. Cell Biol.* 10:9–20.

Glotzer, M., A.W. Murray, and M.W. Kirschner. 1991. Cyclin is degraded by the ubiquitin pathway. *Nature*. 349:132–138.

Godinho, S.A., M. Kwon, and D. Pellman. 2009. Centrosomes and cancer: how cancer cells divide with too many centrosomes. *Cancer Metastasis Rev.* 28:85–98.

Godinho, S.A., R. Picone, M. Burute, R. Dagher, Y. Su, C.T. Leung, K. Polyak, J.S. Brugge, M. Théry, and D. Pellman. 2014. Oncogene-like induction of cellular invasion from centrosome amplification. *Nature*. 510:167–171.

Gogendeau, D., K. Siudeja, D. Gambarotto, C. Pennetier, A.J. Bardin, and R. Basto. 2015. Aneuploidy causes premature differentiation of neural and intestinal stem cells. *Nat Commun*. 6:8894.

Goldstein, A.Y.N., Y.N. Jan, and L. Luo. 2005. Function and regulation of Tumbleweed (RacGAP50C) in neuroblast proliferation and neuronal morphogenesis. *Proc. Natl. Acad. Sci. U. S. A.* 102:3834–3839.

Gönczy, P. 2008. Mechanisms of asymmetric cell division: Flies and worms pave the way. *Nat. Rev. Mol. Cell Biol.* 9:355–366.

Gönczy, P. 2012. Towards a molecular architecture of centriole assembly. *Nat. Rev. Mol. Cell Biol.* 13:425–435.

Gönczy, P., S. Pichler, M. Kirkham, and A.A. Hyman. 1999. Cytoplasmic dynein is required for distinct aspects of MTOC positioning, including centrosome separation, in the one cell stage Caenorhabditis elegans embryo. *J. Cell Biol.* 147:135–150.

Gonzalez, C. 2007. Spindle orientation, asymmetric division and tumour suppression in

Drosophila stem cells. *Nat. Rev. Genet.* 8:462–472.

Goshima, G., M. Mayer, N. Zhang, N. Stuurman, and R.D. Vale. 2008. Augmin: A protein complex required for centrosome-independent microtubule generation within the spindle. *J. Cell Biol.* 181:421–429.

Goshima, G., F. Nédélec, and R.D. Vale. 2005. Mechanisms for focusing mitotic spindle poles by minus end-directed motor proteins. *J. Cell Biol.* 171:229–240.

Goshima, G., R. Wollman, S.S. Goodwin, N. Zhang, J.M. Scholey, R.D. Vale, and N. Stuurman. 2007. Genes required for mitotic spindle assembly in Drosophila S2 cells. *Science (80-.).* 316:417–421.

Gottardo, M., G. Callaini, and M.G. Riparbelli. 2015. The Drosophila centriole – conversion of doublets into triplets within the stem cell niche. *J. Cell Sci.* 128:2437–2442.

Goupil, A., M. Nano, G. Letort, S. Gemble, F. Edwards, O. Goundiam, D. Gogendeau, C. Pennetier, and R. Basto. 2020a. Chromosomes function as a barrier to mitotic spindle bipolarity in polyploid cells. *J. Cell Biol.* 219.

Goupil, A., C. Pennetier, A. Simon, P. Skorski, A. Bardin, and R. Basto. 2020b. Drosophila neural stem cells show a unique dynamic pattern of gene expression that is influenced by environmental factors. *bioRxiv*. 2020.12.04.411991.

Graser, S., Y.D. Stierhof, S.B. Lavoie, O.S. Gassner, S. Lamla, M. Le Clech, and E.A. Nigg. 2007. Cep164, a novel centriole appendage protein required for primary cilium formation. *J. Cell Biol.* 179:321–330.

Gregan, J., S. Polakova, L. Zhang, I.M. Tolić-Nørrelykke, and D. Cimini. 2011. Merotelic kinetochore attachment: Causes and effects. *Trends Cell Biol.* 21:374–381.

Le Gros, M.A., E.J. Clowney, A. Magklara, A. Yen, E. Markenscoff-Papadimitriou, B. Colquitt, M. Myllys, M. Kellis, S. Lomvardas, and C.A. Larabell. 2016. Soft X-Ray Tomography Reveals Gradual Chromatin Compaction and Reorganization during Neurogenesis In Vivo. *Cell Rep.* 17:2125–2136.

Grosskortenhaus, R., B.J. Pearson, A. Marusich, and C.Q. Doe. 2005. Regulation of temporal identity transitions in drosophila neuroblasts. *Dev. Cell*. 8:193–202.

Grosskortenhaus, R., K.J. Robinson, and C.Q. Doe. 2006. Pdm and Castor specify late-born motor neuron identity in the NB7-1 lineage. *Genes Dev.* 20:2618–2627.

Gruss, O.J., R.E. Carazo-Salas, C.A. Schatz, G. Guarguaglini, J. Kast, M. Wilm, N. Le Bot, I. Vernos, E. Karsenti, and I.W. Mattaj. 2001. Ran induces spindle assembly by reversing the inhibitory effect of importin alpha on TPX2 activity. *Cell*. 104:83–93.

Gruss, O.J., M. Wittmann, H. Yokoyama, R. Pepperkok, T. Kufer, H. Silljé, E. karsenti, I.W. Mattaj, I. Vernos, H. Sillje, E. karsenti, I.W. Mattaj, and I. Vernos. 2002. Chromosome-induced microtubule assembly mediated by TPX2 is required for spindle formation in HeLa cells. *Nat. Cell Biol.* 4:871–879.

Guo, H., M. Gao, J. Ma, T. Xiao, L. Zhao, Y. Gao, and Q. Pan. 2007. Analysis of the cellular centrosome in fine-needle aspirations of the breast. *Breast Cancer Res.* 9:R48.

Guo, Z., S. Kozlov, M.F. Lavin, M.D. Person, and T.T. Paull. 2010. ATM activation by oxidative stress. *Science*. 330:517–521.

Guse, A., M. Mishima, and M. Glotzer. 2005. Phosphorylation of ZEN-4/MKLP1 by aurora B

regulates completion of cytokinesis. *Curr. Biol.* 15:778–786.

Haase, J., M.K. Bonner, H. Halas, and A.E. Kelly. 2017. Distinct Roles of the Chromosomal Passenger Complex in the Detection of and Response to Errors in Kinetochore-Microtubule Attachment. *Dev. Cell*. 42:640-654.e5.

Habedanck, R., Y.-D. Stierhof, C.J. Wilkinson, and E.A. Nigg. 2005. The Polo kinase Plk4 functions in centriole duplication. *Nat. Cell Biol.* 7:1140–1146.

Haering, C.H., A.M. Farcas, P. Arumugam, J. Metson, and K. Nasmyth. 2008. The cohesin ring concatenates sister DNA molecules. *Nature*. 454:297–301.

Haering, C.H., J. Löwe, A. Hochwagen, and K. Nasmyth. 2002. Molecular Architecture of SMC Proteins and the Yeast Cohesin Complex C-terminal domains forming a head would be part of. *Mol. Cell*. 9:773–788.

Hagstrom, K.A., V.F. Holmes, N.R. Cozzarelli, and B.J. Meyer. 2002. C. elegans condensin promotes mitotic chromosome architecture, centromere organization, and sister chromatid segregation during mitosis and meiosis. *Genes Dev.* 16:729–742.

Hammond, M.P., and C.D. Laird. 1985. Control of DNA replication and spatial distribution of defined DNA sequences in salivary gland cells of Drosophila melanogaster. *Chromosoma*. 91:279–286.

Hancock, V., J.F. Martin, and R. Lelchuk. 1993. The relationship between human megakaryocyte nuclear DNA content and gene expression. *Br. J. Haematol.* 85:692–697.

Hannak, E., K. Oegema, M. Kirkham, P. Gönczy, B. Habermann, and A.A. Hyman. 2002. The kinetically dominant assembly pathway for centrosomal asters in Caenorhabditis elegans is γ-tubulin dependent. *J. Cell Biol.* 157:591–602.

Hansemann, D. 1897. Die mikroskopische Diagnose der bösartigen Geschwülste. August Hirshwald.

Harris, H., and T. Boveri. 2008. Concerning the origin of malignant tumours by Theodor Boveri. Translated and annotated by Henry Harris. Preface. *J Cell Sci*. 121 Suppl:v–vi.

Harris, P. 1961. Electron microscope study of mitosis in sea urchin blastomeres. *J. Biophys. Biochem. Cytol.* 11:419–431.

Hartmann-Goldstein, I.J. 1967. On the relationship between heterochromatization and variegation in Drosophila, with special reference to temperature sensitive periods. *Genet. Res.* 10:143–159.

Hartwell, L.H., and T.A. Weinert. 1989. Checkpoints: Controls that ensure the order of cell cycle events. *Science (80-.).* 246:629–634.

Hassel, C., B. Zhang, M. Dixon, and B.R. Calvi. 2014. Induction of endocycles represses apoptosis independently of differentiation and predisposes cells to genome instability. *Dev.* 141:112–123.

Hatan, M., V. Shinder, D. Israeli, F. Schnorrer, and T. Volk. 2011. The Drosophila blood brain barrier is maintained by GPCR-dependent dynamic actin structures. *J. Cell Biol.* 192:307–319.

Hayashi, H., K. Kimura, and A. Kimura. 2012. Localized accumulation of tubulin during semi-open mitosis in the Caenorhabditis elegans embryo. *Mol. Biol. Cell*. 23:1688–1699.

Hayden, J.H., S.S. Bowser, and C.L. Rieder. 1990. Kinetochores capture astral microtubules

during chromosome attachment to the mitotic spindle: direct visualization in live newt lung cells. *J. Cell Biol.* 111:1039–1045.

Hayward, D., J. Metz, C. Pellacani, and J.G. Wakefield. 2014. Synergy between multiple microtubule-generating pathways confers robustness to centrosome-driven mitotic spindle formation. *Dev Cell*. 28:81–93.

Hayward, D., and J.G. Wakefield. 2014. Chromatin-mediated microtubule nucleation in Drosophila syncytial embryos. *Commun. Integr. Biol.* 7:e28512.

Heald, R., and A. Khodjakov. 2015. Thirty years of search and capture: The complex simplicity of mitotic spindle assembly. *J. Cell Biol.* 211:1103–1111.

Heald, R., R. Tournebize, T. Blank, R. Sandaltzopoulos, P. Becker, A. Hyman, and E. Karsenti. 1996. Self-organization of microtubules into bipolar spindles around artificial chromosomes in Xenopus egg extracts. *Nature*. 382:420–425.

Helenius, J., G. Brouhard, Y. Kalaidzidis, S. Diez, and J. Howard. 2006. The depolymerizing kinesin MCAK uses lattice diffusion to rapidly target microtubule ends. *Nature*. 441:115–119.

Helming, L., and S. Gordon. 2009. Molecular mediators of macrophage fusion. *Trends Cell Biol.* 19:514–522.

Helmke, K.J., R. Heald, and J.D. Wilbur. 2013. Interplay between spindle architecture and function. 306. 1st ed. Elsevier Inc. 83–125 pp.

Hernández-Vega, A., M. Braun, L. Scharrel, M. Jahnel, S. Wegmann, B.T. Hyman, S. Alberti, S. Diez, and A.A. Hyman. 2017. Local Nucleation of Microtubule Bundles through Tubulin Concentration into a Condensed Tau Phase. *Cell Rep.* 20:2304–2312.

Hernando, E., Z. Nahlé, G. Juan, E. Diaz-Rodriguez, M. Alaminos, M. Hemann, L. Michel, V. Mittal, W. Gerald, R. Benezra, S.W. Lowe, and C. Cordon-Cardo. 2004. Rb inactivation promotes genomic instability by uncoupling cell cycle progression from mitotic control. *Nature*. 430:797–802.

Hime, G., and R. Saint. 1992. Zygotic expression of the pebble locus is required for cytokineses during the postblastoderm mitoses of Drosophila. *Development*. 114:165–171.

Hinchcliffe, E.H., C.A. Day, K.B. Karanjeet, S. Fadness, A. Langfald, K.T. Vaughan, and Z. Dong. 2016. Chromosome missegregation during anaphase triggers p53 cell cycle arrest through histone H3.3 Ser31 phosphorylation. *Nat. Cell Biol.* 18:668–675.

Hirano, T., R. Kobayashi, and M. Hirano. 1997. Condensins, Chromosome Condensation Protein Complexes Containing XCAP-C, XCAP-E and a Xenopus Homolog of the Drosophila Barren Protein. *Cell*. 89:511–521.

Hirano, T., and T.J. Mitchison. 1991. Cell cycle control of higher-order chromatin assembly around naked DNA in vitro. *J. Cell Biol.* 115:1479–1489.

Hirano, T., and T.J. Mitchison. 1994. A heterodimeric coiled-coil protein required for mitotic chromosome condensation in vitro. *Cell*. 79:449–458.

Hochegger, H., S. Takeda, and T. Hunt. 2008. Cyclin-dependent kinases and cell-cycle transitions: Does one fit all? *Nat. Rev. Mol. Cell Biol.* 9:910–916.

van Holde, K.E. 1989. The Proteins of Chromatin. I. Histones BT - Chromatin. K.E. van Holde,

editor. Springer New York, New York, NY. 69–180.

Holdridge, C., and D. Dorsett. 1991. Repression of hsp70 heat shock gene transcription by the suppressor of hairy-wing protein of Drosophila melanogaster. *Mol. Cell. Biol.* 11:1894–1900.

Holguera, I., and C. Desplan. 2018. Neuronal specification in space and time. *Science (80-.).* 362:176–180.

Holland, A.J., and D.W. Cleveland. 2012. Losing balance: The origin and impact of aneuploidy in cancer. *EMBO Rep.* 13:501–514.

Holloway, S.L., M. Glotzer, R.W. King, and A.W. Murray. 1993. Anaphase is initiated by proteolysis rather than by the inactivation of maturation-promoting factor. *Cell*. 73:1393–1402.

Holy, T.E., and S. Leibler. 1994. Dynamic instability of microtubules as an efficient way to search in space. *Proc. Natl. Acad. Sci. U. S. A.* 91:5682–5685.

Homem, C.C.F.F., and J.A. Knoblich. 2012. Drosophila neuroblasts: a model for stem cell biology. *Development*. 139:4297–4310.

Hori, T., and T. Fukagawa. 2012. Establishment of the vertebrate kinetochores. *Chromosom. Res.* 20:547–561.

Horvitz, H.R., and I. Herskowitz. 1992. Mechanisms of asymmetric cell division: Two Bs or not two Bs, that is the question. *Cell*. 68:237–255.

Hou, C., L. Li, Z.S. Qin, and V.G. Corces. 2012. Gene Density, Transcription, and Insulators Contribute to the Partition of the Drosophila Genome into Physical Domains. *Mol. Cell*. 48:471–484.

Howard, A., and S.. Pelc. 1953. Synthesis of deoxyribonucleic acid in normal and irradiated ceils and its relation to chromosome breakage. *Hered. Suppl*. 6:261–273.

Hoyt, M.A., L. Totis, and B.T. Roberts. 1991. S. cerevisiae genes required for cell cycle arrest in response to loss of microtubule function. *Cell*. 66:507–517.

Hsu, L.-C., M. Kapali, J.A. DeLoia, and H.H. Gallion. 2005. Centrosome abnormalities in ovarian cancer. *Int. J. Cancer*. 113:746–751.

Hudson, D.F., P. Vagnarelli, R. Gassmann, and W.C. Earnshaw. 2003. Condensin is required for nonhistone protein assembly and structural integrity of vertebrate mitotic chromosomes. *Dev. Cell*. 5:323–336.

Hunter, A.W., M. Caplow, D.L. Coy, W.O. Hancock, S. Diez, L. Wordeman, and J. Howard. 2003. The kinesin-related protein MCAK is a microtubule depolymerase that forms an ATP-hydrolyzing complex at microtubule ends. *Mol. Cell*. 11:445–457.

Ichijima, Y., K.I. Yoshioka, Y. Yoshioka, K. Shinohe, H. Fujimori, J. Unno, M. Takagi, H. Goto, M. Inagaki, S. Mizutani, and H. Teraoka. 2010. DNA lesions induced by replication stress trigger mitotic aberration and tetraploidy development. *PLoS One*. 5:1–10.

Ingham, P.W., and A. Martinez Arias. 1992. Boundaries and fields in early embryos. *Cell*. 68:221–235.

Inoué, S. 1953. [Polarization optical studies of the mitotic spindle. I. The demonstration of spindle fibers in living cells]. *Chromosoma*. 5:487–500.

Insolera, R., H. Bazzi, W. Shao, K. V Anderson, and S.-H. Shi. 2014. Cortical neurogenesis in the absence of centrioles. *Nat. Neurosci.* 17:1528–1535.

Iourov, I.Y., S.G. Vorsanova, T. Liehr, and Y.B. Yurov. 2009. Aneuploidy in the normal, Alzheimer's disease and ataxia-telangiectasia brain: Differential expression and pathological meaning. *Neurobiol. Dis.* 34:212–220.

Isshiki, T., B. Pearson, S. Holbrook, and C.Q. Doe. 2001. Drosophila neuroblasts sequentially express transcription factors which specify the temporal identity of their neuronal progeny. *Cell*. 106:511–521.

Ito, K., W. Awano, K. Suzuki, Y. Hiromi, and D. Yamamoto. 1997. The Drosophila mushroom body is a quadruple structure of clonal units each of which contains a virtually identical set of neurones and glial cells. *Development*. 124:761–771.

Ivanov, D., and K. Nasmyth. 2007. A Physical Assay for Sister Chromatid Cohesion In Vitro. *Mol. Cell*. 27:300–310.

Jacobs, P.A., W.M. Court Brown, and R. Doll. 1961. Distribution of Human Chromosome Counts in Relation to Age. *Nature*. 191:1178–1180.

Janssen, A., M. Van Der Burg, K. Szuhai, G.J.P.L. Kops, and R.H. Medema. 2011. Chromosome segregation errors as a cause of DNA damage and structural chromosome aberrations. *Science (80-.).* 333:1895–1898.

Januschke, J., and C. Gonzalez. 2008. Drosophila asymmetric division, polarity and cancer. *Oncogene*. 27:6994–7002.

Januschke, J., S. Llamazares, J. Reina, and C. Gonzalez. 2011. Drosophila neuroblasts retain the daughter centrosome. *Nat. Commun.* 2.

Jeganathan, K., L. Malureanu, D.J. Baker, S.C. Abraham, and J.M. Van Deursen. 2007. Bub1 mediates cell death in response to chromosome missegregation and acts to suppress spontaneous tumorigenesis. *J. Cell Biol.* 179:255–267.

Jensen, C.G., and M. Watson. 1999. Inhibition of cytokinesis by asbestos and synthetic fibres. *Cell Biol. Int.* 23:829–840.

Jia, C.-W., L. Wang, Y.-L. Lan, R. Song, L.-Y. Zhou, L. Yu, Y. Yang, Y. Liang, Y. Li, Y.-M. Ma, and S.-Y. Wang. 2015. Aneuploidy in Early Miscarriage and its Related Factors. *Chin. Med. J. (Engl).* 128.

Jiang, H., A. Tian, and J. Jiang. 2016. Intestinal stem cell response to injury: lessons from Drosophila. *Cell. Mol. Life Sci.* 73:3337–3349.

Jiang, K., S. Hua, R. Mohan, I. Grigoriev, K.W. Yau, Q. Liu, E.A. Katrukha, A.F.M. Altelaar, A.J.R. Heck, C.C. Hoogenraad, and A. Akhmanova. 2014. Microtubule Minus-End Stabilization by Polymerization-Driven CAMSAP Deposition. *Dev. Cell*. 28:295–309.

Johnson, R.T., and P.N. Rao. 1970. Mammalian Cell Fusion : Induction of Premature Chromosome Condensation in Interphase Nuclei. *Nature*. 226:717–722.

Jones, K.T. 2008. Meiosis in oocytes: Predisposition to aneuploidy and its increased incidence with age. *Hum. Reprod. Update*. 14:143–158.

Jordan, K.C., V. Schaeffer, K.A. Fischer, E.E. Gray, and H. Ruohola-Baker. 2006. Notch signaling through Tramtrack bypasses the mitosis promoting activity of the JNK pathway in the mitotic-to-endocycle transition of Drosophila follicle cells. *BMC Dev. Biol.* 6:1–12.

Joshi, H.C., M.J. Palacios, L. Mcnamara, and D.W. Cleveland. 1992. Γ-Tubulin is a centrosomal. 356:9–12.

Joyce, E.F., B.R. Williams, T. Xie, C.-T. ting Wu, R.S. Hawley, E.F. Joyce, B.R. Williams, T. Xie, and C.-T. ting Wu. 2012. Identification of Genes That Promote or Antagonize Somatic Homolog Pairing Using a High-Throughput FISH–Based Screen. *PLoS Genet.* 8:e1002667.

Kaláb, P., A. Pralle, E.Y. Isacoff, R. Heald, and K. Weis. 2006. Analysis of a RanGTP-regulated gradient in mitotic somatic cells. *Nature*. 440:697–701.

Kalab, P., R.T. Pu, and M. Dasso. 1999. The Ran GTPase regulates mitotic spindle assembly. *Curr. Biol.* 9:481–484.

Kalab, P., K. Weis, and R. Heald. 2002. Visualization of a Ran-GTP gradient in interphase and mitotic Xenopus egg extracts. *Science (80-.).* 295:2452–2456.

Kamasaki, T., E. O'Toole, S. Kita, M. Osumi, J. Usukura, J.R. McIntosh, and G. Goshima. 2013. Augmin-dependent microtubule nucleation at microtubule walls in the spindle. *J. Cell Biol.* 202:25–33.

Kambadur, R., K. Koizumi, C. Stivers, J. Nagle, S.J. Poole, and W.F. Odenwald. 1998. Regulation of POU genes by castor and hunchback establishes layered compartments in the Drosophila CNS. *Genes Dev.* 12:246–260.

Kaneko, Y., and A.G. Knudson. 2000. Mechanism and relevance of ploidy in neuroblastoma. *Genes Chromosom. Cancer*. 29:89–95.

Kaplan, W.D. 1953. The Influence of Minutes upon Somatic Crossing over in Drosophila Melanogaster. *Genetics*. 38:630–651.

Karabay, A., and R.A. Walker. 1999. The Ncd tail domain promotes microtubule assembly and stability. *Biochem. Biophys. Res. Commun.* 258:39–43.

Karess, R.E., X.J. Chang, K.A. Edwards, S. Kulkarni, I. Aguilera, and D.P. Kiehart. 1991. The regulatory light chain of nonmuscle myosin is encoded by spaghetti-squash, a gene required for cytokinesis in Drosophila. *Cell*. 65:1177–1189.

Karsenti, E., J. Newport, and M. Kirschner. 1984. Respective roles of centrosomes and chromatin in the conversion of microtubule arrays from interphase to metaphase. *J. Cell Biol.* 99.

Katayama, H., K. Sasai, M. Kloc, B.R. Brinkley, and S. Sen. 2008. Aurora kinase-A regulates kinetochore/chromatin associated microtubule assembly in human cells. *Cell Cycle*. 7:2691–2704.

Kaufman, T.C. 2017. A Short History and Description of Drosophila melanogaster Classical Genetics: Chromosome Aberrations, Forward Genetic Screens, and the Nature of Mutations. *Genetics*. 206:665–689.

Kaushal, D., J.J.A. Contos, K. Treuner, A.H. Yang, M.A. Kingsbury, S.K. Rehen, M.J. Mcconnell, M. Okabe, C. Barlow, and J. Chun. 2003. Alteration of Gene Expression by Chromosome Loss in the Postnatal Mouse Brain. 23:5599–5606.

Kaya, A., M. V. Gerashchenko, I. Seim, J. Labarre, M.B. Toledano, and V.N. Gladyshev. 2015. Adaptive aneuploidy protects against thiol peroxidase deficiency by increasing respiration via key mitochondrial proteins. *Proc. Natl. Acad. Sci. U. S. A.* 112:10685–10690.

Kellum, R., and P. Schedl. 1991. A position-effect assay for boundaries of higher order chromosomal domains. *Cell*. 64:941–950.

Kellum, R., and P. Schedl. 1992. A group of scs elements function as domain boundaries in an enhancer-blocking assay. *Mol. Cell. Biol.* 12:2424–2431.

Khodjakov, A., R.W. Cole, B.R. Oakley, and C.L. Rieder. 2000. Centrosome-independent mitotic spindle formation in vertebrates. *Curr. Biol.* 10:59–67.

Khodjakov, A., L. Copenagle, M.B. Gordon, D.A. Compton, and T.M. Kapoor. 2003. Minus-end capture of preformed kinetochore fibers contributes to spindle morphogenesis. *J. Cell Biol.* 160:671–683.

Khodjakov, A., and C.L. Rieder. 1999. The sudden recruitment of gamma-tubulin to the centrosome at the onset of mitosis and its dynamic exchange throughout the cell cycle, do not require microtubules. *J. Cell Biol.* 146:585–596.

Killander, D., and A. Zetterberg. 1965. A quantitative cytochemical investigation of the relationship between cell mass and initiation of DNA synthesis in mouse fibroblasts in vitro. *Exp. Cell Res.* 40:12–20.

Kim, H., J.M. Johnson, R.F. Lera, S. Brahma, and M.E. Burkard. 2017. Anillin Phosphorylation Controls Timely Membrane Association and Successful Cytokinesis. *PLoS Genet.* 13:1–20.

Kim, J., J. Kang, and C.S.M. Chan. 1999. Chromosome Segregation in Saccharomyces cerevisiae. 145:1381–1394.

King, R.W., P.K. Jackson, and M.W. Kirschner. 1994. Mitosis in Transition Review. *Cell*. 79:563–571.

Kingsbury, M.A., B. Friedman, M.J. McConnell, S.K. Rehen, A.H. Yang, D. Kaushal, and J. Chun. 2005. Aneuploid neurons are functionally active and integrated into brain circuitry. *Proc. Natl. Acad. Sci. U. S. A.* 102:6143–6147.

Kirschner, M., and T. Mitchison. 1986. Beyond self-assembly: From microtubules to morphogenesis. *Cell*. 45:329–342.

Kitamura, E., K. Tanaka, S. Komoto, Y. Kitamura, C. Antony, and T.U. Tanaka. 2010. Kinetochores Generate Microtubules with Distal Plus Ends: Their Roles and Limited Lifetime in Mitosis. *Dev. Cell*. 18:248–259.

Kleylein-Sohn, J., B. Pöllinger, M. Ohmer, F. Hofmann, E.A. Nigg, B.A. Hemmings, and M. Wartmann. 2012. Acentrosomal spindle organization renders cancer cells dependent on the kinesin HSET. *J. Cell Sci.* 125:5391–5402.

Knoblich, J.A. 2008. Mechanisms of Asymmetric Stem Cell Division. *Cell*. 132:583–597.

Knouse, K.A., K.E. Lopez, M. Bachofner, and A. Amon. 2018. Chromosome Segregation Fidelity in Epithelia Requires Tissue Architecture. *Cell*. 175:200-211.e13.

Knouse, K.A., J. Wu, C.A. Whittaker, and A. Amon. 2014. Single cell sequencing reveals low levels of aneuploidy across mammalian tissues. *Proc Natl Acad Sci U S A*. 111:13409–13414.

Knowlton, A.L., W. Lan, and P.T. Stukenberg. 2006. Aurora B Is Enriched at Merotelic Attachment Sites, Where It Regulates MCAK. *Curr. Biol.* 16:1705–1710.

Koffa, M.D., C.M. Casanova, R. Santarella, T. Köcher, M. Wilm, and I.W. Mattaj. 2006. HURP

is part of a Ran-dependent complex involved in spindle formation. *Curr. Biol.* 16:743–754.

Kornberg, R.D. 1974. Chromatin Structure: A Repeating Unit of Histones and DNA. *Science (80-.).* 184:868 LP – 871.

Krämer, A., K. Neben, and A.D. Ho. 2005. Centrosome aberrations in hematological malignancies. *Cell Biol. Int.* 29:375–383.

Krzywicka-Racka, A., and G. Sluder. 2011. Repeated cleavage failure does not establish centrosome amplification in untransformed human cells. *J. Cell Biol.* 194:199–207.

Kudryavtsev, B.N., M. V Kudryavtseva, G.A. Sakuta, and G.I. Stein. 1993. Human hepatocyte polyploidization kinetics in the course of life cycle. *Virchows Arch. B. Cell Pathol. Incl. Mol. Pathol.* 64:387–393.

Kuffer, C., A.Y. Kuznetsova, and Z. Storchová. 2013. Abnormal mitosis triggers p53-dependent cell cycle arrest in human tetraploid cells. *Chromosoma*. 122:305–318.

Kulukiana, A., A.J. Holland, B. Vitrec, S. Naika, D.W. Cleveland, and E. Fuchsa. 2015. Epidermal development, growth control, and homeostasis in the face of centrosome amplification. *Proc. Natl. Acad. Sci. U. S. A.* 112:E6311–E6320.

Kuznetsova, A.Y., K. Seget, G.K. Moeller, M.S. de Pagter, J.A.D.M. de Roos, M. Dürrbaum, C. Kuffer, S. Müller, G.J.R. Zaman, W.P. Kloosterman, and Z. Storchová. 2015. Chromosomal instability, tolerance of mitotic errors and multidrug resistance are promoted by tetraploidization in human cells. *Cell Cycle*. 14:2810–2820.

Kwon, M., S.A. Godinho, N.S. Chandhok, N.J. Ganem, A. Azioune, M. Thery, and D. Pellman. 2008. Mechanisms to suppress multipolar divisions in cancer cells with extra centrosomes. *Genes Dev*. 22:2189–2203.

Lacroix, B., G. Letort, L. Pitayu, J. Sallé, M. Stefanutti, G. Maton, A.-M.M. Ladouceur, J.C. Canman, P.S. Maddox, A.S. Maddox, N. Minc, F. Nédélec, and J. Dumont. 2018. Microtubule Dynamics Scale with Cell Size to Set Spindle Length and Assembly Timing. *Dev. Cell*. 45:496-511.e6.

Lambrus, B.G., V. Daggubati, Y. Uetake, P.M. Scott, K.M. Clutario, G. Sluder, and A.J. Holland. 2016. A USP28-53BP1-p53-p21 signaling axis arrests growth after centrosome loss or prolonged mitosis. *J. Cell Biol.* 214:143–153.

Lambrus, B.G., Y. Uetake, K.M. Clutario, V. Daggubati, M. Snyder, G. Sluder, and A.J. Holland. 2015. P53 protects against genome instability following centriole duplication failure. *J. Cell Biol.* 210:63–77.

Lan, W., X. Zhang, S.L. Kline-Smith, S.E. Rosasco, G.A. Barrett-Wilt, J. Shabanowitz, D.F. Hunt, C.E. Walczak, and P.T. Stukenberg. 2004. Aurora B Phosphorylates Centromeric MCAK and Regulates Its Localization and Microtubule Depolymerization Activity. *Curr. Biol.* 14:273–286.

Laprell, F., K. Finkl, and J. Müller. 2017. Propagation of Polycomb-repressed chromatin requires sequence-specific recruitment to DNA. *Science (80-.).* 356:85–88.

Lara-Gonzalez, P., F.G. Westhorpe, and S.S. Taylor. 2012. The spindle assembly checkpoint. *Curr. Biol.* 22:R966–R980.

Larson, K., S.J. Yan, A. Tsurumi, J. Liu, J. Zhou, K. Gaur, D. Guo, T.H. Eickbush, and W.X. Li.

2012. Heterochromatin formation promotes longevity and represses ribosomal RNA synthesis. *PLoS Genet.* 8.

Latif, C., N.R. den Elzen, and M.J. O'Connell. 2004. DNA damage checkpoint maintenance through sustained Chk1 activity. *J. Cell Sci.* 117:3489–3498.

Lawo, S., M. Bashkurov, M. Mullin, M.G. Ferreria, R. Kittler, B. Habermann, A. Tagliaferro, I. Poser, J.R.A.A. Hutchins, B. Hegemann, D. Pinchev, F. Buchholz, J.-M.M. Peters, A.A. Hyman, A.-C.C. Gingras, and L. Pelletier. 2009. HAUS, the 8-Subunit Human Augmin Complex, Regulates Centrosome and Spindle Integrity. *Curr. Biol.* 19:816–826.

Lawo, S., M. Hasegan, G.D. Gupta, and L. Pelletier. 2012. Subdiffraction imaging of centrosomes reveals higher-order organizational features of pericentriolar material. *Nat. Cell Biol.* 14:1148–1158.

Lawrence, M., S. Daujat, and R. Schneider. 2016. Lateral Thinking: How Histone Modifications Regulate Gene Expression. *Trends Genet.* 32:42–56.

Leber, B., B. Maier, F. Fuchs, J. Chi, P. Riffel, S. Anderhub, L. Wagner, A.D. Ho, J.L. Salisbury, M. Boutros, and A. Krämer. 2010. Proteins required for centrosome clustering in cancer cells. *Sci. Transl. Med.* 2:33ra38.

Ledbetter, M.C., and K.R. Porter. 1963. A "MICROTUBULE" IN PLANT CELL FINE STRUCTURE. *J. Cell Biol.* 19:239–250.

Lee, H.O., J.M. Davidson, and R.J. Duronio. 2009. Endoreplication: Polyploidy with purpose. *Genes Dev.* 23:2461–2477.

Lee, T., and L. Luo. 1999. Mosaic analysis with a repressible neurotechnique cell marker for studies of gene function in neuronal morphogenesis. *Neuron*. 22:451–461.

Lefevre, J. 1976. photographic representation and interpretation of the polytene chromosomes of Drosophila melanogaster salivary glands.

Lejeune, J., M. Gautier, and R. Turpin. 1959. [Study of somatic chromosomes from 9 mongoloid children]. *C. R. Hebd. Seances Acad. Sci.* 248:1721–1722.

Levine, M.S., B. Bakker, B. Boeckx, J. Moyett, J. Lu, B. Vitre, D.C. Spierings, P.M. Lansdorp, D.W. Cleveland, D. Lambrechts, F. Foijer, and A.J. Holland. 2017. Centrosome Amplification Is Sufficient to Promote Spontaneous Tumorigenesis in Mammals. *Dev. Cell*. 40:313-322.e5.

Levine, M.S., and A.J. Holland. 2018. The impact of mitotic errors on cell proliferation and tumorigenesis. *Genes Dev.* 32:620–638.

Li, H.-B., M. Muller, I.A. Bahechar, O. Kyrchanova, K. Ohno, P. Georgiev, and V. Pirrotta. 2011. Insulators, Not Polycomb Response Elements, Are Required for Long-Range Interactions between Polycomb Targets in Drosophila melanogaster. *Mol. Cell. Biol.* 31:616–625.

Li, H.B., K. Ohno, H. Gui, and V. Pirrotta. 2013a. Insulators Target Active Genes to Transcription Factories and Polycomb-Repressed Genes to Polycomb Bodies. *PLoS Genet.* 9.

Li, L., and H. Vaessin. 2000. Pan-neural prospero terminates cell proliferation during Drosophila neurogenesis. *Genes Dev.* 14:147–151.

Li, M., X. Fang, D.J. Baker, L. Guo, X. Gao, Z. Wei, S. Han, J.M. Van Deursen, and P. Zhang.

2010. The ATM-p53 pathway suppresses aneuploidy-induced tumorigenesis. *Proc. Natl. Acad. Sci. U. S. A.* 107:14188–14193.

Li, R., and A.W. Murray. 1991. Feedback control of mitosis in budding yeast. *Cell*. 66:519–531.

Li, W., L. Prazak, N. Chatterjee, S. Grüninger, L. Krug, D. Theodorou, and J. Dubnau. 2013b. Activation of transposable elements during aging and neuronal decline in Drosophila. *Nat. Neurosci.* 16:529–531.

Li, X., Z. Chen, and C. Desplan. 2013c. Temporal patterning of neural progenitors in drosophila. 105. 1st ed. Elsevier Inc. 69–96 pp.

Li, X., T. Erclik, C. Bertet, Z. Chen, R. Voutev, S. Venkatesh, J. Morante, A. Celik, and C. Desplan. 2013d. Temporal patterning of Drosophila medulla neuroblasts controls neural fates.

Li, X., and R.B. Nicklas. 1995. Mitotic forces control a cell-cycle checkpoint. *Nature*. 373:630–632.

Li, Z., and G. Goshima. 2011. Identification of a TPX2-Like Microtubule-Associated Protein in Drosophila. *PLoS One*. 6.

Lilly, M.A., and A.C. Spradling. 1996. The Drosophila endocycle is controlled by Cyclin E and lacks a checkpoint ensuring S-phase completion. *Genes Dev.* 10:2514–2526.

Lin, Y.-H., S. Zhang, M. Zhu, T. Lu, K. Chen, Z. Wen, S. Wang, G. Xiao, D. Luo, Y. Jia, L. Li, M. MacConmara, Y. Hoshida, A.G. Singal, A. Yopp, T. Wang, and H. Zhu. 2020. Mice With Increased Numbers of Polyploid Hepatocytes Maintain Regenerative Capacity But Develop Fewer Hepatocellular Carcinomas Following Chronic Liver Injury. *Gastroenterology*. 158:1698-1712.e14.

Linder, R.A., J.P. Greco, F. Seidl, T. Matsui, and I.M. Ehrenreich. 2017. The stress-inducible peroxidase TSA2 underlies a conditionally beneficial chromosomal duplication in Saccharomyces cerevisiae. *G3 Genes, Genomes, Genet.* 7:3177–3184.

Lingle, W.L., W.H. Lutz, J.N. Ingle, N.J. Maihle, and J.L. Salisbury. 1998. Centrosome hypertrophy in human breast tumors: implications for genomic stability and cell polarity. *Proc. Natl. Acad. Sci. U. S. A.* 95:2950–2955.

Lippe, B. 1991. Turner syndrome. *Endocrinol. Metab. Clin. North Am.* 20:121–152.

Livingstone, L.R., A. White, J. Sprouse, E. Livanos, T. Jacks, and T.D. Tlsty. 1992. Altered cell cycle arrest and gene amplification potential accompany loss of wild-type p53. *Cell*. 70:923–935.

López-Sánchez, N., Á. Fontán-Lozano, A. Pallé, V. González-Álvarez, A. Rábano, J.L. Trejo, and J.M. Frade. 2017. Neuronal tetraploidization in the cerebral cortex correlates with reduced cognition in mice and precedes and recapitulates Alzheimer's-associated neuropathology. *Neurobiol. Aging*. 56:50–66.

López-Schier, H., and D. St. Johnston. 2001. Delta signaling from the germ line controls the proliferation and differentiation of the somatic follicle cells during Drosophila oogenesis. *Genes Dev.* 15:1393–1405.

Lorbeck, M.T., N. Singh, A. Zervos, M. Dhatta, M. Lapchenko, C. Yang, and F. Elefant. 2010. The histone demethylase Dmel\Kdm4A controls genes required for life span and male-

specific sex determination in Drosophila. *Gene*. 450:8–17.

Losick, V.P. 2016. Wound-Induced Polyploidy Is Required for Tissue Repair. *Adv. Wound Care*. 5:271–278.

Losick, V.P., D.T. Fox, and A.C. Spradling. 2013. Polyploidization and cell fusion contribute to wound healing in the adult Drosophila epithelium. *Curr. Biol.* 23:2224–2232.

Lozano, E., A.G. Sáez, A.J. Flemming, A. Cunha, and A.M. Leroi. 2006. Regulation of growth by ploidy in Caenorhabditis elegans. *Curr. Biol.* 16:493–498.

Lu, B.Y., C.P. Bishop, and J.C. Eissenberg. 1996. Developmental timing and tissue specificity of heterochromatin-mediated silencing. *EMBO J.* 15:1323–1332.

Luca, F.C., E.K. Shibuya, C.E. Dohrmann, and J. V Ruderman. 1991. Both cyclin A delta 60 and B delta 97 are stable and arrest cells in M-phase, but only cyclin B delta 97 turns on cyclin destruction. *EMBO J.* 10:4311–4320.

Luduena, R.F., and D.O. Woodward. 1973. Isolation and partial characterization of α and β tubulin from outer doublets of sea urchin sperm and microtubules of chick embryo brain. *Proc. Natl. Acad. Sci. U. S. A.* 70:3594–3598.

Lutz, A.M. 1907. A PRELIMINARY NOTE ON THE CHROMOSOMES OF OEligNOTHERA LAMARCKIANA AND ONE OF ITS MUTANTS, O. GIGAS. *Science*. 26:151–152.

Ly, P., and D.W. Cleveland. 2017. Rebuilding Chromosomes After Catastrophe: Emerging Mechanisms of Chromothripsis. *Trends Cell Biol.* 27:917–930.

Ma, J.-Y., S. Li, L.-N. Chen, H. Schatten, X.-H. Ou, and Q.-Y. Sun. 2020. Why is oocyte aneuploidy increased with maternal aging? *J. Genet. Genomics*.

Mable, B.K. 2004. 'Why polyploidy is rarer in animals than in plants': myths and mechanisms. *Biol. J. Linn. Soc.* 82:453–466.

Maddox, P.S., K. Oegema, A. Desai, and I.M. Cheeseman. 2004. "Holo"er than thou: Chromosome segregation and kinetochore function in C. elegans. *Chromosom. Res.* 12:641–653.

Maeshima, K., T. Matsuda, Y. Shindo, H. Imamura, S. Tamura, R. Imai, S. Kawakami, R. Nagashima, T. Soga, H. Noji, K. Oka, and T. Nagai. 2018. A Transient Rise in Free Mg2+ Ions Released from ATP-Mg Hydrolysis Contributes to Mitotic Chromosome Condensation. *Curr. Biol.* 28:444-451.e6.

Magidson, V., C.B. O'Connell, J. Lončarek, R. Paul, A. Mogilner, and A. Khodjakov. 2011. The spatial arrangement of chromosomes during prometaphase facilitates spindle assembly. *Cell*. 146:555–567.

Maiato, H., J. DeLuca, E.D. Salmon, and W.C. Earnshaw. 2004a. The dynamic kinetochore-microtubule interface. *J. Cell Sci.* 117:5461–5477.

Maiato, H., A.M. Gomes, F. Sousa, and M. Barisic. 2017. Mechanisms of Chromosome Congression during Mitosis. *Biol.* 6.

Maiato, H., C.L. Rieder, and A. Khodjakov. 2004b. Kinetochore-driven formation of kinetochore fibers contributes to spindle assembly during animal mitosis. *J. Cell Biol.* 167:831–840.

Manning, A.L., M.S. Longworth, and N.J. Dyson. 2010. Loss of pRB causes centromere dysfunction and chromosomal instability. *Genes Dev.* 24:1364–1376.

Maresca, T.J., A.C. Groen, J.C. Gatlin, R. Ohi, T.J. Mitchison, and E.D. Salmon. 2009. Spindle Assembly in the Absence of a RanGTP Gradient Requires Localized CPC Activity. *Curr. Biol.* 19:1210–1215.

Marsden, M.P.F., and U.K. Laemmli. 1979. Metaphase chromosome structure: Evidence for a radial loop model. *Cell.* 17:849–858.

Marshall, O.J., and A.H. Brand. 2017. Chromatin state changes during neural development revealed by in vivo cell-type specific profiling. *Nat. Commun.* 8:1–9.

Marthiens, V., M.A. Rujano, C. Pennetier, S. Tessier, P. Paul-Gilloteaux, and R. Basto. 2013. Centrosome amplification causes microcephaly. *Nat Cell Biol*. 15:731–740.

Martin, G.M., and C.A. Sprague. 1969. Parasexual Cycle in Cultivated Human Somatic Cells. *Science (80-.).* 166:761 LP – 763.

Mastronarde, D.N., K.L. McDonald, R. Ding, and J.R. McIntosh. 1993. Interpolar spindle microtubules in PTK cells. *J. Cell Biol.* 123:1475–1489.

Matsumoto, T., L. Wakefield, A. Peters, M. Peto, P. Spellman, and M. Grompe. 2021. Proliferative polyploid cells give rise to tumors via ploidy reduction. *Nat. Commun.* 12:646.

Matsumoto, T., L. Wakefield, B.D. Tarlow, and M. Grompe. 2020. In Vivo Lineage Tracing of Polyploid Hepatocytes Reveals Extensive Proliferation during Liver Regeneration. *Cell Stem Cell*. 26:34-47.e3.

Matthies, H.J.G., H.B. McDonald, L.S.B. Goldstein, and W.E. Theurkauf. 1996. Anastral meiotic spindle morphogenesis: Role of the non-claret disjunctional kinesin-like protein. *J. Cell Biol.* 134:455–464.

Maurange, C. 2012. Temporal Specification of Neural Stem Cells. Insights from Drosophila Neuroblasts. *Curr. Top. Dev. Biol.* 98:199–228.

Maurange, C., L. Cheng, and A.P. Gould. 2008. Temporal Transcription Factors and Their Targets Schedule the End of Neural Proliferation in Drosophila. *Cell*. 133:891–902.

Maurange, C., and R. Paro. 2002. A cellular memory module conveys epigenetic inheritance of hedgehog expression during Drosophila wing imaginal disc development. *Genes Dev.* 16:2672–2683.

Mayer, V.W., and A. Aguilera. 1990. High levels of chromosome instability in polyploids of Saccharomyces cerevisiae. *Mutat. Res. Mol. Mech. Mutagen.* 231:177–186.

Mayshar, Y., U. Ben-David, N. Lavon, J.C. Biancotti, B. Yakir, A.T. Clark, K. Plath, W.E. Lowry, and N. Benvenisty. 2010. Identification and classification of chromosomal aberrations in human induced pluripotent stem cells. *Cell Stem Cell*. 7:521–531.

McCrann, D.J., H.G. Nguyen, M.R. Jones, and K. Ravid. 2008. Vascular smooth muscle cell polyploidy: An adaptive or maladaptive response? *J. Cell. Physiol.* 215:588–592.

McDonald, K.L., E.T. O'Toole, D.N. Mastronarde, and J.R. McIntosh. 1992. Kinetochore microtubules in PTK cells. *J. Cell Biol.* 118:369–383.

McEwen, B.F., A.B. Heagle, G.O. Cassels, K.F. Buttle, and C.L. Rieder. 1997. Kinetochore fiber maturation in PtK1 cells and its implications for the mechanisms of chromosome congression and anaphase onset. *J. Cell Biol.* 137:1567–1580.

McGuire, S.E., P.T. Le, A.J. Osborn, K. Matsumoto, and R.L. Davis. 2003. Spatiotemporal

rescue of memory dysfunction in Drosophila. *Science*. 302:1765–1768.

McNally, F.J., K. Okawa, A. Iwamatsu, and R.D. Vale. 1996. Katanin, the microtubule-severing ATPase, is concentrated at centrosomes. *J. Cell Sci.* 109:561–567.

Meena, J.K., A. Cerutti, C. Beichler, Y. Morita, C. Bruhn, M. Kumar, J.M. Kraus, M.R. Speicher, Z.-Q. Wang, H.A. Kestler, F. d'Adda di Fagagna, C. Günes, and K.L. Rudolph. 2015. Telomerase abrogates aneuploidy-induced telomere replication stress, senescence and cell depletion. *EMBO J.* 34:1371–1384.

Mehrotra, S., S.B. Maqbool, A. Kolpakas, K. Murnen, and B.R. Calvi. 2008. Endocycling cells do not apoptose in response to DNA rereplication genotoxic stress. *Genes Dev.* 22:3158–3171.

Meireles, A.M., K.H. Fisher, N. Colombié, J.G. Wakefield, and H. Ohkura. 2009. Wac: A new augmin subunit required for chromosome alignment but not for acentrosomal microtubule assembly in female meiosis. *J. Cell Biol.* 184:777–784.

Meitinger, F., J. V. Anzola, M. Kaulich, A. Richardson, J.D. Stender, C. Benner, C.K. Glass, S.F. Dowdy, A. Desai, A.K. Shiau, and K. Oegema. 2016. 53BP1 and USP28 mediate p53 activation and G1 arrest after centrosome loss or extended mitotic duration. *J. Cell Biol.* 214:155–166.

Mennella, V., B. Keszthelyi, K.L. McDonald, B. Chhun, F. Kan, G.C. Rogers, B. Huang, and D.A. Agard. 2012. Subdiffraction-resolution fluorescence microscopy reveals a domain of the centrosome critical for pericentriolar material organization. *Nat. Cell Biol.* 14:1159–1168.

Meraldi, P., R. Honda, and E.A. Nigg. 2002. Aurora-A overexpression reveals tetraploidization as a major route to centrosome amplification in p53-/- cells. *EMBO J.* 21:483–492.

Meshorer, E., and T. Misteli. 2006. Chromatin in pluripotent embryonic stem cells and differentiation. *Nat. Rev. Mol. Cell Biol.* 7:540–546.

Meshorer, E., D. Yellajoshula, E. George, P.J. Scambler, D.T. Brown, and T. Misteli. 2006. Hyperdynamic plasticity of chromatin proteins in pluripotent embryonic stem cells. *Dev. Cell*. 10:105–116.

Métivier, M., E. Gallaud, A. Thomas, A. Pascal, J.P. Gagné, G.G. Poirier, D. Chrétien, R. Gibeaux, L. Richard-Parpaillon, C. Benaud, and R. Giet. 2020. Drosophila Tubulin-Specific Chaperone E Recruits Tubulin around Chromatin to Promote Mitotic Spindle Assembly. *Curr. Biol.* 1–12.

Metz, C.W. 1914. Chromosome studies in the Diptera. I. A preliminary survey of five different types of chromosome groups in the genus Drosophila. *J. Exp. Zool.* 17:45–59.

Meunier, S., and I. Vernos. 2012. Microtubule assembly during mitosis - from distinct origins to distinct functions? *J Cell Sci*. 125:2805–2814.

Michel, L.S., V. Liberal, A. Chatterjee, R. Kirchwegger, B. Pasche, W. Gerald, M. Dobles, P.K. Sorger, V.V.V.S. Murty, and R. Benezra. 2001. MAD2 haplo-insufficiency causes premature anaphase and chromosome instability in mammalian cells. *Nature*. 409:355–359.

Mikkelsen, T.S., M. Ku, D.B. Jaffe, B. Issac, E. Lieberman, G. Giannoukos, P. Alvarez, W. Brockman, T.K. Kim, R.P. Koche, W. Lee, E. Mendenhall, A. O'Donovan, A. Presser, C. Russ, X. Xie, A. Meissner, M. Wernig, R. Jaenisch, C. Nusbaum, E.S. Lander, and B.E.

Bernstein. 2007. Genome-wide maps of chromatin state in pluripotent and lineage-committed cells. *Nature*. 448:553–560.

Millet, C., and S. Makovets. 2016. Aneuploidy as a mechanism of adaptation to telomerase insufficiency. *Curr. Genet.* 62:557–564.

Mitchison, T., and M. Kirschner. 1984. Dynamic instability of microtubule growth. *Nature*. 312:237–242.

Mitchison, T.J., and M.W. Kirschner. 1985a. Properties of the kinetochore in vitro. I. Microtubule nucleation and tubulin binding. *J. Cell Biol.* 101:755–765.

Mitchison, T.J., and M.W. Kirschner. 1985b. Properties of the kinetochore in vitro. II. Microtubule capture and ATP-dependent translocation. *J. Cell Biol.* 101:766–777.

Moehrle, A., and R. Paro. 1994. Spreading the silence: Epigenetic transcriptional regulation during Drosophila development. *Dev. Genet.* 15:478–484.

Mohri, H. 1968. Amino-acid composition of “Tubulin” constituting microtubules of sperm flagella. *Nature*. 217:1053–1054.

Mollova, M., K. Bersell, S. Walsh, J. Savla, L.T. Das, S.Y. Park, L.E. Silberstein, C.G. Dos Remedios, D. Graham, S. Colan, and B. Kühn. 2013. Cardiomyocyte proliferation contributes to heart growth in young humans. *Proc. Natl. Acad. Sci. U. S. A.* 110:1446–1451.

Molnar, M., and M. Sipiczki. 1993. Polyploidy in the haplontic yeast Schizosaccharomyces pombe: construction and analysis of strains. *Curr. Genet.* 24:45–52.

Morgan, D.O. 1995. Principles of CDK regulation. *Nature*. 374:131–134.

Morin, X., and Y. Bellaïche. 2011. Mitotic Spindle Orientation in Asymmetric and Symmetric Cell Divisions during Animal Development. *Dev. Cell*. 21:102–119.

Moritz, M., M.B. Braunfeld, J.W. Sedat, B. Alberts, and D.A. Agard. 1995. Microtubule nucleation by gamma-tubulin-containing rings in the centrosome. *Nature*. 378:638–640.

Morrison, S.J., and J. Kimble. 2006. Asymmetric and symmetric stem-cell divisions in development and cancer. *Nature*. 441:1068–1074.

Morrow, C.J., A. Tighe, V.L. Johnson, M.I.F. Scott, C. Ditchfield, and S.S. Taylor. 2005. Bub1 and aurora B cooperate to maintain BubR1-mediated inhibition of APC/CCdc20. *J. Cell Sci.* 118:3639–3652.

Mountain, V., C. Simerly, L. Howard, A. Ando, G. Schatten, and D.A. Compton. 1999. The kinesin-related protein, HSET, opposes the activity of Eg5 and cross-links microtubules in the mammalian mitotic spindle. *J. Cell Biol.* 147:351–366.

Muller, H.J. 1925. Why Polyploidy is Rarer in Animals Than in Plants. *Am. Nat.* 59:346–353.

Muller, H.J. 1930. Types of visible variations induced by X-rays inDrosophila. *J. Genet.* 22:299–334.

Murata-Hori, M., and Y.L. Wang. 2002. The kinase activity of aurora B is required for kinetochore-microtubule interactions during mitosis. *Curr. Biol.* 12:894–899.

Murata, T., S. Sonobe, T.I. Baskin, S. Hyodo, S. Hasezawa, T. Nagata, T. Horio, and M. Hasebe. 2005. Microtubule-dependent microtubule nucleation based on recruitment of γ-tubulin in higher plants. *Nat. Cell Biol.* 7:961–968.

Muravyova, E., A. Golovnin, E. Gracheva, A. Parshikov, T. Belenkaya, V. Pirrotta, and P. Georgiev. 2001. Loss of Insulator Activity by Paired Su(Hw) Chromatin Insulators. *Science (80-.).* 291:495 LP – 498.

Musacchio, A., and E.D. Salmon. 2007. The spindle-assembly checkpoint in space and time. *Nat. Rev. Mol. Cell Biol.* 8:379–393.

Myers, S.M., and I. Collins. 2016. Recent findings and future directions for interpolar mitotic kinesin inhibitors in cancer therapy. *Future Med. Chem.* 8:463–489.

Nachury, M. V., T.J. Maresca, W.C. Salmon, C.M. Waterman-Storer, R. Heald, and K. Weis. 2001. Importin β is a mitotic target of the small GTPase ran in spindle assembly. *Cell*. 104:95–106.

Nagata, Y., Y. Muro, and K. Todokoro. 1997a. Thrombopoietin-induced polyploidization of bone marrow megakaryocytes is due to a unique regulatory mechanism in late mitosis. *J. Cell Biol.* 139:449–457.

Nagata, Y., H. Nagahisa, T. Nagasawa, and K. Todokoro. 1997b. Regulation of megakaryocytopoiesis by thrombopoietin and stromal cells. *Leukemia*. 11:435–438.

Nandakumar, S., O. Grushko, and L.A. Buttitta. 2020. Polyploidy in the adult drosophila brain. *Elife*. 9:1–25.

Nano, M., and R. Basto. 2016. The Janus soul of centrosomes: a paradoxical role in disease? *Chromosom. Res*. 24:127–144.

Nano, M., S. Gemble, A. Simon, C. Pennetier, V. Fraisier, V. Marthiens, and R. Basto. 2019. Cell-Cycle Asynchrony Generates DNA Damage at Mitotic Entry in Polyploid Cells. *Curr. Biol.* 29:3937-3945.e7.

Nasmyth, K., and C.H. Haering. 2009. Cohesin: Its roles and mechanisms. *Annu. Rev. Genet.* 43:525–558.

Neef, R., U.R. Klein, R. Kopajtich, and F.A. Barr. 2006. Cooperation between mitotic kinesins controls the late stages of cytokinesis. *Curr. Biol.* 16:301–307.

Nicholson, J.M., J.C. Macedo, A.J. Mattingly, D. Wangsa, J. Camps, V. Lima, A.M. Gomes, S. Dória, T. Ried, E. Logarinho, and D. Cimini. 2015. Chromosome mis-segregation and cytokinesis failure in trisomic human cells. *Elife*. 4:1–23.

Nicklas, R.B., D.F. Kubai, and T.S. Hays. 1982. Spindle microtubules and their mechanical associations after micromanipulation in anaphase. *J. Cell Biol.* 95:91–104.

Nigg, E.A. 2002. Centrosome aberrations: cause or consequence of cancer progression? *Nat. Rev. Cancer*. 2:815–825.

Nogales, E., M. Whittaker, R.A. Milligan, and K.H. Downing. 1999. High-resolution model of the microtubule. *Cell*. 96:79–88.

Nora, E.P., B.R. Lajoie, E.G. Schulz, L. Giorgetti, I. Okamoto, N. Servant, T. Piolot, N.L. van Berkum, J. Meisig, J. Sedat, J. Gribnau, E. Barillot, N. Blüthgen, J. Dekker, and E. Heard. 2012. Spatial partitioning of the regulatory landscape of the X-inactivation centre. *Nature*. 485:381–385.

Norbury, C., and P. Nurse. 1992. Animal cell cycles and their control. *Annu. Rev. Biochem.* 61:441–470.

Nordman, J., S. Li, T. Eng, D. MacAlpine, and T.L. Orr-Weaver. 2011. Developmental control

of the DNA replication and transcription programs. *Genome Res.* 21:175–181.

Nordman, J.T., E.N. Kozhevnikova, C.P. Verrijzer, A. V. Pindyurin, E.N. Andreyeva, V. V. Shloma, I.F. Zhimulev, and T.L. Orr-Weaver. 2014. DNA copy-number control through inhibition of replication fork progression. *Cell Rep.* 9:841–849.

Notta, F., M. Chan-Seng-Yue, M. Lemire, Y. Li, G.W. Wilson, A.A. Connor, R.E. Denroche, S. Ben Liang, A.M.K. Brown, J.C. Kim, T. Wang, J.T. Simpson, T. Beck, A. Borgida, N. Buchner, D. Chadwick, S. Hafezi-Bakhtiari, J.E. Dick, L. Heisler, M.A. Hollingsworth, E. Ibrahimov, G.H. Jang, J. Johns, L.G.T. Jorgensen, C. Law, O. Ludkovski, I. Lungu, K. Ng, D. Pasternack, G.M. Petersen, L.I. Shlush, L. Timms, M.S. Tsao, J.M. Wilson, C.K. Yung, G. Zogopoulos, J.M.S. Bartlett, L.B. Alexandrov, F.X. Real, S.P. Cleary, M.H. Roehrl, J.D. McPherson, L.D. Stein, T.J. Hudson, P.J. Campbell, and S. Gallinger. 2016. A renewed model of pancreatic cancer evolution based on genomic rearrangement patterns. *Nature*. 538:378–382.

Novak, Z.A., P.T. Conduit, A. Wainman, and J.W. Raff. 2014. Asterless licenses daughter centrioles to duplicate for the first time in Drosophila embryos. *Curr. Biol.* 24:1276–1282.

Novitski, E., and G. Braver. 1954. An Analysis of Crossing over within a Heterozygous Inversion in Drosophila Melanogaster. *Genetics*. 39:197–209.

Novotny, T., R. Eiselt, and J. Urban. 2002. Hunchback is required for the specification of the early sublineage of neuroblast 7-3 in the Drosophila central nervous system. *Development*. 129:1027–1036.

O. Wasteneys, G., and R. E. Williamson. 1989. Reassembly of microtubules in Nitella tasmanica: assembly of cortical microtubules in branching clusters and its relevance to steady-state microtubule assembly. *J. Cell Sci.* 93:705 LP – 714.

O'Brien, L.E., S.S. Soliman, X. Li, and D. Bilder. 2011. Altered modes of stem cell division drive adaptive intestinal growth. *Cell*. 147:603–614.

O'Connell, C.B., J. Lončarek, P. Kaláb, and A. Khodjakov. 2009. Relative contributions of chromatin and kinetochores to mitotic spindle assembly. *J. Cell Biol.* 187:43–51.

O'Donnell, K.H., C.T. Chen, and P.C. Wensink. 1994. Insulating DNA directs ubiquitous transcription of the Drosophila melanogaster alpha 1-tubulin gene. *Mol. Cell. Biol.* 14:6398–6408.

Oakley, B.R. 1992. γ-Tubulin: the microtubule organizer? *Trends Cell Biol.* 2:1–5.

Oakley, B.R., C.E. Oakley, Y. Yoon, and M.K. Jung. 1990. Gamma-tubulin is a component of the spindle pole body that is essential for microtubule function in Aspergillus nidulans. *Cell*. 61:1289–1301.

Oakley, C.E., and B.R. Oakley. 1989. Identification of γ-tubulin, a new member of the tubulin superfamily encoded by mipA gene of Aspergillus nidulans. *Nature*. 338:662–664.

Ohashi, A. 2016. Different cell fates after mitotic slippage: From aneuploidy to polyploidy. *Mol. Cell. Oncol.* 3:1–3.

Ohashi, A., M. Ohori, K. Iwai, Y. Nakayama, T. Nambu, D. Morishita, T. Kawamoto, M. Miyamoto, T. Hirayama, M. Okaniwa, H. Banno, T. Ishikawa, H. Kandori, and K. Iwata. 2015. Aneuploidy generates proteotoxic stress and DNA damage concurrently with p53-mediated post-mitotic apoptosis in SAC-impaired cells. *Nat. Commun.* 6.

Ohtsubo, M., H. Okazaki, and T. Nishimoto. 1989. The RCC1 protein, a regulator for the onset of chromosome condensation locates in the nucleus and binds to DNA. *J. Cell Biol.* 109:1389–1397.

Ohtsubo, M., A.M. Theodoras, J. Schumacher, J.M. Roberts, and M. Pagano. 1995. Human cyclin E, a nuclear protein essential for the G1-to-S phase transition. *Mol. Cell. Biol.* 15:2612–2624.

Olins, A.L., and D.E. Olins. 1974. Spheroid Chromatin Units (ν Bodies). *Science (80-.).* 183:330 LP – 332.

Oromendia, A.B., S.E. Dodgson, and A. Amon. 2012. Aneuploidy causes proteotoxic stress in yeast. *Genes Dev*. 26:2696–2708.

Orr-weaver, T.L. 2015. When bigger is better: the role of polyploidy in organogenesis. *Trends Genet*. 31:307–315.

Orr-Weaver, T.L., and A.C. Spradling. 1986. Drosophila chorion gene amplification requires an upstream region regulating s18 transcription. *Mol. Cell. Biol.* 6:4624–4633.

Orr, B., and D.A. Compton. 2013. A double-edged sword: How oncogenes and tumor suppressor genes can contribute to chromosomal instability. *Front. Oncol.* 3 JUN:1–14.

Orr, H.A. 1990. "Why Polyploidy is Rarer in Animals Than in Plants" Revisited. *Am. Nat.* 136:759–770.

Öst, A., A. Lempradl, E. Casas, M. Weigert, T. Tiko, M. Deniz, L. Pantano, U. Boenisch, P.M. Itskov, M. Stoeckius, M. Ruf, N. Rajewsky, G. Reuter, N. Iovino, C. Ribeiro, M. Alenius, S. Heyne, T. Vavouri, and J.A. Pospisilik. 2014. Paternal diet defines offspring chromatin state and intergenerational obesity. *Cell*. 159:1352–1364.

Otto, S.P. 2007. The Evolutionary Consequences of Polyploidy. *Cell*. 131:452–462.

Øvrebø, J.I., B.A. Edgar, J.I. Ovrebo, and B.A. Edgar. 2018. Polyploidy in tissue homeostasis and regeneration. *Dev.* 145.

Pack, S.D., R.J. Weil, A.O. Vortmeyer, W. Zeng, J. Li, H. Okamoto, M. Furuta, E. Pak, I.A. Lubensky, E.H. Oldfield, and Z. Zhuang. 2005. Individual adult human neurons display aneuploidy: Detection by fluorescence in situ hybridization and single neuron PCR. *Cell Cycle*. 4:1758–1760.

Pampalona, J., C. Frías, A. Genescà, and L. Tusell. 2012. Progressive telomere dysfunction causes cytokinesis failure and leads to the accumulation of polyploid cells. *PLoS Genet.* 8.

Pandit, S.K., B. Westendorp, and A. De Bruin. 2013. Physiological significance of polyploidization in mammalian cells. *Trends Cell Biol.* 23:556–566.

Pandita, T.K., and C. Richardson. 2009. Chromatin remodeling finds its place in the DNA double-strand break response. *Nucleic Acids Res.* 37:1363–1377.

Parada, L.A., P.G. McQueen, and T. Misteli. 2004. Tissue-specific spatial organization of genomes. *Genome Biol.* 5:R44.

Passerini, V., E. Ozeri-Galai, M.S. De Pagter, N. Donnelly, S. Schmalbrock, W.P. Kloosterman, B. Kerem, and Z. Storchová. 2016. The presence of extra chromosomes leads to genomic instability. *Nat. Commun.* 7.

Paulson, J.R., and U.K. Laemmli. 1977. The structure of histone-depleted metaphase

chromosomes. *Cell*. 12:817–828.

Pavelka, N., G. Rancati, J. Zhu, W.D. Bradford, A. Saraf, L. Florens, B.W. Sanderson, G.L. Hattem, and R. Li. 2010. Aneuploidy confers quantitative proteome changes and phenotypic variation in budding yeast. *Nature*. 468:321–325.

Pearson, B.J., and C.Q. Doe. 2003. Regulation of neuroblast competence in Drosophila. *Nature*. 425:624–628.

Pearson, M.J. 1974. Polyteny and the Functional Significance of the Polytene Cell Cycle. *J. Cell Sci.* 15:457 LP – 479.

Van De Peer, Y., E. Mizrachi, and K. Marchal. 2017. The evolutionary significance of polyploidy. *Nat. Rev. Genet.* 18:411–424.

Peng, C.Y., P.R. Graves, R.S. Thoma, Z. Wu, A.S. Shaw, and H. Piwnica-Worms. 1997. Mitotic and G2 checkpoint control: Regulation of 14-3-3 protein binding by phosphorylation of Cdc25c on serine-216. *Science (80-.).* 277:1501–1505.

Pepling, M.E. 2016. Nursing the oocyte. *Science (80-.).* 352:35–36.

Pera, F., and B. Rainer. 1973. Studies of multipolar mitoses in euploid tissue cultures. I. Somatic reduction to exactly haploid and triploid chromosome sets. *Chromosoma*. 42:71–86.

Pereanu, W., D. Shy, and V. Hartenstein. 2005. Morphogenesis and proliferation of the larval brain glia in Drosophila. *Dev. Biol.* 283:191–203.

Peter, M., J. Nakagawa, M. Dorée, J.C. Labbé, and E.A. Nigg. 1990. In vitro disassembly of the nuclear lamina and M phase-specific phosphorylation of lamins by cdc2 kinase. *Cell*. 61:591–602.

Peters, J.M. 2002. The anaphase-promoting complex: Proteolysis in mitosis and beyond. *Mol. Cell*. 9:931–943.

Petry, S., C. Pugieux, F.J. Neḑeĺec, and R.D. Vale. 2011. Augmin promotes meiotic spindle formation and bipolarity in Xenopus egg extracts. *Proc. Natl. Acad. Sci. U. S. A.* 108:14473–14478.

Pfau, S.J., R.E. Silberman, K.A. Knouse, and A. Amon. 2016. Aneuploidy impairs hematopoietic stem cell fitness and is selected against in regenerating tissues in vivo. *Genes Dev*. 30:1395–1408.

Pfeiffer, B.D., T.T.B. Ngo, K.L. Hibbard, C. Murphy, A. Jenett, J.W. Truman, and G.M. Rubin. 2010. Refinement of tools for targeted gene expression in Drosophila. *Genetics*. 186:735–755.

Phan, T.P., A.L. Maryniak, C.A. Boatwright, J. Lee, A. Atkins, A. Tijhuis, D.C. Spierings, H. Bazzi, F. Foijer, P.W. Jordan, T.H. Stracker, and A.J. Holland. 2021. Centrosome defects cause microcephaly by activating the 53BP1-USP28-TP53 mitotic surveillance pathway. *EMBO J.* 40:1–18.

Piekny, A.J., and M. Glotzer. 2008. Anillin is a scaffold protein that links RhoA, actin, and myosin during cytokinesis. *Curr. Biol.* 18:30–36.

Pihan, G.A., A. Purohit, J. Wallace, H. Knecht, B. Woda, P. Quesenberry, and S.J. Doxsey. 1998. Centrosome defects and genetic instability in malignant tumors. *Cancer Res.* 58:3974–3985.

Pimpinelli, S., and C. Goday. 1989. Unusual kinetochores and chromatin diminution in Parascaris. *Trends Genet.* 5:310–315.

Pines, J. 1995. Cyclins and cyclin-dependent kinases: A biochemical view. *Biochem. J.* 308:697–711.

Pines, J., and T. Hunter. 1991. Human cyclins A and B1 are differentially located in the cell and undergo cell cycle-dependent nuclear transport. *J. Cell Biol.* 115:1–17.

Potapova, T.A., C.W. Seidel, A.C. Box, G. Rancati, and R. Li. 2016. Transcriptome analysis of tetraploid cells identifes cyclin D2 as a facilitator of adaptation to genome doubling in the presence of p53. *Mol. Biol. Cell*. 27:3065–3084.

Poulton, J.S., J.C. Cuningham, and M. Peifer. 2014. Acentrosomal Drosophila epithelial cells exhibit abnormal cell division, leading to cell death and compensatory proliferation. *Dev Cell*. 30:731–745.

Prasad, A., and E. Alizadeh. 2019. Cell Form and Function: Interpreting and Controlling the Shape of Adherent Cells. 37. Elsevier Ltd.

Purvis, J.E., K.W. Karhohs, C. Mock, E. Batchelor, A. Loewer, and G. Lahav. 2012. P53 Dynamics Control Cell Fate. *Science (80-.).* 336:1440–1444.

Quinn, M.E., Q. Goh, M. Kurosaka, D.G. Gamage, M.J. Petrany, V. Prasad, and D.P. Millay. 2017. Myomerger induces fusion of non-fusogenic cells and is required for skeletal muscle development. *Nat. Commun.* 8:1–9.

Quintyne, N.J., J.E. Reing, D.R. Hoffelder, S.M. Gollin, and W.S. Saunders. 2005. Spindle multipolarity is prevented by centrosomal clustering. *Science (80-.).* 307:127–129.

Rando, O.J., and H.Y. Chang. 2009. Genome-Wide Views of Chromatin Structure. *Annu. Rev. Biochem.* 78:245–271.

Rao, P.N., and R.T. Johnson. 1970. Mammalian Cell Fusion : Studies on the Regulation of DNA Synthesis and Mitosis. *Nature*. 225:159–164.

Ravid, K., J. Lu, J.M. Zimmet, and M.R. Jones. 2002. Roads to polyploidy: The megakaryocyte example. *J. Cell. Physiol.* 190:7–20.

Rebollo, E., P. Sampaio, J. Januschke, S. Llamazares, H. Varmark, and C. González. 2007. Functionally Unequal Centrosomes Drive Spindle Orientation in Asymmetrically Dividing Drosophila Neural Stem Cells. *Dev. Cell*. 12:467–474.

Redemann, S., J. Baumgart, N. Lindow, M. Shelley, E. Nazockdast, A. Kratz, S. Prohaska, J. Brugués, S. Fürthauer, and T. Müller-Reichert. 2017. C. elegans chromosomes connect to centrosomes by anchoring into the spindle network. *Nat. Commun.* 8:1–13.

Reed, B.H., and T.L. Orr-Weaver. 1997. The Drosophila gene morula inhibits mitotic functions in the endo cell cycle and the mitotic cell cycle. *Development*. 124:3543–3553.

Rehen, S.K., M.J. McConnell, D. Kaushal, M.A. Kingsbury, A.H. Yang, and J. Chun. 2001. Chromosomal variation in neurons of the developing and adult mammalian nervous system. *Proc. Natl. Acad. Sci. U. S. A.* 98:13361–13366.

Rehen, S.K., Y.C. Yung, M.P. Mccreight, D. Kaushal, A.H. Yang, B.S. V Almeida, M.A. Kingsbury, M.S. Cabral, M.J. Mcconnell, B. Anliker, M. Fontanoz, and J. Chun. 2005. Constitutional Aneuploidy in the Normal Human Brain. 25:2176–2180.

Reilein, A., S. Yamada, and W.J. Nelson. 2005. Self-organization of an acentrosomal

microtubule network at the basal cortex of polarized epithelial cells. *J. Cell Biol.* 171:845–855.

Ren, Q., T. Awasaki, Y.-F. Huang, Z. Liu, and T. Lee. 2016. Cell Class-Lineage Analysis Reveals Sexually Dimorphic Lineage Compositions in the Drosophila Brain. *Curr. Biol.* 26:2583–2593.

De Renty, C., M.L. DePamphilis, and Z. Ullah. 2014. Cytoplasmic localization of p21 protects trophoblast giant cells from DNA damage induced apoptosis. *PLoS One*. 9:1–15.

Resende, L.P., A. Monteiro, R. Bras, T. Lopes, C.E. Sunkel, R. Brás, T. Lopes, C.E. Sunkel, R. Bras, T. Lopes, and C.E. Sunkel. 2018. Aneuploidy in intestinal stem cells promotes gut dysplasia in Drosophila. *J Cell Biol*. 217:3930–3946.

Rhys, A.D., P. Monteiro, C. Smith, M. Vaghela, T. Arnandis, T. Kato, B. Leitinger, E. Sahai, A. McAinsh, G. Charras, and S.A. Godinho. 2018. Loss of E-cadherin provides tolerance to centrosome amplification in epithelial cancer cells. *J. Cell Biol.* 217:195–209.

Rhyu, M.S., L.Y. Jan, and Y.N. Jan. 1994. Asymmetric distribution of numb protein during division of the sensory organ precursor cell confers distinct fates to daughter cells. *Cell*. 76:477–491.

Ricke, R.M., and J.M. Van Deursen. 2011. Correction of microtubule-kinetochore attachment errors: Mechanisms and role in tumor suppression. *Semin. Cell Dev. Biol.* 22:559–565.

Rieder, C.L. 1981. The structure of the cold-stable kinetochore fiber in metaphase PtK1 cells. *Chromosoma*. 84:145–158.

Rieder, C.L. 2005. Kinetochore fiber formation in animal somatic cells: Dueling mechanisms come to a draw. *Chromosoma*. 114:310–318.

Rieder, C.L., and S.P. Alexander. 1990. Kinetochores are transported poleward along a single astral microtubule during chromosome attachment to the spindle in newt lung cells. *J. Cell Biol.* 110:81–95.

Rieder, C.L., R.W. Cole, A. Khodjakov, and G. Sluder. 1995. The checkpoint delaying anaphase in response to chromosome monoorientation is mediated by an inhibitory signal produced by unattached kinetochores. *J. Cell Biol.* 130:941–948.

Rieder, C.L., E.A. Davison, L.C. Jensen, L. Cassimeris, and E.D. Salmon. 1986. Oscillatory movements of monooriented chromosomes and their position relative to the spindle pole result from the ejection properties of the aster and half-spindle. *J. Cell Biol.* 103:581–591.

Rieder, C.L., and E.D. Salmon. 1994. Motile kinetochores and polar ejection forces dictate chromosome position on the vertebrate mitotic spindle. *J. Cell Biol.* 124:223–233.

Ring, D., R. Hubble, and M. Kirschner. 1982. Mitosis in a cell with multiple centrioles. *J. Cell Biol.* 94:549–556.

Ringrose, L., and R. Paro. 2007. Polycom/Trithorax response elements and epigenetic memory of cell identity. *Development*. 134:223–232.

Rivera, T., C. Ghenoiu, M. Rodríguez-Corsino, S. Mochida, H. Funabiki, and A. Losada. 2012. Xenopus Shugoshin 2 regulates the spindle assembly pathway mediated by the chromosomal passenger complex. *EMBO J.* 31:1467–1479.

Roseman, R.R., V. Pirrotta, and P.K. Geyer. 1993. The su(Hw) protein insulates expression of

the Drosophila melanogaster white gene from chromosomal position-effects. *EMBO J.* 12:435–442.

Ross, D.W. 1999. The human genome: information content and structure. *Hosp. Pract. (1995)*. 34:49-54,56-60,65.

Roth, L.E., and E.W. Daniels. 1962. Electron microscopic studies of mitosis in amebae. II. The giant ameba Pelomyxa carolinensis. *J. Cell Biol.* 12:57–78.

Roth, L.E., S.W. Obetz, and E.W. Daniels. 1960. Electron microscopic studies of mitosis in amebae. I. Amoeba proteus. *J. Biophys. Biochem. Cytol.* 8:207–220.

Rudkin, G.T. 1969. Non replicating DNA in Drosophila. *Genetics*. 61:Suppl:227-38.

Rudkin, G.T. 1972. Replication in polytene chromosomes. *Results Probl. Cell Differ.* 4:59–85.

Rué, P., and A. Martinez Arias. 2015. Cell dynamics and gene expression control in tissue homeostasis and development. *Mol. Syst. Biol.* 11:792.

Rusan, N.M., and M. Peifer. 2007. A role for a novel centrosome cycle in asymmetric cell division. *J. Cell Biol.* 177:13–20.

Rusan, N.M., U. Serdar Tulu, C. Fagerstrom, and P. Wadsworth. 2002. Reorganization of the microtubule array in prophase/prometaphase requires cytoplasmic dynein-dependent microtubule transport. *J. Cell Biol.* 158:997–1003.

Russo, A., F. Pacchierotti, D. Cimini, N.J. Ganem, A. Genescà, A.T. Natarajan, S. Pavanello, G. Valle, and F. Degrassi. 2015. Genomic instability: Crossing pathways at the origin of structural and numerical chromosome changes. *Environ. Mol. Mutagen.* 56:563–580.

Sabat-Pośpiech, D., K. Fabian-Kolpanowicz, I.A. Prior, J.M. Coulson, and A.B. Fielding. 2019. Targeting centrosome amplification, an Achilles' heel of cancer. *Biochem. Soc. Trans.* 47:1209–1222.

Sabino, D., D. Gogendeau, D. Gambarotto, M. Nano, C. Pennetier, F. Dingli, G. Arras, D. Loew, and R. Basto. 2015. Moesin is a major regulator of centrosome behavior in epithelial cells with extra centrosomes. *Curr. Biol.* 25:879–889.

Salimian, K.J., E.R. Ballister, E.M. Smoak, S. Wood, T. Panchenko, M.A. Lampson, and B.E. Black. 2011. Feedback control in sensing chromosome biorientation by the aurora B kinase. *Curr. Biol.* 21:1158–1165.

Sampaio, P., E. Rebollo, H. Varmark, C.E. Sunkel, and C. González. 2001. Organized microtubule arrays in γ-tubulin-depleted Drosophila spermatocytes. *Curr. Biol.* 11:1788–1793.

Sampath, S.C., R. Ohi, O. Leismann, A. Salic, A. Pozniakovski, and H. Funabiki. 2004. The chromosomal passenger complex is required for chromatin-induced microtubule stabilization and spindle assembly. *Cell*. 118:187–202.

Sansregret, L., and C. Swanton. 2017. The role of aneuploidy in cancer evolution. *Cold Spring Harb. Perspect. Med.* 7:1–17.

Santarella, R.A., M.D. Koffa, P. Tittmann, H. Gross, and A. Hoenger. 2007. HURP Wraps Microtubule Ends with an Additional Tubulin Sheet That Has a Novel Conformation of Tubulin. *J. Mol. Biol.* 365:1587–1595.

Sanz-Gómez, N., A. Freije, L. Ceballos, S. Obeso, J.R. Sanz, F. García-Reija, C. Morales-Angulo, and A. Gandarillas. 2018. Response of head and neck epithelial cells to a DNA damage-

differentiation checkpoint involving polyploidization. *Head Neck*. 40:2487–2497.

Sanz-Gómez, N., I. de Pedro, B. Ortigosa, D. Santamaría, M. Malumbres, G. de Cárcer, and A. Gandarillas. 2020. Squamous differentiation requires G2/mitosis slippage to avoid apoptosis. *Cell Death Differ.* 27:2451–2467.

Sato, N., K. Mizumoto, M. Nakamura, K. Nakamura, M. Kusumoto, H. Niiyama, T. Ogawa, and M. Tanaka. 1999. Centrosome abnormalities in pancreatic ductal carcinoma. *Clin. cancer Res. an Off. J. Am. Assoc. Cancer Res.* 5:963–970.

Sattler, M.C., C.R. Carvalho, and W.R. Clarindo. 2016. The polyploidy and its key role in plant breeding. *Planta*. 243:281–296.

Saunders, W.S. 1993. Mitotic spindle pole separation. *Trends Cell Biol.* 3:432–437.

Saura, A.O., A.J. Saura, and V. Sorsa. 1999. Polytene chromosome maps on the internet–the first 18 months. *In* Europ. Dros. Res. Conf. 202.

Schaeffer, V., C. Althauser, H.R. Shcherbata, W.-M. Deng, and H. Ruohola-Baker. 2004. Notch-Dependent Fizzy-Related/Hec1/Cdh1 Expression Is Required for the Mitotic-to-Endocycle Transition in Drosophila Follicle Cells. *Curr. Biol.* 14:630–636.

Scheer, U. 2014. Historical roots of centrosome research: Discovery of Boveri's microscope slides in Würzburg. *Philos. Trans. R. Soc. B Biol. Sci.* 369.

Schmidt, H., C. Rickert, T. Bossing, O. Vef, J. Urban, and G.M. Technau. 1997. The Embryonic Central Nervous System Lineages ofDrosophila melanogaster. *Dev. Biol.* 189:186–204.

Schneiderman, J.I., S. Goldstein, and K. Ahmad. 2010. Perturbation analysis of heterochromatin-mediated gene silencing and somatic inheritance. *PLoS Genet.* 6.

Schoenfelder, K.P., and D.T. Fox. 2015. The expanding implications of polyploidy. *J Cell Biol*. 209:485–491.

Schoenfelder, K.P., R.A. Montague, S. V. Paramore, A.L. Lennox, A.P. Mahowald, and D.T. Fox. 2014. Indispensable pre-mitotic endocycles promote aneuploidy in the Drosophila rectum. *Dev.* 141:3551–3560.

Schoenfelder, S., M. Furlan-Magaril, B. Mifsud, F. Tavares-Cadete, R. Sugar, B.M. Javierre, T. Nagano, Y. Katsman, M. Sakthidevi, S.W. Wingett, E. Dimitrova, A. Dimond, L.B. Edelman, S. Elderkin, K. Tabbada, E. Darbo, S. Andrews, B. Herman, A. Higgs, E. LeProust, C.S. Osborne, J.A. Mitchell, N.M. Luscombe, and P. Fraser. 2015. The pluripotent regulatory circuitry connecting promoters to their long-range interacting elements. *Genome Res.* 25:582–597.

Schotta, G., A. Ebert, and G. Reuter. 2003. SU(VAR)3-9 is a Conserved Key Function in Heterochromatic Gene Silencing. *Genetica*. 117:149–158.

Schukken, K.M., and F. Foijer. 2018. CIN and Aneuploidy: Different Concepts, Different Consequences. *BioEssays*. 40:1–9.

Schwartz, Y.B., D. Linder-Basso, P. V Kharchenko, M.Y. Tolstorukov, M. Kim, H.-B. Li, A.A. Gorchakov, A. Minoda, G. Shanower, A.A. Alekseyenko, N.C. Riddle, Y.L. Jung, T. Gu, A. Plachetka, S.C.R. Elgin, M.I. Kuroda, P.J. Park, M. Savitsky, G.H. Karpen, and V. Pirrotta. 2012. Nature and function of insulator protein binding sites in the Drosophila genome. *Genome Res.* 22:2188–2198.

Schweizer, N., N. Pawar, M. Weiss, and H. Maiato. 2015. An organelle-exclusion envelope

assists mitosis and underlies distinct molecular crowding in the spindle region. *J. Cell Biol.* 210:695–704.

Sedat, J., and L. Manuelidis. 1978. A direct approach to the structure of eukaryotic chromosomes. *Cold Spring Harb. Symp. Quant. Biol.* 42 Pt 1:331–350.

Selmecki, A., A. Forche, and J. Berman. 2006. Formation in Drug-Resistant. *Science (80-.).* 367–370.

Selmecki, A.M., K. Dulmage, L.E. Cowen, J.B. Anderson, and J. Berman. 2009. Acquisition of aneuploidy provides increased fitness during the evolution of antifungal drug resistance. *PLoS Genet.* 5:1–16.

Seong, K.H., D. Li, H. Shimizu, R. Nakamura, and S. Ishii. 2011. Inheritance of stress-induced, ATF-2-dependent epigenetic change. *Cell*. 145:1049–1061.

Serçin, Ö., J.C. Larsimont, A.E. Karambelas, V. Marthiens, V. Moers, B. Boeckx, M. Le Mercier, D. Lambrechts, R. Basto, C. Blanpain, O. Sercin, J.C. Larsimont, A.E. Karambelas, V. Marthiens, V. Moers, B. Boeckx, M. Le Mercier, D. Lambrechts, R. Basto, C. Blanpain, Ö. Serçin, J.C. Larsimont, A.E. Karambelas, V. Marthiens, V. Moers, B. Boeckx, M. Le Mercier, D. Lambrechts, R. Basto, and C. Blanpain. 2016. Transient PLK4 overexpression accelerates tumorigenesis in p53-deficient epidermis. *Nat. Cell Biol.* 18:100–110.

Sexton, T., E. Yaffe, E. Kenigsberg, F. Bantignies, B. Leblanc, M. Hoichman, H. Parrinello, A. Tanay, and G. Cavalli. 2012. Three-dimensional folding and functional organization principles of the Drosophila genome. *Cell*. 148:458–472.

Shcherbata, H.R., C. Althauser, S.D. Findley, and H. Ruohola-Baker. 2004. The mitotic-to-endrocycle switch in Drosophila follicle cells is executed by Notch-dependent regulation of G1/S, G2/M and M/G1 cell-cycle transitions. *Development*. 131:3169–3181.

Sheltzer, J.M., E.M. Torres, M.J. Dunham, and A. Amon. 2012. Transcriptional consequences of aneuploidy. *Proc Natl Acad Sci U S A*. 109:12644–12649.

Shepherd, C.E., Y. Yang, and G.M. Halliday. 2018. Region- and Cell-specific Aneuploidy in Brain Aging and Neurodegeneration. *Neuroscience*. 374:326–334.

Sher, N., J.R. Von Stetina, G.W. Bell, S. Matsuura, K. Ravid, and T.L. Orr-Weaver. 2013. Fundamental differences in endoreplication in mammals and Drosophila revealed by analysis of endocycling and endomitotic cells. *Proc. Natl. Acad. Sci. U. S. A.* 110:9368–9373.

Sherr, C.J. 1994. G1 phase progression: cycling on cue. *Cell*. 79:551–555.

Sieben, C.J., K.B. Jeganathan, G.G. Nelson, I. Sturmlechner, C. Zhang, W.H. Van Deursen, B. Bakker, F. Foijer, H. Li, D.J. Baker, and J.M. Van Deursen. 2020. BubR1 allelic effects drive phenotypic heterogeneity in mosaic-variegated aneuploidy progeria syndrome. *J. Clin. Invest.* 130:171–188.

Siegel, J.J., and A. Amon. 2012. New Insights into the Troubles of Aneuploidy. *Annu. Rev. Cell Dev. Biol.* 28:189–214.

Sigrist, S.J., and C.F. Lehner. 1997. Drosophila fizzy-related down-regulates mitotic cyclins and is required for cell proliferation arrest and entry into endocycles. *Cell*. 90:671–681.

Sikirzhytski, V., V. Magidson, J.B. Steinman, J. He, M. Le Berre, I. Tikhonenko, J.G. Ault, B.F. McEwen, J.K. Chen, H. Sui, M. Piel, T.M. Kapoor, and A. Khodjakov. 2014. Direct

kinetochore-spindle pole connections are not required for chromosome segregation. *J. Cell Biol.* 206:231–243.

Sikirzhytski, V., F. Renda, I. Tikhonenko, V. Magidson, B.F. McEwen, and A. Khodjakov. 2018. Microtubules assemble near most kinetochores during early prometaphase in human cells. *J. Cell Biol.* 217:2647–2659.

Silkworth, W.T., I.K. Nardi, L.M. Scholl, and D. Cimini. 2009. Multipolar spindle pole coalescence is a major source of kinetochore mis-attachment and chromosome mis-segregation in cancer cells. *PLoS One*. 4:e6564.

Silverman-Gavrila, R. V, and A. Wilde. 2006. Ran is required before metaphase for spindle assembly and chromosome alignment and after metaphase for chromosome segregation and spindle midbody organization. *Mol Biol Cell*. 17:2069–2080.

Simon, J.A., and J.W. Tamkun. 2002. Programming off and on states in chromatin: mechanisms of Polycomb and trithorax group complexes. *Curr. Opin. Genet. Dev.* 12:210–218.

Sinclair, D.A.R., R.C. Mottus, and T.A. Grigliatti. 1983. Genes which suppress position-effect variegation in Drosophila melanogaster are clustered. *Mol. Gen. Genet. MGG*. 191:326–333.

Sir, J.H., M. Pütz, O. Daly, C.G. Morrison, M. Dunning, J. V. Kilmartin, and F. Gergely. 2013. Loss of centrioles causes chromosomal instability in vertebrate somatic cells. *J. Cell Biol.* 203:747–756.

Siudeja, K., and A.J. Bardin. 2017. Somatic recombination in adult tissues: What is there to learn? *Fly*. 11:121–128.

Siudeja, K., S. Nassari, L. Gervais, P. Skorski, S. Lameiras, D. Stolfa, M. Zande, V. Bernard, T.R. Frio, A.J. Bardin, T. Rio Frio, A.J. Bardin, T.R. Frio, and A.J. Bardin. 2015. Frequent Somatic Mutation in Adult Intestinal Stem Cells Drives Neoplasia and Genetic Mosaicism during Aging. *Cell Stem Cell*. 17:663–674.

Skora, A.D., and A.C. Spradling. 2010. Epigenetic stability increases extensively during Drosophila follicle stem cell differentiation. *Proc. Natl. Acad. Sci. U. S. A.* 107:7389–7394.

Skyldberg, B., K. Fujioka, A.C. Hellström, L. Sylvén, B. Moberger, and G. Auer. 2001. Human papillomavirus infection, centrosome aberration, and genetic stability in cervical lesions. *Mod. Pathol. an Off. J. United States Can. Acad. Pathol. Inc*. 14:279–284.

Slattery, M., L. Ma, R.F. Spokony, R.K. Arthur, P. Kheradpour, A. Kundaje, N. Nègre, A. Crofts, R. Ptashkin, J. Zieba, A. Ostapenko, S. Suchy, A. Victorsen, N. Jameel, A.J. Grundstad, W. Gao, J.R. Moran, E.J. Rehm, R.L. Grossman, M. Kellis, and K.P. White. 2014. Diverse patterns of genomic targeting by transcriptional regulators in Drosophila melanogaster. *Genome Res.* 24:1224–1235.

Slautterback, D.B. 1963. Cytoplasmic Microtubules. I. Hydra. *J. Cell Biol.* 18:367–388.

Smith, A. V., and T.L. Orr-Weaver. 1991. The regulation of the cell cycle during Drosophila embryogenesis: The transition to polyteny. *Development*. 112:997–1008.

Smith, C.D., S. Shu, C.J. Mungall, and G.H. Karpen. 2007. The Release 5.1 Annotation of Drosophila melanogaster Heterochromatin. *Science (80-.).* 316:1586 LP – 1591.

Somma, M.P., B. Fasulo, G. Cenci, E. Cundari, M. Gatti, N. Richerche, B. Molecolare, and R. La. 2002. Cytokinesis genes and multinucleation. 13:2448–2460.

Sonnen, K.F., L. Schermelleh, H. Leonhardt, and E.A. Nigg. 2012. 3D-structured illumination microscopy provides novel insight into architecture of human centrosomes. *Biol. Open*. 1:965–976.

Spéder, P., and A.H. Brand. 2014. Gap junction proteins in the blood-brain barrier control nutrient-dependent reactivation of Drosophila neural stem cells. *Dev. Cell*. 30:309–321.

Spitz, F., and E.E.M. Furlong. 2012. Transcription factors: from enhancer binding to developmental control. *Nat. Rev. Genet.* 13:613–626.

Stearns, T., L. Evans, and M. Kirschner. 1991. γ-Tubulin is a highly conserved component of the centrosome. *Cell*. 65:825–836.

Stebbins, G.L. 1947. Types of Polyploids: Their Classification and Significance. M.B.T.-A. in G. Demerec, editor. Academic Press. 403–429.

Steffen, P.A., and L. Ringrose. 2014. What are memories made of? How polycomb and trithorax proteins mediate epigenetic memory. *Nat. Rev. Mol. Cell Biol.* 15:340–356.

Steigemann, P., C. Wurzenberger, M.H.A. Schmitz, M. Held, J. Guizetti, S. Maar, and D.W. Gerlich. 2009. Aurora B-Mediated Abscission Checkpoint Protects against Tetraploidization. *Cell*. 136:473–484.

Stern, C. 1936. Somatic Crossing over and Segregation in Drosophila Melanogaster. *Genetics*. 21:625–730.

Stern, S., Y. Fridmann-Sirkis, E. Braun, and Y. Soen. 2012. Epigenetically Heritable Alteration of Fly Development in Response to Toxic Challenge. *Cell Rep.* 1:528–542.

Von Stetina, J.R., L.E. Frawley, Y. Unhavaithaya, and T.L. Orr-Weaver. 2018. Variant cell cycles regulated by Notch signaling control cell size and ensure a functional blood-brain barrier. *Dev.* 145.

Steubing, R.W., S. Cheng, W.H. Wright, Y. Numajiri, and M.W. Berns. 1991. Laser induced cell fusion in combination with optical tweezers: The laser cell fusion trap. *Cytometry*. 12:505–510.

Stewénius, Y., L. Gorunova, T. Jonson, N. Larsson, M. Höglund, N. Mandahl, F. Mertens, F. Mitelman, and D. Gisselsson. 2005. Structural and numerical chromosome changes in colon cancer develop through telomere-mediated anaphase bridges, not through mitotic multipolarity. *Proc. Natl. Acad. Sci. U. S. A.* 102:5541–5546.

Stingele, S., G. Stoehr, K. Peplowska, J. Cox, M. Mann, and Z. Storchova. 2012. Global analysis of genome, transcriptome and proteome reveals the response to aneuploidy in human cells. *Mol. Syst. Biol.* 8.

Storchová, Z., A. Breneman, J. Cande, J. Dunn, K. Burbank, E. O'Toole, and D. Pellman. 2006. Genome-wide genetic analysis of polyploidy in yeast. *Nature*. 443:541–547.

Storchova, Z., and D. Pellman. 2004. From polyploidy to aneuploidy, genome instability and cancer. *Nat Rev Mol Cell Biol*. 5:45–54.

Stork, T., D. Engelen, A. Krudewig, M. Silies, R.J. Bainton, and C. Klämbt. 2008. Organization and function of the blood-brain barrier in Drosophila. *J. Neurosci.* 28:587–597.

Strome, S., J. Powers, M. Dunn, K. Reese, C.J. Malone, J. White, G. Seydoux, and W. Saxton.

2001. Spindle dynamics and the role of γ-tubulin in early Caenorhabditis elegans embryos. *Mol. Biol. Cell*. 12:1751–1764.

Struhl, G., and K. Basler. 1993. Organizing activity of wingless protein in Drosophila. *Cell*. 72:527–540.

Sudakin, V., G.K.T. Chan, and T.J. Yen. 2001. Checkpoint inhibition of the APC/C in HeLa cells is mediated by a complex of BUBR1, BUB3, CDC20, and MAD2. *J. Cell Biol.* 154:925–936.

Sugimoto-Shirasu, K., and K. Roberts. 2003. "Big it up": Endoreduplication and cell-size control in plants. *Curr. Opin. Plant Biol.* 6:544–553.

Sunkel, C.E., and D.M. Glover. 1988. polo, a mitotic mutant of Drosophila displaying abnormal spindle poles. *J. Cell Sci.* 89 (Pt 1):25–38.

Sunkel, C.E., R. Gomes, P. Sampaio, J. Perdigão, and C. González. 1995. γ-Tubulin is required for the structure and function of the microtubule organizing centre in Drosophila neuroblasts. *EMBO J.* 14:28–36.

Suster, M.L., L. Seugnet, M. Bate, and M.B. Sokolowski. 2004. Refining GAL4-driven transgene expression in Drosophila with a GAL80 enhancer-trap. *Genesis*. 39:240–245.

Suzuki, T., M. Kaido, R. Takayama, and M. Sato. 2013. A temporal mechanism that produces neuronal diversity in the Drosophila visual center. *Dev. Biol.* 380:12–24.

Szabad, J., H.J. Bellen, and K.J. Venken. 2012. An assay to detect in vivo Y chromosome loss in Drosophila wing disc cells. *G3*. 2:1095–1102.

Taapken, S.M., B.S. Nisler, M.A. Newton, T.L. Sampsell-Barron, K.A. Leonhard, E.M. McIntire, and K.D. Montgomery. 2011. Karyotypic abnormalities in human induced pluripotent stem cells and embryonic stem cells. *Nat. Biotechnol.* 29:313–314.

Tamori, Y., and W.M. Deng. 2013. Tissue Repair through Cell Competition and Compensatory Cellular Hypertrophy in Postmitotic Epithelia. *Dev. Cell*. 25:350–363.

Tan, L., and T.M. Kapoor. 2011. Examining the dynamics of chromosomal passenger complex (CPC)-dependent phosphorylation during cell division. *Proc. Natl. Acad. Sci. U. S. A.* 108:16675–16680.

Tanaka, K., N. Mukae, H. Dewar, V. Breugel, E.K. James, A.R. Prescott, C. Antony, T.U. Tanaka, M. van Breugel, E.K. James, A.R. Prescott, C. Antony, and T.U. Tanaka. 2005. Supplementary Information Molecular mechanisms of kinetochore capture by spindle microtubules. *Nature*. 434:987–994.

Tanaka, T.U., N. Rachidi, C. Janke, G. Pereira, M. Galova, E. Schiebel, M.J.R. Stark, and K. Nasmyth. 2002. Evidence that the Ipl1-Sli15 (Aurora Kinase-INCENP) complex promotes chromosome bi-orientation by altering kinetochore-spindle pole connections. *Cell*. 108:317–329.

Tang, Y.C., B.R. Williams, J.J. Siegel, and A. Amon. 2011. Identification of aneuploidy-selective antiproliferation compounds. *Cell*. 144:499–512.

Tanos, B.E., H.J. Yang, R. Soni, W.J. Wang, F.P. Macaluso, J.M. Asara, and M.F.B. Tsou. 2013. Centriole distal appendages promote membrane docking, leading to cilia initiation. *Genes Dev.* 27:163–168.

Taylor, A.M., J. Shih, G. Ha, G.F. Gao, X. Zhang, A.C. Berger, S.E. Schumacher, C. Wang, H. Hu, J. Liu, A.J. Lazar, S.J. Caesar-Johnson, J.A. Demchok, I. Felau, M. Kasapi, M.L. Ferguson,

C.M. Hutter, H.J. Sofia, R. Tarnuzzer, Z. Wang, L. Yang, J.C. Zenklusen, J. (Julia) J. Zhang, S. Chudamani, J. Liu, L. Lolla, R. Naresh, T. Pihl, Q. Sun, Y. Wan, Y. Wu, J. Cho, T. DeFreitas, S. Frazer, N. Gehlenborg, G. Getz, D.I. Heiman, J. Kim, M.S. Lawrence, P. Lin, S. Meier, M.S. Noble, G. Saksena, D. Voet, H.H.H. Zhang, B. Bernard, N. Chambwe, V. Dhankani, T. Knijnenburg, R. Kramer, K. Leinonen, Y. Liu, M. Miller, S. Reynolds, I. Shmulevich, V. Thorsson, W. Zhang, R. Akbani, B.M. Broom, A.M. Hegde, Z. Ju, R.S. Kanchi, A. Korkut, J. Li, H. Liang, S. Ling, W. Liu, Y. Lu, G.B. Mills, K.S. Ng, A. Rao, M. Ryan, J.J. Wang, J.N. Weinstein, J. (Julia) J. Zhang, A. Abeshouse, J. Armenia, D. Chakravarty, W.K. Chatila, I. de Bruijn, J. Gao, B.E. Gross, Z.J. Heins, R. Kundra, K. La, M. Ladanyi, A. Luna, M.G. Nissan, A. Ochoa, S.M. Phillips, E. Reznik, F. Sanchez-Vega, C. Sander, N. Schultz, R. Sheridan, S.O. Sumer, Y. Sun, B.S. Taylor, et al. 2018. Genomic and Functional Approaches to Understanding Cancer Aneuploidy. *Cancer Cell*. 33:676-689.e3.

Telzer, B.R., M.J. Moses, and J.L. Rosenbaum. 1975. Assembly of microtubules onto kinetochores of isolated mitotic chromosomes of HeLa cells. *Proc. Natl. Acad. Sci. U. S. A.* 72:4023–4027.

Terada, Y., Y. Uetake, and R. Kuriyama. 2003. Interaction of Aurora-A and centrosomin at the microtubule-nucleating site in Drosophila and mammalian cells. *J. Cell Biol.* 162:757–763.

Thompson, S.L., and D.A. Compton. 2010. Proliferation of aneuploid human cells is limited by a p53-dependent mechanism. *J. Cell Biol.* 188:369–381.

Thompson, S.L., and D.A. Compton. 2011. Chromosome missegregation in human cells arises through specific types of kinetochore-microtubule attachment errors. *Proc. Natl. Acad. Sci. U. S. A.* 108:17974–17978.

Tian, F.-Y., and C.J. Marsit. 2018. Environmentally Induced Epigenetic Plasticity in Development: Epigenetic Toxicity and Epigenetic Adaptation. *Curr. Epidemiol. reports*. 5:450–460.

Tilney, L.G., J. Bryan, D.J. Bush, K. Fujiwara, M.S. Mooseker, D.B. Murphy, and D.H. Snyder. 1973. Microtubules: Evidence for 13 protofilaments. *J. Cell Biol.* 59:267–275.

Tobey, R.A., L.R. Gurley, C.E. Hildebrand, R.L. Ratliff, and R.A. Walters. 1973. Sequential biochemical events in preparation for DNA replication and mitosis. United States.

Torosantucci, L., M. De Luca, G. Guarguaglini, P. Lavia, and F. Degrassi. 2008. Localized RanGTP Accumulation Promotes Microtubule Nucleation at Kinetochores in Somatic Mammalian Cells. *Mol. Biol. Cell*. 19:1873–1882.

Torres, E.M., N. Dephoure, A. Panneerselvam, C.M. Tucker, C.A. Whittaker, S.P. Gygi, M.J. Dunham, and A. Amon. 2010. Identification of aneuploidy-tolerating mutations. *Cell*. 143:71–83.

Torres, E.M., T. Sokolsky, C.M. Tucker, L.Y. Chan, M. Boselli, M.J. Dunham, and A. Amon. 2007. Effects of aneuploidy on cellular physiology and cell division in haploid yeast. *Science (80-.).* 317:916–924.

Torres, E.M., B.R. Williams, and A. Amon. 2008. Aneuploidy: Cells losing their balance. *Genetics*. 179:737–746.

Toso, A., J.R. Winter, A.J. Garrod, A.C. Amaro, P. Meraldi, and A.D. McAinsh. 2009.

Kinetochore-generated pushing forces separate centrosomes during bipolar spindle assembly. *J. Cell Biol.* 184:365–372.

Trakala, M., S. Rodríguez-Acebes, M. Maroto, C.E. Symonds, D. Santamaría, S. Ortega, M. Barbacid, J. Méndez, and M. Malumbres. 2015. Functional Reprogramming of Polyploidization in Megakaryocytes. *Dev. Cell*. 32:155–167.

Tran, K.D., and C.Q. Doe. 2008. Pdm and Castor close successive temporal identity windows in the NB3-1 lineage. *Development*. 135:3491–3499.

Trieselmann, N., and A. Wilde. 2002. Ran localizes around the microtubule spindle in vivo during mitosis in Drosophila embryos. *Curr. Biol.* 12:1124–1129.

Tsompana, M., and M.J. Buck. 2014. Chromatin accessibility: A window into the genome. *Epigenetics and Chromatin*. 7:1–16.

Tsou, M.-F.B., W.-J. Wang, K.A. George, K. Uryu, T. Stearns, and P. V Jallepalli. 2009. Polo kinase and separase regulate the mitotic licensing of centriole duplication in human cells. *Dev. Cell*. 17:344–354.

Tulu, U.S., C. Fagerstrom, N.P. Ferenz, and P. Wadsworth. 2006. Molecular requirements for kinetochore-associated microtubule formation in mammalian cells. *Curr. Biol.* 16:536–541.

Uehara, R., R. s Nozawa, A. Tomioka, S. Petry, R.D. Vale, C. Obuse, and G. Goshima. 2009. The augmin complex plays a critical role in spindle microtubule generation for mitotic progression and cytokinesis in human cells. *Proc. Natl. Acad. Sci. U. S. A.* 106:6998–7003.

Uhlmann, F., D. Wernic, M.-A. Poupart, E. V Koonin, and K. Nasmyth. 2000. Cleavage of Cohesin by the CD Clan Protease Separin Triggers Anaphase in Yeast. *Cell*. 103:375–386.

Ullah, Z., M.J. Kohn, R. Yagi, L.T. Vassilev, and M.L. DePamphilis. 2008. Differentiation of trophoblast stem cells into giant cells is triggered by p57/Kip2 inhibition of CDK1 activity. *Genes Dev.* 22:3024–3026.

Ullah, Z., C.Y. Lee, and M.L. DePamphilis. 2009. Cip/Kip cyclin-dependent protein kinase inhibitors and the road to polyploidy. *Cell Div.* 4:1–15.

Unhavaithaya, Y., and T.L. Orr-Weaver. 2012. Polyploidization of glia in neural development links tissue growth to blood-brain barrier integrity. *Genes Dev.* 26:31–36.

Upender, M.B., J.K. Habermann, L.M. McShane, E.L. Korn, J.C. Barrett, M.J. Difilippantonio, and T. Ried. 2004. Chromosome transfer induced aneuploidy results in complex dysregulation of the cellular transcriptome in immortalized and cancer cells. *Cancer Res.* 64:6941–6949.

Urata, Y., S.J. Parmelee, D.A. Agard, and J.W. Sedat. 1995. A three-dimensional structural dissection of Drosophila polytene chromosomes. *J. Cell Biol.* 131:279–295.

Urbach, R., and G.M. Technau. 2003. Molecular markers for identified neuroblasts in the developing brain of Drosophila. *Development*. 130:3621–3637.

Vanneste, D., V. Ferreira, and I. Vernos. 2011. Chromokinesins: localization-dependent functions and regulation during cell division. *Biochem. Soc. Trans.* 39:1154–1160.

Varmark, H., S. Llamazares, E. Rebollo, B. Lange, J. Reina, H. Schwarz, and C. Gonzalez. 2007. Asterless Is a Centriolar Protein Required for Centrosome Function and Embryo

Development in Drosophila. *Curr. Biol.* 17:1735–1745.

Vaziri, C., S. Saxena, Y. Jeon, C. Lee, K. Murata, Y. Machida, N. Wagle, D.S. Hwang, and A. Dutta. 2003. A p53-dependent checkpoint pathway prevents rereplication. *Mol. Cell*. 11:997–1008.

Vermeulen, K., D.R. Van Bockstaele, and Z.N. Berneman. 2003. The cell cycle: a review of regulation, deregulation and therapeutic targets in cancer. *Cell Prolif.* 36:131–149.

Vitrea, B., A.J. Holland, A. Kulukian, O. Shoshani, M. Hirai, Y. Wanga, M. Maldonado, T. Cho, J. Boubaker, D.A. Swing, L. Tessarollo, S.M. Evans, E. Fuchs, and D.W. Cleveland. 2015. Chronic centrosome amplification without tumorigenesis. *Proc. Natl. Acad. Sci. U. S. A.* 112:E6321–E6330.

Vorobjev, I.A., and Y.S. Chentsov. 1982. Centrioles in the cell cycle. I. Epithelial cells. *J. Cell Biol.* 93:938–949.

Wainman, A., D.W. Buster, T. Duncan, J. Metz, A. Ma, D. Sharp, and J.G. Wakefield. 2009. A new Augmin subunit, Msd1, demonstrates the importance of mitotic spindle-templated microtubule nucleation in the absence of functioning centrosomes. *Genes Dev.* 23:1876–1881.

Walczak, C.E., S. Cai, and A. Khodjakov. 2010. Mechanisms of chromosome behaviour during mitosis. *Nat Rev Mol Cell Biol*. 11:91–102.

Walczak, C.E., and R. Heald. 2008. Mechanisms of mitotic spindle assembly and function. *Int. Rev. Cytol.* 265:111–158.

Waldeyer, W. 1888. Ueber Karyokinese und ihre Beziehungen zu den Befruchtungsvorgängen. *Arch. für mikroskopische Anat.* 32:1.

Walker, D.H., and J.L. Maller. 1991. Role for cyclin A in the dependence of mitosis on completion of DMA replication. *Nature*. 354:314–317.

Wang, M., R.B. Nagle, B.S. Knudsen, A.E. Cress, and G.C. Rogers. 2020. Centrosome loss results in an unstable genome and malignant prostate tumors. *Oncogene*. 39:399–413.

Wang, X., H. Willenbring, Y. Akkari, Y. Torimaru, M. Foster, M. Al-Dhalimy, E. Lagasse, M. Finegold, S. Olson, and M. Grompe. 2003. Cell fusion is the principal source of bone-marrow-derived hepatocytes. *Nature*. 422:897–901.

Wangsa, D., I. Quintanilla, K. Torabi, M. Vila-Casadesús, A. Ercilla, G. Klus, Z. Yuce, C. Galofré, M. Cuatrecasas, J.J. Lozano, N. Agell, D. Cimini, A. Castells, T. Ried, and J. Camps. 2018. Near-tetraploid cancer cells show chromosome instability triggered by replication stress and exhibit enhanced invasiveness. *FASEB J.* 32:3502–3517.

Warburton, D., K. Anyane-Yeboa, P. Taterka, C.Y. Yu, and D. Olsen. 1991. Mosaic variegated aneuploidy with microcephaly: a new human mitotic mutant? *Ann. Genet.* 34:287–292.

Watanabe, S., G. Shioi, Y. Furuta, and G. Goshima. 2016. Intra-spindle Microtubule Assembly Regulates Clustering of Microtubule-Organizing Centers during Early Mouse Development. *Cell Rep.* 15:54–60.

Watson, E.D., and J.C. Cross. 2005. Development of structures and transport functions in the mouse placenta. *Physiology*. 20:180–193.

Weaver, B.A., A.D. Silk, C. Montagna, P. Verdier-Pinard, and D.W. Cleveland. 2007. Aneuploidy acts both oncogenically and as a tumor suppressor. *Cancer Cell*. 11:25–36.

Weaver, B.A.A., and D.W. Cleveland. 2007. Aneuploidy: Instigator and Inhibitor of Tumorigenesis: Figure 1. *Cancer Res.* 67:10103–10105.

Weisenberg, R.C., G.G. Borisy, and E.W. Taylor. 1968. The Colchicine-Binding Protein of Mammalian Brain and Its Relation to Microtubules. *Biochemistry*. 7:4466–4479.

Weiss, E., and M. Winey. 1996. The Saccharomyces cerevisiae spindle pole body duplication gene MPS1 is part of a mitotic checkpoint. *J. Cell Biol.* 132:111–123.

Wiese, C., A. Wilde, M.S. Moore, S.A. Adam, A. Merdes, and Y. Zheng. 2001. Role of importin-beta in coupling Ran to downstream targets in microtubule assembly. *Science*. 291:653–656.

Wilkins, B.J., N.A. Rall, Y. Ostwal, T. Kruitwagen, K. Hiragami-Hamada, M. Winkler, Y. Barral, W. Fischle, and H. Neumann. 2014. A cascade of histone modifications induces chromatin condensation in mitosis. *Science (80-.).* 343:77–80.

Williams, B.R., V.R. Prabhu, K.E. Hunter, C.M. Glazier, C. a Whittaker, D.E. Housman, and A. Amon. 2008. Aneuploidy Affects Proliferation and Spontaneous Immortalization in Mammalian Cells. *Science (80-.).* 322:703–709.

Winkelmann, M., P. Pfitzer, and W. Schneider. 1987. Significance of polyploidy in megakaryocytes and other cells in health and tumor disease. *Klin. Wochenschr.* 65:1115–1131.

Winkler, H. 1916. Über die experimentelle Erzeugung von Pflanzen mit abweichenden Chromosomenzahlen. Zeitschr. f. Bot. 8. 1920. *Verbreitung und Ursache der Parthenogenes. im Pflanzen-und Tierreiche. Jena*.

de Wit, E., F. Greil, and B. van Steensel. 2007. High-resolution mapping reveals links of HP1 with active and inactive chromatin components. *PLoS Genet.* 3:e38.

Witt, P.L., H. Ris, and G.G. Borisy. 1980. Origin of kinetochore microtubules in Chinese hamster ovary cells. *Chromosoma*. 81:483–505.

Witt, P.L., H. Ris, and G.G. Borisy. 1981. Structure of kinetochore fibers: microtubule continuity and inter-microtubule bridges. *Chromosoma*. 83:523–540.

Wittmann, T., A. Hyman, and A. Desai. 2001. The spindle: A dynamic assembly of microtubules and motors. *Nat. Cell Biol.* 3.

Wittmann, T., M. Wilm, E. Karsenti, and I. Vernos. 2000. TPX2, a novel Xenopus MAP involved in spindle pole organization. *J. Cell Biol.* 149:1405–1418.

Wollman, R., E.N. Cytrynbaum, J.T. Jones, T. Meyer, J.M. Scholey, and A. Mogilner. 2005. Efficient chromosome capture requires a bias in the “search-and-capture” process during mitotic-spindle assembly. *Curr. Biol.* 15:828–832.

Wong, Y.L., J. V. Anzola, R.L. Davis, M. Yoon, A. Motamedi, A. Kroll, C.P. Seo, J.E. Hsia, S.K. Kim, J.W. Mitchell, B.J. Mitchell, A. Desai, T.C. Gahman, A.K. Shiau, and K. Oegema. 2015. Reversible centriole depletion with an inhibitor of Polo-like kinase 4. *Science (80-.).* 348:1155–1160.

Woodruff, J.B. 2018. Assembly of Mitotic Structures through Phase Separation. *J. Mol. Biol.* 430:4762–4772.

Woodruff, J.B., B. Ferreira Gomes, P.O. Widlund, J. Mahamid, A. Honigmann, and A.A. Hyman. 2017. The Centrosome Is a Selective Condensate that Nucleates Microtubules

by Concentrating Tubulin. *Cell*. 169:1066-1077.e10.

Wordeman, L., and T.J. Mitchison. 1995. Identification and partial characterization of mitotic centromere- associated kinesin, a kinesin-related protein that associates with centromeres during mitosis. *J. Cell Biol.* 128:95–105.

Xiang, J., J. Bandura, P. Zhang, Y. Jin, H. Reuter, and B.A. Edgar. 2017. EGFR-dependent TOR-independent endocycles support Drosophila gut epithelial regeneration. *Nat. Commun.* 8:1–13.

Xiao, C., M. Grzonka, C. Gerards, M. Mack, R. Figge, and H. Bazzi. 2020. Gradual centriole maturation associates with the mitotic surveillance pathway in mouse development. 1–12.

Xing, L. 2012. Osteoclast fusion and regulation by RANKL-dependent and independent factors. *World J. Orthop.* 3:212.

Yagi, M., T. Miyamoto, Y. Sawatani, K. Iwamoto, N. Hosogane, N. Fujita, K. Morita, K. Ninomiya, T. Suzuki, K. Miyamoto, Y. Oike, M. Takeya, Y. Toyama, and T. Suda. 2005. DC-STAMP is essential for cell-cell fusion in osteoclasts and foreign body giant cells. *J. Exp. Med.* 202:345–351.

Yang, A.H., D. Kaushal, S.K. Rehen, K. Kriedt, M.A. Kingsbury, M.J. McConnell, and J. Chun. 2003. Chromosome Segregation Defects Contribute to Aneuploidy in Normal Neural Progenitor Cells. *J. Neurosci.* 23:10454–10462.

Yang, C.P., and S.S. Fan. 2008. Drosophila mars is required for organizing kinetochore microtubules during mitosis. *Exp Cell Res*. 314:3209–3220.

Yang, J., and M.H. Shen. 2006. Polyethylene Glycol-Mediated Cell Fusion BT - Nuclear Reprogramming: Methods and Protocols. S. Pells, editor. Humana Press, Totowa, NJ. 59–66.

Yang, L., J. Titlow, D. Ennis, C. Smith, J. Mitchell, F.L. Young, S. Waddell, D. Ish-Horowicz, and I. Davis. 2017. Single molecule fluorescence in situ hybridisation for quantitating post-transcriptional regulation in Drosophila brains. *Methods*. 126:166–176.

Yao, C., U. Rath, H. Maiato, D. Sharp, J. Girton, K.M. Johansen, and J. Johansen. 2012. A nuclear-derived proteinaceous matrix embeds the microtubule spindle apparatus during mitosis. *Mol. Biol. Cell*. 23:3532–3541.

Ye, Y., M. Li, L. Gu, X. Chen, J. Shi, X. Zhang, and C. Jiang. 2017. Chromatin remodeling during in vivo neural stem cells differentiating to neurons in early Drosophila embryos. *Cell Death Differ*. 24:409–420.

Yim, A.P.C. 1982. Some flow-cytofluorimetric studies of the nuclear ploidy of mouse hepatocytes: III. Further observations on early changes in nuclear ploidy of mouse hepatocytes following various experimental procedures. *Br. J. Exp. Pathol.* 63:458–461.

Yona, A.H., Y.S. Manor, R.H. Herbst, G.H. Romano, A. Mitchell, M. Kupiec, Y. Pilpel, and O. Dahan. 2012. Chromosomal duplication is a transient evolutionary solution to stress. *Proc. Natl. Acad. Sci. U. S. A.* 109:21010–21015.

Yost, S., B. de Wolf, S. Hanks, A. Zachariou, C. Marcozzi, M. Clarke, R.M. de Voer, B. Etemad, E. Uijttewaal, E. Ramsay, H. Wylie, A. Elliott, S. Picton, A. Smith, S. Smithson, S. Seal, E. Ruark, G. Houge, J. Pines, G.J.P.L. Kops, and N. Rahman. 2017. Biallelic TRIP13 mutations predispose to Wilms tumor and chromosome missegregation. *Nat. Genet.* 49:1148–

1151.

Yu, F., C.T. Kuo, and Y.N. Jan. 2006. Drosophila Neuroblast Asymmetric Cell Division: Recent Advances and Implications for Stem Cell Biology. *Neuron*. 51:13–20.

Yurov, Y.B., I.Y. Iourov, S.G. Vorsanova, T. Liehr, A.D. Kolotii, S.I. Kutsev, F. Pellestor, A.K. Beresheva, I.A. Demidova, V.S. Kravets, V. V. Monakhov, and I. V. Soloviev. 2007. Aneuploidy and confined chromosomal mosaicism in the developing human brain. *PLoS One*. 2:4–9.

Yurov, Y.B., S.G. Vorsanova, I.A. Demidova, A.D. Kolotii, I. V. Soloviev, and I.Y. Iourov. 2018. Mosaic Brain Aneuploidy in Mental Illnesses: An Association of Low-level post-zygotic Aneuploidy with Schizophrenia and Comorbid Psychiatric Disorders. *Curr. Genomics*. 19:163–172.

Yurov, Y.B., S.G. Vorsanova, T. Liehr, A.D. Kolotii, and I.Y. Iourov. 2014. X chromosome aneuploidy in the Alzheimer's disease brain. *Mol. Cytogenet.* 7:1–7.

Zack, T.I., S.E. Schumacher, S.L. Carter, A.D. Cherniack, G. Saksena, B. Tabak, M.S. Lawrence, C.Z. Zhang, J. Wala, C.H. Mermel, C. Sougnez, S.B. Gabriel, B. Hernandez, H. Shen, P.W. Laird, G. Getz, M. Meyerson, and R. Beroukhim. 2013. Pan-cancer patterns of somatic copy number alteration. *Nat. Genet.* 45:1134–1140.

Zahn, J.M., S. Poosala, A.B. Owen, D.K. Ingram, A. Lustig, A. Carter, A.T. Weeraratna, D.D. Taub, M. Gorospe, K. Mazan-Mamczarz, E.G. Lakatta, K.R. Boheler, X. Xu, M.P. Mattson, G. Falco, M.S.H. Ko, D. Schlessinger, J. Firman, S.K. Kummerfeld, W.H. Wood, A.B. Zonderman, S.K. Kim, and K.G. Becker. 2007. AGEMAP: A gene expression database for aging in mice. *PLoS Genet.* 3:2326–2337.

Zanet, J., A. Freije, M. Ruiz, V. Coulon, J.R. Sanz, J. Chiesa, and A. Gandarillas. 2010. A mitosis block links active cell cycle with human epidermal differentiation and results in endoreplication. *PLoS One*. 5.

Zhai, Y., P.J. Kronebusch, P.M. Simon, and G.G. Borisy. 1996. Microtubule dynamics at the G2/M transition: abrupt breakdown of cytoplasmic microtubules at nuclear envelope breakdown and implications for spindle morphogenesis. *J. Cell Biol.* 135:201–214.

Zhang, B., S. Mehrotra, W.L. Ng, and B.R. Calvi. 2014a. Low Levels of p53 Protein and Chromatin Silencing of p53 Target Genes Repress Apoptosis in Drosophila Endocycling Cells. *PLoS Genet.* 10.

Zhang, S., Q. Chen, Q. Liu, Y. Li, X. Sun, L. Hong, S. Ji, C. Liu, J. Geng, W. Zhang, Z. Lu, Z.Y. Yin, Y. Zeng, K.H. Lin, Q. Wu, Q. Li, K.K.I.K.K.I. Nakayama, K.K.I.K.K.I. Nakayama, X. Deng, R.L. Johnson, L. Zhu, D. Gao, L. Chen, and D. Zhou. 2017. Hippo Signaling Suppresses Cell Ploidy and Tumorigenesis through Skp2. *Cancer Cell*. 31:669-684.e7.

Zhang, S., I. Mercado-Uribe, Z. Xing, B. Sun, J. Kuang, and J. Liu. 2014b. Generation of cancer stem-like cells through the formation of polyploid giant cancer cells. *Oncogene*. 33:116–128.

Zheng, Y., M.K. Jung, and B.R. Oakley. 1991. γ-Tubulin is present in Drosophila melanogaster and homo sapiens and is associated with the centrosome. *Cell*. 65:817–823.

Zheng, Y., M.L. Wong, B. Alberts, and T. Mitchison. 1995. Nucleation of microtubule assembly by a gamma-tubulin-containing ring complex. *Nature*. 378:578–583.

Zhiteneva, A., J.J. Bonfiglio, A. Makarov, T. Colby, P. Vagnarelli, E.C. Schirmer, I. Matic, and

W.C. Earnshaw. 2017. Mitotic post-translational modifications of histones promote chromatin compaction in vitro. *Open Biol.* 7.

Zhu, J., M. Adli, J.Y. Zou, G. Verstappen, M. Coyne, X. Zhang, T. Durham, M. Miri, V. Deshpande, P.L. De Jager, D.A. Bennett, J.A. Houmard, D.M. Muoio, T.T. Onder, R. Camahort, C.A. Cowan, A. Meissner, C.B. Epstein, N. Shoresh, and B.E. Bernstein. 2013. Genome-wide chromatin state transitions associated with developmental and environmental cues. *Cell*. 152:642–654.

Zhu, Q., and A.A. Wani. 2010. Histone modifications: crucial elements for damage response and chromatin restoration. *J. Cell. Physiol.* 223:283–288.

Zielke, N., K.J. Kim, V. Tran, S.T. Shibutani, M.J. Bravo, S. Nagarajan, M. Van Straaten, B. Woods, G. Von Dassow, C. Rottig, C.F. Lehner, S.S. Grewal, R.J. Duronio, and B.A. Edgar. 2011. Control of Drosophila endocycles by E2F and CRL4 CDT2. *Nature*. 480:123–127.

Zybina, T.G., and E. V Zybina. 2005. Cell reproduction and genome multiplication in the proliferative and invasive trophoblast cell populations of mammalian placenta. *Cell Biol. Int.* 29:1071–1083.

RÉSUMÉ

La plupart de nos cellules sont diploïdes possédant deux copies de chaque chromosome. Lors de la mitose, la formation d'un fuseau bipolaire avec un centrosome à chaque pôle permet la ségrégation correcte des chromosomes, essentielle au maintien de la stabilité génétique. Il existe néanmoins des variations du contenu chromosomique comme la polyploïdie, définit comme le doublement de l'ensemble des chromosomes et l'aneuploïdie, définie comme la perte ou le gain de chromosomes entiers. Bien qu'observées, la fréquence des cellules aneuploïdes dans les tissus d'un organisme sain reste controversée. De façon importante, la duplication du génome et l'aneuploïdie sont associées à des pathologies et sont considérées comme des caractéristiques au cancer. En effet, un nombre anormal de chromosomes est souvent associé à une instabilité chromosomique. Toutefois le rôle et les implications de ces variations dans l'initiation et la progression de tumeur restent peu compris.

J'ai d'abord étudié les conséquences de la polyploïdie sur la division des cellules. J'ai utilisé des approches *in vivo* et *in vitro* en induisant la polyploïdisation par défaut de cytocinèse dans des cellules souches neurales de drosophile et des cellules cancéreuses humaines. L'analyse de leur mitose m'a permis de découvrir que la présence de chromosomes et de centrosomes en excès conduisait invariablement à la formation de fuseaux multipolaires. En modélisant les cellules polyploïdes, j'ai découvert qu'au-delà de la quantité, la conformation spatiale de l'ADN contribuait à cette multipolarité. Des perturbations expérimentales au niveau de l'ADN et du fuseau m'ont permis de démontrer que la présence d'ADN en excès agissait comme une barrière physique bloquant la coalescence des multiples pôles et par conséquent empêchant la bipolarité. De façon intéressante, j'ai réussi à restaurer la bipolarité en supprimant la «barrière d'ADN» par ablation avec laser ou en augmentant la longueur des microtubules pour contourner celle-ci. Alors que l'amplification centrosomale était considérée comme unique acteur, mes résultats identifient l'excès d'ADN comme contributeur clef de la multipolarité et de l'instabilité chromosomique typique des cellules polyploïdes.

Je me suis ensuite intéressée à l'aneuploïdie, dont la fréquence en contexte sain reste un sujet de débat intense. De plus, les outils développés jusqu'à présent pour évaluer le taux d'aneuploïdie manque d'une dimension temporelle. J'ai donc généré un outil génétique innovant de visualisation et de suivi des cellules aneuploïdes *in vivo* chez la drosophile. J'ai utilisé l'expression de la GFP comme gène rapporteur, contrôlée par le système GAL4/UAS et son inhibition par GAL80. Ainsi, la perte aléatoire du chromosome contenant la séquence du GAL80 entraine l'apparition d'un signal GFP dans les cellules aneuploïdes. Celles-ci peuvent donc être facilement détectées et suivies en temps-réel dans les tissus. En utilisant ce système, j'ai découvert que la perte de chromosome était un évènement très rare dans les tissus de la mouche. Cet outil combiné à d'autres marqueurs fluorescents et/ou utilisé dans divers contextes génétiques aidera à la compréhension de la genèse et du devenir des cellules aneuploïdes *in vivo*.

De plus, j'ai constaté que le cerveau de la larve présentait un nombre important de cellules GFP. De manière surprenante, ces cellules ne résultaient pas de la perte d'un chromosome mais de la perte d'expression du gène *GAL80*. Ces résultats inattendus ont de fortes implications pour la communauté des drosophilistes qui utilise quotidiennement ce système GAL4/GAL80. J'ai aussi découvert que les cellules souches neurales présentaient un mosaïsme dans l'expression des gènes, qui diffèrent d'autres organes et s'adaptent à des stimuli environnementaux. Ceci représente possiblement un niveau de plasticité dans le cerveau nécessaire à la diversité neuronale, l'adaptation et la survie.

MOTS CLÉS

Fuseau mitotique / Polyploïdie / Aneuploïdie / Neuroblastes / GAL4/GAL80

ABSTRACT

Most animal cells are diploid, containing two copies of each chromosome. Establishment of proper bipolar mitotic spindle containing two centrosomes, one at each pole contributes to accurate chromosome segregation. This is essential for the maintenance of genome stability, tissue and organism homeostasis. However, numerical deviations to the diploid set are observed in healthy tissues. Polyploidy is the doubling of the whole chromosome set and aneuploidy concerns the gain or loss of whole chromosomes. Importantly, whole genome duplications and aneuploidy have also been associated to pathological conditions. For example, variations to genome content are associated with chromosome instability and cancer development, however their exact contribution to cancer genome remains poorly understood.

In the first part of my PhD project, I investigated the consequences of polyploidy during cell division. I found that the presence of extra DNA and extra centrosomes generated invariably multipolar spindles. Then I identified contributors to the multipolar status using in vivo approaches in *Drosophila* neural stem cells and *in vitro* culture of cancer cells. Further I combined DNA and spindle perturbations with computer modelling and found that in polyploid cells, the presence of excessive DNA acts as a physical barrier blocking spindle pole coalescence and bipolarity. Indeed, laser ablation to disrupt and increase in microtubule stability and length to bypass the DNA-barrier could rescue bipolar spindle formation. This discovery challenges the current view that suggested extra-centrosomes as only contributor to spindle multipolarity and provides a rational to understand chromosome instability typical of polyploid cells.

The aim of the second part of my PhD project was to generate a novel tool to quantitively probe chromosome loss *in vivo* in *Drosophila* tissues. Aneuploidy has been observed in various physiological tissues, however the frequency of this error remained highly debatable. In addition, tools developed so far to assess aneuploidy lack a temporal dimension. To circumvent this, I used the expression of a GFP report gene driven by the GAL4/UAS system and its inhibition by GAL80. In principle, the random loss of the chromosome carrying the GAL80 sequence leads to GFP appearance in aneuploid cells that can therefore be followed in live tissues. I found that chromosome loss was extremely infrequent in most tissues of the wild type fly. This tool combined with fluorescent marker and/or tested in various genetic background, will help understanding mechanisms behind aneuploidy genesis and outcome *in vivo*.

While developing this tool, I discovered that in the larval brain, GFP cells where not a by-product of chromosome loss but rather an unexpected mis-regulation in the expression of the *GAL80* gene. These results have strong implications for the *Drosophila* community as it can result in false positive in clonal experiments. Further, I discovered a mosaicism and plasticity of the *Drosophila* brain in neural stem cells for gene expression which differs from other organs and that is influenced by environmental stimuli. This possibly reflects a certain level of plasticity in the brain necessary for neuronal diversity, adaptation and survival.

KEYWORDS

Mitotic spindle / Polyploidy / Aneuploidy / Neuroblasts / GAL4/GAL80